AWARD NUMBER: W81XWH-16-1-0474

TITLE: An association of unique microRNA turnover machinery with prostate cancer progression

PRINCIPAL INVESTIGATOR: Hsieh, Jer-Tsong

CONTRACTING ORGANIZATION: UT Southwestern Medical Center
5323 harry Hines Blvd., Dallas, TX 75390

REPORT DATE: JANUARY 2022

TYPE OF REPORT: Final

PREPARED FOR: U.S. Army Medical Research and Materiel Command
Fort Detrick, Maryland 21702-5012

REPORT DOCUMENTATION PAGE

Form Approved
OMB No. 0704-0188

1. REPORT DATE	2. REPORT TYPE	3. DATES COVERED
JANUARY 2022	Final	09/15/2016 - 09/14/2021

An association of unique microRNA turnover machinery with prostate cancer progression

5a. CONTRACT NUMBER
W81XWH-16-1-0474

5b. GRANT NUMBER
PC150136

5c. PROGRAM ELEMENT NUMBER

6. AUTHOR(S)
Jer-Tsong Hsieh

E-Mail: jt.hsieh@utsouthwestern.edu

5d. PROJECT NUMBER

5e. TASK NUMBER

5f. WORK UNIT NUMBER

7. PERFORMING ORGANIZATION NAME(S) AND ADDRESS(ES)

UT Southwestern Medical Center
5323 Harry Hines Blvd.,
Dallas, TX 75390

8. PERFORMING ORGANIZATION REPORT NUMBER

9. SPONSORING / MONITORING AGENCY NAME(S) AND ADDRESS(ES)

U.S. Army Medical Research and Materiel Command
Fort Detrick, Maryland 21702-5012

10. SPONSOR/MONITOR'S ACRONYM(S)

11. SPONSOR/MONITOR'S REPORT NUMBER(S)

12. DISTRIBUTION / AVAILABILITY STATEMENT

Approved for Public Release; Distribution Unlimited

13. SUPPLEMENTARY NOTES

14. ABSTRACT

Prostate cancer (PCa) is still incurable when cancer cells undergo epithelial-to-mesenchymal transition (EMT) and acquire cancer stem cell (CSC) phenotypes to become metastatic therapy- and castration-resistant PCa (t-CRPC). In this study, we demonstrate that IFNγ can induce EMT in PCa cells via the JAK-STAT1 signaling pathway, leading to the transcription of interferon-induced tetratricopeptide repeat 5 (IFIT5). We also unveil a new function of IFIT5 complex in degrading precursor microRNAs (pre-miRNA) that include pre-miR-363 from the miR-106a-363 cluster as well as pre-miR-101 and pre-miR-128. Mechanistically, STAT1-mediated induction of IFIT5 appears to facilitate the acquisition of stemness properties by accelerating specific microRNAs (such as miR-128 and miR-101) turnover, which is resulted in BMI1 and SOX2 elevation. Overall, this study provides a new understanding of the role of IFN-STAT1-IFIT5-mediated microRNA turnover in the acquisition of stemness properties in PCa and also highlights STAT1 as a potent therapeutic target in preventing the outgrowth of t-CRPC.

15. SUBJECT TERMS

NONE LISTED

16. SECURITY CLASSIFICATION OF:			17. LIMITATION OF ABSTRACT	18. NUMBER OF PAGES	19a. NAME OF RESPONSIBLE PERSON
a. REPORT	b. ABSTRACT	c. THIS PAGE			USAMRMC
Unclassified	Unclassified	Unclassified	Unclassified	122	19b. TELEPHONE NUMBER *(include area code)*

TABLE OF CONTENTS

1. INTRODUCTION

Prostate cancer (PCa) is ranked the second lethal disease among US men; the majority of mortality is resulted from the metastatic castration resistant PCa (CRPC) relapse from hormonal therapy. Epithelial-to-mesenchymal transition (EMT) has been identified as a key mechanism leading to metastatic disease. Thus, developing effective targeted therapy to EMT becomes a high priority of PCa management.

Clinically, recurrent CRPC is resistant to chemotherapy; the underlying mechanism(s) is not fully understood. One of the possible theories to explain the recurrence and ineffectiveness of cancer treatment is the cancer stem cell (CSC) model in which a subset of tumor cells is responsible for cancer initiation and progression as well as cancer recurrence. These CSCs share with normal stem cells the properties of self-renewal, immortal and differentiation into a variety of cell types including heterogeneous lineages of cancer cells. In addition, CSC can re-grow from a few cells resistant to therapy and left behind. Until now, it is known several potential molecular pathways associated with CSC development in PCa; these pathways also overlap with pathways leading to EMT. In this study, interferon (IFN) is shown to be a potent facilitator for EMT and CSC in PCa.

In order to develop “effective agent”, microRNA now becomes an emerging avenue of cancer therapy. MicroRNA (miRNA) is a short RNA molecule that has been shown to regulate 60% cellular mRNA with high specificity (sequence recognition) and efficiency (multi-miRNAs to one mRNA or one miRNA to multi-mRNAs). In general, based on their function, miRNA can be divided into oncomir (promoting cancer development) and tumor suppressor (inhibiting cancer development). This project is to unveil a protein complex as new machinery of controlling multiple tumor suppressive miRNA degradation that leads to cancer metastasis and CSC development. The goal of this proposal is to unveil its mechanism of action, the control of gene expression and its clinical applicability as prognostic marker. Specifically, understanding the mechanism of action of this protein complex will help us to design better miRNAs as therapeutic to avoid its degradation after delivery. Unveiling the regulation by stromal factor will provide us more understanding the impact of tumor microenvironment on cancer progression. Evaluating clinical correlation from minimal invasive liquid biopsy will offer a new tool to distinguish aggressive cancer from indolent disease. Overall, the outcome of this study has provided a new regulatory mechanism of miRNA homeostasis, which is also applicable to other cancer types. Most significantly, this proposal offers new therapeutic strategies of repurposing FDA-approved targeted therapeutics to CRPC patients; the outcome of this study is expected to have an immediate clinical impact on PCa therapy.

2. KEYWORDS

Epithelial-to-mesenchymal transition, cancer stem cell, IFIT5, XRN1 microRNA, microRNA turn over.

3. ACCOMPLISHMENTS

Major goals and accomplishments

Aim 1 Dissect the mechanism of IFIT5-mediated miRNA turnover.

Major Task: Unveil new machinery of miRNA turnover**.**

Milestone: Unveil a new regulatory mechanism of miRNA turnover by IFIT5 and publish two review papers**.**

Aim 2 Determine the regulation of IFIT5 gene in PCa progression.

Major Task: Identify key regulator(s) and inducer(s) of IFIT5 gene expression**.**

Milestone: Unveil IFIT5 as a bona fide IFN-regulated gene via STAT-JAK signaling pathway and publish two peer-reviewed papers.

Aim 3 Evaluate IFIT5 as a prognostic marker in PCa patients.

Major Task: Determine IFIT5 as a potential prognostic marker for prostate cancer.

Milestone: Unveil IFIT5 as a bona fide IFN-regulated gene via STAT-JAK signaling pathway. Completed with paper publication.

What was accomplished under these goals?

(1) major activities

- Perform miR array to identify miR-363 as a potential tumor suppressor miR in PCa acquired EMT phenotypes.
- Perform RNA pull down and LC/MS-MS assays to identify specific binding of IFIT5 to miR-363.
- Perform in vitro transcription of pre-miRNA and miRNA turnover assay.
- Design gene-specific knockdown using shRNA technology.
- Employ CRISPR/Cas9 technology to permanently delete p53 and Rb in PCa cell lines.
- Characterize prostate CSC using in vitro prostatsphere, biomarkers and in vivo tumorigenic assay.
- Analyze clinical correlation of IFN-regulated genes with PCa progression.
- Evaluate the therapeutic efficacies of STAT1 inhibitor in CRPC xenograft model.

(2) Specific objective

We have established that IFN promotes EMT and CSC of PCa via IFIT5-elicited turnover of several tumor suppressor miRNAs.

We have identified potent inhibitors for CRPC treatment.

(3) Significant results or key outcomes

Our studies demonstrate IFNγ as a potent facilitator in cancer metastasis in which IFIT5, an IFNγ-regulated gene, appears to be a critical downstream effector with significant clinical prevalence. Mechanistically, we unveil a new functional role of IFIT5 in modulating turnover of several tumor suppressor miRNAs. Targeting IFN-mediated signaling pathway (i.e., STAT-JAK) with FDA-approved small molecule inhibitors exhibits excellent efficacy to overcome castration resistance of PCa.

What opportunities for training and professional development have the project provided?
This project provides excellent training opportunities for molecular cell biology, tumor biology and pathohistologic techniques.

How were the results disseminated to communities of interest?
We have published three manuscripts. Also, we are submitting abstract to report these new discoveries in 2021 SBUR annual meeting and ready to submit one additional paper.

What do you plan to do during the next reporting period to accomplish the goals?
N/A

4. IMPACT

What was the impact on the development of the principal discipline(s) of the project? What was the impact on other disciplines?
This project highlights several functional roles of IFN in PCa progression including induction of EMT and CSC. This study also demonstrates that the unique oncogenic function of IFIT5 is to modulate turnover of several tumor suppressor microRNAs (miRNAs). By determining its clinical correlation, the elevated IFIT5 is associated with PCa progression, which could be used as a prognostic biomarker(s) for lethality of PCa. Knowing IFIT5 as a bona fide IFN-regulated gene via STAT-JAK signaling pathway, we further explore the efficacy of several FDA-approved small molecule inhibitors specific to STAT1 or JAK1 using clinically relevant animal model and the results support repurposing these inhibitors on therapy- and castration-resistant prostate cancer patients.

What was the impact on technology transfer?
Nothing to Report.

What was the impact on society beyond science and technology?
Nothing to report.

5. CHANGES/PROBLEMS

Changes in approach and reasons for change
Nothing to report

Actual or anticipated problems or delays and actions or plans to resolve them

Nothing to report

Changes that had a significant impact on expenditures
Nothing to report

Significant changes in use or care of human subjects, vertebrate animals, biohazards, and/or select agents
Significant changes in use or care of human subjects
Nothing to report

Significant changes in use or care of vertebrate animals
Nothing to report

Significant changes in use of biohazards and/or select agents
Nothing to report

6. PRODUCTS

- **Publications, conference papers, and presentations**

  Lo, U., Pong, R.C., Yang, D., Gandee, L., Hernandez, E., Dang, A., Lin, C-J., Santoyo, J., Ma, S-H., Sonavane, R., Huang, J., Tseng, S-F., Moro, L., Arbini A.A., Kaour, P., Raj, G., He, D., Lai, C.H., Lin, H., Hsieh, J.T. (2019) Interferon-γ induces epithelial-to-mesenchymal transition in prostate cancer via a new mechanism of microRNA processing. Cancer Res., 79:1098-1112. PMID30504123

  Lo, U., Bao, J., Cen, J., Yeh, H., Luo, J., Tan, W., Hsieh, J.T. (2019) Interferon-induced IFIT5 promotes epithelial-to-mesenchymal transition leading to renal cancer invasion. Am. J. Clin. Exp. Urol., 7:31-45. PMID30906803

  Lin CJ, Lo UG, Hsieh JT. (2018) The regulatory pathways leading to stem-like cells underlie prostate cancer progression. Asian J Androl., 21:233-240. PMID: 30178777

  Lo, U., Lee, C.F., Lee, M.S., Hsieh, J.T. (2017) The role and mechanism of epithelial-to-mesenchymal transition in prostate cancer progression. Int. J. Mol. Sci., 18: pii: E2079. PMID28973968

- **Books or other non-periodical, one-time publications.**
  Nothing to report
- **Other publications, conference papers and presentations**.
  Nothing to report
- **Website(s) or other Internet site(s)**
  Nothing to report
- **Technologies or techniques**
  Nothing to report
- **Inventions, patent applications, and/or licenses**

Nothing to report

- **Other Products**
  Nothing to report

7. PARTICIPANTS AND OTHER COLLABORATING ORGANIZATIONS

Name: U-Ging Lo

Project Role:	Research Scientist
Researcher Identifier (e.g. ORCID ID):	none
Nearest person month worked:	12.0
Contribution to Project:	Performed all experiments and analyzed data.
Funding Support:	No change

Name: Payal Kapur

Project Role:	collaborator
Researcher Identifier (e.g. ORCID ID):	none
Nearest person month worked:	0.36
Contribution to Project:	Analyzed histopathologic data.
Funding Support:	No change

Has there been a change in the active other support of the PD/PI(s) or senior/key personnel since the last reporting period?
Nothing to Report.

What other organizations were involved as partners?
Nothing to Report.

8. SPECIAL REPORTING REQUIREMENTS

None.

9. APPENDIX

Four publications and one manuscript ready for submission.

STAT1-IFIT5 signaling activation by interferon potentiates lineage plasticity of castration-resistant prostate cancer

U-Ging Lo[1], Yu-An Chen[1,2], Junjie Cen[3], Su Deng[4], Junghang Luo[3], Haiyen Zhau[5], Lin Ho[6], Chih-Ho Lai[2], Ping Mu[4], Leland W.K. Chung[6], and Jer-Tsong Hsieh[1]

[1]Department of Urology, University of Texas Southwestern Medical Center, Dallas, TX 75390, USA; [2]Department of Microbiology and Immunology, Graduate Institute of Biomedical Sciences, College of Medicine, Chang Gung University, Taoyuan, Taiwan; [3]Department of Urology, First Affiliated Hospital, Sun Yat-sen University, Guangdong, China; [4]Department of Molecular Biology, University of Texas Southwestern Medical Center, Dallas, TX 75390, USA; [5]Uro-Oncology Research, Department of Medicine, Cedars-Sinai Medical Center, Los Angeles, California, USA; [6]Department of Life Sciences, National Chung Hsing University, Taichung, Taiwan.

Running Title: The role of interferon-STAT1 signaling pathway in cell plasticity

All authors don't have any conflict of interest

Corresponding author: Jer-Tsong Hsieh, Ph.D., jt.hsieh@utsouthwestern.edu,

Phone: 214-648-3988; Fax: 214-648-8786; 5323 Harry Hines Blvd., J8-134 Dallas, TX 75390 USA.

Abstract

In the past few years, cell plasticity in prostate cancer (PCa) has emerged as an important mechanism of therapeutic- and castration-resistant PCa (t-CRPC), which has been characterized as a biologic process of lineage development from stem cell. In addition to the impact of genetic alterations on PCa cell plasticity, other exogeneous factors are known to induce neuroendocrine differentiation in PCa. In this study, we reported interferon as a potent inducer of PCa cell plasticity, which is supported by significant elevation of interferon (IFN)-inducible STAT1-driven genes in metastatic PCa. Inhibition of JAK-STAT1 signaling suppresses the self-renewal capacity of PCa stem cell (PSCS) *in vitro* and attenuates tumor growth *in vivo*. Mechanistically, STAT1-mediated induction of IFIT5, a unique downstream effector, appears to facilitate the acquisition of stemness properties in PCSCs by accelerating specific microRNAs (such as miR-128 and miR-101) turnover, which is resulted in BMI1 and SOX2 elevation. Consistently, knocking down IFIT5 in t-CRPC cell can attenuate sphere forming ability *in vitro*, and decreased tumor incidence *in vivo*. Overall, this study provides a new understanding of the role of IFN-STAT1-IFIT5-mediated microRNA turnover in the acquisition of stemness properties in PCa and also highlights STAT1 as a potent therapeutic target in preventing the outgrowth of t-CRPC.

Introduction

Prostate adenocarcinoma (PCa) remains to be the leading cause of cancer incidence and the second leading cause of cancer-related deaths in men of the United States[1]. Androgen deprivation therapy (ADT) remains to be the primary therapeutic strategy for advanced PCa[2-5]. Despite drugs targeting androgen receptor (AR) signaling or androgen synthesis is effective on the regression of metastatic hormone naive tumor, the onset of therapeutic- and castration-resistant (t-CRPC) phenotype becomes inevitable, which is considered as a lethal disease. Data derived from clinical specimens or cell model or transgenic mouse models suggest that distinct genetic alterations[6-11] are associated with the appearance of t-CRPC from androgen-deprived condition, which are related with lineage plasticity of CRPC cells. Meanwhile, accumulating evidence indicate that t-CRPC cells often display neuroendocrine-like phenotypes[12]. In general, normal stem cell is an ingredient component in lineage plasticity, however, cancer stem cell (CSC) population not only possess self-renewal properties and trans-differentiation into different lineages[13-15] but also lose homeostatic regulation. For example, the presence of CSC in PCa can be related with cancer recurrence, metastasis and therapeutic resistance[16-18]. In addition to genetic alterations[19], several paracrine factors have been shown to induce de-differentiation into stem-like status of PCa cells[20]. Recently, we observed that IFIT5, a bone fide interferon (IFN)-inducible gene, is able to facilitate PCa epithelial-to-mesenchymal transition that is considered as trans-differentiation of adenocarcinoma. Also, significant elevation of serum IFNγ was found in PCa patients after ADT[21]. However, whether IFN plays any role in prostate CSC development is largely unknown. In this study, we demonstrate that activation of Janus kinases (JAK)- signal transducer and activator of transcription 1 (STAT1) pathway in PCa cells after IFN treatment or long-term ADT is associated with prostate cancer stem cell (PCSC) activities as well as neuroendocrine phenotypes. Parallel with known genetic hallmarks, we have detailed upstream molecular driver(s) leading to lineage plasticity and explored clinically applicable targeted strategy for preventing t-CRPC progression.

Results

Clinical relevance of STAT1 in metastatic PCa is associated with PCSCs phenotypes.

Gene set enrichment analysis (GSEA) of TCGA PCa dataset (Fig. 1A and 1B) indicated that either type I or II IFN-induced genes (Fig. S1A) are highly enriched in PCa patients with lymph node metastasis (N1), compared to N0 cohort. IFN related DNA damage resistance signature (IRDS)

genes, included a subset of STAT1-driven genes, have been associated with the progression of many malignancies[22,23], and are significantly enriched in N1 PCa patients compared to N0 PCa patients (Fig. S1B). STAT1 is an exclusive transcriptional factor activated by IFNγ stimulation. Based on the TCGA PCa dataset, significant elevation of STAT1 level is detected in high stage PCa patients (Fig. 1C), lymph node metastasis (Fig. 1D), or high-grade tumor specimens (Fig. S1C) as well as other malignancies (Fig. S1D). We further explored the relationship between IFN-regulated downstream effectors and the status of STAT1 gene expression in PCa patients and found significant clinical correlation from the most of effectors (Fig. 1E), which are also elevated in N1 patients (Fig. 1F). These data support the role of IFN-STAT1 signaling pathway in PCa progression.

Recent data [9,19]indicated that loss of TP53 and RB1 increases SOX2 expression that is associated with the lineage plasticity of PCa cells. To demonstrate PCSC capabilities using prostasphere forming assay[24], we observed that the number of prostasphere in sgTP53/RB1 LNCaP cells is significantly higher than that in vector control cells (Fig. 1G). Furthermore, we checked other PCSC-associated markers. In particular, human prostate basal cells expressing high level of tumor-associated calcium signal transducer 2 (Trop2) and CD49f are considered as progenitor stem cell population evidenced by enhanced sphere formation and self-renewal capability[25,26]. Meanwhile, CD44 and CD133 are well-known surface markers of PCSCs[27,28]. The significantly increased expression of CD44, CD133, CD49f and TROP2 in sgTP53/RB1 LNCaP cells (Fig. S1E) further supported its PCSC phenotypes. Moreover, elevated STAT1 levels are detected in the sgTP53/RB1 LNCaP cells (Fig. 1H), as well as in the prostaspheres (S) derived from several PCa lines compared with monolayer culture (M) (Fig. 1I and S1F). We further examined the role of STAT1 and its upstream regulator-JAK in prostasphere formation using small molecule inhibitors (SMIs) Fludarabine[29] and Ruxolitinib[30] specifically targeting STAT1 and JAK, respectively. Both SMIs significantly suppressed prostasphere formation of sgTP53/RB1 LNCaP (Fig. 1J and S1G), Du145 (Fig. 1K and S1H), and 22Rv1 (Fig. S1I and S1J) cells, indicating JAK-STAT1 signaling is critical for the acquisition of PCSC.

Interferon-elicited signaling is associated with the neuroendocrine phenotypes of PCa

ARCaP line is initially characterized as AR-repressive prostate cancer cells derived from a patient with ascites metastasis after failure of ADT; apparently, this cell line contains heterogenous cell population based on morphology and expression profile of biomarker[31-34]. Therefore, by single

cell cloning followed by RNA-seq, five gene clusters were categorized by their distinct function in three ARCaP sublines (IIF11, Fast and IIB5) (Fig. 2A). In particular, the Ingenuity pathway analyses demonstrate that cluster 2 genes associated with IIF11 subline are highly involved in the IFN signaling pathway (Fig. 2B). Indeed, GSEA confirms that IIF11 subline has enriched expression of genes involved in IFNα (Fig. 2C, S2A and Table S1) and IFNγ response (Fig. 2D, S2B and Table S1). Based on proteomic profile among PCa cell lines, neuroendocrine transcriptional factor (BRN2 and SOX2) and biomarkers (SYP and CgA) are correlated with STAT1 expression (Fig. 2E).

Similar correlation was observed in sgTP53/RB1 LNCaP9 exhibiting neuroendocrine phenotypes (Fig. S2C) or castration resistant C4-2B MDVR35-37 (Fig. S2D); targeting STAT1 by Fludarabine is able to inhibit the expression of these genes in C4-2B MDVR line (Fig. S2E). On the other hand, IFNβ can enhance the expression of these genes in Du145 cells (Fig. S2F). These data support the inductive role of IFN in neuroendocrine differentiation of PCa cells.

Furthermore, RNA-seq result indicated that 18 out of 45 IRDS genes are significantly higher in IIF11 subline than Fast or IIB5 subline (Table S2). Among these 18 IRDS genes, a subset of 10 STAT1-driven genes (IFI44, IFI44L, IFI6, IFIT1, IFIT3, IFITM1, MX1, MX2, OAS1 and OAS3) are positively correlated with STAT1 expression level in clinical TCGA PCa dataset (Fig. 1E) and are significantly elevated in PCa patients with lymph node metastasis (Fig. 1F). Therefore, we determine to examine the differential expression of these ten IFN-induced STAT1-driven genes among PCa lines. Indeed, IIF11 subline has the highest expression level of all ten genes among examined PCa lines (Fig. 2F). On the other hand, treatment with either Fludarabine or Ruxolitinib results in significant downregulation of all ten genes in IIF11 subline (Fig. 2G), suggesting they are downstream to JAK-STAT1 signaling axis. Meanwhile, expression level of STAT1, IFI44, IFI6, IFIT1, IFIT3, MX1, MX2, OAS1 and OAS3 are significantly increased in either Du145 tumor sphere (Fig. S2G). Overall, this evidence demonstrated emerging activation of JAK-STAT1 signaling and its downstream target genes may contribute to the acquisition of cancer stemness properties of castration resistant PCa lines.

By intraperitoneal administration of Fludarabine (20 mg/kg) into IIF11 tumors, we observed significant growth delay compared to vehicle control (Left panel in Fig. 2H), which corresponds with the reduction of protein expression of phospho-STAT1, STAT1, IFIT5, BMI1, SOX2, and

NANOG (Right panel in Fig. 2H). Apparently, STAT1 represents a potent therapeutic target for t-CRPC.

STAT1 signaling-induced IFIT5 upregulation facilitates the acquisition of stemness properties in PCa

In response to IFNγ treatment, we observed a significant induction of IFIT5 (Fig. S3A), which is abolished by STAT1 knockdown (Fig. S3B) or Fludarabine treatment (Fig. 3A). The dose-dependent inhibitory effect of Fludarabine on IFIT5 induction is also observed in PC3 cells treated with IFNβ (Fig. S3C). Clinically, elevated IFIT5 is associated with PCa progression (Fig. 1F and 3B) and predicts poor overall survival in PCa patients (Fig. 3C). A positive correlation between STAT1 and IFIT5 seen in PCa (Fig. 1E) is also observed in breast (Fig. 3D), brain and kidney cancers (Fig. S3D). Moreover, elevated IFIT5 gene promoter activities (Fig. 3E), mRNA (Fig. 3F) and protein (Fig. 3G) is associated with prostaspheres formation.

Based on the profile of IFIT5 expression in several PCa lines (Fig. S3E), IFIT5 expression vector was transfected into either LNCaP or 22Rv1 cells (Fig. S3F) and the result indicated that IFIT5 significantly facilitates the number and size of prostasphere formation of both cells (Fig. 3H and 3I). In contrast, IFIT5 knockdown Du145 cells (Fig. 3J) exhibit significantly lower number of prostasphere compared with control Du145 cells (Fig. 3K). Consistent with *in vitro* observation, the incidence of Du145 tumorigenesis is significantly reduced in IFIT5 knockdown Du145 cells (Fig. 3L), which is similar with their tumor size and weight (Fig. 3M, Table S3 and S4). Overall, IFIT5, a bone fide STAT1-induced gene, is critical for maintaining PCSC capabilities.

IFIT5 modulates BMI1, SOX2 and NANOG gene expression underlying PCSC capabilities.

Among numerous CSC-associated genes, Polycomb complex protein Bmi-1 (BMI1)[38], SOX2[39-43]and NANOG[44] have been associated with human PCSC activities. We found, similar to IFIT5, these three genes are significantly elevated in prostaspheres derived from several PCa lines (Fig. 4A). The presence of IFIT5 in LNCaP or 22Rv1 line can induce mRNA expression of BMI1, SOX2 and NANOG (Fig. 4B and S4A). In contrast, IFIT5 knockdown in Du145 cells significantly decrease prostasphere formation (Fig. 3K) and the expression of BMI1, SOX2 and NANOG (Fig. 4C). Meanwhile, there is an apparent time-dependent mRNA expression among BMI1, SOX2, NANOG and IFIT5 during prostasphere formation (Fig. 4D, S4B and S4C), which is paralleled with JAK-STAT1 signaling activation (Fig. 4E). Also, the significant elevation of TROP2, CD49f,

CD44 and CD133 mRNA level representing PCSC biomarkers, is observed in IFIT5-overexpressing LNCaP cells (Fig. 4F). In addition to SOX2 elevation in sgTP53/RB1 LNCaP cells, both BMI1 and NANOG mRNA levels were elevated (Fig. S4D), as expected, elevated SOX2 and BMI protein levels but not NANOG were observed (Fig. S4D). On the other hand, BMI1 and SOX2 was significantly downregulated at mRNA and protein level after IFIT5 knockdown in sgTP53/RB1 LNCaP cells (Fig. 4G and 4H), which is closely associated with prostasphere formation (Fig. 4I).

Clinical PCa dataset also demonstrated a positive correlation between IFIT5 and BMI1 or SOX2 expression in PCa adenocarcinoma (PRAD) (Fig. 4J) as well as other malignancies such as renal cancer (KIRC), Glioblastoma multiform (GBM) and breast cancer (BRCA) (Fig. S4E). However, no significant correlation between IFIT5 and NANOG was found in PRAD (Fig. 4J) or other malignancies (data not shown). Similarly, a positive correlation between STAT1 and BMI1 expression was also found in PRAD (Fig. 4J), Pan kidney cancer cohort (KIPAN) and GBM (Fig. S4F). Overall, clinical data further support the regulatory network between STAT1-IFIT5 axis and BMI1 and SOX2 expression in PCa.

The mechanism of IFIT5-elicited PCSC activities is mediated by specific precursor microRNA (pre-miRNA) turnover

IFIT5 is known to regulate viral RNA turnover[45-47], our recent study[48] unveiled a novel functional role of IFIT5 in degrading specific pre-miRNA including miR-101 and miR-128. We therefore examined both miR-101 and miR-128 levels in IFIT5-elicited prostaspheres and found significant downregulation of both mature miRs in prostaspheres derived from different PCa lines (Fig. 5A), which appear to be dose-dependent suppression by IFIT5 overexpression (Fig. S5A). We further investigated whether miR-128 or miR-101 can target BMI1, SOX2 or NANOG mRNA. The 3'UTR of BMI1 and NANOG mRNA was predicted to match with the seed sequence of miR-128 (Fig. S5B) and the 3'UTR of SOX2 and BMI1 mRNA was predicted to match with the seed sequence of miR-101 (Fig. S5C). Indeed, miR-128 overexpression is able to decrease BMI1 and NANOG mRNA level (Fig. 5B and S5D) and miR-101 overexpression is able to decrease BMI1 and SOX2 expression (Fig. 5C and S5D). Functionally, the presence of miR-128 or miR-101 can inhibit prostasphere formation of Du145 or 22RV1 cell (Fig. 5D and 5E).

To examine the mechanism of IFIT5-elicited PCSC activities is mediated by the degradation of both miRNAs, we transfected two mutant forms of pre-miR-128 (Fig. 5F) and pre-miR-101 (Fig.

5G) into IFIT5-expressing Du145 cell; the DSmut can resist IFIT5-medicated degradation and the SSmut is sensitive to IFIT5-medicated degradation. Therefore, in the presence of DSmut of each pre-miR, the significant reduction of corresponding target gene was observed but SSmut didn't change or slightly increase the corresponding target gene expression (Middle panel in Fig. 5F and 5G). As expected, the IFIT5-resistant DSmut can significantly inhibit prostasphere formation but IFIT5-sensitive SSmut has an opposite activity (Right panel in Fig. 5F and G). Similar observation was found in prostasphere formation of 22Rv1 (Fig. S5E) or LNCaP cells (Fig. S5F). Overall, these data support that the turnover of miR-101 or -128 modulated by IFIT5 plays a central role in PSCS activities.

Interferon potentiates the acquisition of cancer stemness properties via STAT1-IFIT5 axis

Until now, the impact of IFN on PCSC is not well studied. As shown in Fig. 6A, all 3 IFNs alone can increase prostasphere formation of sgTP53/RB1 LNCaP cells cultured with basal DMEM without B27, bFGF and EGF that are key ingredients to support the growth of prostasphere medium, suggesting IFNs are potent stimulatory factors in PCSC development. This phenomenon is further supported by that IFNγ exhibits a dose-dependent stimulatory effect on the induction of CSC-related genes (such as BMI1, SOX2, NANOG, CD133, CD44, CD49f and TROP2) (Fig. 6B) as well as prostasphere formation (Fig. S6A) in 22Rv1 cells. The similar impact of type I or type II IFN on prostasphere formation (Fig. S6B) and upregulation of STAT1, IFIT5, BMI1, SOX2 and NANOG gene expression (Fig. S6C) are also observed in Du145 cells. Fludarabine is able to diminish IFNβ-induced prostasphere formation of Du145 cells (Fig. S6D). Knowing elevated STAT1 in sgTP53/RB1 LNCaP cells (Fig. 1H), IFNγ treatment is expected to increase prostasphere formation under supplement-free culture condition (Fig. 6C) along with IFIT5 induction (Fig. S6E). Furthermore, by knocking down STAT1 or IFIT5 in sgTP53/RB1 LNCaP cells, we observed significant reduction of the inductive effect of IFNγ on prostasphere formation (Fig. 6D and 6E). Similarly, Fludarabine exhibits therapeutic efficacy using *in vivo* tumor model of sgTP53/RB1 LNCaP (Left panel in Fig. 6F), which also shows good targeting efficiency (Right panel in Fig. 6F).

In contrast, both miR-128 or miR-101 level was elevated in both gene knockdown conditions (Fig. 6G). Functionally, overexpression of native miR-128 or DSmut 128 is able to antagonize IFNγ-induced prostasphere formation in Du145 cells (Fig. 6H), supporting the central role of STAT1-IFIT5-miR turnover in IFN-induced PCSC. Since SOX2 and BMI1 are the target genes of miR-

101 or miR-128 in PCa line (Fig. 5F and 5G), we examined their roles in IFN-induced PCSC. First, SOX2 knockdown in the shTP53/RB1 LNCaP cells didn't change STAT1 level (Fig. S6F) but significantly diminished prostasphere formation (Fig. S6G). Furthermore, BMI inhibitor-PTC-209 (Fig. S6H) exhibits a dose-dependent inhibition of prostasphere formation of Du145 cells (Fig. S6I) and sgTP53/RB1-LNCaP cells (Fig. S6J). Taken together, these data support the critical role of SOX2 or BMI1in PCSC activities.

ADT followed by STAT1 signaling activation confers PSCS properties

Accumulating evidence implies that ADT ultimately facilitates the lineage plasticity in PCa undergoing neuroendocrine differentiation (NED). Noticeably, STAT1 and IFIT5 proteins (Fig. 7A) as well as BMI1 and SOX2 mRNA (Fig. 7B) are significantly elevated in the CRPC line, C4-2B MDVR that is able to form more prostaspheres than the parental cells (Fig. 7C). To investigate whether the acquired stemness properties in CRPC cells is due to prolonged androgen-deprived (AD) condition, we cultured the parental C4-2B cells in 10% Charcoal Stripped-FBS (CS-FBS) - supplemented with Phenol Red free RPMI medium for 3 weeks. Although additional Enzalutamide (ENZ, 10μM) treatment could further enhance the AD-induced BMI1 and SOX2 (Fig. 7D) as well as STAT1 and IFIT5 mRNA levels (Fig. S7A), it didn't reflect on the protein expression from these genes (Fig. 7E). On the other hand, following the upregulation of STAT1 and phosphorylated STAT1 (Fig. 7E), a significant induction of IFNγ-inducible STAT1-driven genes are seen in C4-2B cells cultured under AD condition with additional ENZ (Fig. S7B). Nevertheless, additional ENZ treatment only slightly enhanced prostasphere formation of C4-2B compared with AD condition alone (Fig. 7F). Similar result is also observed in 22Rv1 cells (Fig. S7C). In contrast, the prostasphere forming ability of castration-resistant C4-2B MDVR line is significantly abolished when the cells are primarily cultured in regular serum condition for 2 weeks (Fig. 7G). Apparently, Fludarabine is a potent agent in inhibiting PCSC activities from C4-2B MDVR (Fig. 7H and 7I), C4-2B in AD (Fig. S7D) or 22RV1 treated with ENZ (Fig. S7E), which support the central role of STAT1-IFIT5 pathway in castration-elicited PCSC.

DISCUSSION

PCa is a typical androgen-dependent disease thus ADT is considered the most effective regimen to treat metastatic hormone naïve PCa; almost all patients eventually develop CRPC, which is

associated with the majority of mortality of this disease. Although many new agents have been introduced for these patients, inevitably, CRPC acquires resistance to become t-CRPC, which is considered as a lethal disease without effective targeted therapy. Approximately, 20-25% t-CRPC patients recurred from ADT harbor neuroendocrine cell features from classical adenocarcinoma PCa (ADPC), also, these cells exhibit ADT- or radio-resistance. Thus, understanding the molecular driver(s) leading to the onset of NEPC can certainly lead us to develop new therapeutic strategies for the recurrent t-CRPC.

In general, ADPC cells exhibit differentiated luminal cell markers. In contrast, NEPC cells express neuronal biomarkers and neuronal factors secretion in an endocrine fashion. Based on distinct phenotypes among ADPC and NEPC, lineage plasticity is likely manifested as reversible or irreversible changes in cellular 'identity', whereby cells take on an alternative morphologic, phenotypic, or epigenetic state. During ADT-related lineage plasticity, differentiated tumor cells acquire new phenotypes, in some cases reverting back to a more 'stem-like' state followed by re-differentiating towards an alternative 'cell fate' in order to bypass therapeutic pressure. Mechanisms empowering the lineage plasticity in PCa are also critical for the onset of NED in t-CRPC patients. Loss of function or mutation in Rb and TP53 gene in ADPC[9,19,49] or N-MYC amplification[50,51] or overexpression of Aurora A kinase[52,53] is considered as key intrinsic genetic drivers that are associated with the expression of PCSC genes such as SOX2 or BMI1. The elevation of SOX2 can lead to upregulation of BRN2 (neuronal transcription factor) and Synaptophysin (SYP, neuronal biomarker) associated with NEPC[42], and BMI1+SOX2+ cells drive the recurrence of PCa[54].

Previously, we demonstrated the promoting role of IFN in epithelial-to-mesenchymal transition of PCa[48] since significant elevation of IFN levels are found in the serum of PCa patients receiving ADT[21,55,56]. Furthermore, IRDS comprised a subset of IFN-induced genes are highly associated with therapeutic resistance to chemotherapy[23]. A more recent analysis of TCGA PCa dataset indicated that elevation of IRDS is correlated with decreased disease-free survival in PCa patients[22]. Meanwhile, a study focused on germline variation suggested that IRDS is more prevalent in the tumor specimens derived from African American PCa patients with higher incidence and mortality rate, compared to European American cohorts[22,57]. Taken together, IFN-elicited signaling pathway is highly involved in PCa progression.

STAT1 or 2 is essential components in the IFN-induced signaling pathway. In response to type I or type II IFN stimulation, JAK-mediated phosphorylation of STAT leads to its activation and nuclear translocation. Activated STAT1 or 2 binds to the IFN-stimulated response element (ISRE) in the promoter region and induce transcriptional activation of IFN-stimulated genes (ISGs). Indeed, STAT1 and several STAT1-driven IRDS genes are highly upregulated not only in the cohort of PCa patients with lymph node metastasis (Fig. 1D) but also in several PCa lines with acquired lineage plasticity (Fig. 1H). In particular, we found STAT1 signaling is highly activated in both sgTP53/RB1-LNCaP and androgen-deprived C4-2B lines with enhanced PCSC properties and increased sphere forming abilities (Fig. 1H, 1J, 7A and 7C). Meanwhile, a significant enrichment of IFN responsive genes and activation of STAT1 signaling are also observed in ARCaP subline with NEPC features (Fig. 2A-2F). Functionally, the upregulation of STAT1 and STAT1-driven genes in several CRPC lines lead to enhanced PCSC capabilities (Fig. S7B, 7E, 7F) that can provide pro-survival advantage of ADPC under ADT as well as facilitate trans-differentiation into metastatic cells with mesenchymal phenotypes or recurrent cells with neuroendocrine phenotypes.

Mechanistically, IFIT5, an interferon-induced protein with tetratricopeptide repeats that can bind to 5'end viral RNA and cause its degradation, plays a key downstream effector in modulating stemness gene expression (Fig. 4B and 4C), which is also supported by clinical data (Fig. 4J). In addition to its functional role in viral RNA degradation, the unique function of IFIT5 in PCa cells is to modulate the turnover of miR subpopulation via recognizing the 5'end specific structure of precursor form (Fig. 5F and 5G); similar observations were found in renal and bladder cancer cells[48,58]. Noticeably, either miR-101 or -128, the target of IFIT5, is able to degrade BMI1 or SOX2 mRNA leading to the suppression of PCSC activities (Fig. 5B-5E).

By targeting STAT1 or JAK activation with specific inhibitors such as Fludarabine or Ruxolitinib, our data clearly demonstrated that JAK-STAT1 axis is a critical pathway associated with PCSC and NED (Fig. 1J, S1G, 2G and S2E). Also, Fludarabine, FDA-approved chronic lymphocytic leukemia therapeutic, exhibited a potent efficacy in suppressing t-CRPC tumor (Fig. 2H and 6F). This result support the re-purposing this agent on t-CRPC treatment, which is expected to have an immediate impact on overall survival of PCa patients.

MATERIALS AND METHODS

Cell lines

Cells obtained from ATCC (Manassas, VA): LNCaP and Du145 cells are maintained in RPMI-1640 medium supplemented with 10% Fetal bovine serum (FBS), and CWR-22Rv1 cells are maintained in DMEM medium supplemented with 10% FBS. C4-2 and ARCaP single cell clones (Fast, IIB5 and IIF11) maintained in RPMI-1640 medium supplemented with 10% FBS were obtained from Dr. Leland Chung (Cider-Sinai Medical Center, Los Angeles, CA). C4-2B parental (with the same medium as C4-2) and C4-2B MDVR cell lines are given by Dr. Allen Gao (UC Davis, CA); C4-2B MDVR line is cultured in 10% Charcoal Stripped-FBS-supplemented Phenol Red free RPMI medium (CS-FBS) with additional 20μM enzalutamide (ENZ). LNCaP-sgNT (CRISPR-control) and LNCaP-sgTP53/RB1 CRISPR-knockout cell lines are given by Dr. Ping Mu (UT Southwestern Medical Center, TX). Stable IFIT5-shRNA knockdown (shIFIT5) and control (shCon) prostate cell lines were generated from Du145, Du145 and LNCaP sgTP53/RB1 cell lines using pLKO-shIFIT5 plasmid generated by Academia Sinica, Taipei, Taiwan. Stable IFIT5-overexpressing (IFIT5) and control (Vec) cell lines were generated from 22Rv1, C4-2 and LNCaP cell lines using pcDNA3.1-3XFlag-IFIT5 plasmid given by Dr. Collins (UC Berkeley, CA). All these cell lines were authenticated with the short tandem repeat (STR) profiling by Genomic Core in UT Southwestern Medical Center (UTSW) periodically and Mycoplasma testing was performed by MycoAlert® kit (Lonza Inc. Walkersville, MD) to ensure Mycoplasma-free condition.

Cell transfection

Cells ($2.5x10^5$) were seeded in 60-mm dish at 60-70% confluence before transfection. According to manufacturer's protocol, transfection of plasmids was using either Xfect Reagent (Clontech) or EZ Plex transfection reagent (EZPLEX). Transient transfection was carried out 48 hrs post-transfection to harvest cell for further analyses. In addition, the stable clones were established after 3 weeks of culture at the antibiotic selective medium.

In vitro prostatesphere formation assay

Cells were counted and seeded into 96-well ultra-low attachment plate (Corning) at density of 250 cells/per well in DMEM (Gibco) supplemented with B-27 supplement (Gibco), recombinant human basic Fibroblast Growth Factor (bFGF, 10ng/ml, Gibco) and human Epidermal Growth Factor (hEGF, 20ng/ml, Gibco). Inhibitors (Fludarabine or Ruxolitinib) or interferons were added

to the culture medium prior to seeding the cells. Formation of sphere was observed and quantified under microscope at Week 1 or 2 after seeding.

SSMut and DSMut precursor miRNA-expression plasmid constructs

Native miR-128 or miR-101 expressing plasmid (Genecopoeia) was used as a template to generate mutant pre-miR-128 with 5'-six nucleotides single stranded overhang (pre-SS6Mut-miR-128) or double-stranded blunt end (pre-DSMut-miR-128), as well as mutant pre-miR-101 with 5'-nine nucleotides single stranded overhang (pre-SS9Mut-miR-101) or double-stranded blunt end (pre-DSMut-miR-101) constructs using site-directed mutagenesis.

RNA isolation and quantitative real-time RT-PCR (qRT-PCR)

Total RNA was isolated and purified using Maxwell® 16 miRNA Tissue kit or Maxwell® 16 LEV Simply RNA Tissue Kit (Promega). Small RNA from total RNA (2 μg) was subjected to miScript II RT kit (QIAGEN) then 2.5 μl cDNA was applied to a 25-μL reaction volume using miScript SYBR Green PCR kit (QIAGEN) in iCycler thermal cycler (Bio-Rad). The relative expression levels of matured miRNAs from each sample were determined by normalizing to SNORD95 small RNA. Large RNA from total RNA (2 μg) was subjected to iScript^{TM} Adv cDNA kit (BioRad) then 2.5 μl cDNA was applied to a 25-μL reaction volume using iTaq Universal SYBR® Green Supermix (BioRad) in iCycler thermal cycler (Bio-Rad). All primer sequences are listed in Table S1. The relative expression levels of BMI1, Lin28, NANOG, SOX2 and IFIT5 mRNA from each sample were determined by normalizing to 18S mRNA. All quantitative data of miRNA or mRNA expression level were analyzed using ΔCt (Ct value normalized to internal snord95 miRNA or 18S RNA) and ΔΔCt (difference between the ΔCt of control and experimental groups) values to obtain the fold change after normalizing with control group.

Western blot analysis

Cells were lysed in lysis buffer [50mMTris-HCl (pH 7.5), 150 mM NaCl, 0.1% Triton X-100, 1 mM sodium orthovanadate, 1 mM sodium fluoride, 1 mM sodium pyrophosphate, 10 mg/mL, aprotinin, 10 mg/mL leupeptin, 2 mM phenylmethylsulfonyl fluoride, and 1 mM EDTA] for 30 mins on ice. Cell lysates were spin down at 20,000 xg for 20 mins at 4°C. Protein extracts were subjected to SDS-PAGE using Bolt 4-12% Bis-Tris Plus gel (Invitrogen), and transferred to nitrocellulose membrane using Trans-Blot Turbo Transfer system (BIORAD). Membranes were incubated with primary antibodies against IFIT5, Lin28, NANOG (ProteinTech), BMI1, SOX2 (Cell Signaling Technology), as well as GAPDH and STAT1 (Santa Cruz Biotechnology) at 4 °C

for 16-18 hrs, and horseradish peroxidase-conjugated secondary antibodies at room temperature for 2 hrs. Results were visualized with ECL chemiluminescent detection system (Pierce ThermoScientific). The relative protein expression level in each sample was normalized to GAPDH.

***In vivo* tumor incidence and experimental therapy study**

All animal works were approved by the Institutional Animal Care and Use Committee from UTSW. Serial dilutions of stable shCon or shIFIT5-knockdown Du145 cells mixed 1:1 with Matrigel (BD Biosciences) were injected subcutaneously into male SCID (6 weeks-old) mice. The incidence of Du145 tumor was determined 8 weeks after injection followed by measurement of tumor weights and tumor volumes. The tumor volume was determined by caliper and calculated (length × width × width)/2.

Initially, 1.5 million ARCaP-F11 or 5 million LNCaP sgTP53/RB1 cells mixed 1:1 with Matrigel (BD Biosciences) were injected subcutaneously into both flanks of SCID (6 weeks-old) mice. When tumor volume reached 100 mm^3, mice were then randomly distributed into 3 groups: Fludarabine (10 or 20 mg/kg, i.p.) was administered 5 days per week for 2 weeks and the control received 10% DMSO. Tumor growth rate was measured at Day 0, 4, 7, 11, 14, 18, 21 and 25 after treatment. The average tumor volumes of each group were calculated according to the equation of volume = (length × width × width)/2.

Statistics analysis

Statistics analyses were performed by using GraphPad Prism software. Statistical significance was evaluated using Student *t*-test. *P<0.05, **P<0.001 or ***P<0.0001 was considered a significant difference between compared groups and marked with asterisks.

ACKNOWLEDGMENTS
This work was supported by grants from the United States Army (W81XWH-16-1-0474 to JTH).

REFERENCES

1 Siegel, R. L., Miller, K. D., Fuchs, H. E. & Jemal, A. Cancer Statistics, 2021. *CA Cancer J Clin* **71**, 7-33, doi:10.3322/caac.21654 (2021).

2 Chi, K. N. *et al.* Patient-reported outcomes following abiraterone acetate plus prednisone added to androgen deprivation therapy in patients with newly diagnosed metastatic castration-naive prostate cancer (LATITUDE): an international, randomised phase 3 trial. *Lancet Oncol* **19**, 194-206, doi:10.1016/S1470-2045(17)30911-7 (2018).

3 Dong, Y. *et al.* The need for androgen deprivation therapy in patients with intermediate-risk prostate cancer treated with dose-escalated external beam radiation therapy. *Can J Urol* **24**, 8656-8662 (2017).

4 Gandaglia, G. *et al.* Use of Concomitant Androgen Deprivation Therapy in Patients Treated with Early Salvage Radiotherapy for Biochemical Recurrence After Radical Prostatectomy: Long-term Results from a Large, Multi-institutional Series. *Eur Urol* **73**, 512-518, doi:10.1016/j.eururo.2017.11.020 (2018).

5 Wallis, C. J. D. *et al.* Comparison of Abiraterone Acetate and Docetaxel with Androgen Deprivation Therapy in High-risk and Metastatic Hormone-naive Prostate Cancer: A Systematic Review and Network Meta-analysis. *Eur Urol* **73**, 834-844, doi:10.1016/j.eururo.2017.10.002 (2018).

6 Aparicio, A. M. *et al.* Combined Tumor Suppressor Defects Characterize Clinically Defined Aggressive Variant Prostate Cancers. *Clin Cancer Res* **22**, 1520-1530, doi:10.1158/1078-0432.CCR-15-1259 (2016).

7 Beltran, H. *et al.* Divergent clonal evolution of castration-resistant neuroendocrine prostate cancer. *Nat Med* **22**, 298-305, doi:10.1038/nm.4045 (2016).

8 Li, Y. *et al.* SRRM4 Drives Neuroendocrine Transdifferentiation of Prostate Adenocarcinoma Under Androgen Receptor Pathway Inhibition. *Eur Urol* **71**, 68-78, doi:10.1016/j.eururo.2016.04.028 (2017).

9 Mu, P. *et al.* SOX2 promotes lineage plasticity and antiandrogen resistance in TP53- and RB1-deficient prostate cancer. *Science* **355**, 84-88, doi:10.1126/science.aah4307 (2017).

10 Tan, H. L. *et al.* Prostate adenocarcinomas aberrantly expressing p63 are molecularly distinct from usual-type prostatic adenocarcinomas. *Mod Pathol* **28**, 446-456, doi:10.1038/modpathol.2014.115 (2015).

11 Zhou, Z., Flesken-Nikitin, A. & Nikitin, A. Y. Prostate cancer associated with p53 and Rb deficiency arises from the stem/progenitor cell-enriched proximal region of prostatic ducts. *Cancer Res* **67**, 5683-5690, doi:10.1158/0008-5472.CAN-07-0768 (2007).

12 Zhang, X. *et al.* SRRM4 Expression and the Loss of REST Activity May Promote the Emergence of the Neuroendocrine Phenotype in Castration-Resistant Prostate Cancer. *Clin Cancer Res* **21**, 4698-4708, doi:10.1158/1078-0432.CCR-15-0157 (2015).

13 Maitland, N. J. & Collins, A. A tumour stem cell hypothesis for the origins of prostate cancer. *BJU Int* **96**, 1219-1223, doi:10.1111/j.1464-410X.2005.05744.x (2005).

14 Yu, C., Yao, Z., Jiang, Y. & Keller, E. T. Prostate cancer stem cell biology. *Minerva Urol Nefrol* **64**, 19-33 (2012).

15 Zhang, K. *et al.* Current Stem Cell Biomarkers and Their Functional Mechanisms in Prostate Cancer. *Int J Mol Sci* **17**, doi:10.3390/ijms17071163 (2016).

16 Ricci, E. *et al.* Increased expression of putative cancer stem cell markers in the bone marrow of prostate cancer patients is associated with bone metastasis progression. *Prostate* **73**, 1738-1746, doi:10.1002/pros.22689 (2013).

17 Seiler, D. *et al.* Enrichment of putative prostate cancer stem cells after androgen deprivation: upregulation of pluripotency transactivators concurs with resistance to androgen deprivation in LNCaP cell lines. *Prostate* **73**, 1378-1390, doi:10.1002/pros.22685 (2013).
18 Zhang, L. *et al.* Tumorspheres derived from prostate cancer cells possess chemoresistant and cancer stem cell properties. *J Cancer Res Clin Oncol* **138**, 675-686, doi:10.1007/s00432-011-1146-2 (2012).
19 Ku, S. Y. *et al.* Rb1 and Trp53 cooperate to suppress prostate cancer lineage plasticity, metastasis, and antiandrogen resistance. *Science* **355**, 78-83, doi:10.1126/science.aah4199 (2017).
20 Lin, C. J. *et al.* The paracrine induction of prostate cancer progression by caveolin-1. *Cell Death Dis* **10**, 834, doi:10.1038/s41419-019-2066-3 (2019).
21 Tazaki, E. *et al.* Serum cytokine profiles in patients with prostate carcinoma. *Exp Ther Med* **2**, 887-891, doi:10.3892/etm.2011.286 (2011).
22 Tang, W. *et al.* IFNL4-DeltaG Allele Is Associated with an Interferon Signature in Tumors and Survival of African-American Men with Prostate Cancer. *Clin Cancer Res* **24**, 5471-5481, doi:10.1158/1078-0432.CCR-18-1060 (2018).
23 Weichselbaum, R. R. *et al.* An interferon-related gene signature for DNA damage resistance is a predictive marker for chemotherapy and radiation for breast cancer. *Proc Natl Acad Sci U S A* **105**, 18490-18495, doi:10.1073/pnas.0809242105 (2008).
24 Bahmad, H. F. *et al.* Sphere-Formation Assay: Three-Dimensional in vitro Culturing of Prostate Cancer Stem/Progenitor Sphere-Forming Cells. *Front Oncol* **8**, 347, doi:10.3389/fonc.2018.00347 (2018).
25 Garraway, I. P. *et al.* Human prostate sphere-forming cells represent a subset of basal epithelial cells capable of glandular regeneration in vivo. *Prostate* **70**, 491-501, doi:10.1002/pros.21083 (2010).
26 Goldstein, A. S. *et al.* Trop2 identifies a subpopulation of murine and human prostate basal cells with stem cell characteristics. *Proc Natl Acad Sci U S A* **105**, 20882-20887, doi:10.1073/pnas.0811411106 (2008).
27 Kalantari, E. *et al.* Co-Expression of Putative Cancer Stem Cell Markers CD44 and CD133 in Prostate Carcinomas. *Pathol Oncol Res* **23**, 793-802, doi:10.1007/s12253-016-0169-z (2017).
28 Soner, B. C. *et al.* Induced growth inhibition, cell cycle arrest and apoptosis in CD133+/CD44+ prostate cancer stem cells by flavopiridol. *Int J Mol Med* **34**, 1249-1256, doi:10.3892/ijmm.2014.1930 (2014).
29 Frank, D. A., Mahajan, S. & Ritz, J. Fludarabine-induced immunosuppression is associated with inhibition of STAT1 signaling. *Nat Med* **5**, 444-447, doi:10.1038/7445 (1999).
30 Turk, C. *et al.* The impact of JAK/STAT inhibitor ruxolitinib on the genesis of lymphoproliferative diseases. *Turk J Med Sci* **49**, 661-674, doi:10.3906/sag-1807-152 (2019).
31 Zhau, H. Y. *et al.* Androgen-repressed phenotype in human prostate cancer. *Proc Natl Acad Sci U S A* **93**, 15152-15157, doi:10.1073/pnas.93.26.15152 (1996).
32 Zhau, H. E. *et al.* Epithelial to mesenchymal transition (EMT) in human prostate cancer: lessons learned from ARCaP model. *Clin Exp Metastasis* **25**, 601-610, doi:10.1007/s10585-008-9183-1 (2008).

33 He, H. *et al.* Progressive epithelial to mesenchymal transitions in ARCaP E prostate cancer cells during xenograft tumor formation and metastasis. *Prostate* **70**, 518-528, doi:10.1002/pros.21086 (2010).

34 He, H. *et al.* Differential expression of the alpha2 chain of the interleukin-13 receptor in metastatic human prostate cancer ARCaPM cells. *Prostate* **70**, 993-1001, doi:10.1002/pros.21133 (2010).

35 Liu, C., Armstrong, C., Zhu, Y., Lou, W. & Gao, A. C. Niclosamide enhances abiraterone treatment via inhibition of androgen receptor variants in castration resistant prostate cancer. *Oncotarget* **7**, 32210-32220, doi:10.18632/oncotarget.8493 (2016).

36 Liu, C. *et al.* Niclosamide and Bicalutamide Combination Treatment Overcomes Enzalutamide- and Bicalutamide-Resistant Prostate Cancer. *Mol Cancer Ther* **16**, 1521-1530, doi:10.1158/1535-7163.MCT-16-0912 (2017).

37 Lombard, A. P. *et al.* Wntless promotes cellular viability and resistance to enzalutamide in castration-resistant prostate cancer cells. *Am J Clin Exp Urol* **7**, 203-214 (2019).

38 Hu, J. *et al.* BTF3 sustains cancer stem-like phenotype of prostate cancer via stabilization of BMI1. *J Exp Clin Cancer Res* **38**, 227, doi:10.1186/s13046-019-1222-z (2019).

39 Vaddi, P. K., Stamnes, M. A., Cao, H. & Chen, S. Elimination of SOX2/OCT4-Associated Prostate Cancer Stem Cells Blocks Tumor Development and Enhances Therapeutic Response. *Cancers (Basel)* **11**, doi:10.3390/cancers11091331 (2019).

40 Srinivasan, D., Senbanjo, L., Majumdar, S., Franklin, R. B. & Chellaiah, M. A. Androgen receptor expression reduces stemness characteristics of prostate cancer cells (PC3) by repression of CD44 and SOX2. *J Cell Biochem*, doi:10.1002/jcb.27573 (2018).

41 Rybak, A. P. & Tang, D. SOX2 plays a critical role in EGFR-mediated self-renewal of human prostate cancer stem-like cells. *Cell Signal* **25**, 2734-2742, doi:10.1016/j.cellsig.2013.08.041 (2013).

42 Metz, E. P., Wilder, P. J., Dong, J., Datta, K. & Rizzino, A. Elevating SOX2 in prostate tumor cells upregulates expression of neuroendocrine genes, but does not reduce the inhibitory effects of enzalutamide. *J Cell Physiol* **235**, 3731-3740, doi:10.1002/jcp.29267 (2020).

43 Jia, X. *et al.* SOX2 promotes tumorigenesis and increases the anti-apoptotic property of human prostate cancer cell. *J Mol Cell Biol* **3**, 230-238, doi:10.1093/jmcb/mjr002 (2011).

44 Jeter, C. R. *et al.* NANOG promotes cancer stem cell characteristics and prostate cancer resistance to androgen deprivation. *Oncogene* **30**, 3833-3845, doi:10.1038/onc.2011.114 (2011).

45 Zhang, B., Liu, X., Chen, W. & Chen, L. IFIT5 potentiates anti-viral response through enhancing innate immune signaling pathways. *Acta Biochim Biophys Sin (Shanghai)* **45**, 867-874, doi:10.1093/abbs/gmt088 (2013).

46 Katibah, G. E. *et al.* tRNA binding, structure, and localization of the human interferon-induced protein IFIT5. *Mol Cell* **49**, 743-750, doi:10.1016/j.molcel.2012.12.015 (2013).

47 Chico, V. *et al.* IFIT5 Participates in the Antiviral Mechanisms of Rainbow Trout Red Blood Cells. *Front Immunol* **10**, 613, doi:10.3389/fimmu.2019.00613 (2019).

48 Lo, U. G. *et al.* IFNgamma-Induced IFIT5 Promotes Epithelial-to-Mesenchymal Transition in Prostate Cancer via miRNA Processing. *Cancer Res* **79**, 1098-1112, doi:10.1158/0008-5472.CAN-18-2207 (2019).

49 Zhou, Z. *et al.* Synergy of p53 and Rb deficiency in a conditional mouse model for metastatic prostate cancer. *Cancer Res* **66**, 7889-7898, doi:10.1158/0008-5472.CAN-06-0486 (2006).

50 Yin, Y. *et al.* N-Myc promotes therapeutic resistance development of neuroendocrine prostate cancer by differentially regulating miR-421/ATM pathway. *Mol Cancer* **18**, 11, doi:10.1186/s12943-019-0941-2 (2019).

51 Dardenne, E. *et al.* N-Myc Induces an EZH2-Mediated Transcriptional Program Driving Neuroendocrine Prostate Cancer. *Cancer Cell* **30**, 563-577, doi:10.1016/j.ccell.2016.09.005 (2016).

52 Beltran, H. *et al.* A Phase II Trial of the Aurora Kinase A Inhibitor Alisertib for Patients with Castration-resistant and Neuroendocrine Prostate Cancer: Efficacy and Biomarkers. *Clin Cancer Res* **25**, 43-51, doi:10.1158/1078-0432.CCR-18-1912 (2019).

53 Mosquera, J. M. *et al.* Concurrent AURKA and MYCN gene amplifications are harbingers of lethal treatment-related neuroendocrine prostate cancer. *Neoplasia* **15**, 1-10, doi:10.1593/neo.121550 (2013).

54 Yoo, Y. A. *et al.* The Role of Castration-Resistant Bmi1+Sox2+ Cells in Driving Recurrence in Prostate Cancer. *J Natl Cancer Inst* **111**, 311-321, doi:10.1093/jnci/djy142 (2019).

55 Mahon, K. L. *et al.* Cytokine profiling of docetaxel-resistant castration-resistant prostate cancer. *Br J Cancer* **112**, 1340-1348, doi:10.1038/bjc.2015.74 (2015).

56 Tanji, N. *et al.* Circulating Cytokine Levels in Patients with Prostate Cancer: Effects of Neoadjuvant Hormonal Therapy and External-beam Radiotherapy. *Anticancer Res* **35**, 3379-3383 (2015).

57 Wang, B. D. *et al.* Identification and Functional Validation of Reciprocal microRNA-mRNA Pairings in African American Prostate Cancer Disparities. *Clin Cancer Res* **21**, 4970-4984, doi:10.1158/1078-0432.CCR-14-1566 (2015).

58 Huang, J. *et al.* The roles and mechanism of IFIT5 in bladder cancer epithelial-mesenchymal transition and progression. *Cell Death Dis* **10**, 437, doi:10.1038/s41419-019-1669-z (2019).

FIGURES AND FIGURE LEGENDS

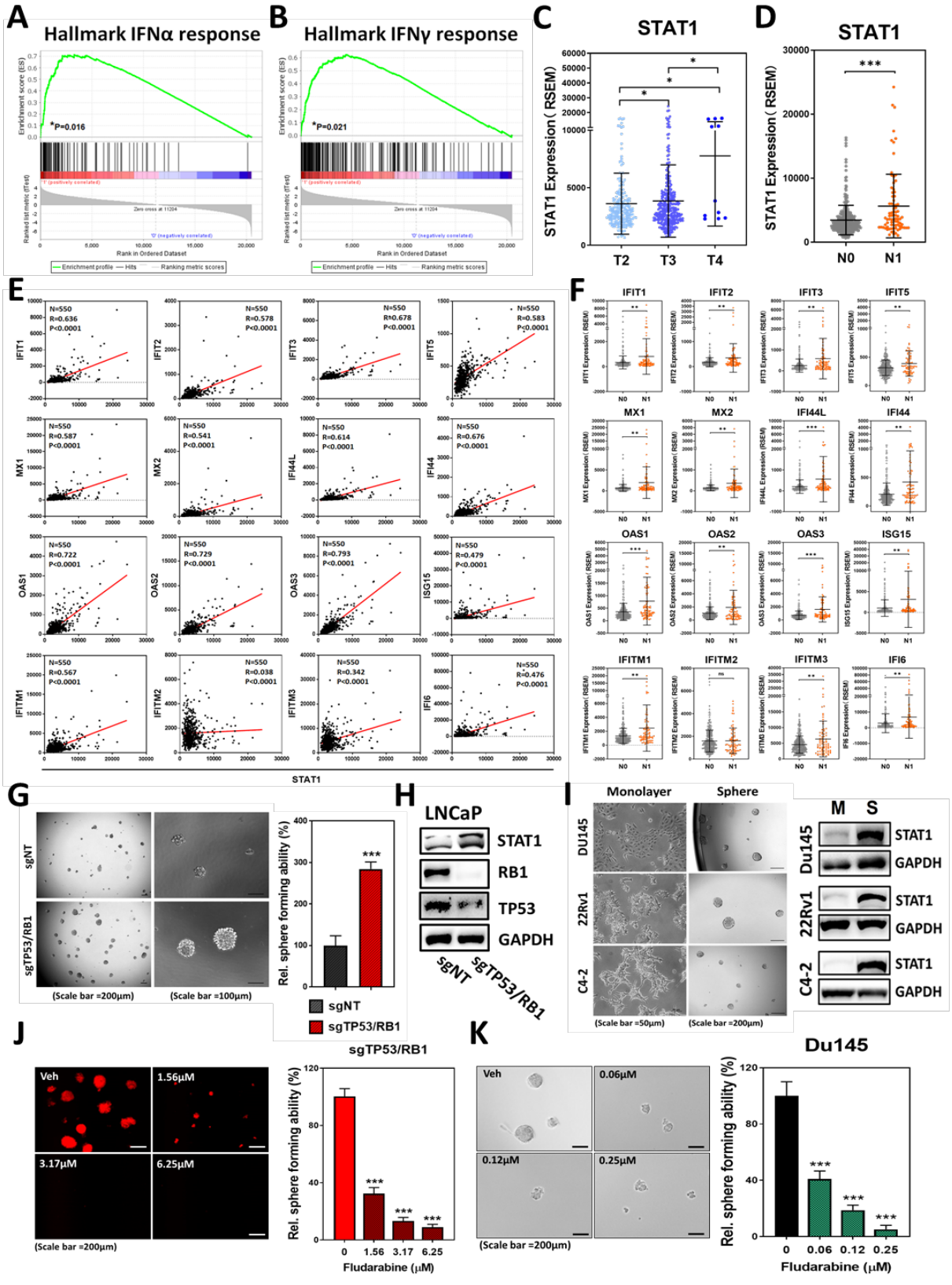

Figure 1. Emergence of STAT1 in advanced PCa contributes to the acquisition of self-renewal capacity in PCSCs. (A-B) GSEA identifying enrichment of upregulated genes associated with IFNα and IFNγ response in the tumor specimens of PCa patients with lymph node metastasis (N1, n=80), compared to cohort without metastasis (N0, n=345). (C) TCGA PCa dataset demonstrating STAT1 expression level among T2 (n=187), T3 (n=293) and T4 (n=11) stage of PCa patients. (D) TCGA PCa dataset demonstrating elevation of STAT1 in PCa patients with lymph node metastasis (N1, n=80), compared to cohort without metastasis (N0, n=345). (E) Clinical correlation of STAT1 with interferon response-associated genes (N=550) based on TCGA PCa dataset analysis. (F) Expression level of interferon response-associated genes in PCa patients with lymph node metastasis (N1, n=80), compared to cohort without metastasis (N0, n=345) (ns=no significant differences, *p<0.05, **p<0.001, ***p<0.0001) (G) The sphere forming ability of sgTP53/RB1-LNCaP cell, compared to vector control (sgNT) (***P<0.0001). (H) Protein level of STAT1, RB1 and TP53 in sgTP53/RB1-LNCaP cell, compared to vector control (sgNT). (I) Left: Morphology of Du145, 22Rv1 and C4-2 cells under adherent monolayer or ultra-low attachment sphere culture condition. Right: STAT1 protein expression in the sphere (S) derived from each PCa line, compared to corresponding monolayer (M) culture. (J-K) Dose-dependent impact of Fludarabine on the sphere forming ability of sgTP53/RB1-LNCaP cells and Du145 cells (***p<0.0001).

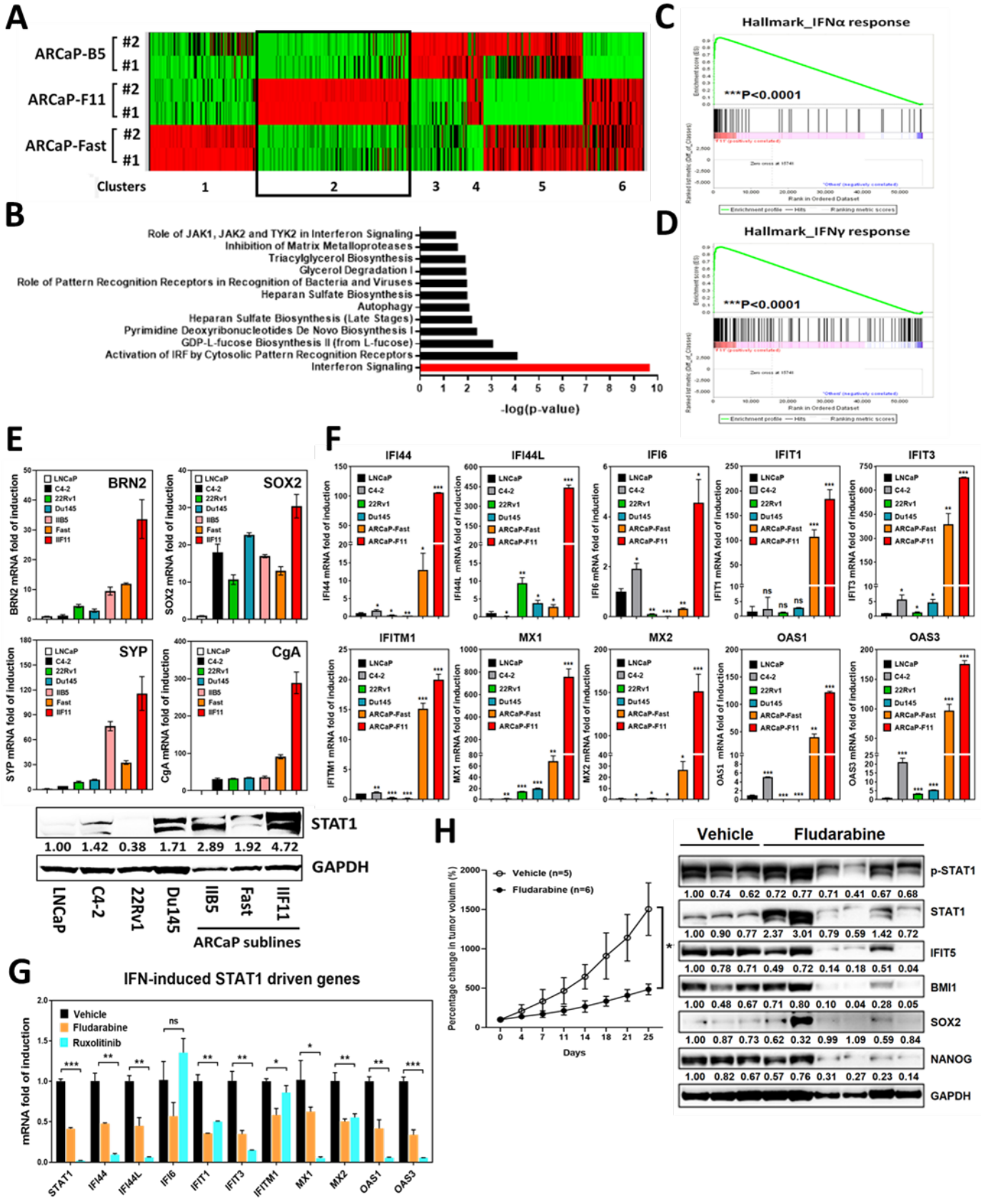
A
ARCaP-B5
ARCaP-F11
ARCaP-Fast
#2
#1
Clusters
1
2
3
4
5
6
B
Role of JAK1, JAK2 and TYK2 in Interferon Signaling
Inhibition of Matrix Metalloproteases
Triacylglycerol Biosynthesis
Glycerol Degradation I
Role of Pattern Recognition Receptors in Recognition of Bacteria and Viruses
Heparan Sulfate Biosynthesis
Autophagy
Heparan Sulfate Biosynthesis (Late Stages)
Pyrimidine Deoxyribonucleotides De Novo Biosynthesis I
GDP-L-fucose Biosynthesis II (from L-fucose)
Activation of IRF by Cytosolic Pattern Recognition Receptors
Interferon Signaling
-log(p-value)
C
Hallmark_IFNα response
***P<0.0001
Rank in Ordered Dataset
D
Hallmark_IFNγ response
***P<0.0001
Rank in Ordered Dataset
E
BRN2
SOX2
SYP
CgA
LNCaP
C4-2
22Rv1
Du145
IIB5
Fast
IIF11
STAT1
1.00 1.42 0.38 1.71 2.89 1.92 4.72
GAPDH
LNCaP
C4-2
22Rv1
Du145
IIB5
Fast
IIF11
ARCaP sublines
F
IFI44
IFI44L
IFI6
IFIT1
IFIT3
IFITM1
MX1
MX2
OAS1
OAS3
LNCaP
C4-2
22Rv1
Du145
ARCaP-Fast
ARCaP-F11
G
IFN-induced STAT1 driven genes
Vehicle
Fludarabine
Ruxolitinib
mRNA fold of induction
STAT1
IFI44
IFI44L
IFI6
IFIT1
IFIT3
IFITM1
MX1
MX2
OAS1
OAS3
H
Vehicle (n=5)
Fludarabine (n=6)
Percentage change in tumor volumn (%)
Days
Vehicle
Fludarabine
p-STAT1
1.00 0.74 0.62 0.72 0.77 0.71 0.41 0.67 0.68
STAT1
1.00 0.90 0.77 2.37 3.01 0.79 0.59 1.42 0.72
IFIT5
1.00 0.78 0.71 0.49 0.72 0.14 0.18 0.51 0.04
BMI1
1.00 0.48 0.67 0.71 0.80 0.10 0.04 0.28 0.05
SOX2
1.00 0.87 0.73 0.62 0.32 0.99 1.09 0.59 0.84
NANOG
1.00 0.82 0.67 0.57 0.76 0.31 0.27 0.23 0.14
GAPDH

Figure 2. STAT1-IFIT5 signaling activation is emerged during the advanced progression of PCa toward CRPC and NePCa (A) Heat map illustrating the gene expression profile among three ARCaP sublines-IIB5, IIF11 and Fast. (B) The ingenuity pathway analysis suggesting significantly enrichment of IFN signaling pathway genes in IIF11, compared to Fast and IIB5 sublines. (C-D) GSEA identifying enrichment of genes associated with IFNα and IFNγ response in IIF11 subline, compared to Fast and IIB5 sublines. (E) Upper: Screening of BRN2, SOX2, SYP and CgA mRNA levels among PCa lines including ARCaP sublines. Lower: STAT1 protein level among screened PCa lines including ARCaP sublines. (F) Expression level of ten IFN-inducible STAT1-driven genes among PCa lines including ARCaP sublines (*$p<0.05$, **$p<0.001$, ***$p<0.0001$). (G) Expression of ten IFN-inducible STAT1-driven genes in ARCaP-IIF11 subline treated with Fludarabine (1 μM) or Ruxolitinib (2.5 μM) for 48hrs. (*$p<0.05$, **$p<0.001$, ***$p<0.0001$) (H) Left: The impact of Fludarabine (20 mg/kg) on the sub-cutaneous ARCaP-IIF11 tumor growth (**$p<0.001$). Right: Expression of phospho-STAT1, STAT1, IFIT5, BMI1, SOX2 and Nanog protein levels in the ARCaP-IIF11 tumors treated with fludarabine (20mg/kg), compared to vehicle control.

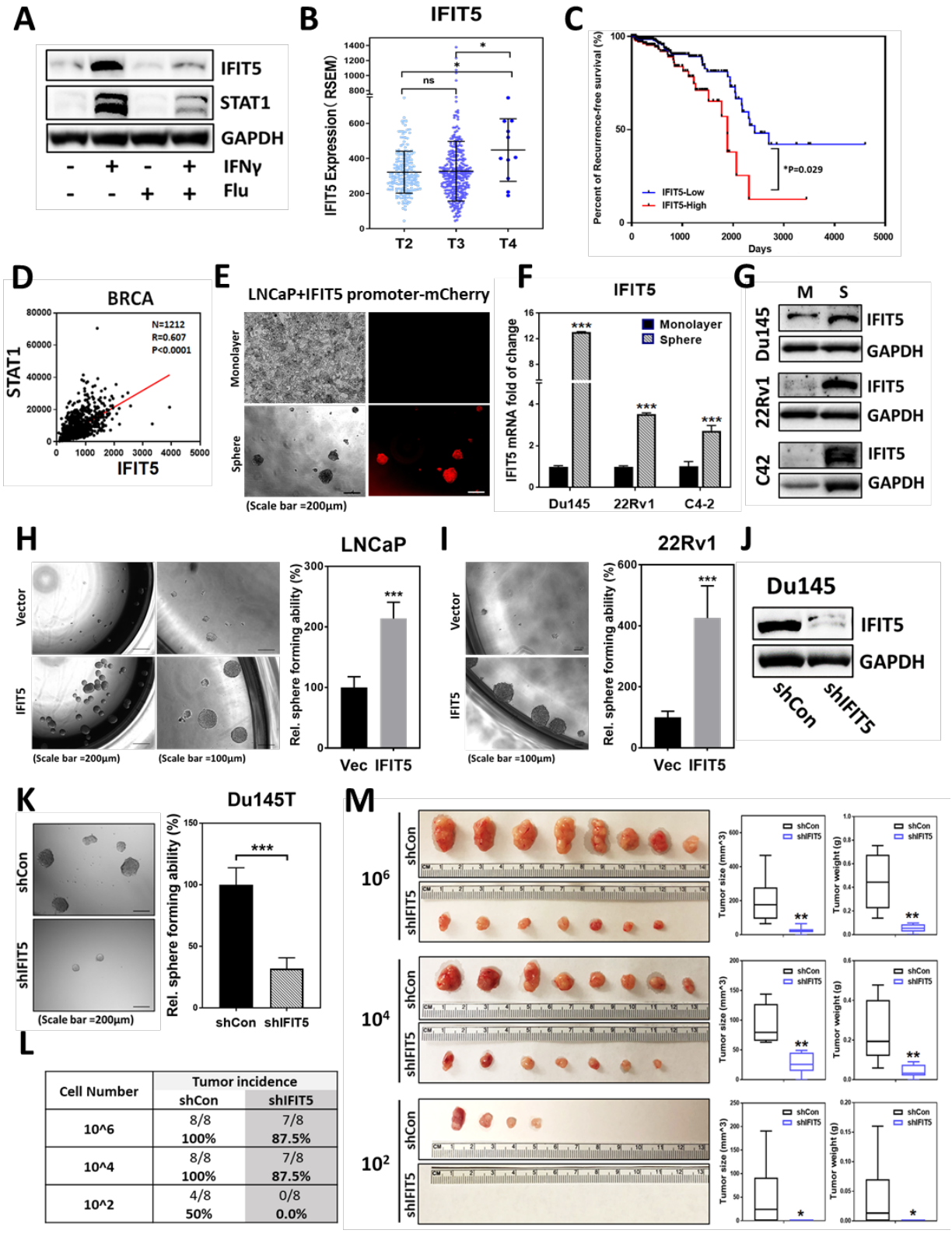

Cell Number	Tumor incidence	
	shCon	shIFIT5
10^6	8/8 100%	7/8 87.5%
10^4	8/8 100%	7/8 87.5%
10^2	4/8 50%	0/8 0.0%

Figure 3. STAT1-mediated induction of IFIT5 facilitates the emergence of stemness properties in PCa (A) Impact of fludarabine-mediated STAT1 inhibition on IFNγ-induced IFIT5 protein upregulation in Du145 cell. (B) TCGA PCa dataset demonstrating IFIT5 expression level among T2 (n=187), T3 (n=293) and T4 (n=11) stage of PCa patients. (C) Kaplan-meier survival curve of PCa patients grouped into IFIT5-high and IFIT5-low cohorts. (D) TCGA dataset demonstrating the clinical correlation of IFIT5 with STAT1 in Breast invasive carcinoma (BRCA, N=1212). (E) Expression of IFIT5 promoter-driven mCherry fluorescent protein in tumor sphere derived from LNCaP cells, compared to monolayer adherent culture. (F) Upregulation of IFIT5 mRNA level in the sphere (S) derived from each PCa line, compared to corresponding monolayer (M) culture (***$p<0.0001$). (G) IFIT5 protein upregulation in the sphere (S) derived from each PCa line, compared to corresponding monolayer (M) culture. (H-I) The impact of IFIT5-overexpression on sphere forming ability of LNCaP and 22Rv1 cells, compared to vector control (Vec). (***$p<0.0001$) (J) shRNA knockdown of IFIT5 in Du145 cells. (K) The impact of IFIT5 knockdown on sphere forming ability of Du145 cells, compared to control shRNA (shCon) (***$p<0.0001$). (L) The tumor incidence of subcutaneous injected IFIT5-knockdown (shIFIT5) Du145 cells at 10^6, 10^4 and 10^2 cell number, compared to shCon cohort. (M) Quantified size and weight of subcutaneous IFIT5-knockdown Du145 tumors, compared to shCon cohort (*$p<0.05$, **$p<0.001$).

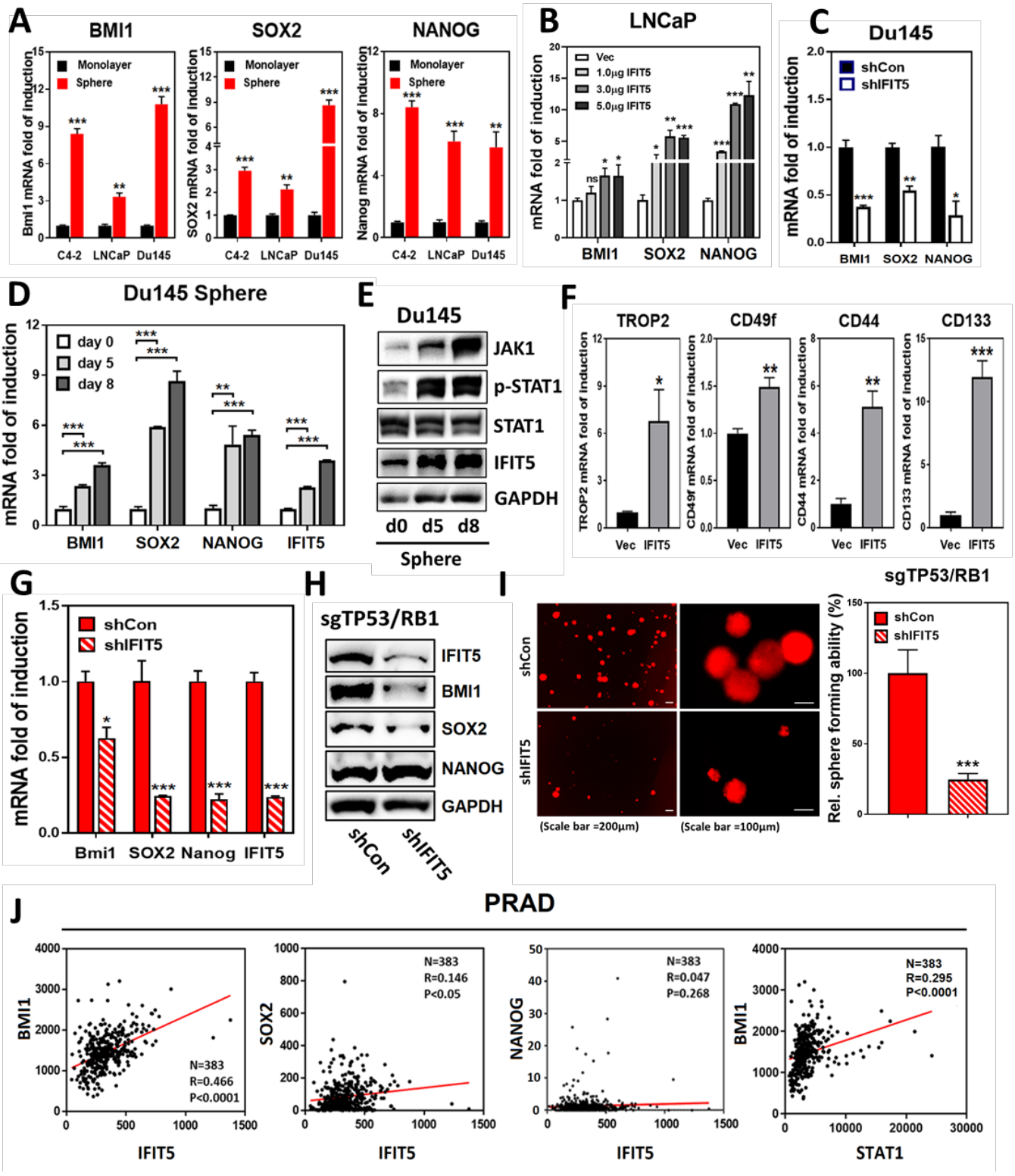
A
BMI1
SOX2
NANOG
Monolayer
Sphere
Bmi1 mRNA fold of induction
SOX2 mRNA fold of Induction
Nanog mRNA fold of induction
C4-2 LNCaP Du145
B
LNCaP
Vec
1.0μg IFIT5
3.0μg IFIT5
5.0μg IFIT5
mRNA fold of induction
BMI1 SOX2 NANOG
C
Du145
shCon
shIFIT5
mRNA fold of induction
BMI1 SOX2 NANOG
D
Du145 Sphere
day 0
day 5
day 8
mRNA fold of induction
BMI1 SOX2 NANOG IFIT5
E
Du145
JAK1
p-STAT1
STAT1
IFIT5
GAPDH
d0 d5 d8
Sphere
F
TROP2
CD49f
CD44
CD133
TROP2 mRNA fold of induction
CD49f mRNA fold of induction
CD44 mRNA fold of induction
CD133 mRNA fold of induction
Vec IFIT5
G
shCon
shIFIT5
mRNA fold of induction
Bmi1 SOX2 Nanog IFIT5
H
sgTP53/RB1
IFIT5
BMI1
SOX2
NANOG
GAPDH
shCon
shIFIT5
I
sgTP53/RB1
shCon
shIFIT5
(Scale bar =200μm)
(Scale bar =100μm)
Rel. sphere forming ability (%)
shCon
shIFIT5
J
PRAD
BMI1
IFIT5
N=383
R=0.466
P<0.0001
SOX2
IFIT5
N=383
R=0.146
P<0.05
NANOG
IFIT5
N=383
R=0.047
P=0.268
BMI1
STAT1
N=383
R=0.295
P<0.0001

Figure 4. IFIT5 impacts on prostate cancer stemness via regulating Bmi1, Sox2 and Nanog
(A) Expression level of BMI1, Sox2 and Nanog mRNA in spheres derived from Du145, LNCaP and 22Rv1 cell lines, compared to each corresponding monolayer adherent culture (**p<0.001, ***P<0.0001). (B) Dose-dependent upregulation of BMI1, SOX2, NANOG in IFIT5-overexpressed LNCaP cells, compared to vector control (ns, no significance, *p<0.05, **p<0.001, ***p<0.0001). (C) Expression level of BMI1, SOX2, Nanog and IFIT5 in IFIT5-knockdown Du145 cells, compared to control vector (shCon) (*p<0.05, **p<0.001, ***p<0.0001). (D) Induction of BMI1, SOX2, NANOG and IFIT5 gene upregulation during Du145 tumor sphere formation (*p<0.05, **p<0.001, ***p<0.0001). (E) Induction of JAK1, phospho-STAT1, STAT1 and IFIT5 protein upregulation during Du145 tumor sphere formation at Day 5 and Day 8 post-seeding. (F) Expression level of TROP2, CD49f, CD44 and CD133 mRNA in IFIT5-overexpressing LNCaP cells, compared to vector control (Vec) (*p<0.05, **p<0.001, ***p<0.0001). (G-H) mRNA and protein level of BMI1, SOX2, NANOG and IFIT5 in IFIT5-knockdown (shIFIT5) sgTP53/RB1-LNCaP cells, compared to control vector (shCon) (*p<0.05, ***p<0.0001). (I) Reduction of tumor sphere formation in IFIT5-knockdown sgTP53/RB1-LNCaP cells, compared to control vector (shCon) (***p<0.0001). (J) TCGA dataset demonstrating the clinical correlation of IFIT5 or STAT1 with BMI1, SOX2 or NANOG in Prostate adenocarcinoma (PRAD, N=383).

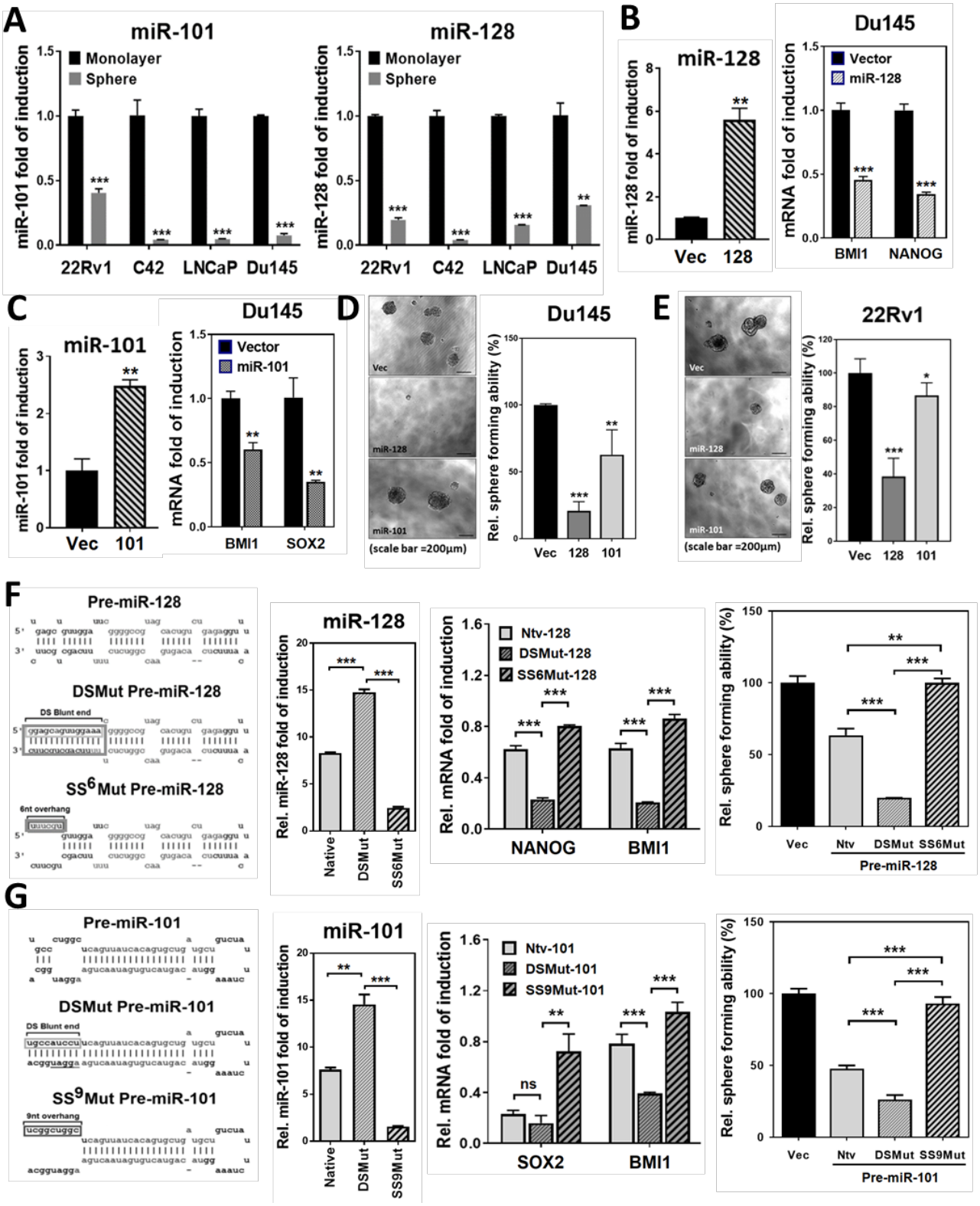
A
miR-101
miR-101 fold of induction
Monolayer
Sphere
22Rv1 C42 LNCaP Du145
miR-128
miR-128 fold of induction
B
miR-128
Vec 128
Du145
Vector
miR-128
mRNA fold of induction
BMI1 NANOG
C
miR-101
Vec 101
Du145
Vector
miR-101
BMI1 SOX2
D
Du145
Rel. sphere forming ability (%)
Vec 128 101
(scale bar =200μm)
E
22Rv1
Rel. sphere forming ability (%)
Vec 128 101
(scale bar =200μm)
F
Pre-miR-128
DSMut Pre-miR-128
DS Blunt end
SS6Mut Pre-miR-128
6nt overhang
miR-128
Rel. miR-128 fold of induction
Native DSMut SS6Mut
Ntv-128
DSMut-128
SS6Mut-128
Rel. mRNA fold of induction
NANOG BMI1
Rel. sphere forming ability (%)
Vec Ntv DSMut SS6Mut
Pre-miR-128
G
Pre-miR-101
DSMut Pre-miR-101
DS Blunt end
SS9Mut Pre-miR-101
9nt overhang
miR-101
Rel. miR-101 fold of induction
Native DSMut SS9Mut
Ntv-101
DSMut-101
SS9Mut-101
Rel. mRNA fold of induction
SOX2 BMI1
Rel. sphere forming ability (%)
Vec Ntv DSMut SS9Mut
Pre-miR-101

Figure 5. IFIT5 promotes the expression of PCSC-associated regulators via targeting miRNA biogenesis at precursor level (A) Expression level of miR-101 and miR-128 in spheres derived from 22Rv1, C4-2, LNCaP and Du145 cell lines, compared to each corresponding monolayer adherent culture (***p<0.0001). (B) The impact of miR-128 overexpression on Nanog and Bmi1 level in Du145 cells (**p<0.001, ***p<0.0001), compared to vector control. (C) The impact of miR-101 overexpression on SOX2 and BMI1 level in Du145 cells (**p<0.001), compared to vector control. (D-E) The impact of miR-128 and miR-101 on the tumor sphere formation of Du145 and 22Rv1 cells (*p<0.05, **p<0.001, ***p<0.0001). (F) Left: Mutation of nucleotides (box) for generating blunt 5'-end double stranded pre-miR-128 (DSMut pre-miR-128) or 5'-end 6 nucleotides single stranded pre-miR-128 (SS^6Mut pre-miR-128). Both mature miR-128 and miR-128* sequences were shown in lighter gray. Middle: The effect of Native, DSMut or SS^6Mut pre-miR-128 on the expression level of mature miR-128 in Du145 cells (***P<0.0001). The impact of Native, DSMut or SS^6Mut pre-miR-128 on the expression level of NANOG and BMI1 mRNA in Du145 cells (***P<0.0001). Right: The impact of Native, DSMut or SS^6Mut pre-miR-128 on the sphere formation of Du145 cells. (**p<0.001, ***p<0.0001). (G) Left: Mutation of nucleotides (box) for generating blunt 5'-end double stranded pre-miR-101 (DSMut pre-miR-101) or 5'-end 9 nucleotides single stranded pre-miR-101 (SSMut pre-miR-101). Both mature miR-101 and miR-101* sequences were shown in lighter gray. Middle: The effect of Native, DSMut or SS^9Mut pre-miR-101 on the expression level of mature miR-101 in Du145 cells (**p<0.001, ***p<0.0001). The impact of Native, DSMut or SS^9Mut pre-miR-101 on the expression level of SOX2 and BMI1 mRNA in Du145 cells (ns, No significance, **p<0.001, ***p<0.0001). Right: The impact of Native, DSMut or SS^9Mut pre-miR-101 on the sphere formation of Du145 cells (***p<0.0001).

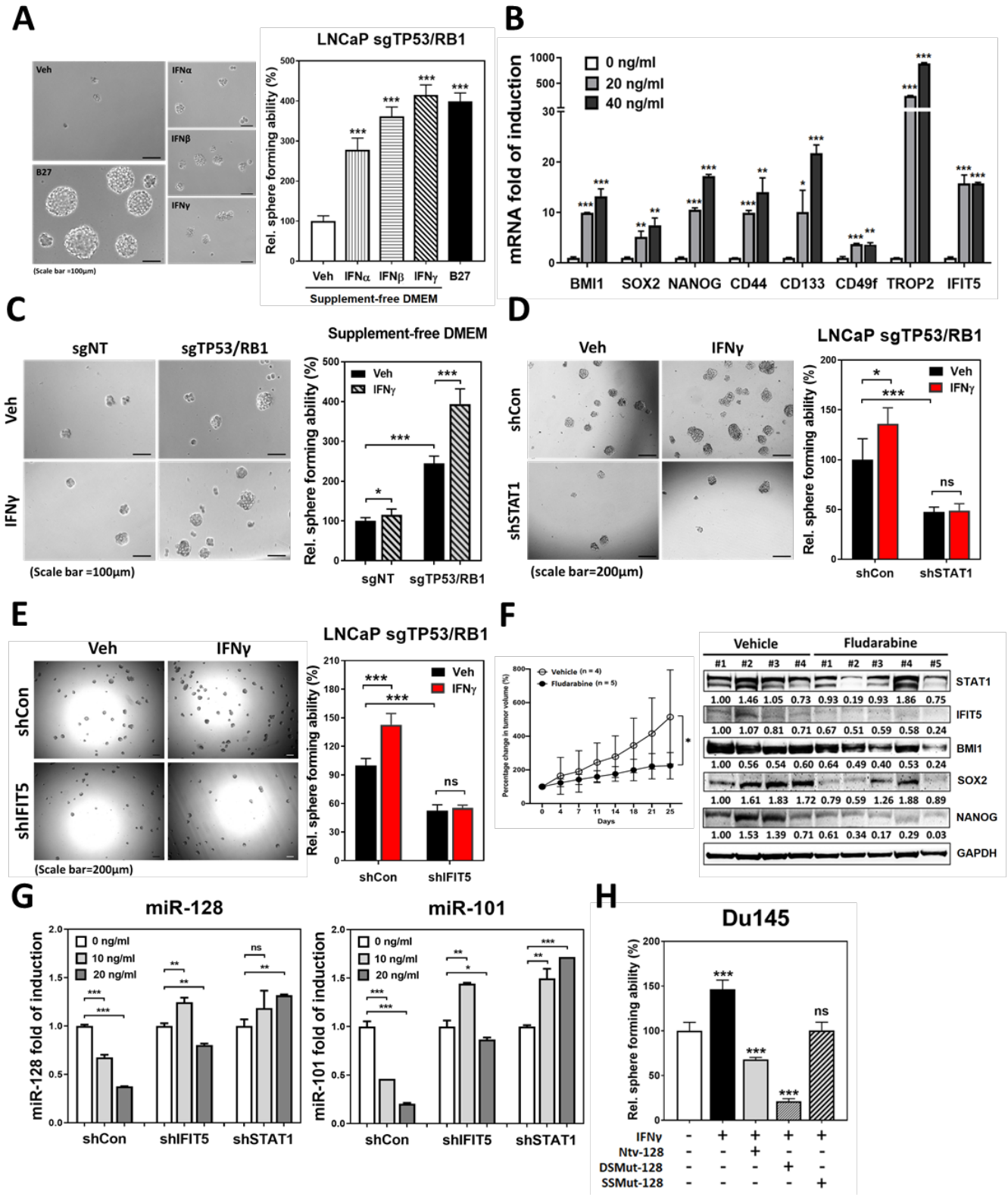
A
Veh
IFNα
IFNβ
B27
IFNγ
(Scale bar =100μm)
LNCaP sgTP53/RB1
Rel. sphere forming ability (%)
Veh
IFNα
IFNβ
IFNγ
B27
Supplement-free DMEM
B
mRNA fold of induction
0 ng/ml
20 ng/ml
40 ng/ml
BMI1
SOX2
NANOG
CD44
CD133
CD49f
TROP2
IFIT5
C
sgNT
sgTP53/RB1
Veh
IFNγ
(Scale bar =100μm)
Supplement-free DMEM
Rel. sphere forming ability (%)
Veh
IFNγ
sgNT
sgTP53/RB1
D
Veh
IFNγ
shCon
shSTAT1
(scale bar=200μm)
LNCaP sgTP53/RB1
Rel. sphere forming ability (%)
Veh
IFNγ
ns
shCon
shSTAT1
E
Veh
IFNγ
shCon
shIFIT5
(Scale bar=200μm)
LNCaP sgTP53/RB1
Rel. sphere forming ability (%)
Veh
IFNγ
ns
shCon
shIFIT5
F
Vehicle (n = 4)
Fludarabine (n = 5)
Percentage change in tumor volume (%)
Days
Vehicle
Fludarabine
#1
#2
#3
#4
#1
#2
#3
#4
#5
STAT1
1.00 1.46 1.05 0.73 0.93 0.19 0.93 1.86 0.75
IFIT5
1.00 1.07 0.81 0.71 0.67 0.51 0.59 0.58 0.24
BMI1
1.00 0.56 0.54 0.60 0.64 0.49 0.40 0.53 0.24
SOX2
1.00 1.61 1.83 1.72 0.79 0.59 1.26 1.88 0.89
NANOG
1.00 1.53 1.39 0.71 0.61 0.34 0.17 0.29 0.03
GAPDH
G
miR-128
miR-128 fold of induction
0 ng/ml
10 ng/ml
20 ng/ml
shCon
shIFIT5
shSTAT1
miR-101
miR-101 fold of induction
0 ng/ml
10 ng/ml
20 ng/ml
shCon
shIFIT5
shSTAT1
H
Du145
Rel. sphere forming ability (%)
IFNγ
Ntv-128
DSMut-128
SSMut-128

Figure 6. Interferon-STAT1-IFIT5 signaling potentiates the acquisition of cancer stemness properties in PCa (A) The impact of type I and Type II IFN treatment on the sphere formation of sgTP53/RB1 LNCaP cells cultured within supplement-free DMEM condition (***p<0.0001). (B) The dose-dependent impact of IFNγ treatment on the induction of IFIT5 and cancer stemness-associated genes in 22Rv1 cells (**p<0.001, ***p<0.0001). (C) The impact of IFNγ on the self-renewal capacity of sgTP53/RB1-LNCaP cells under supplement-free DMEM culture condition, compared to sgNT control (*p<0.05, ***p<0.0001). (D-E) The impact of IFIT5- or STAT1-knockdown on the IFNγ-facilitated sgTP53/RB1-LNCaP sphere formation, compared to control vector (shCon) (ns, No significance, *P<0.05, ***p<0.0001). (F) Left: The impact of Fludarabine (10 mg/kg) on LNCaP sgTP53/RB1 tumor growth (*p<0.05). Right: Expression of STAT1, IFIT5, BMI1, NANOG and SOX2 protein levels in the shTP53/RB1-LNCaP tumors treated with fludarabine (10 mg/kg), compared to vehicle control. Fludarabine was administrated through intraperitoneal injection at consecutive 5 days per week, for total 2 weeks. (G) The impact of IFIT5- or STAT1-knockdown on the IFNγ-induced miR-128 or miR-101 downregulation, compared to control vector (shCon) (ns, No significance, *p<0.05, **p<0.001, ***p<0.0001). (H) The impact of mutant miR-128 on the IFNγ-facilitated sphere formation in Du145 cells (ns, No significance, ***p<0.0001).

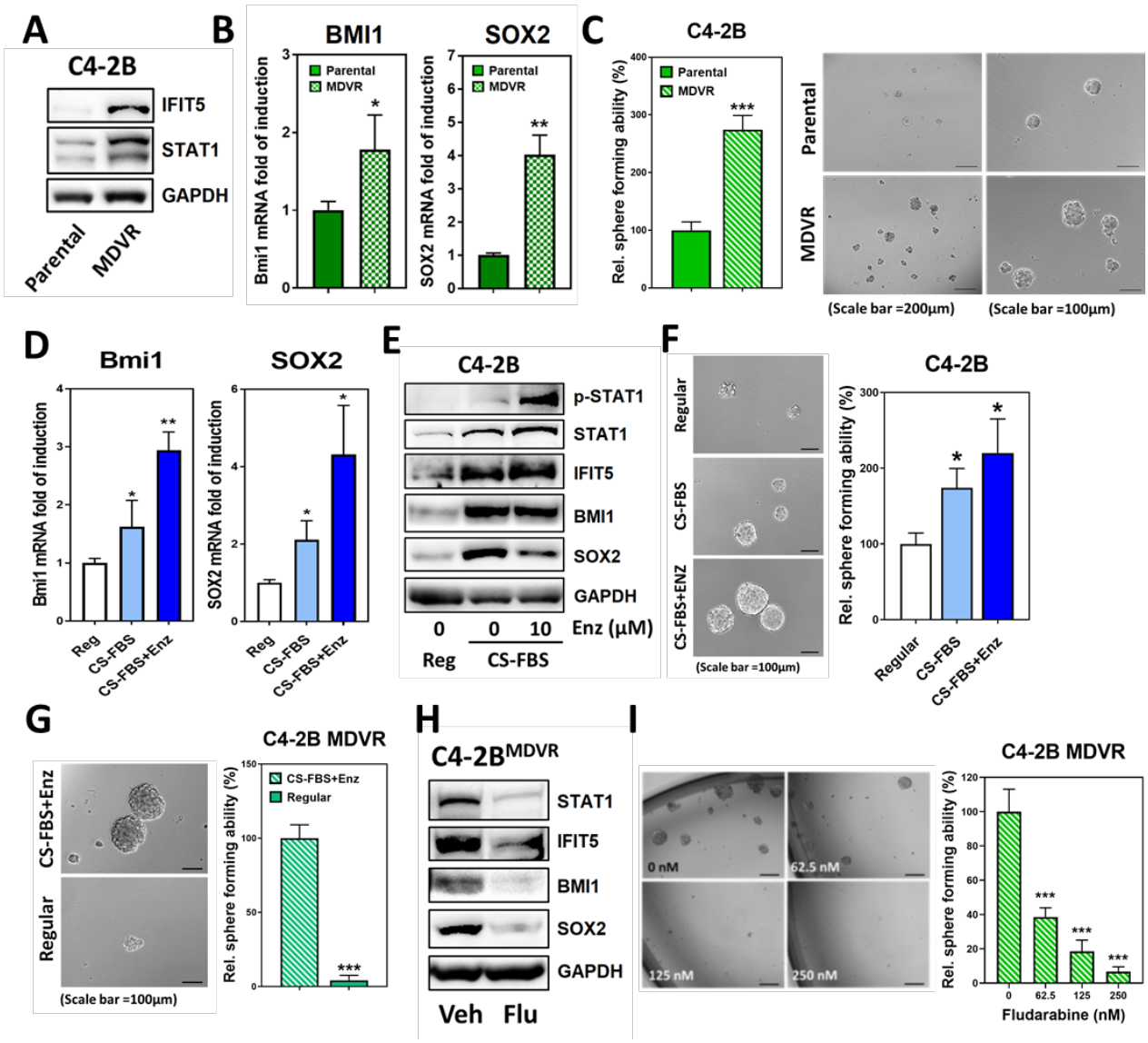
A
C4-2B
IFIT5
STAT1
GAPDH
Parental
MDVR
B
BMI1
SOX2
Parental
MDVR
Bmi1 mRNA fold of induction
SOX2 mRNA fold of induction
C
C4-2B
Parental
MDVR
Rel. sphere forming ability (%)
(Scale bar =200μm)
(Scale bar =100μm)
D
Bmi1
SOX2
Bmi1 mRNA fold of induction
SOX2 mRNA fold of induction
Reg
CS-FBS
CS-FBS+Enz
E
C4-2B
p-STAT1
STAT1
IFIT5
BMI1
SOX2
GAPDH
0 0 10 Enz (μM)
Reg CS-FBS
F
Regular
CS-FBS
CS-FBS+ENZ
(Scale bar =100μm)
C4-2B
Rel. sphere forming ability (%)
G
CS-FBS+Enz
Regular
(Scale bar =100μm)
C4-2B MDVR
Rel. sphere forming ability (%)
H
C4-2B MDVR
STAT1
IFIT5
BMI1
SOX2
GAPDH
Veh Flu
I
0 nM
62.5 nM
125 nM
250 nM
C4-2B MDVR
Rel. sphere forming ability (%)
Fludarabine (nM)

Figure 7. STAT1 signaling activation confers CSC properties in castration-resistance PCa (A) Elevation of STAT1 and IFIT5 protein in C4-2B MDVR cells, compared to C4-2B parental line. (B) Expression level of BMI1 and SOX2 mRNA in C4-2B MDVR cells, compared to C4-2B parental line (*p<0.05, **p<0.001). (C) The sphere forming ability of C4-2B MDVR cells, compared to C4-2B parental line (***p<0.0001). (D) Induction of BMI1 and SOX2 gene upregulation in C4-2B cells cultured in CS-FBS-supplemented phenol red-free RPMI without (CS-FBS) or with 10 μM enzalutamide (CS-FBS+Enz), compared to regular culture condition (Reg). (*p<0.05, ***p<0.0001). (E) Expression level of phosphorylated STAT1, STAT1, IFIT5, BMI1, Sox2 and Nanog proteins in C4-2B cells cultured in CS-FBS-supplemented phenol Red free RPMI without (CS-FBS) or with 10μM enzalutamide (CS-FBS+Enz), compared to regular culture condition (Reg). (F) The sphere forming ability of C4-2B cells primarily cultured in CS-FBS-supplemented pheno red-free RPMI without (CS-FBS) or with 10 μM enzalutamide (CS-FBS+Enz) for 2 weeks, compared to regular culture condition (Reg). (*p<0.05). (G) The sphere forming ability of C4-2B MDVR cells primarily cultured in regular condition for 2 weeks, compared with culture condition of CS-FBS-supplemented phenol Red free RPMI with 20μM enzalutamide (CS-FBS+Enz) (***p<0.0001). (H) The expression level of STAT1, IFIT5, Bmi1, SOX2 and Nanog proteins in C4-2B MDVR cells treated with fludarabine (500 nM, 48 hrs). (I) The sphere forming ability of C4-2B MDVR cells treated with increased dose of fludarabine during sphere culture.

SUPPLEMENTARY FIGURES AND TABLE

A

HALLMARK Pathways	SIZE	ES	NES	NOM p-val
G2M_CHECKPOINT	186	0.6271	2.0058	0.00442
INTERFERON_ALPHA_RESPONSE	92	0.7136	1.9032	0.01552
E2F_TARGETS	189	0.6480	1.8732	0.01831
INTERFERON_GAMMA_RESPONSE	196	0.6224	1.8533	0.02113
PI3K_AKT_MTOR_SIGNALING	104	0.3397	1.4749	0.03279

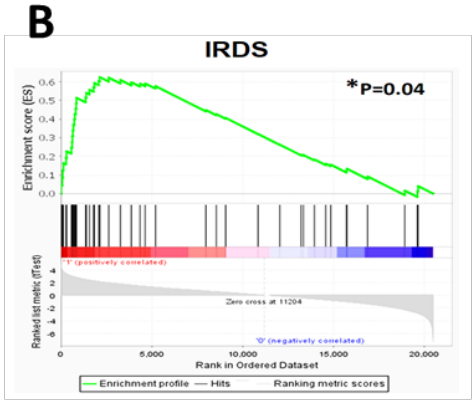

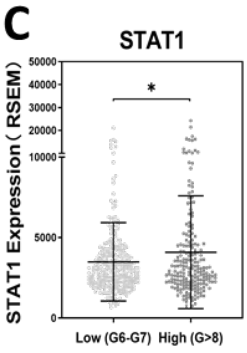

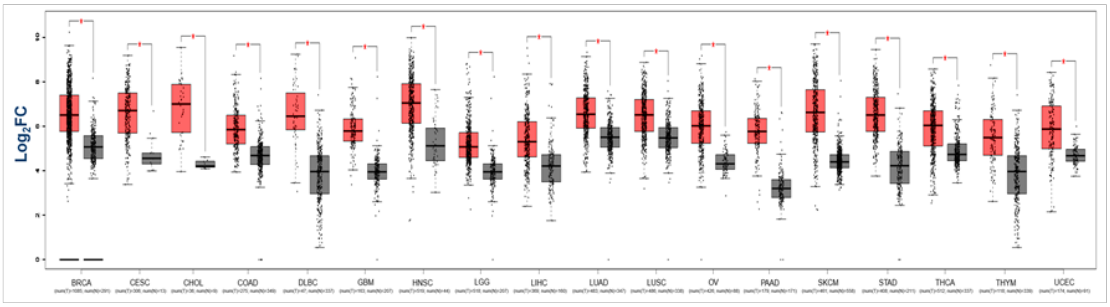

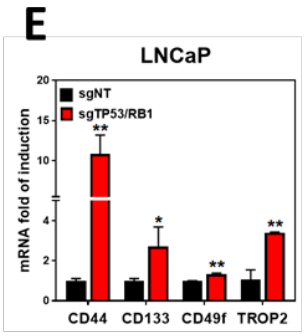

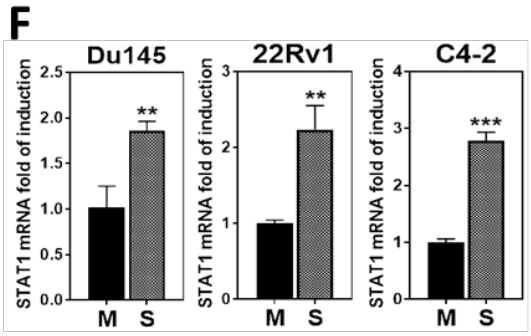

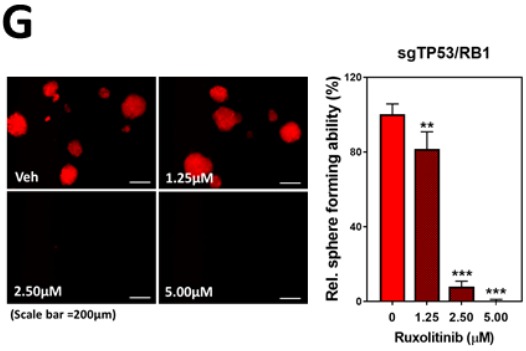

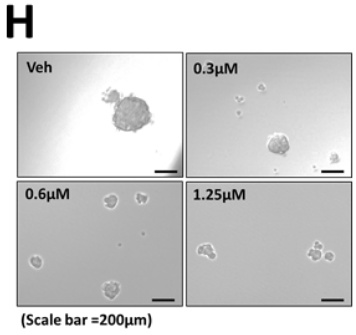

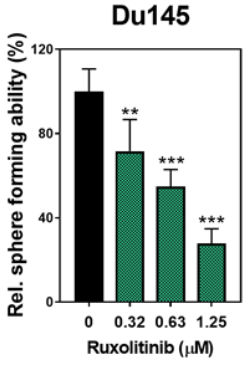

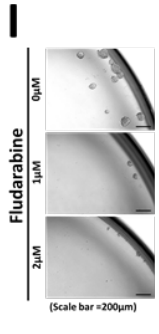

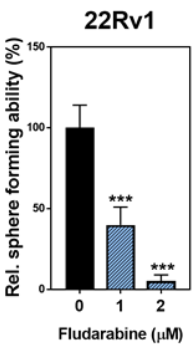

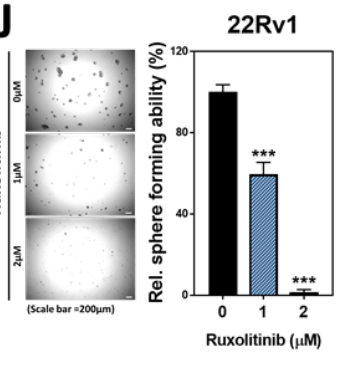

Figure S1. (A) GSEA identifying enrichment of upregulated genes associated with demonstrated pathways in PCa patients with lymph node metastasis (N1, n=80), compared to cohort without metastasis (N0, n=345). (B) GSEA identifying enrichment of IRDS genes in the tumor specimens of PCa patients with lymph node metastasis (N1, n=80), compared to cohort without metastasis (N0, n=345). (C) TCGA PCa dataset demonstrating STAT1 expression level among low (Gleason score=6 and 7, n=292) and High (Gleason score >8, n=206) grade tumor specimens from PCa patients. (*$p<0.05$). (D) GEPIA analysis of STAT1 expression level among tumor (red) and normal (gray) specimens derived from different malignancies (*$p<0.01$) (http://gepia.cancer-pku.cn/index.html). (E) Expression level of cancer stemness-associated genes (CD44, CD133, CD49f and TROP2) in sgTP53/RB1-LNCaP cell, compared to control vector (sgNT) (*$p<0.05$, **$p<0.001$, ***$p<0.0001$). (F) Induction of STAT1 mRNA upregulation in the sphere (S) derived from each PCa line, compared to corresponding monolayer (M) culture. (G-H) Dose-dependent impact of Ruxolitinib on the sphere forming ability of sgTP53/RB1-LNCaP and Du145 cells (**$p<0.001$, ***$p<0.0001$). (I-J) Dose-dependent impact of Fludarabine or Ruxolitinib on the sphere forming ability of 22Rv1 cells (***$p<0.0001$).

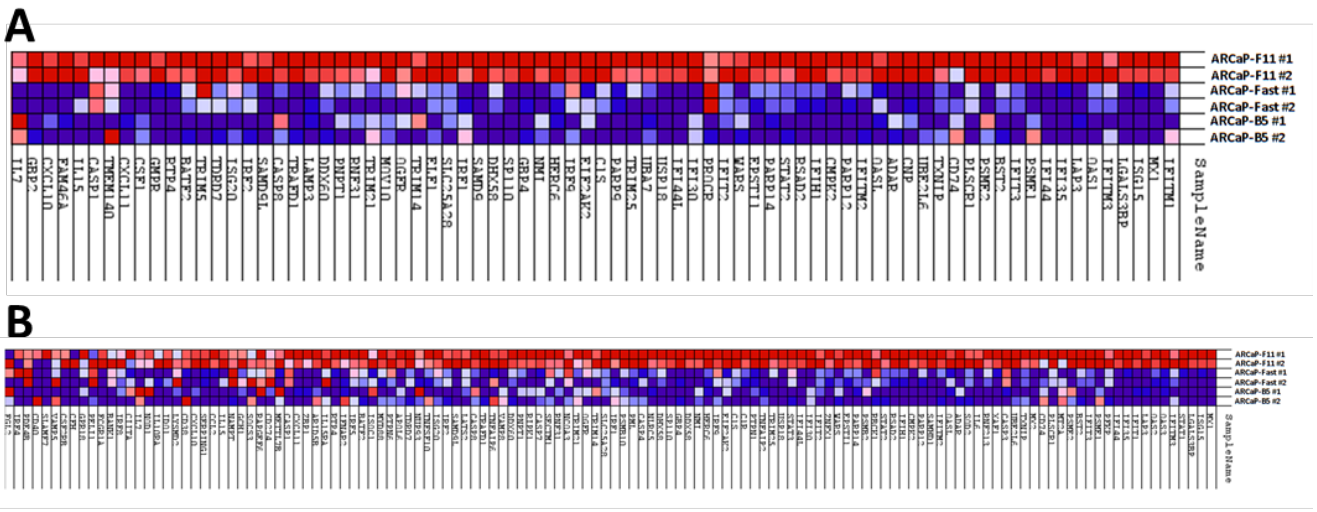
A
ARCaP-F11 #1
ARCaP-F11 #2
ARCaP-Fast #1
ARCaP-Fast #2
ARCaP-B5 #1
ARCaP-B5 #2
SampleName
B
SampleName

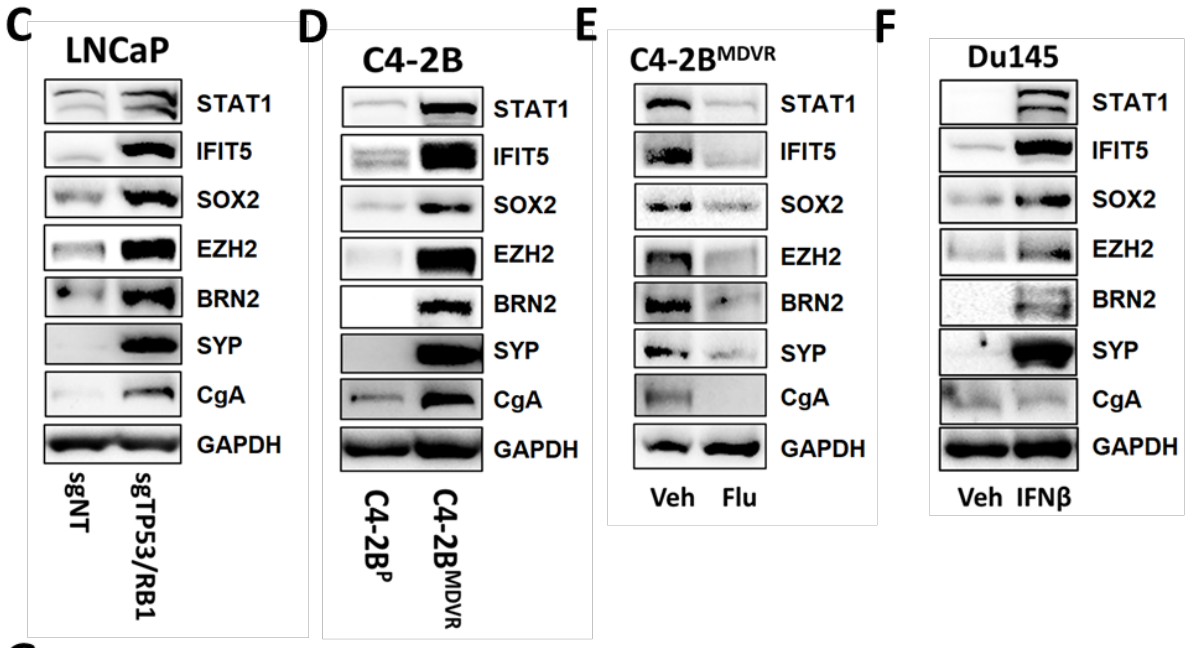
C
LNCaP
STAT1
IFIT5
SOX2
EZH2
BRN2
SYP
CgA
GAPDH
sgNT
sgTP53/RB1
D
C4-2B
STAT1
IFIT5
SOX2
EZH2
BRN2
SYP
CgA
GAPDH
C4-2BP
C4-2BMDVR
E
C4-2BMDVR
STAT1
IFIT5
SOX2
EZH2
BRN2
SYP
CgA
GAPDH
Veh
Flu
F
Du145
STAT1
IFIT5
SOX2
EZH2
BRN2
SYP
CgA
GAPDH
Veh
IFNβ

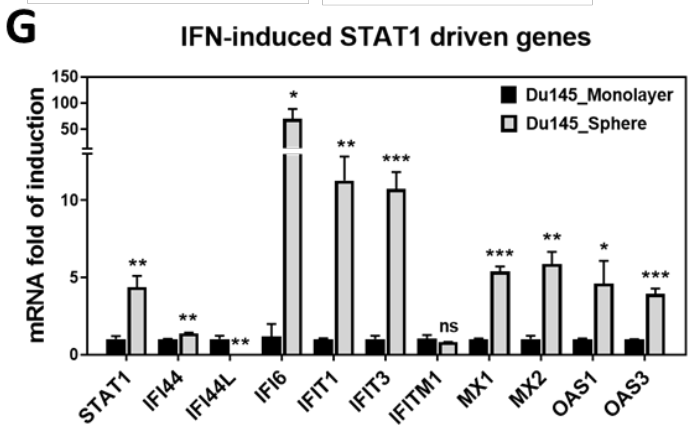
G
IFN-induced STAT1 driven genes
mRNA fold of induction
Du145_Monolayer
Du145_Sphere
STAT1
IFI44
IFI44L
IFI6
IFIT1
IFIT3
IFITM1
MX1
MX2
OAS1
OAS3
ns

Fig. S2 (A) GSEA-identified enrichment of IFNα response-associated genes in ARCaP-F11 subline, compared to ARCaP-Fast and ARCaP-B5 sublines. (B) GSEA-identified enrichment of IFNγ response-associated genes in ARCaP-F11 subline, compared to ARCaP-Fast and ARCaP-B5 sublines. (C) Protein expression level of STAT1, IFIT5, SOX2, EZH2, BRN2, SYP, and CgA in sgTP53/RB1-LNCaP cell, compared to sgNT control. (D) Expression level of STAT1, IFIT5, SOX2, EZH2, BRN2, SYP and CgA proteins among C4-2B parental and MDVR lines. (E) Downregulation of STAT1, IFIT5, SOX2, EZH2, BRN2, SYP and CgA proteins in C4-2B MDVR line treated with Fludarabine (500nM, 48hrs). (F) Induction of STAT1, IFIT5, SOX2, EZH2, BRN2, SYP and CgA proteins in Du145 cells treated with IFNβ (20 ng/ml, 48 hrs). (G) Expression of ten IFN-inducible STAT1-driven genes in Du145 tumor spheres, compared to monolayer adherent culture (*$p<0.05$, **$p<0.001$, ***$p<0.0001$).

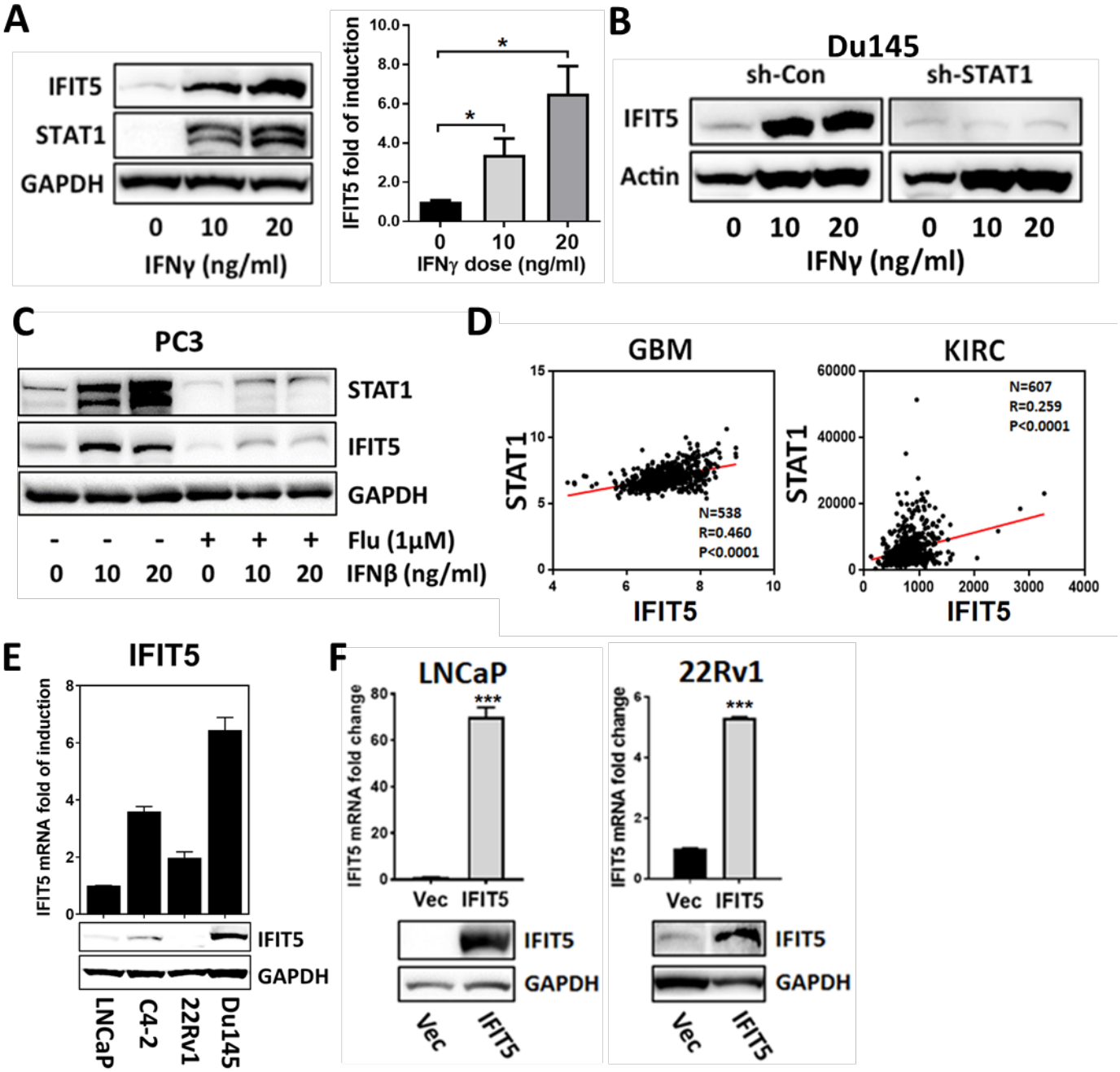
A
IFIT5
STAT1
GAPDH
0 10 20
IFNγ (ng/ml)
IFIT5 fold of induction
IFNγ dose (ng/ml)
B
Du145
sh-Con
sh-STAT1
IFIT5
Actin
0 10 20 0 10 20
IFNγ (ng/ml)
C
PC3
STAT1
IFIT5
GAPDH
- - - + + + Flu (1μM)
0 10 20 0 10 20 IFNβ (ng/ml)
D
GBM
KIRC
STAT1
IFIT5
N=538
R=0.460
P<0.0001
N=607
R=0.259
P<0.0001
E
IFIT5
IFIT5 mRNA fold of induction
IFIT5
GAPDH
LNCaP
C4-2
22Rv1
Du145
F
LNCaP
22Rv1
IFIT5 mRNA fold change
***
Vec IFIT5
IFIT5
GAPDH
Vec
IFIT5

Figure S3. (A) IFNγ induced upregulation of IFIT5 protein and mRNA in Du145 cells. (B) Impact of STAT1 shRNA knockdown on IFNγ-induced upregulation of IFIT5 protein in Du145 cells. (C) Impact of fludarabine-mediated STAT1 inhibition on IFNγ-induced upregulation of IFIT5 protein in PC3 cells. (D) TCGA dataset demonstrating the clinical correlation of IFIT5 with STAT1 in Gliblastoma Multiform (GBM, N=538), and Kidney renal clear cell carcinoma (KIRC, N=607). (E) Expression level of IFIT5 mRNA and protein among listed PCa lines. (F) Level of IFIT5 mRNA and protein in IFIT5-overexpressing (IFIT5) LNCaP and 22Rv1 cells, compared to vector control (Vec) (***$p<0.0001$).

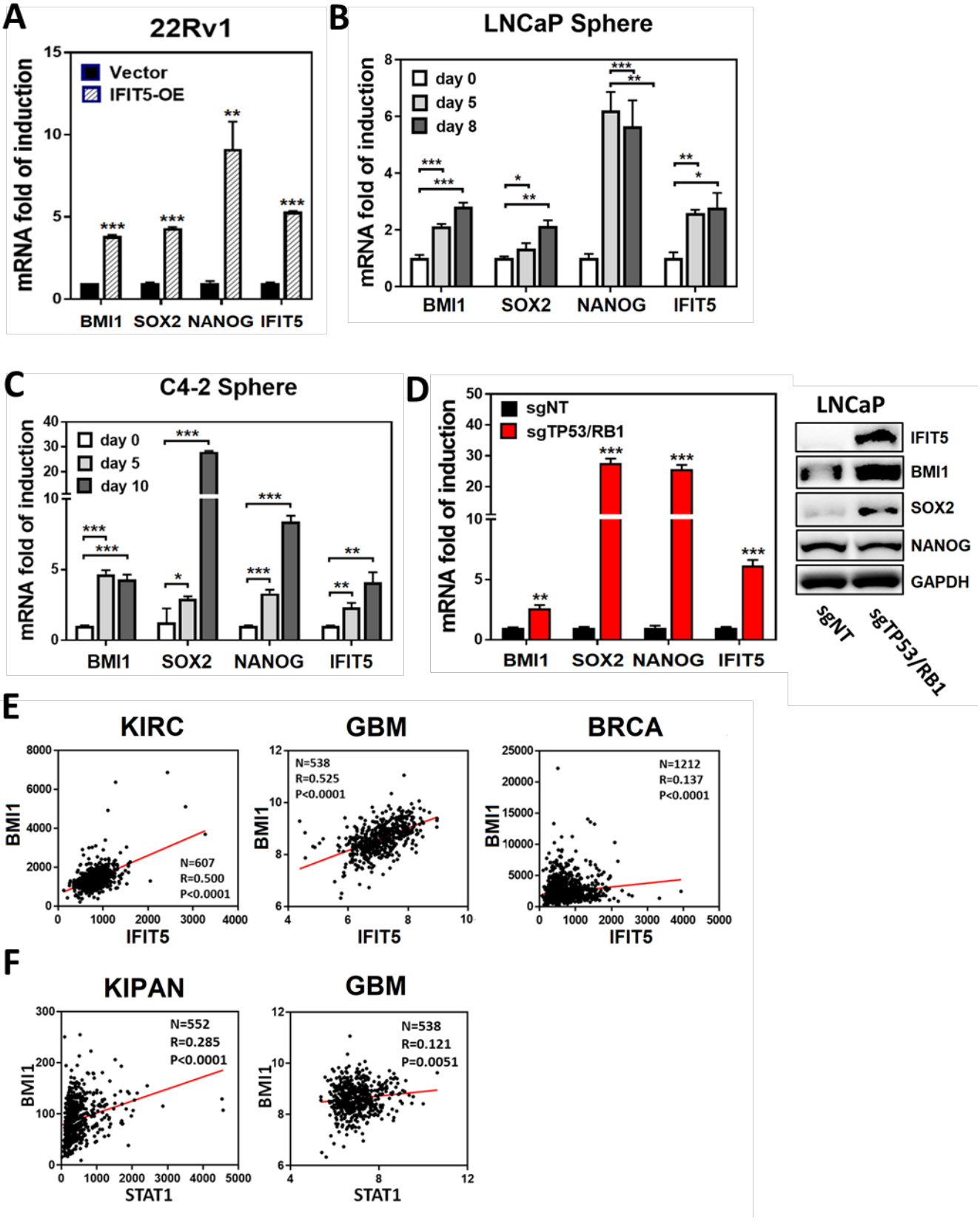
A
22Rv1
mRNA fold of induction
Vector
IFIT5-OE
BMI1 SOX2 NANOG IFIT5
B
LNCaP Sphere
mRNA fold of induction
day 0
day 5
day 8
BMI1 SOX2 NANOG IFIT5
C
C4-2 Sphere
mRNA fold of induction
day 0
day 5
day 10
BMI1 SOX2 NANOG IFIT5
D
mRNA fold of induction
sgNT
sgTP53/RB1
BMI1 SOX2 NANOG IFIT5
LNCaP
IFIT5
BMI1
SOX2
NANOG
GAPDH
sgNT
sgTP53/RB1
E
KIRC
BMI1
IFIT5
N=607
R=0.500
P<0.0001
GBM
BMI1
IFIT5
N=538
R=0.525
P<0.0001
BRCA
BMI1
IFIT5
N=1212
R=0.137
P<0.0001
F
KIPAN
BMI1
STAT1
N=552
R=0.285
P<0.0001
GBM
BMI1
STAT1
N=538
R=0.121
P=0.0051

Figure S4. (A) Expression level of Bmi1, Sox2, Nanog and IFIT5 in IFIT5-overexpressed 22Rv1 cells, compared to vector control (**p<0.001, ***p<0.0001). (B-C) Induction of BMI1, SOX2, Nanog and IFIT5 gene upregulation during LNCaP and C4-2 tumor sphere formation (*p<0.05, **p<0.001, ***p<0.0001). (D) mRNA and protein upregulation of BMI1, SOX2, NANOG and IFIT5 in sgTP53/RB1-LNCaP cell, compared to control vector (sgNT). (E) TCGA dataset demonstrating the clinical correlation of IFIT5 with BMI1 in Kidney renal clear cell carcinoma (KIRC, N=607), Gliblastoma Multiform (GBM, N=538), and Breast invasive carcinoma (BRCA, N=1212) (F) TCGA dataset demonstrating the clinical correlation of STAT1 with BMI1 in Pan Kidney cancer cohort (KIPAN, N=552) and Glioblastoma Multiform (GBM, N=538).

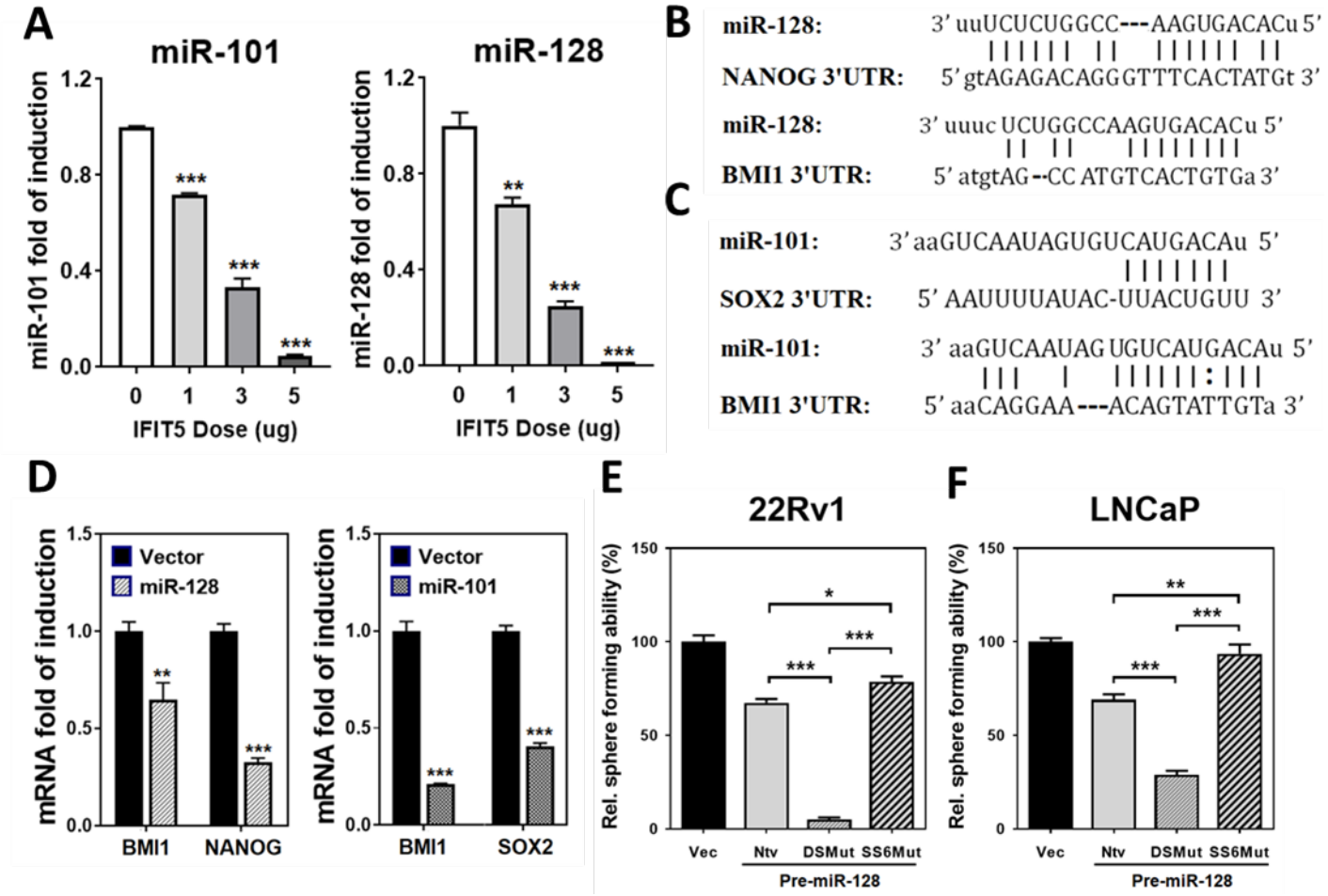
A
miR-101
miR-101 fold of induction
IFIT5 Dose (ug)
miR-128
miR-128 fold of induction
IFIT5 Dose (ug)
B
miR-128: 3' uuUCUCUGGCC---AAGUGACACu 5'
NANOG 3'UTR: 5' gtAGAGACAGGGTTTCACTATGt 3'
miR-128: 3' uuuc UCUGGCCAAGUGACACu 5'
BMI1 3'UTR: 5' atgtAG--CC ATGTCACTGTGa 3'
C
miR-101: 3' aaGUCAAUAGUGUCAUGACAu 5'
SOX2 3'UTR: 5' AAUUUUAUAC-UUACUGUU 3'
miR-101: 3' aaGUCAAUAG UGUCAUGACAu 5'
BMI1 3'UTR: 5' aaCAGGAA---ACAGTATTGTa 3'
D
mRNA fold of induction
Vector
miR-128
BMI1
NANOG
mRNA fold of induction
Vector
miR-101
BMI1
SOX2
E
22Rv1
Rel. sphere forming ability (%)
Vec
Ntv
DSMut
SS6Mut
Pre-miR-128
F
LNCaP
Rel. sphere forming ability (%)
Vec
Ntv
DSMut
SS6Mut
Pre-miR-128

Figure S5. (A) Dose-dependent impact of IFIT5-overexpression on the level of miR-101 and miR-128 expression in 22Rv1 cells (**p<0.001, ***p<0.0001). (B) Representative matched nucleotide sequences between the seed region of miR-128 and the 3'UTR of Nanog and Bmi1 mRNA. (C) Representative matched nucleotide sequences between the seed region of miR-101 and the 3'UTR of Sox2 and Bmi1 mRNA (D) Left: The impact of miR-128 overexpression on BMI1 and NANOG level in 22Rv1 cells (**p<0.001, ***p<0.0001). Right: The impact of miR-101 overexpression on BMI1 and SOX2 level in 22Rv1 cells (***p<0.0001). (E-F) The impact of Native, DSMut or SS6Mut pre-miR-128 on the sphere formation of 22Rv1 and LNCaP cells. (*p<0.05, **p<0.001, ***p<0.0001).

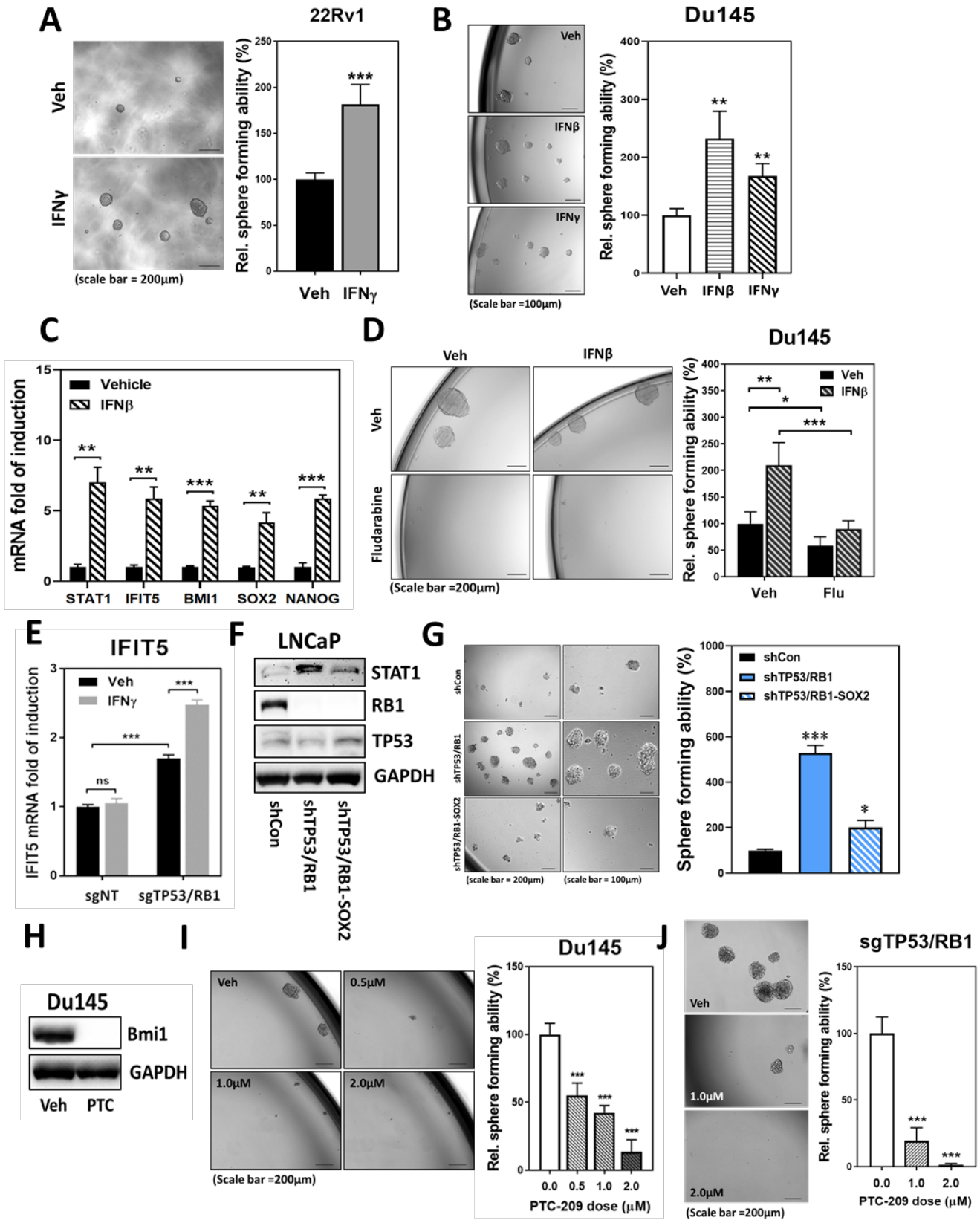
A
22Rv1
Veh
IFNγ
(scale bar = 200μm)
Rel. sphere forming ability (%)
***
Veh
IFNγ
B
Du145
Veh
IFNβ
IFNγ
(Scale bar =100μm)
Rel. sphere forming ability (%)
**
**
Veh
IFNβ
IFNγ
C
mRNA fold of induction
Vehicle
IFNβ
**
**
***
**
***
STAT1
IFIT5
BMI1
SOX2
NANOG
D
Veh
IFNβ
Veh
Fludarabine
(Scale bar =200μm)
Du145
Rel. sphere forming ability (%)
**
*
***
Veh
IFNβ
Veh
Flu
E
IFIT5
IFIT5 mRNA fold of induction
Veh
IFNγ
***
***
ns
sgNT
sgTP53/RB1
F
LNCaP
STAT1
RB1
TP53
GAPDH
shCon
shTP53/RB1
shTP53/RB1-SOX2
G
shCon
shTP53/RB1
shTP53/RB1-SOX2
(scale bar = 200μm)
(scale bar = 100μm)
Sphere forming ability (%)
shCon
shTP53/RB1
shTP53/RB1-SOX2
***
*
H
Du145
Bmi1
GAPDH
Veh
PTC
I
Veh
0.5μM
1.0μM
2.0μM
(Scale bar =200μm)
Du145
Rel. sphere forming ability (%)
***
***
***
0.0
0.5
1.0
2.0
PTC-209 dose (μM)
J
Veh
1.0μM
2.0μM
(Scale bar =200μm)
sgTP53/RB1
Rel. sphere forming ability (%)
***
***
0.0
1.0
2.0
PTC-209 dose (μM)

Fig. S6 (A) The impact of IFNγ on 22Rv1 tumor sphere formation (***p<0.0001). (B) The impact of IFNβ and IFNγ on the sphere formation of Du145 cells (**p<0.001) (C) IFNβ-induced upregulation of STAT1, IFIT5, BMI1, SOX2 and Nanog in Du145 cells (**p<0.001, ***p<0.0001). (D) The impact of fludarabine on the IFNβ-facilitated sphere forming ability of Du145 cells (*p<0.05, **p<0.001, *p<0.0001). (E) The impact of IFNγ on the induction of IFIT5 in sgTP53/RB1-LNCaP cells, compared to sgNT control (ns, No significance, ***p<0.0001). (F) Protein level of STAT1, RB1 and TP53 in shTP3/RB1 LNCaP cells with additional knockdown of SOX2. (G) The sphere forming ability of shTP3/RB1 LNCaP cells with additional knockdown of SOX2. (*p<0.05, *p<0.0001). (H) Suppression of Bmi1 protein level in Du145 cells treated with BMI1 inhibitor PTC-209 (500 nM, 48 hrs). (I-J) PTC-209-mediated dose-dependent suppression on the sphere formation of Du145 and sgTP53/RB1-LNCaP cells (***p<0.0001).

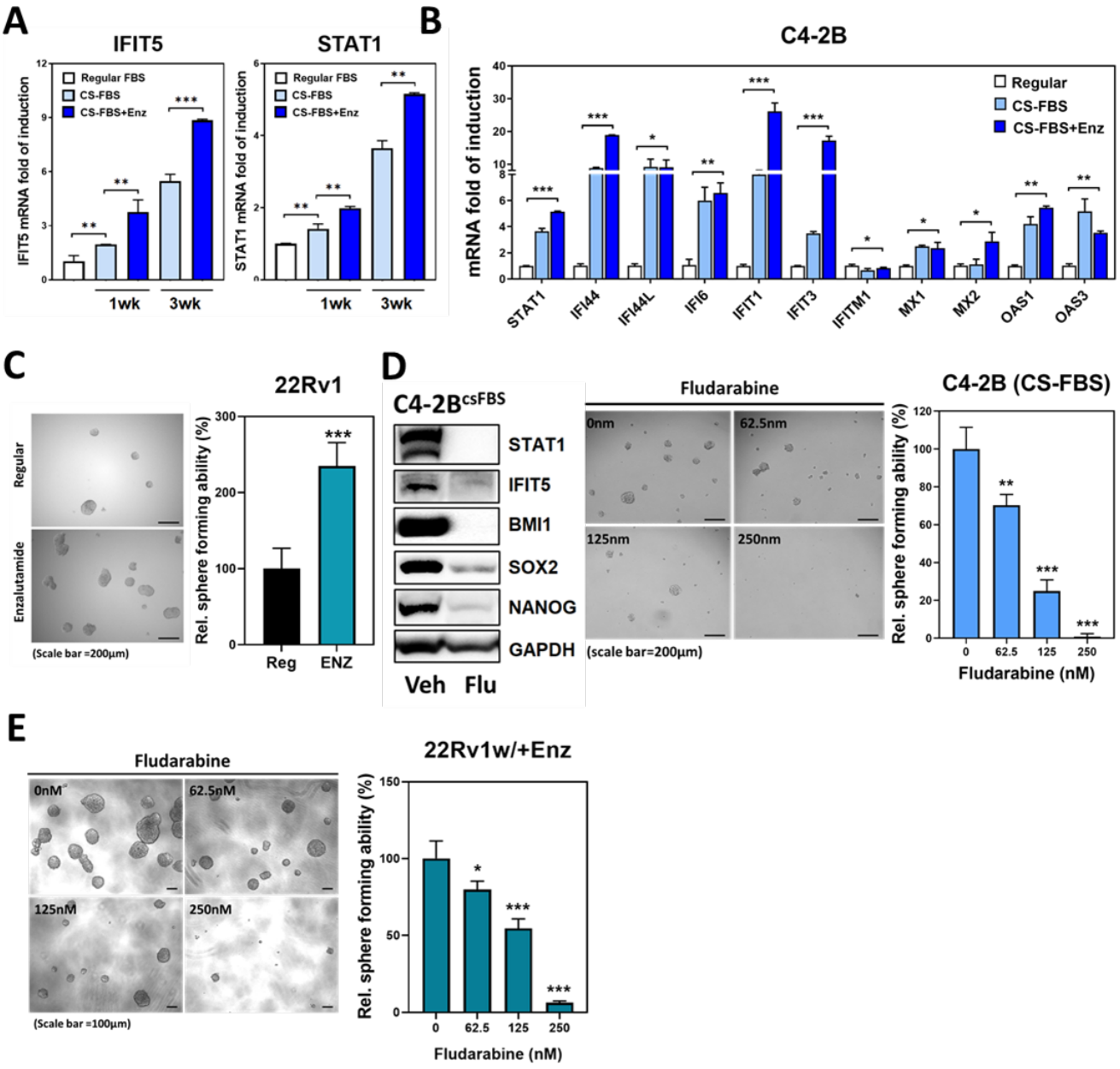
A
IFIT5
STAT1
Regular FBS
CS-FBS
CS-FBS+Enz
IFIT5 mRNA fold of induction
STAT1 mRNA fold of induction
1wk
3wk
B
C4-2B
mRNA fold of induction
Regular
CS-FBS
CS-FBS+Enz
STAT1
IFI44
IFI44L
IFI6
IFIT1
IFIT3
IFITM1
MX1
MX2
OAS1
OAS3
C
22Rv1
Regular
Enzalutamide
(Scale bar =200μm)
Rel. sphere forming ability (%)
Reg
ENZ
D
C4-2B^csFBS
STAT1
IFIT5
BMI1
SOX2
NANOG
GAPDH
Veh
Flu
Fludarabine
0nm
62.5nm
125nm
250nm
(scale bar=200μm)
C4-2B (CS-FBS)
Rel. sphere forming ability (%)
Fludarabine (nM)
E
Fludarabine
0nM
62.5nM
125nM
250nM
(Scale bar =100μm)
22Rv1w/+Enz
Rel. sphere forming ability (%)
Fludarabine (nM)

Fig. S7 (A) Time-dependent elevation of STAT1 or IFIT5 mRNA level in C4-2B cells cultured in CS-FBS-supplemented phenol red-free RPMI without or with additional 10 μM enzalutamide (**p<0.001, ***p<0.0001). (B) Induction of ten IFN-inducible STAT1-driven genes in C4-2B primarily cultured with CS-FBS without or with additional enzalutamide (10 μM), compared to regular medium (*p<0.05, **p<0.001, ***p<0.0001). (C) The sphere forming ability of 22Rv1 cells primarily cultured in androgen-deprived condition with 5 μM enzalutamide (ENZ), compared to regular condition (Reg) (***p<0.0001). (D) Left: The impact of fludarabine treatment (500 nM, 48 hrs) on the expression level of STAT1, IFIT5, BMI1, SOX2 and Nanog proteins in C4-2B cells primarily cultured in CS-FBS-supplemented phenol red-free RPMI for 3 wks. Middle-Right: The dose-dependent impact of fludarabine on the sphere forming ability of C4-2B cells primarily cultured in CS-FBS-supplemented phenol red-free RPMI for 2 weeks (*p<0.05, ***p<0.0001). (E) The dose-dependent impact of fludarabine on the sphere forming ability of 22Rv1 cells primarily cultured in androgen-deprived condition with 5 μM Enzalutamide for 2 weeks (*p<0.05, ***p<0.0001).

Supplementary Table 1. GSEA identifying genes enriched in listed pathways in ARCaP-IIF11 cell, compared to ARCaP-Fast and ARCaP-IIB5 sublines.

NAME	NOM p-val	SIZE	ES	NES	FDR q-val
HALLMARK_INTERFERON_GAMMA_RESPONSE	<0.0001	197	0.902104	1.113394	0.9031964
HALLMARK_INTERFERON_ALPHA_RESPONSE	<0.0001	94	0.941871	1.106214	0.8066409
HALLMARK_PI3K_AKT_MTOR_SIGNALING	<0.0001	104	0.803492	1.211047	1
HALLMARK_KRAS_SIGNALING_DN	<0.0001	194	0.779206	1.186822	1
HALLMARK_HEDGEHOG_SIGNALING	0.22166666	35	0.81645	1.163759	1
HALLMARK_XENOBIOTIC_METABOLISM	0.31441048	198	0.699175	1.150249	1
HALLMARK_UV_RESPONSE_UP	0.125	155	0.599276	1.136887	0.9761724
HALLMARK_REACTIVE_OXIGEN_SPECIES_PATHWAY	0.22	46	0.848599	1.11999	0.97129846
HALLMARK_HEME_METABOLISM	0.2646503	191	0.597934	1.101115	0.72334665
HALLMARK_ADIPOGENESIS	0.24584104	195	0.628668	1.098276	0.6762306
HALLMARK_MITOTIC_SPINDLE	0.26055047	198	0.562246	1.077838	0.73321736
HALLMARK_FATTY_ACID_METABOLISM	0.26741996	157	0.586373	1.034118	0.8529015
HALLMARK_APICAL_JUNCTION	0.32026145	195	0.533531	1.023842	0.8157521
HALLMARK_APICAL_SURFACE	0.30769232	44	0.633561	1.01972	0.76893455
HALLMARK_DNA_REPAIR	0.4385965	143	0.565447	1.005199	0.7779733
HALLMARK_MYOGENESIS	0.57918555	199	0.538736	0.956211	0.91874576
HALLMARK_COMPLEMENT	0.6229261	195	0.500121	0.955069	0.88064915
HALLMARK_OXIDATIVE_PHOSPHORYLATION	0.4385965	198	0.650016	0.951478	0.84035134
HALLMARK_E2F_TARGETS	0.5671642	198	0.641151	0.945224	0.8144215
HALLMARK_MTORC1_SIGNALING	0.5260223	198	0.562164	0.926194	0.82797027
HALLMARK_NOTCH_SIGNALING	0.7170213	32	0.469431	0.856663	0.9837505
HALLMARK_CHOLESTEROL_HOMEOSTASIS	0.776699	73	0.444428	0.855078	0.9440868
HALLMARK_G2M_CHECKPOINT	0.7185501	198	0.583791	0.836091	0.9330952
HALLMARK_BILE_ACID_METABOLISM	0.73491377	112	0.473109	0.736843	1
HALLMARK_MYC_TARGETS_V2	0.85532993	58	0.56871	0.693345	0.98105043

Supplementary Table 2. RNA-seq analysis of 18 IRDS genes express among three ARCaP sublines.

SYMBOL	ARCaP-Fast		ARCaP-F11		ARCaP-B5	
	#1	#2	#1	#2	#1	#2
HERC6	4.49	3.61	21.78	21.27	3.32	1.56
IFI35	31.38	17.03	141.94	130.35	17.60	18.57
IFI44	9.43	8.77	127.44	110.95	5.35	2.30
IFI44L	0.10	0.09	31.56	24.25	0.00	0.00
IFI6	43.78	38.08	758.43	409.52	8.77	14.59
IFIT1	13.46	13.98	141.94	121.02	18.46	8.17
IFIT3	36.17	36.70	121.07	121.73	20.32	17.60
IFITM1	232.70	173.10	478.44	414.74	49.86	295.20
LAMP3	3.06	3.92	11.60	9.94	3.87	3.09
LGALS3BP	132.93	119.13	367.33	334.67	107.54	120.59
MX1	14.90	9.35	310.43	242.32	2.38	1.61
MX2	3.65	2.81	83.37	55.98	0.53	0.54
OAS1	49.19	46.94	175.29	164.83	13.38	22.80
OAS3	58.60	52.72	230.60	223.30	59.22	42.95
OASL	18.29	27.18	55.90	65.06	14.17	11.49
PLSCR1	55.92	47.67	105.25	100.17	13.58	22.44
STAT1	45.17	40.59	265.54	256.62	31.23	31.21
USP18	1.46	1.40	31.96	24.73	1.37	1.14

Supplementary Table 3. Tumor size of sub-cutaneous injected Du145-shCon and Du145-shIFIT5 lines.

Cell number	1X10^6		1X10^4		1X10^2	
	shCon	shIFIT5	shCon	shIFIT5	shCon	shIFIT5
Tumor size (mm^3)	466.80	65.40	143.60	49.40	190.40	0.00
	296.50	33.50	128.10	49.40	98.10	0.00
	222.30	26.20	125.50	33.50	71.90	0.00
	205.90	25.10	94.10	26.20	47.70	0.00
	147.10	25.10	65.40	25.10	0.00	0.00
	110.50	16.70	65.40	16.70	0.00	0.00
	87.00	14.10	65.40	14.10	0.00	0.00
	65.40	0.00	63.30	0.00	0.00	0.00
Average (mm^3)	200.18±132.41	25.76±18.95	93.85±33.83	26.80±17.12	51.01±68.14	0.00±0.00
P value	0.003620		0.000240		0.026303	

Supplementary Table 4. Tumor weight of sub-cutaneous injected Du145-shCon and Du145-shIFIT5 lines.

Cell number	1X10^6		1X10^4		1X10^2	
	shCon	shIFIT5	shCon	shIFIT5	shCon	shIFIT5
Tumor weight (g)	0.75	0.10	0.48	0.09	0.16	0.00
	0.68	0.09	0.43	0.08	0.08	0.00
	0.67	0.08	0.32	0.06	0.05	0.00
	0.61	0.07	0.25	0.03	0.03	0.00
	0.28	0.04	0.14	0.03	0.00	0.00
	0.26	0.03	0.13	0.03	0.00	0.00
	0.21	0.02	0.12	0.02	0.00	0.00
	0.14	0.00	0.06	0.00	0.00	0.00
Average (g)	0.45±0.25	0.06±0.03	0.24±0.16	0.05±0.03	0.08±0.06	0.00±0.00
P value	0.001522		0.005140		0.040319	

Published OnlineFirst November 30, 2018; DOI: 10.1158/0008-5472.CAN-18-2207

Molecular Cell Biology

Cancer Research

IFNγ-Induced IFIT5 Promotes Epithelial-to-Mesenchymal Transition in Prostate Cancer via miRNA Processing

U-Ging Lo[1], Rey-Chen Pong[1], Diane Yang[1], Leah Gandee[1], Elizabeth Hernandez[1], Andrew Dang[1], Chung-Jung Lin[1], John Santoyo[1], Shihong Ma[1], Rajni Sonavane[1], Jun Huang[2], Shu-Fen Tseng[3], Loredana Moro[4], Arnaldo A. Arbini[5], Payal Kapur[6], Ganesh V. Raj[1], Dalin He[2], Chih-Ho Lai[7], Ho Lin[8], and Jer-Tsong Hsieh[1,9]

Abstract

IFNγ, a potent cytokine known to modulate tumor immunity and tumoricidal effects, is highly elevated in patients with prostate cancer after radiation. In this study, we demonstrate that IFNγ can induce epithelial-to-mesenchymal transition (EMT) in prostate cancer cells via the JAK–STAT signaling pathway, leading to the transcription of IFN-stimulated genes (ISG) such as IFN-induced tetratricopeptide repeat 5 (IFIT5). We unveil a new function of IFIT5 complex in degrading precursor miRNAs (pre-miRNA) that includes pre-miR-363 from the miR-106a-363 cluster as well as pre-miR-101 and pre-miR-128, who share a similar 5′-end structure with pre-miR-363. These suppressive miRNAs exerted a similar function by targeting EMT transcription factors in prostate cancer cells. Depletion of IFIT5 decreased IFNγ-induced cell invasiveness *in vitro* and lung metastasis *in vivo*. IFIT5 was highly elevated in high-grade prostate cancer and its expression inversely correlated with these suppressive miRNAs. Altogether, this study unveils a pro-metastatic role of the IFNγ pathway via a new mechanism of action, which raises concerns about its clinical application.

Significance: A unique IFIT5–XRN1 complex involved in the turnover of specific tumor suppressive microRNAs is the underlying mechanism of IFNγ-induced epithelial-to-mesenchymal transition in prostate cancer.

See related commentary by Liu and Gao, p. 1032

Introduction

IFNγ is first characterized as a cytokine associated with antivirus and antitumor activities during cell-mediated innate immune response (1, 2). Mechanistically, IFNs can activate JAK–STAT signaling pathway leading to the transcriptional activation of a variety of IFN-stimulated genes (ISG), resulting in diverse biologic responses (3). Among ISGs, IFN-induced tetratricopeptide repeat (IFIT) family members are highly inducible. They are viral RNA-binding proteins (4) and a part of antiviral defense mechanisms. Among IFIT orthologs, human IFIT1, IFIT2, and IFIT3 form a complex through the tetratricopeptide repeats (TPR) to degrade viral RNA. However, the functional role of IFIT5 is not fully understood because it acts solely as a monomer that can not only bind directly to viral RNA molecules via its convoluted RNA-binding cleft, but also endogenous cellular RNAs with a 5′-end phosphate cap, including transfer RNAs (tRNA; refs. 5, 6). In this study, we demonstrate a new function of IFIT5 in regulating miRNAs turnover.

miRNAs regulate approximately 60% of protein-coding genes via posttranscriptional suppression, mRNA degradation, or translation inhibition (7, 8). Many miRNAs associated with different stages of tumor development are regulated at transcriptional or posttranscriptional level (9). Unlike most eukaryotic protein genes, several miRNAs such as miR-106a-363 (10) and miR-17-92 are clustered together to generate a polycistronic primary transcript (11–13), which implies a complicated regulation of miRNA biogenesis. For example, miR-363 belongs to the polycistronic miR-106a-363 cluster containing six miRNAs. Unlike the other five miRNAs with similar seed sequences and functions as the oncogenic miR-17-92 cluster (14), the seed sequence of miR-363 is distinct from the rest of miRNAs, suggesting different function. Indeed, based on the specific interaction with IFIT5, miR-363 biogenesis is mediated by miRNA turnover, which appears to be a new function of IFIT5.

[1]Department of Urology, University of Texas Southwestern Medical Center, Dallas, Texas. [2]Department of Urology, The First Affiliated Hospital, Medical School of Xi'an Jiaotong University, Xi'an China. [3]Department of Bioengineering, University of Texas at Arlington, Arlington, Texas. [4]Institute of Biomembranes, Bioenergetics and Molecular Biotechnologies, National Research Council, Bari, Italy. [5]Department of Pathology, NYU Langone Medical Center, New York, New York. [6]Department of Pathology, University of Texas Southwestern Medical Center, Dallas, Texas. [7]Department of Microbiology and Immunology, Graduate Institute of Biomedical Sciences, College of Medicine, Chang Gung University, Taoyuan, Taiwan. [8]Department of Life Sciences, National Chung Hsing University, Taichung, Taiwan. [9]Department of Biotechnology, Kaohsiung Medical University, Kaohsiung, Taiwan, Republic of China.

Note: Supplementary data for this article are available at Cancer Research Online (http://cancerres.aacrjournals.org/).

Corresponding Author: Jer-Tsong Hsieh, University of Texas Southwestern Medical Center, Harry Hines Blvd., Dallas, TX 75390. Phone: 214-648-3988; Fax: 214-648-8786; E-mail: jt.hsieh@utsouthwestern.edu

doi: 10.1158/0008-5472.CAN-18-2207

Published OnlineFirst November 30, 2018; DOI: 10.1158/0008-5472.CAN-18-2207

Based on the mechanism of IFIT5-elicied miR-363 degradation, additional miRNAs such as miR-101 and miR-128 are subjected to IFIT5 complex and target several epithelial-to-mesenchymal transition (EMT) transcriptional factors. Clinically, loss of these miRNAs is associated with tumor grade of prostate cancer, which is inversely correlated with elevated IFIT5 mRNA level. However, IFIT5 mRNA expression is correlated with ZEB1 and Slug mRNA expression in prostate cancer specimens. Taken together, IFIT5 regulated by IFNγ is involved in unique miRNA degradation that can promote EMT, leading to prostate cancer metastasis.

Materials and Methods

Cell lines

Cells were obtained from ATCC: LAPC4 in Iscove DMEM containing 10% FBS; RWPE-1 in keratinocyte medium containing 10% FBS; LNCaP and PC3 in RPMI1640 medium containing 10% FBS. All the DAB2IP-KD and control (Con) prostate cell lines (such as RWPE1, PC3, and LAPC4) were described previously (15). Stable IFIT5-knockdown (KD; shIFIT5) and control (shCon) prostatic cell lines were generated from PC3, LAPC4-KD, RWPE1-KD, and C4-2Neo cell lines using pLKO-shIFIT5. Stable IFIT5-overexpressing (IFIT5) and control (Vec) cell lines were generated from LAPC4-Con, RWPE1-Con, and C4-2D2 cell lines using pcDNA3.1-3XFlag-IFIT5 plasmid from Dr. Collins (5). All these cell lines were used within 20 passages and authenticated with the short tandem repeat (STR) profiling by Genomic Core in UT Southwestern (UTSW) periodically and *Mycoplasma* testing was performed by MycoAlert Kit (Lonza Walkersville Inc.) every quarterly to ensure *Mycoplasma*-free.

In vitro transcription of pre-miRNA and RNA pull-down assay

The PCR-amplified DNA fragment of T7- precursor-miRNAs (pre-miRNA; Supplementary Table S1) was separated by 2% agarose gel electrophoresis and purified using Mermaid SPIN Kit (MP Biomedicals) then subjected to *in vitro* transcription assay using T7 High Yield RNA Synthesis Kit (New England Biolabs). The pre-miRNA molecules were treated with DNase I for 15 minutes at 25°C and purified by acid phenol–chloroform extraction and ethanol precipitation at −20°C for 1 hour. The molecular size and sequence of each purified precursor miRNA was confirmed by gel electrophoresis using 15% TBE-Urea gel and qRT-PCR, respectively.

The *in vitro* transcribed pre-miRNA was subjected to RNA pull-down assay using Pierce Magnetic RNA-Protein Pull-Down Kit (ThermoScientific). An approximate 100 pmol of pre-miRNA were incubated with 10X RNA Ligase reaction buffer, RNase inhibitor, Biotinylated Cytidine Bisphosphate, and T4 RNA ligase at 16°C for 16 hours. The biotinylated pre-miRNA was then purified and incubated with streptavidin magnetic beads for 30 minutes at room temperature. Whole cell lysates (200 μg) were incubated with the biotinylated pre-miRNA beads at 4°C for 1 hour. After elution, proteins–pre-miRNA complex was separated by SDS-PAGE using Bolt 4% to 12% Bis-Tris Plus gel and stained with Coomassie blue then subjected to LC/MS-MS analysis. For identifying the interaction between mutant pre-miR-363s (SS6Mut, DSMut) and IFIT5 or miRNA processing machinery, the proteins–pre-miRNA complex was subjected to Western blot analysis and blotted by using primary antibodies against IFIT5, Dicer, or Drosha proteins.

In vitro pre-miRNA degradation assay

The *in vitro* transcribed pre-miRNAs were incubated with recombinant IFIT5 protein and/or XRN1 (New England Biolab) at 37°C, then the RNA-containing buffer were collected at indicated time points and subjected to 15% TBE-Urea gel electrophoresis. To quantify the degradation of precursor miRNA, the 15% TBE-Urea gel was then stained with GelRed Nucleic Acid Gel Stains (VWR) and visualized under UV light in the AlphaImager device (Protein Simple). The RNA bands were quantified by Multiplex band analysis (AlphaView Software) and the rate of degradation was calculated from each time point normalized to time zero.

Migration and invasion assay

Cells ($4–10 \times 10^4$) in the serum-free medium were plated on the upper chamber (8-μm pore size) of Transwell (Corning) with or without Matrigel for invasion or migration assay, respectively, whereas bottom chamber contained medium supplemented with 10% FBS. After 5 days, cells in the bottom chamber were fixed by 4% paraformaldehyde, stained, and visualized under microscope. Quantification of migratory cells was carried out with Crystal Violet staining and measurement at OD_{555nm}. Each experiment was performed in triplicates.

Animal model

All animal work was approved by the Institutional Animal Care and Use Committee from UTSW. Stable clones of PC3-shCon or -shIFIT5 were infected with luciferase lentivirus. One million PC3 cells pretreated with vehicle (PBS) or IFNγ (20 ng/mL, 48 hours) were resuspended in 50 μL PBS and then injected into the tail vein of male SCID mice, followed by intravenous injection of IFNγ (5 ng/mL,) weekly for 4 weeks. At eighth-week post-injection, lung metastasis of PC3 tumor was observed by bioluminescent imaging (BLI) using IVIS system then lungs were excised, fixed in 10% formalin, paraffin-embedded, and stained with hematoxylin and eosin for pathologic identification of tumor nodules presented in the lung parenchyma.

Clinical specimens and *ex vivo* culture of patient-derived prostate cancer explants

A total of 41 prostate cancer specimens obtained from UT Southwestern Tissue Bank were collected from 6-mm core punch from radical prostectomy and examined by pathologist to determine tumor grade then subjected to RNA extraction and 12 fresh prostate cancer tissues were obtained from men undergoing radical prostatectomy at UT Southwestern University Hospital.

The *ex vivo* culture was performed as previously described (16). Briefly, fresh prostate cancer tissue was dissected into 1 mm^3 cube and placed on a Gelatin sponge (Novartis) bathed in RPMI1640 media supplemented with 10% heat-inactivated FBS, 100 units/mL penicillin–streptomycin, 0.01 mg/mL hydrocortisone, and 0.01 mg/mL insulin (Sigma). In addition, to the media, was added either vehicle, IFNγ (25 ng/mL) or IFNγ (100 ng/mL). Tissues were cultured at 37 °C for 48 hours then snap-freeze in liquid nitrogen for RNA purification. The Institutional Review Board of UTSW approved the tissue procurement protocol for this study and written informed consent was obtained from all patients.

Published OnlineFirst November 30, 2018; DOI: 10.1158/0008-5472.CAN-18-2207

Statistical analysis

Statistics analyses were performed by using GraphPad Prism software. Statistical significance was evaluated using Student *t* test. $P < 0.05$ or $P < 0.0001$ was considered a significant difference between compared groups and marked with an asterisk. The statistical association between miR-363, miR-101, miR-128, and IFIT5 expression among different grades of human prostate cancer was evaluated with regression correlation analysis.

Results

The specific regulation of miR-363 expression

IFNγ is known to modulate cancer immunity and increase cytotoxicity. In addition, we observed that IFNγ was able to induce the expression of Slug and ZEB1, both are potent EMT transcription factors, in prostate cancer cell lines C4-2 (Fig. 1A) and PC3 cells (Supplementary Fig. S1A) in a dose-dependent manner. In contrast, Disabled homolog 2–interacting protein (DAB2IP) protein expression was reduced in treated cells (Fig. 1A; Supplementary Fig. S1A). We have previously identified DAB2IP as an EMT inhibitor in prostate cancer (15, 17). Thus, we believe that the mechanism of IFNγ-induced EMT is mediated through DAB2IP-regulated pathway. Because emerging evidence demonstrates a critical role of miRNA in EMT process, we decided to profile miRNA between DAB2IP-positive and -KD cells. From miRNA microarray screening (Supplementary Fig. S1B), a significant reduction of miR-363 (1176 folds decrease) was detected in DAB2IP-KD cells. The

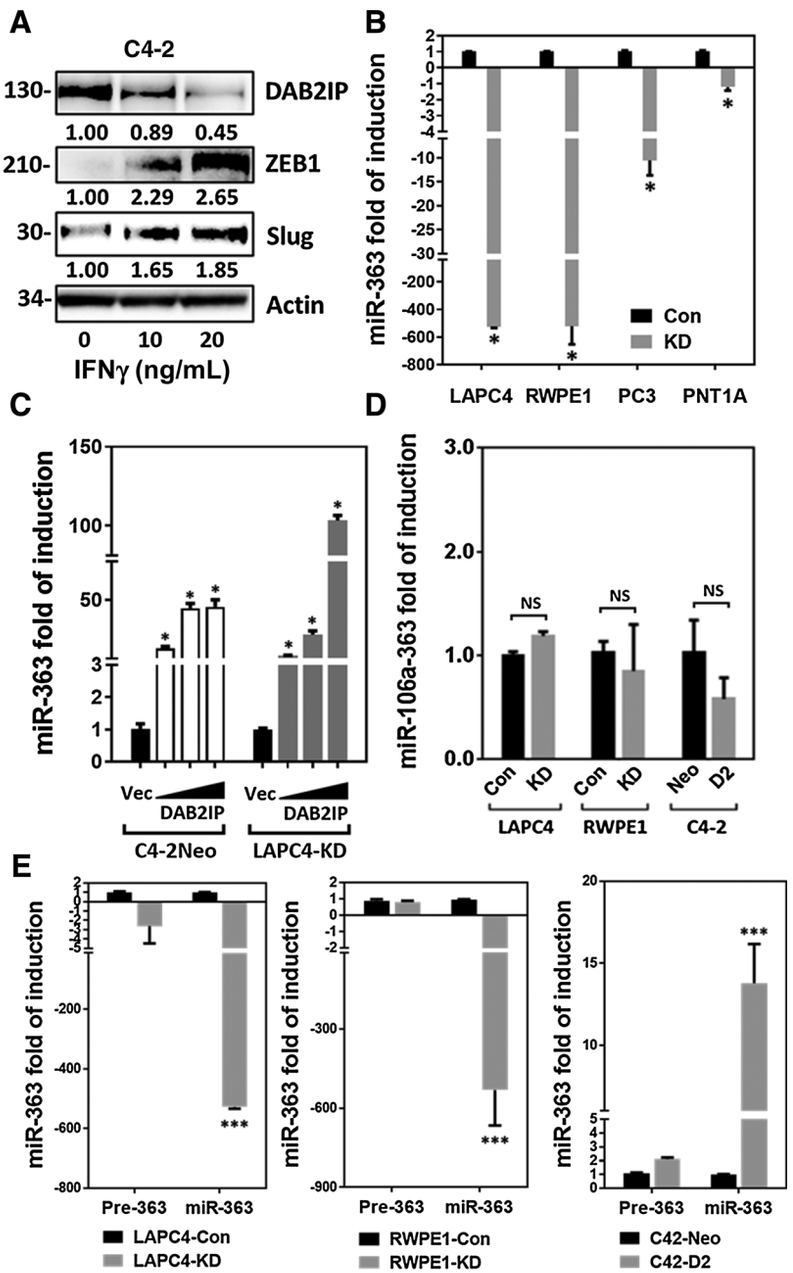

Figure 1.
The effect of DAB2IP on miR-363 expression in prostate cell lines. **A,** Induced expression of DAB2IP, ZEB1, and Slug protein level in C42 cells after treated with IFNγ for 48 hours. **B,** Expression levels of miR-363 in DAB2IP-KD prostate cell lines after normalizing to the Con cell of each cell line pair. *, $P < 0.05$. **C,** Induction of miR-363 by ectopic expression of DAB2IP in C4-2Neo and LAPC4-KD cell lines. Fold change of miR-363 levels were normalized to vector control. *, $P < 0.05$. **D,** Expression levels of primary miR-106a-363 in DAB2IP-positive and -negative sublines after normalizing to the Con cell of each cell line pair. NS, no significant differences. **E,** Expression levels of precursor miR-363 and mature miR-363 in DAB2IP-positive and -negative cells after normalizing to the control vector of each cell line pair. ***, $P < 0.0001$. Quantitative qRT-PCR data of miR-363 expression level were analyzed using ΔC_t (C_t value normalized to internal snord95 miRNAs) and $\Delta\Delta C_t$ (difference between the ΔC_t of control and each experimental group) values to obtain the fold change after normalizing with vector control.

Published OnlineFirst November 30, 2018; DOI: 10.1158/0008-5472.CAN-18-2207

downregulation of miR-363 in DAB2IP-KD cells was further validated in immortalized normal prostatic epithelial cell (RWPE1 and PNT1A) and prostate cancer lines (LAPC-4 and PC3; Fig. 1B). Ectopic expression of DAB2IP in C4-2Neo or LAPC4-KD cells (Fig. 1C) was able to induce mature miR-363 levels, indicating that DAB2IP could modulate miR-363 expression.

miR-363 is located in the polycistronic miR-106a-363 cluster that is first transcribed into a single primary miRNA containing the entire sequence of the cluster genes. We therefore examined

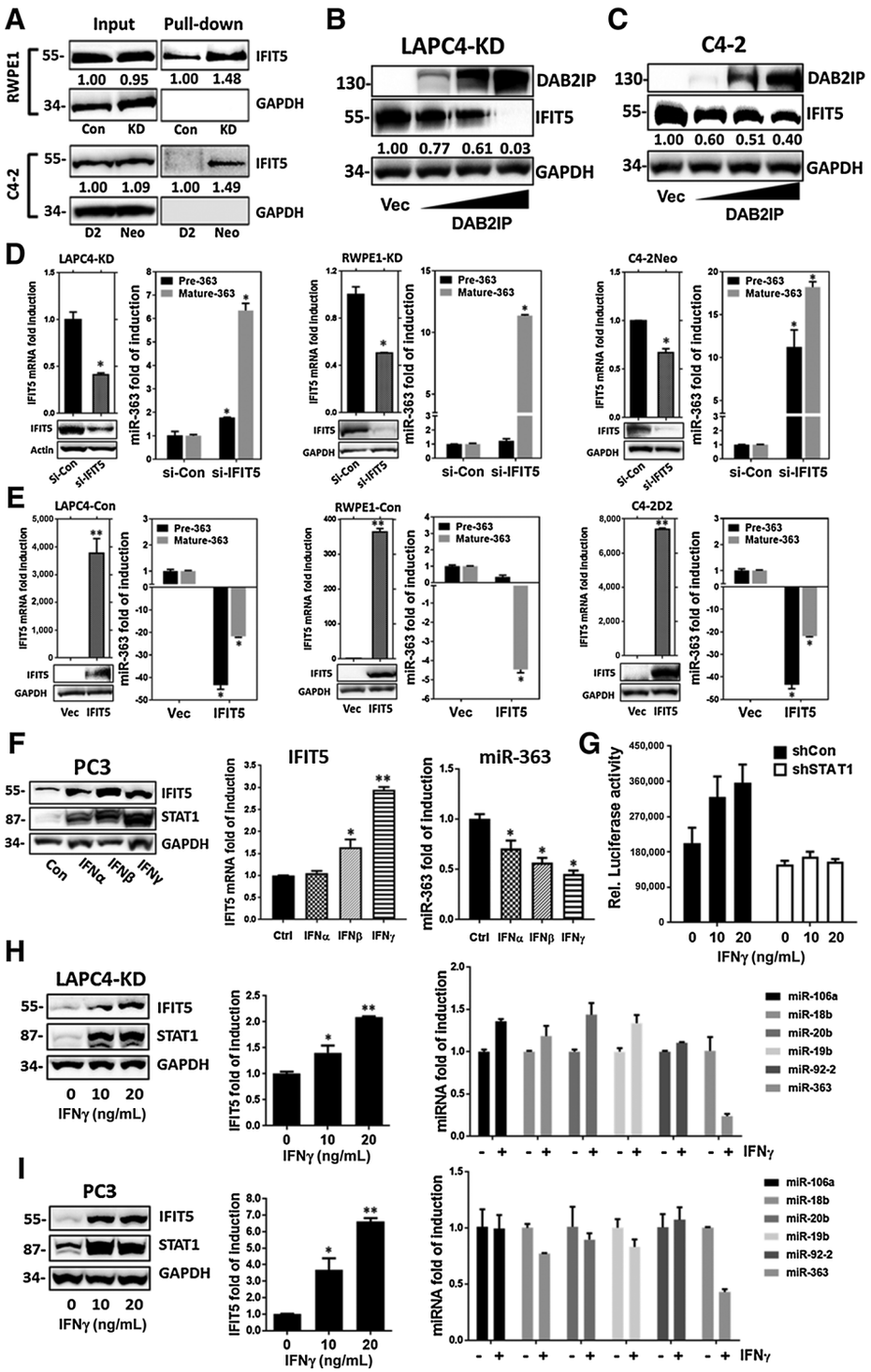

Figure 2.

The impact of IFIT5 on miR-363 maturation from the miR-106a-363 cluster. **A,** The interaction between IFIT5 protein and pre-miR-363 in DAB2IP-positive and -negative cells using RNA pull-down assay. **B** and **C,** Suppression of IFIT5 protein expression by ectopic transfecting DAB2IP into LAPC4-KD (**B**) and C4-2Neo (**C**) cells after normalizing with the control vector (Vec). **D,** Expression levels of precursor and mature miR-363 in IFIT5-siRNA KD (si-IFIT5) LAPC4-KD, RWPE1-KD, and C4-2Neo cells after normalizing to control siRNA (si-Con; *, $P < 0.05$). **E,** Expression levels of precursor and mature miR-363 in IFIT5-overexpressing (IFIT5) LAPC4-Con, RWPE1-Con, and C4-2D2 cells after normalizing to control vector (Vec; *, $P < 0.05$). **F,** Left and middle, induction of IFIT5 protein and mRNA level by IFNα, IFNβ, and IFNγ treatment for 48 hours in PC3 cells, compared with vehicle control. *, $P < 0.05$. Right, expression level of miR-363 in PC3 cells treated with IFNα, IFNβ, and IFNγ for 48 hours after normalizing to vehicle control. *, $P < 0.05$. **G,** IFNγ-induced IFIT5 promoter activity in PC3 cells with shRNA KD of STAT1 (shSTAT1), compared with control shRNA (shCon). Relative (Rel.) luciferase activity was normalized with protein concentration. **H** and **I,** Left and middle, dose-dependent induction of IFIT5 protein and mRNA level in LAPC4-KD and PC3 cells treated with IFNγ for 48 hours, compared with vehicle control. *, $P < 0.05$; **, $P < 0.0001$. Right, induction levels of mature miRNAs (miR-106a, miR-18b, miR-20b, miR-19b-2, miR-92a-2, and miR-363) in LAPC4-KD and PC3 cells treated with IFNγ (+, 20 ng/mL) for 48 hours, compared with vehicle control (−). *, $P < 0.05$. All quantitative data of IFIT5 mRNA or miRNA expression level were analyzed using ΔC_t (C_t value normalized to internal 18S RNA or snord95 miRNA) and $\Delta\Delta C_t$ (difference between the ΔC_t of control and experimental groups) values to obtain the fold change after normalizing with control group.

Published OnlineFirst November 30, 2018; DOI: 10.1158/0008-5472.CAN-18-2207

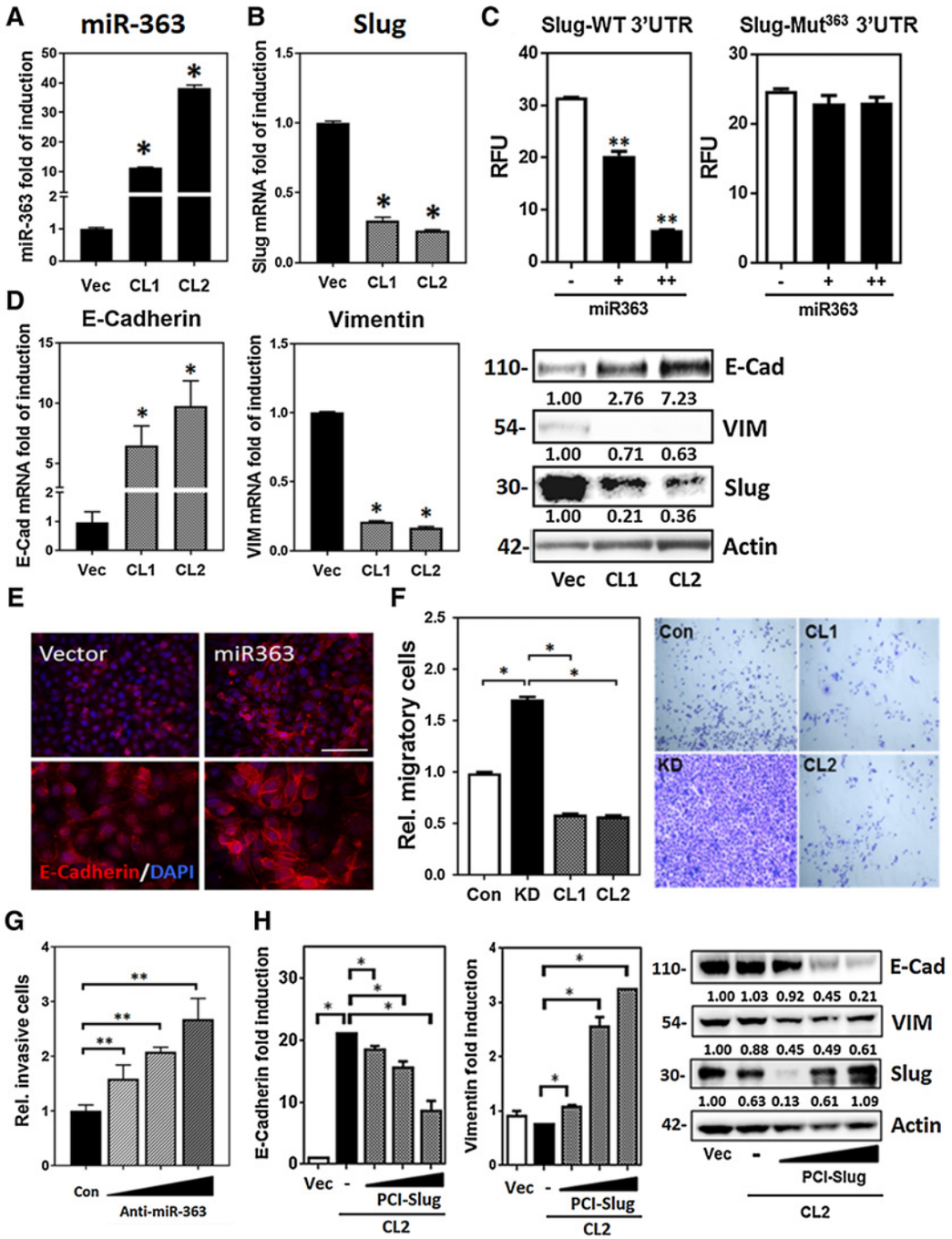

Figure 3.

The inhibitory effect of miR-363 on EMT by targeting Slug. **A,** Upregulation of miR-363 in RWPE1-KD cells transfected with pCMV-miR-363 plasmid after normalizing with vector control. *, $P < 0.05$. **B,** Reduction of Slug mRNA expression and protein level in miR-363–expressing RWPE1-KD cells after normalizing to vector control. *, $P < 0.05$. CL, stable clone of miR-363-expressing RWPE1-KD cells. **C,** Luciferase reporter assay in RWPE1-KD cells cotransfected with psiCHECK2-slug-WT 3′UTR or psiCHECK2-Slug Mut363 3′UTR and pCMV-miR363 or empty vector (−). Luciferase activity unit is plotted as *Renilla* to Firefly luciferase activity (RFU). Each bar represents mean ± SD of four replicated experiments. **, $P < 0.0001$. **D,** Induced mRNA and protein expression of E-cadherin, Slug, and vimentin in miR-363–expressing RWPE1-KD cells after normalizing to vector control. *, $P < 0.05$. **E,** Immunofluorescence staining of E-cadherin protein expression in miR-363–expressing RWPE1-KD cells, compared with vector control. **F,** Transwell migration assay in miR-363–expressing RWPE1-KD cells. Transmigrated RWPE1 cells were observed by crystal violet staining and quantified at OD 555 nm. Each bar represents mean ± SD of three replicated experiments. *, $P < 0.05$. **G,** Transwell invasion assay in RWPE1-Con transfected with different dose of anti-miR-363. Transmigrated cells were stained with crystal violet and quantified at OD 555 nm. Each bar represents mean ± SD of three replicated experiments. **, $P < 0.05$. **H,** E-cadherin and vimentin mRNA and protein expression level after restoration of slug in miR-363–expressing RWPE1-KD cells, compared with vector control (*, $P < 0.05$). All quantitative data of mRNA or miRNA expression level were analyzed using ΔC_t (C_t value normalized to internal 18S RNA or snord95 miRNA) and $\Delta\Delta C_t$ (difference between the ΔC_t of control vector and experimental groups) values to obtain the fold change after normalizing with vector control.

Published OnlineFirst November 30, 2018; DOI: 10.1158/0008-5472.CAN-18-2207

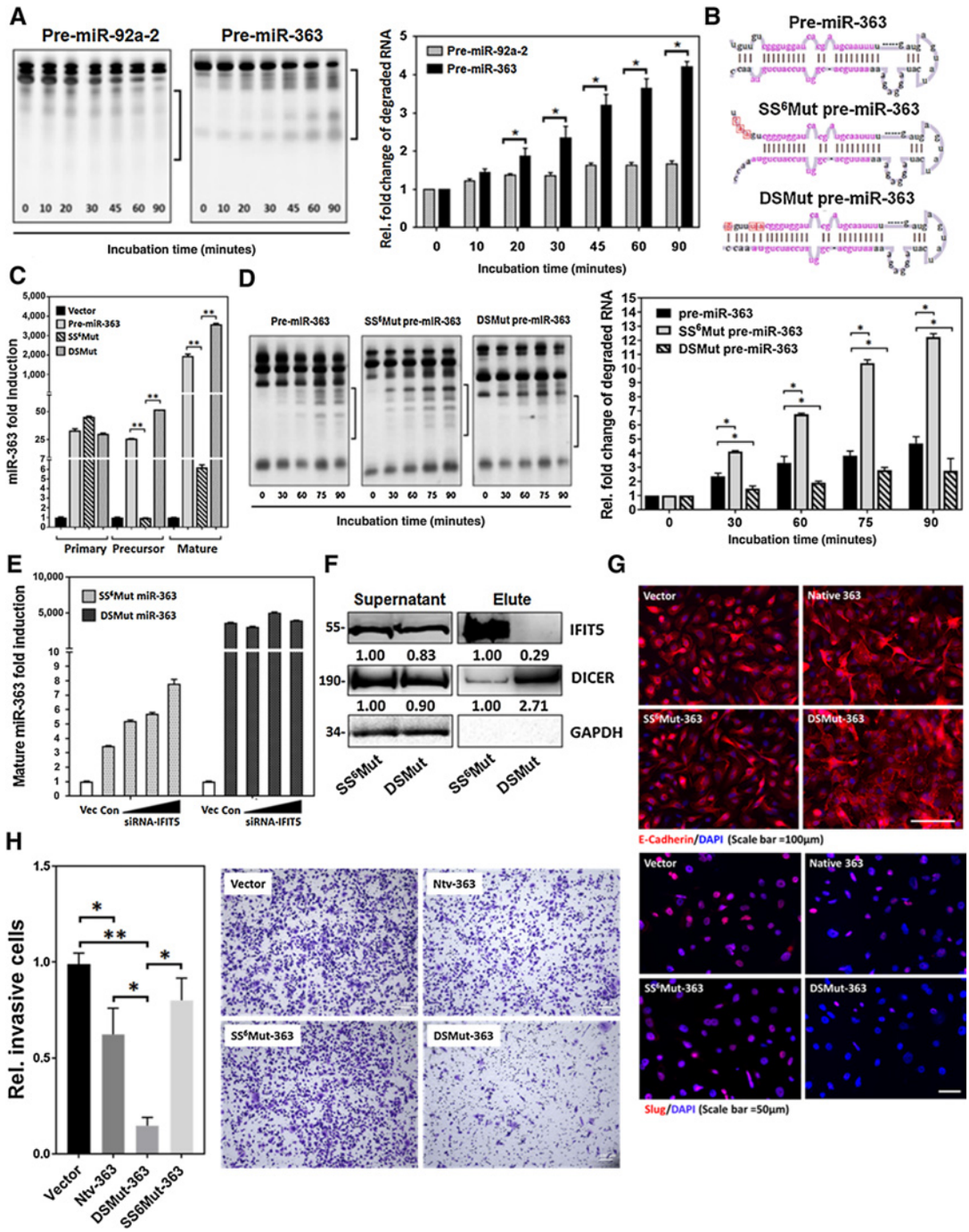

Figure 4.

The effect of IFIT5 on pre-miR-363 degradation *in vitro*. **A,** Time-dependent change of degraded pre-miR-92a-2 and pre-miR-363 fragments (bracket) after incubation with IFIT5 protein complex at 37°C normalized with 0 min. *, $P < 0.05$. **B,** Mutation of nucleotides (red box) for generating 5′-end six nucleotides single-stranded pre-miR-363 (SS6Mut pre-miR-363) and blunt 5′-end double stranded pre-miR-363 (DSMut pre-miR-363). Both mature miR-363 and miR-363* sequences are shown in pink. **C,** Expression levels of primary, precursor, and mature miR-363 in LAPC4-KD cells transfected with Native, SS6Mut, or DSMut pre-miR-363 plasmids for 24 hours after normalizing with the vector control. **D,** Time-dependent degradation of native, SS6Mut, and DSMut pre-miR-363 fragments (bracket) after incubation with IFIT5 protein at 37°C; each time point was normalized with 0 min. *, $P < 0.05$. **E,** Dose-dependent induction of mature miR-363 in cells transfected with SS6Mut pre-miR-363 or DSMut pre-miR-363 plasmids and IFIT5 siRNA after normalizing with the control vector (Vec). Con, control siRNA. **F,** Interaction between IFIT5 protein and SS6Mut or DSMut pre-miR-363 RNA molecules using RNA pull-down assay. **G,** Immunofluorescence staining of E-cadherin and Slug in mutant pre-miR-363–overexpressed RWPE1-KD cells, compared with vector control. **H,** The effect of Native, DSMut-, or SS6Mut-pre-miR-363 on cell invasion in PC3 cells. Cells invaded at the lower bottom at the Transwell were stained with crystal violet and counted. Each bar represents mean ± SD of nine fields of counted cell numbers. *, $P < 0.05$; **, $P < 0.0001$. All quantitative data of miR-363 expression level were analyzed using ΔC_t (C_t value normalized to internal snord95 miRNA) and $\Delta\Delta C_t$ (difference between the ΔCt of control vector and experimental groups) values to obtain the fold change after normalizing with vector control.

Published OnlineFirst November 30, 2018; DOI: 10.1158/0008-5472.CAN-18-2207

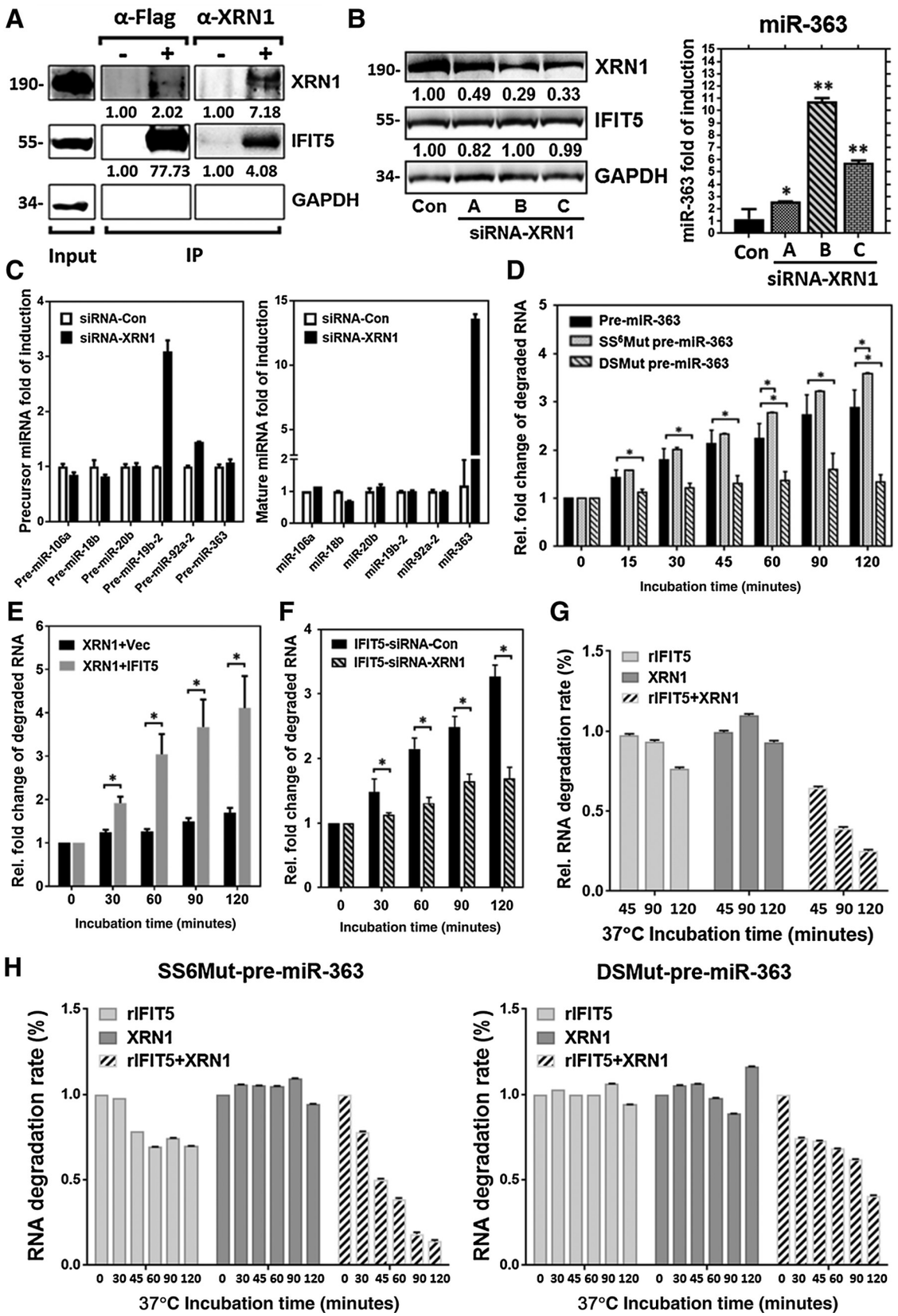

Published OnlineFirst November 30, 2018; DOI: 10.1158/0008-5472.CAN-18-2207

the effect of DAB2IP on the expression levels of primary transcript of miR-106a-363. In contrast to the significant downregulation of mature miR-363 in DAB2IP-KD cells, the expression levels of either primary miR-106a-363 (Fig. 1D) or pre-miR-363 (Fig. 1E) were similar between DAB2IP-positive and -KD cells. Noticeably, among the miRNA members in the miR-106a-363 cluster, only mature miR-363 levels dramatically decreased in DAB2IP-KD cells (i.e., LAPC4-KD and RWPE-1-KD; Fig. 1E; Supplementary Fig. S1C and S1D). However, only mature miR-363 levels increased significantly in C4-2D (Fig. 1E; Supplementary Fig. S1E) with ectopic expression of DAB2IP. These findings indicate that DAB2IP specifically regulates miR-363 maturation from the miR-106a-363 cluster.

Effect of IFIT5 on the biogenesis of miR-363

To elucidate the machinery responsible for miR-363 maturation process, the protein candidates were pulled down by synthetic pre-miR-363 RNA and subjected to LC/MS-MS analysis. IFIT5 (Supplementary Table S2) is consistently showing higher affinity with pre-miR-363 among all three DAB2IP-negative cell lines (LAPC-KD, RWPE1-KD, and C4-2Neo) when compared with DAB2IP-positive cell lines, LAPC4-Con, RWPE1-Con, and C4-2D2, respectively. Moreover, IFIT5 appeared to be a viral-RNA-binding protein, which match with our criteria while searching for a RNA-interacting protein as a potential candidate from the pre-miR-363 RNA pull-down results. The steady-state levels of IFIT5 mRNA and protein were inversely correlated with DAB2IP (Supplementary Fig. S2A). IFIT5 has not been shown to bind to miRNAs; therefore, the interaction between pre-miR-363 and IFIT5 was confirmed in DAB2IP-negative and -positive prostate cancer cell lines (Fig. 2A). This inhibitory effect of DAB2IP on IFIT5 expression was also demonstrated by the ectopic expression of DAB2IP in LAPC4-KD (Fig. 2B), C4-2 (Fig. 2C), and LNCaP cells (Supplementary Fig. S2B).

To determine the role of IFIT5 in miR-363 maturation, we used siRNA to KD IFIT5 in DAB2IP-negative cells. In LAPC4-KD cells treated with several IFIT5 small-interfering RNA (siRNA), the elevated levels of mature miR-363 were detected, which was inversely correlated with the reduction of the endogenous IFIT5 mRNA levels (Supplementary Fig. S2C). Because IFIT5-C siRNA exhibited high efficiency, this siRNA was further tested with RWPE1-KD cells and data showed a significant elevation of mature miR-363 (Supplementary Fig. S2D). Despite the significantly elevated mature miR-363 in IFIT5-siRNA KD cells (Fig. 2D; Supplementary Fig. S2E), the levels of mature miR-106a, miR-18b, miR-20b, miR-19b-2, miR-92a-2 remained relatively unchanged (Supplementary Fig. S2F). However, we ectopically expressed IFIT5 in DAB2IP-positive cells and observed a significant reduction of mature miR-363 levels but not other mature miRNAs from the same cluster (Fig. 2E; Supplementary Fig. S2G). Overall, our finding indicates that IFIT5 can specifically inhibit miR-363 maturation from the miR-106a-363 cluster.

Effect of IFNs on the biogenesis of miR-363 in prostate cancer cells

Knowing IFIT5 as a typical ISG, we further confirmed that all IFNs can induce IFIT5 in PC3 cells (Fig. 2F). Meanwhile, a significant reduction of miR-363 was observed under the same condition (Fig. 2F). Among three IFNs, the type II IFN, IFNγ, has the most potent effect on inducing IFIT5 mRNA and suppressing miR-363. We therefore, used IFNγ to examine its impact on IFIT5 downstream target miRNAs. We first identified that the induction of IFIT5 mRNA by IFNγ was the result of transcriptional activation mediated by STAT1 signaling using IFIT5 gene promoter construct (Fig. 2G). Moreover, a dose-dependent induction of IFIT5 protein and mRNA by IFNγ was detected in LAPC4-KD and PC3 cells (Fig. 2H and I) and significantly reduce mature miR-363 levels compared with other miRNAs in miR-106a-363 cluster (Fig. 2H and I). These data support a key mediator role of IFIT5 in IFNγ-mediated miR-363 suppression. Noticeably, the other member of IFIT family, such as IFIT1, was absent in PC3 cell after IFNγ treatment in contrast to RWPE1 cell (Supplementary Fig. S2H), implying IFIT5 plays a unique role in prostate cancer progression.

The functional role of miR-363 in EMT

Based on the predicted sequences and gene profiling, Slug/SNAI2 mRNA appears to be a potential target gene of miR-363. By transfecting miR-363 vector into DAB2IP-KD cells, the suppression of Slug/SNAI2 mRNA levels was detected in miR-363 expressing cells compared with controls (Fig. 3A and B; Supplementary Fig. S3A). Using both wild-type Slug/SNAI2 3′UTR (Slug-WT3′UTR) and mutant Slug/SNAI2 3′UTR (Slug-Mut^{363}3′UTR) luciferase reporter genes, a significant reduction of the Slug-WT3′UTR but not the Slug-Mut^{363}3′UTR activity was detected in RWPE-1-KD (Fig. 3C) and LAPC4-KD cells (Supplementary Fig. S3B).

Slug/SNAI2 is known to promote EMT by suppressing E-cadherin. As expected, an elevation of E-cadherin mRNA and protein was observed in miR-363 overexpressing RWPE1-KD (Fig. 3D and E) and LAPC4-KD cells (Supplementary Fig. S3C). In contrast, vimentin, a mesenchymal marker, was suppressed (Fig. 3D; Supplementary Fig. S3C). Functionally, ectopic expression of miR-363 was able to reduce cell migration in RWPE1-KD (Fig. 3F) and LAPC4-KD cells (Supplementary Fig. S3D). Noticeably, cells collected from the bottom chamber of a

Figure 5.

Interaction between XRN1 with IFIT5 leading to pre-miR-363 degradation *in vitro*. **A,** Interaction between IFIT5 and XRN1 proteins using immunoprecipitation by Flag and XRN1 antibodies, respectively. **B,** Left, KD of XRN1 in LAPC4-KD cells using siRNA. Right, induction of mature miR-363 in LAPC4-KD cells transfected with XRN1 siRNA after normalizing with the control siRNA (Con). *, $P < 0.05$; **, $P < 0.0001$. **C,** Expression levels of precursor and mature miRNAs (miR-106a, miR-18b, miR-20b, miR-19b-2, miR-92a-2, and miR-363) in XRN1-KD (siRNA-XRN1) LAPC4-KD cells after normalizing with the control siRNA (siRNA-Con). **D,** Time-dependent change of degraded native, SS6Mut, and DSMut pre-miR-363 fragments after incubation with immunoprecipitated XRN1 protein at 37°C after normalizing with 0 minute. *, $P < 0.05$. **E,** Time-dependent change of degraded SS6Mut pre-miR-363 fragments after incubation with immunoprecipitated XRN1 alone (XRN1+Vec) or XRN1-IFIT5 complex (XRN1+IFIT5) at 37°C after normalizing with 0 minute. *, $P < 0.05$. **F,** Time-dependent change of degraded SS6Mut pre-miR-363 after incubation with the immunocomplex derived from cells transfected with IFIT5 and control siRNA (IFIT5+siRNA-Con) or XRN1 siRNA (IFIT5+siRNA-XRN1) at 37°C after normalizing with 0 minute. *, $P < 0.05$. **G,** Degradation of native pre-miR-363 after incubation with recombinant IFIT5 protein (rIFIT5), XRN1 enzyme (XRN1), or combination of XRN1 and rIFIT5 at 37°C after normalizing with 0 minute. **H,** Degradation of SS6Mut- or DSMut-pre-miR-363 after incubation with rIFIT5, XRN1, or combination of XRN1 and rIFIT5 at 37°C after normalizing with 0 minute. Quantitative data of miR-363 expression level were analyzed using ΔC_t (C_t value normalized to internal snord95 miRNA) and $\Delta\Delta C_t$ (difference between the ΔC_t of control vector and experimental groups) values to obtain the fold change after normalizing with vector control.

Published OnlineFirst November 30, 2018; DOI: 10.1158/0008-5472.CAN-18-2207

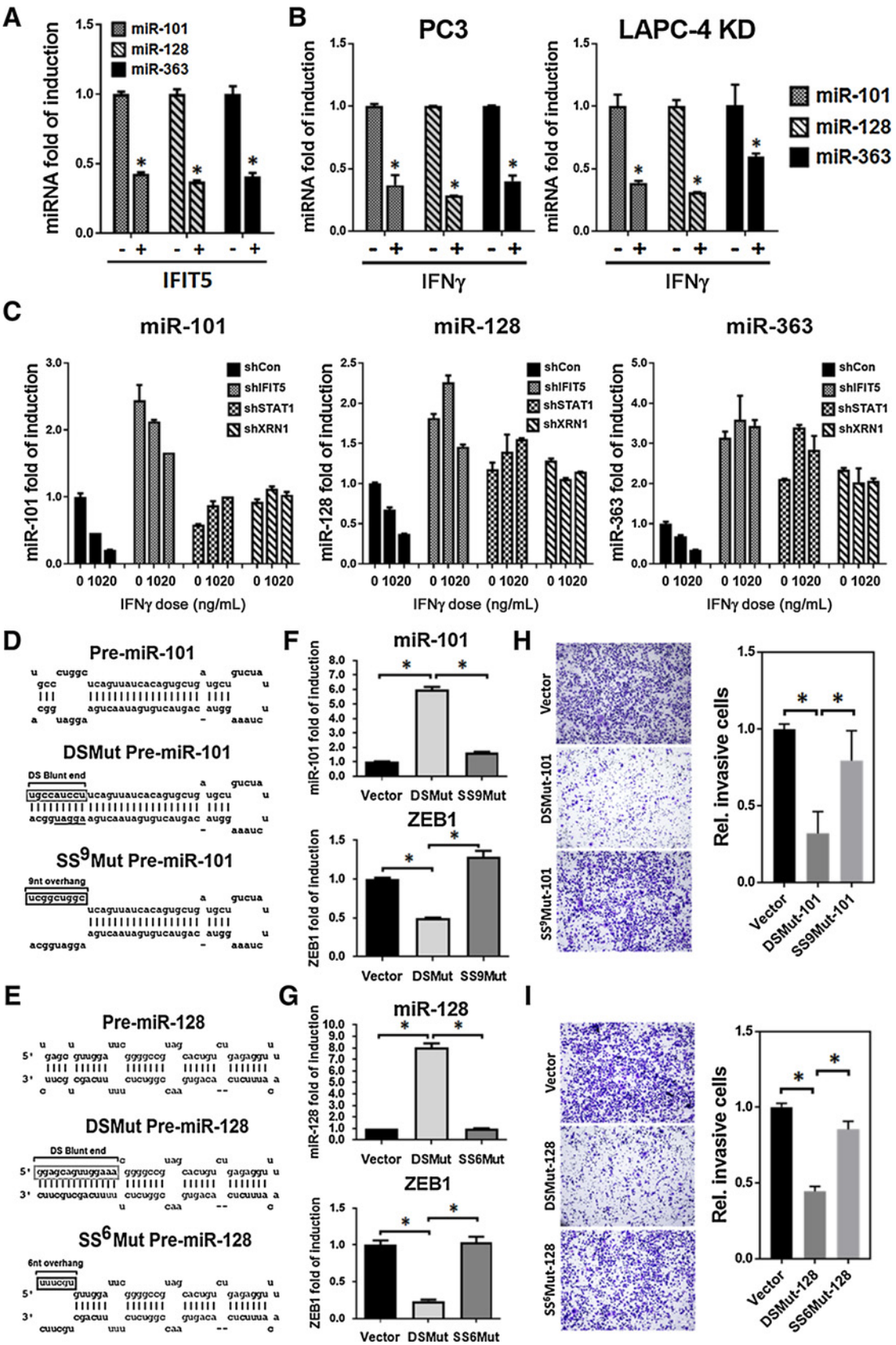

Transwell exhibited lower miR-363 levels than those from the upper chamber (Supplementary Fig. S3D). In contrast, inhibition of miR-363 in RWPE1-Con (Fig. 3G), Du145, and C4-2 cells (Supplementary Fig. S3E) increased cell invasion and migration, respectively. Moreover, restored Slug/SNAI2 levels in miR-363–expressing cells were resulted in a dose-dependent reduction of E-cadherin and elevation in vimentin in RWPE1-KD (Fig. 3H) and LAPC4-KD cells (Supplementary Fig. S3F). These data indicate that miR-363 can suppress EMT by targeting Slug in prostate cancer.

The mechanism of IFIT5 on miR-363 turnover at precursor level

IFIT5 has been suggested to suppress virus replication by targeting the 5′-phosphate end of single-stranded viral RNAs for rapid turnover (6). Thus, we examined whether IFIT5 has a direct impact on the stability of pre-miR-363. In fact, pre-miR-363 RNA prepared from *in vitro* transcription was relatively stable at 37°C (Supplementary Fig. S4A) but quickly degraded in the presence of IFIT5 protein complex (Supplementary Fig. S4A), indicating that the degradation of pre-miR-363 is accelerated by the IFIT5 protein complex. To examine the specificity of IFIT5 in the acceleration of pre-miR-363 degradation, we found no significant change for *in vitro* degradation rate of pre-miR-92a-2 (immediate adjacent to miR-363) under the same condition (Fig. 4A). Previous studies (4, 5) indicate that IFIT5 protein binds to viral RNA molecules at either 5′-phosphate cap or 5′-tri-phosphate group. By comparing the 5′-end structure between pre-miR-92a-2 and pre-miR-363, we hypothesized that a single nucleotide (uracil) overhang in pre-miR-363, in contrast to the double-stranded blunt end in pre-miR-92a-2, is critical for IFIT5 recognition. Therefore, we generated two mutant pre-miR-363 constructs: one with 5′-end six nucleotides single-stranded overhang (SS^6Mut) and the other with double-stranded blunt end (DSMut; Fig. 4B) to test their stabilities. The *in vivo* result (Fig. 4C; Supplementary Fig. S4B) indicated that the expression levels of pre-miR363 or mature miR-363 derived from SS^6Mut were significantly lower than those from native or DSMut form (Fig. 4C; Supplementary Fig. S4B), indicating that the 5′-end structure of pre-miR-363 dictates the stability of miR-363 maturation. By determining the *in vitro* degradation rates of native, pre-SS^6Mut- and pre-DSMut -miR-363 RNA molecules, as we expected, pre-SS^6Mut-miR-363 was very sensitive to IFIT5 whereas pre-DSMut-miR-363 was the most resistant one (Fig. 4D). Furthermore, we observed a steady elevation of SS^6Mut -derived mature miR-363 level in a dose-dependent manner in the presence of an incremental IFIT5 siRNA, whereas the expression of mature DSMut-miR-363 was not impacted by IFIT5 siRNA (Fig. 4E). Meanwhile, using RNA pull-down assay, pre-SS^6Mut-miR-363 exhibited higher affinity to IFIT5 protein than pre-DSMut -miR-363 (Fig. 4F). Noticeably, the biogenesis of these artificial constructs is similar to native one (Fig. 4C; Supplementary Fig. S4B). As expected, all these precursor constructs exhibited low binding affinity to Drosha (Supplementary Fig. S4C), compared with the primary transcript containing both miR-92a-2 and miR-363 (Pri-92a-2+363). However, pre-DSMut-miR-363 exhibited the highest binding affinity to DICER among native and pre-SS^6Mut-miR-363 (Supplementary Fig. S4C), suggesting IFIT5 could prevent Dicer from binding to pre-miR-363. Knowing the high stability of pre-DSMut-miR-363 *in vivo*, it exhibited more potent effect on inhibiting EMT (Supplementary Fig. S4D) evidenced by elevated E-cadherin and reduced Slug protein expression in RWPE1 (Fig. 4G) and PC3 cells (Supplementary Fig. S4E). Also, DSMut exhibited a greater impact on diminishing PC3 and LAPC4-KD cell invasion (Fig. 4H; Supplementary Fig. S4F) and migration (Supplementary Fig. S4F). These data conclude that IFIT5 recognizes the unique 5′-end overhanging structure of pre-miR-363 for its degradation.

To further demonstrate the specificity of this unique 5′-end structure of pre-miRNA, we also generated a mutant construct of pre-miR-92a-2 with single nucleotide at 5′-overhang (SS^1Mut pre-miR-92a-2; Supplementary Fig. S4G), which is similar to the 5′-end of pre-miR-363 (Fig. 4B). Using RNA pull-down assay, we observed an increased interaction between SS^1Mut pre-miR-92a-2 and IFIT5 protein, compared with native pre-miR-92a-2 (Supplementary Fig. S4G). Moreover, the degradation rate of pre-SS^1Mut-miR-92a-2 increased in the presence of IFIT5 complex, compared with that of pre-miR-92a-2 (Supplementary Fig. S4H). Thus, the 5′-end overhanging structure of pre-miRNAs dictates IFIT5-elicited miRNA turnover.

The role of XRN1 in IFIT5-mediated miR-363 turnover

Although IFIT5 can elicit miR-363 turnover, IFIT5 does not possess ribonuclease activity. To determine whether a ribonuclease is associated with the IFIT5–pre-miR-363 complex, we further examined LC/MS-MS results derived from pre-miR-363 pull-down protein candidates and identified an exoribonuclease candidate-XRN1. XRN1 is known to regulate mRNA stability via cleavage of de-capped 5′-monophosphorylated mRNA (18, 19) and a recent study also implied its potential role in miRNA turnover (20). Indeed, an interaction was observed between IFIT5 and XRN1 protein in LAPC4-Con cells transfected with Flag-tagged IFIT5 (Fig. 5A). Meanwhile, an interaction between endogenous IFIT5 and XRN1 protein is also observed in PC3 cells

Figure 6.

The impact of IFIT5–XRN1 on pre-miRNA degradation and EMT of prostate cancer cells. **A,** Expression level of mature miR-101, miR-128, and miR-363 in IFIT5-overexpressed (+) PC3 cells, compared with vector control (−) *, $P < 0.05$. **B,** Expression level of miR-101, miR-128, and miR-363 in PC3 and LAPC4-KD cells treated with IFNγ (+), compared with control vector (−) *, $P < 0.05$. **C,** Expression level of miR-101, miR-128, and miR-363 in PC3 cells treated with IFNγ after KD of IFIT5 (shIFIT5), STAT1 (shSTAT1), or XRN1 (shXRN1), compared with vector control (shCon). **D,** Mutation of nucleotides (box) for generating blunt 5′-end double-stranded pre-miR-101 (DSMut pre-miR-101) and 5′-end nine nucleotides single-stranded pre-miR-101 (SS9Mut pre-miR-101). Gray, mature miR-101 and miR-101* sequence. **E,** Mutation of nucleotides (box) for generating blunt 5′-end double-stranded pre-miR-128 (DSMut pre-miR-128) and 5′-end six nucleotides single-stranded pre-miR-128 (SS6Mut pre-miR-128). Gray, mature miR-128 and miR-128* sequence. **F,** The effect of DSMut or SS9Mut pre-miR-101 on the expression level of mature miR-101 and ZEB1 mRNA (*, $P < 0.05$) after normalizing to vector control. **G,** The effect of DSMut or SS6Mut pre-miR-128 on the expression level of mature miR-128 and ZEB1 mRNA. *, $P < 0.05$. **H,** The effect of DSMut or SS9Mut pre-miR-101 on the cell invasion in PC3 cells. Cells invaded at the lower bottom at the Transwell were stained with crystal violet and counted. Each bar represents mean ± SD of nine fields of counted cell numbers. *, $P < 0.05$. **I,** The effect of DSMut or SS6Mut pre-miR-128 on the cell invasion in PC3 cells. Cells invaded at the lower bottom at the Transwell were stained with crystal violet and counted. Each bar represents mean ± SD of nine fields of counted cell numbers. *, $P < 0.05$. All quantitative data of miRNA or mRNA expression level were analyzed using ΔC_t (C_t value normalized to internal snord95 miRNA or 18S RNA) and $\Delta\Delta C_t$ (difference between the ΔC_t of control and experimental groups) values to obtain the fold change after normalizing with control.

Published OnlineFirst November 30, 2018; DOI: 10.1158/0008-5472.CAN-18-2207

(Supplementary Fig. S5A). Also, the expression levels of miR-363 were correlated with the diminished level of XRN1 protein (Fig. 5B; Supplementary Fig. S5B). Similar to IFIT5-KD, data from XRN1-KD cells clearly demonstrated that only mature miR-363 exhibited a significant accumulation whereas the levels of other mature miRNAs (miR-106a, miR-18b, miR-20b, miR-19b-2, and miR-92a-2) remained relatively unchanged (Fig. 5C). By incubating XRN1 immunocomplex (Supplementary Fig. S5C) with native, SS^{6}Mut or DSMut pre-miR-363 RNA *in vitro*, a significantly increased degradation of both native and pre-SS^{6}Mut-miR-363 was detected in a time-dependent manner, whereas pre-DSMut-miR-363 levels remained relatively unchanged (Fig. 5D; Supplementary Fig. S5C), implying that the IFIT5 binding structure in the 5′-end of pre-miR-363 is critical for recruiting XRN1. In addition, by increasing IFIT5 expression in XRN1-positive LAPC4-Con cells, XRN1–IFIT5 immunocomplex apparently increased the *in vitro* degradation of SS^{6}Mut-pre-miR-363 compared with control (XRN1 alone; Fig. 5E; Supplementary Fig. S5D). However, knocking down XRN1 in IFIT5-overexpressing LAPC4-Con cells diminished the *in vitro* degradation rate of pre-SS^{6}Mut-miR-363 after incubation with IFIT5 (Fig. 5F; Supplementary Fig. S5E). These findings provide further evidence for the specific function of IFIT5–XRN1 complex in miR-363 turnover. In addition, using recombinant IFIT5 protein with or without XRN1 enzyme, the result (Fig. 5G; Supplementary Fig. S5F) clearly indicated that both IFIT5 and XRN1 proteins are required to degrade pre-miR-363 transcript *in vitro*. Similarly, the pre-SS^{6}Mut-miR-363 is more sensitive to rIFIT5–XRN1 complex-mediated degradation than pre-DSMut-miR-363 (Fig. 5H; Supplementary Fig. S5G). Overall, these data demonstrate that the IFIT5–XRN1 complex is responsible for the degradation of pre-miR-363.

The effect of IFNγ on miR-101, miR-128, and miR-363 processing mediated by IFIT5

To survey additional miRNAs subjected to IFIT5-mediated precursor miRNA degradation, we performed miRNA microarray screening in IFIT5-overexpressing LAPC4-Con and IFIT5-siRNA KD LAPC4-KD cells (Supplementary Table S3). In particular, among IFIT5-regulated miRNA candidates, both miR-101 and miR-128 appear to have 5′-end single nucleotide overhang structure similar to the pre-miR-363 (Supplementary Table S3) and exhibit tumor suppressor function. We further confirmed that the presence of IFIT5 reduced the expression of mature miR-101 and miR-128 as well as miR-363 in PC3 cell line (Fig. 6A). In contrast, IFIT5-KD in LAPC4-KD cells increased the expression of all three miRNAs (Supplementary Fig. S6A). Also, XRN1 KD in IFIT5-expressing cells could rescue the expression levels of mature miR-363, miR-101 and miR-128 (Supplementary Fig. S6B), indicating the requirement of XRN1 in IFIT5 complex in degrading these miRNAs. Similarly, IFNγ treatment resulted in reducing the expression of miR-101, miR-128, and miR-363 (Fig. 6B). This inhibitory effect of IFNγ can be reversed or diminished by knocking down IFIT5, STAT1, or XRN1 (Fig. 6C). Similarly, overexpression of DAB2IP in PC3 cells also diminished the inhibitory effect of IFNγ on the suppression of miR-101, miR-128, and miR-363 level (Supplementary Fig. S6C), supporting the key role of IFIT5 in IFNγ-elicited precursor miRNAs processing. Based on the 3′UTR sequence, ZEB1 mRNA was predicted as a common target for both miR-101 and miR-128 (Supplementary Fig. S6D), and the results indeed indicated that both miR-101 and miR-128 could suppress ZEB1 mRNA levels (Supplementary Fig. S6D).

By comparing the precursor structures of miR-101 and miR-128, it appeared that both pre-miR-101 and pre-miR-128 have similar 5′-end structure with pre-miR-363 (Supplementary Table S3), we therefore generated two mutant constructs: one with 5′-end single stranded overhang (SSMut) and the other with double-stranded blunt end (DSMut; Fig. 6D and E) to test their expression in IFIT5-expressing PC3 and LAPC4-KD cell lines. As we expected, DSMuts were resistant to IFIT5-elicited miRNA degradation and resulted in elevated expression of mature miRNA in PC3 (Fig. 6F and G) and LAPC4-KD cells (Supplementary Fig. S6E and S6F). Again, DSMuts appeared to degrade ZEB1 more efficiently in PC3 (Fig. 6F and G) and LAPC4-KD cells (Supplementary Fig. S6E and S6F), which are correlated with the suppression of cell invasion in PC3 cells (Fig. 6H and I) and cell migration in LAPC4-KD cells (Supplementary Fig. S6E and S6F). Overall, the effect of IFIT5–XRN1 complex on pre-miR-101/128/363 processing is unique with respect to the similar 5′-end overhang structure.

Effect of IFNγ on EMT mediated by IFIT5

Based on the mechanism of action of IFIT5–XRN1 complex in the degradation of miRNAs that can target EMT factors, we further examined whether IFNγ could elicit EMT by suppressing these miRNAs via STAT1 signal axis and its downstream effector–IFIT5/XRN1 complex. Indeed, IFNγ treatment increased the PC3 cell invasion (Fig. 7A) and migration (Supplementary Fig. S7A) that was diminished in the absence of STAT1 or IFIT5 (Fig. 7A; Supplementary Fig. S7A), which is consistent with the expression of EMT factors (Slug and ZEB1) or decrease in the mesenchymal marker (vimentin) or increase in the epithelial marker (E-cadherin; Fig. 7B and C). As we expected, the expression of all these three miRNAs was inhibited by IFNγ in a dose-dependent manner (Fig. 6C) and IFNγ failed to suppress the expression of these miRNAs in the absence of XRN1, STAT1, or IFIT5 (Fig. 6C) in which no induction of Slug and ZEB1 mRNA was detected (Fig. 7D). Similarly, the effect of IFNγ on Slug and ZEB1 mRNA induction can be diminished in cells transiently transfected with miR-101, miR-128, or miR-363 (Supplementary Fig. S7B).

Apparently, IFNγ is capable of inducing EMT at low concentrations that are not antitumorigenic or antiproliferation (Supplementary Fig. S7C); its direct antitumor activity is known at much higher concentration (>1,000 ng/mL; ref. 21). These data provide new evidence that IFNγ is a potent inducer of EMT via STAT1–IFIT5/XRN1 signal axis of miRNA regulation.

The clinical correlation of IFIT5, miRNAs, and EMT biomarkers in prostate cancer

To examine the *in vivo* effect of IFNγ on prostate cancer metastasis and the role of IFIT5 in this event, we treated control and IFIT5-KD PC3 cells with IFNγ for 48 hours then cells were injected intravenously into SCID animal via tail vein. IFNγ treatment significantly increases the number and size of metastatic nodules at lung parenchyma, in contrast, loss of IFIT5 dramatically reduces metastasis of prostate cancer with or without IFNγ (Fig. 7E and F; Supplementary Table S4). Furthermore, we demonstrated the effect of IFNγ on EMT clinically, we used an *ex vivo* culture system (16) using human prostate cancer specimens and data indicated that IFNγ was able to induce the expression of IFIT5, ZEB1, Slug (Fig. 7G), and

Published OnlineFirst November 30, 2018; DOI: 10.1158/0008-5472.CAN-18-2207

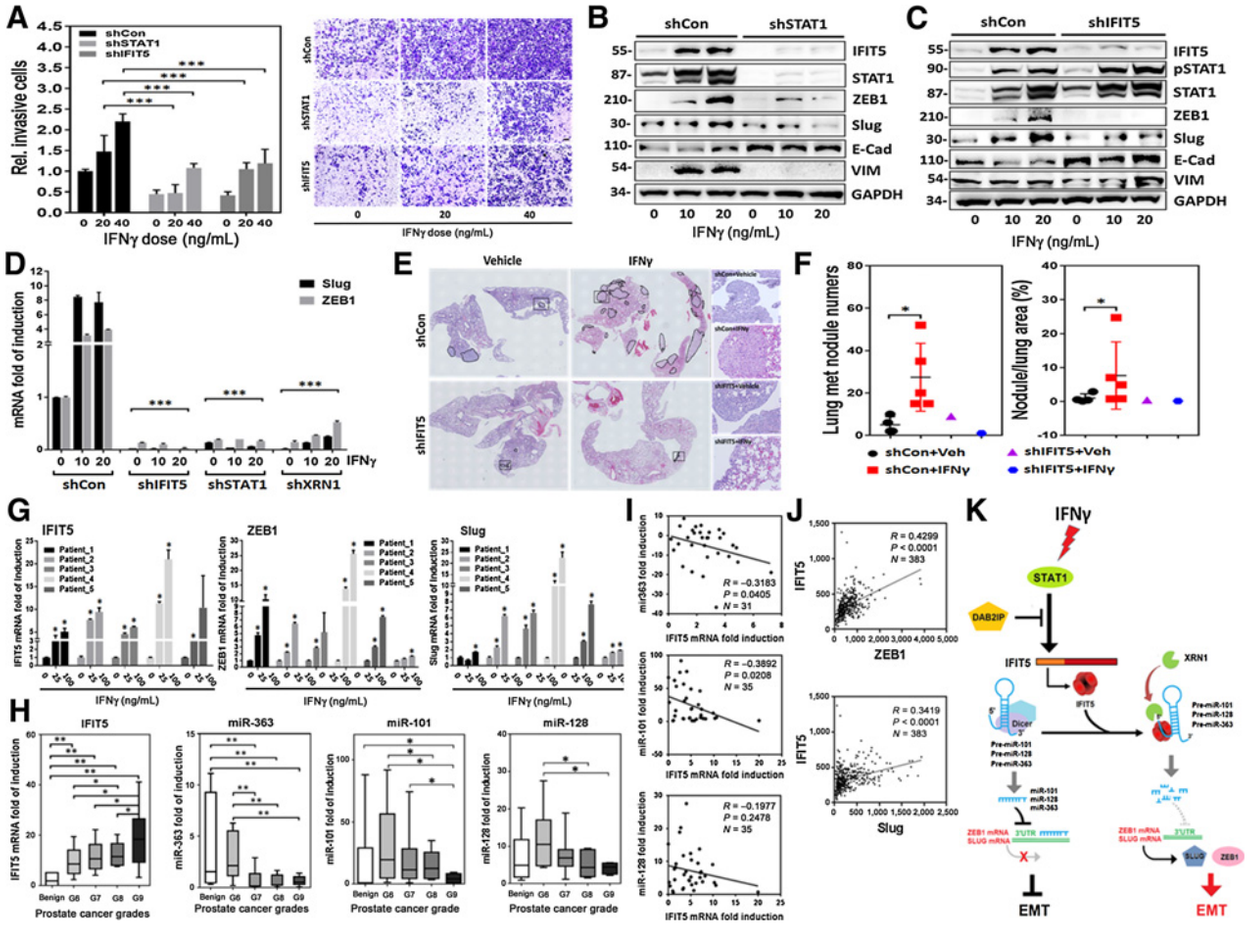

Figure 7.

IFNγ elicits its impact on EMT via activating IFIT5–XRN1-mediated miRNA turnover through STAT1 signaling pathway. **A,** Transwell invasion of STAT1- or IFIT5-KD (shSTAT1, shIFIT5) PC3 cells after treatment of IFNγ for 48 hours, compared with vector control (shCon). Invaded cells were stained with crystal violet and quantified at OD 555 nm (scale bar, 100 μm). Each bar represents mean ± SD of three replicated experiments. ***, $P < 0.0001$. **B** and **C,** Induction of IFIT5, E-cadherin, and mesenchymal factors (ZEB1, Slug, and vimentin) in STAT1- or IFIT5-KD (shSTAT1 or shIFIT5) PC3 cell lines in response to IFNγ treatment, compared with PC3 cells with control vector (shCon). **D,** IFNγ-induced expression level of Slug and ZEB1 mRNA in PC3 cells with KD of IFIT5 (shIFIT5), STAT1 (shSTAT1), or XRN1 (shXRN1), compared with vector control (shCon). ***, $P < 0.0001$. **E,** Hematoxylin and eosin staining of lung tissue derived from mice receiving tail vein intravenous injection of IFIT5-KD PC3 cells (PC3-shIFIT5) pretreated with vehicle (Veh, PBS) or IFNγ (20 ng/mL), compared with PC3 cells transfected with control vector (shCon). The black dotted line-circles region indicate the presence of metastatic nodules observed at lung parenchyma. Representative tumor nodules from each group are shown at right side panels (scale bar, 100 μm). **F,** Comparison of tumor nodule numbers and comparative area ratio in the lung parenchyma among each group. *, $P < 0.05$. **G,** Induction level of IFIT5, ZEB1, and Slug mRNA expression in *ex vivo* culture of human prostate cancer specimens treated with IFNγ for 48 hours, compared with vehicle control. *, $P < 0.05$. **H,** Relative expression level of IFIT5 mRNA and mature miR-363, miR-101, and miR-128 level in human prostate cancer specimens derived from different grades including benign ($N = 10$), G6 ($N = 9$), G7($N = 9$), G8($N = 6$), and G9($N = 7$). *, $P < 0.05$; **, $P < 0.0001$. **I,** Clinical correlation of miR-363, miR-101, and miR-128 with IFIT5 mRNA expression in human prostate cancer specimens graded from benign, G6 to G9. **J,** Clinical correlation between IFIT5 and ZEB1 or Slug mRNA level in prostate cancer from TCGA prostate cancer dataset. **K,** Schematic representing IFN-induced IFIT5-mediated precursor miRNA degradation leading to EMT in cancer. All quantitative data of mRNA or miRNA expression level were analyzed using ΔC_t (C_t value normalized to internal 18S RNA or snord95 miRNA) and $\Delta\Delta C_t$ (difference between the ΔC_t of control and experimental groups) values to obtain the fold change after normalizing with control.

vimentin (Supplementary Fig. S7D) genes whereas miR-363, miR-101, and miR-128 levels were significantly suppressed by IFNγ treatment (Supplementary Fig. S7E). Meanwhile, the level of miR-363, miR-101, and miR-128 in these *ex vivo* specimens is inversely correlated with the clinic-pathologic stage of prostate cancer patient donors (Supplementary Table S5; Supplementary Fig. S7F). We also surveyed the expression status of IFIT5 from different grades of prostate cancer specimens and data (Fig. 7H) indicate that IFIT5 mRNA levels were significantly elevated in the high-grade prostate cancer. As expected, the expression pattern of miR-363, miR-101, and miR-128 levels was opposite to that of IFIT5 (Fig. 7H), which is consistent with our observation from tissue culture cell lines. In contrast, miR-92a-2 and miR-19b-2 known as oncomirs, exhibited an elevated expression pattern in prostate cancer tissues compared with normal tissues (Supplementary Fig. S7G), supporting the specificity of IFIT5 on miRNA degradation. Meanwhile, data from prostate cancer specimens also demonstrated a similar

Published OnlineFirst November 30, 2018; DOI: 10.1158/0008-5472.CAN-18-2207

correlation between IFIT5 mRNA and miR-363 or miR-101 (Fig. 7I). In addition, analyses of EMT factors or markers in a The Cancer Genome Atlas (TCGA) prostate cancer dataset demonstrated a positive correlation between IFIT5 and ZEB1 (or Slug; Fig. 7J), and vimentin (Supplementary Fig. S7H).

Discussion

A recent study using whole exon and whole transcriptome sequencing of patients with metastatic tumors demonstrated a strong correlation between cancer metastasis and the expression of interferon-induced genes or EMT. Prostate cancer is often found to have many different kinds of infiltrated immune cells such as macrophages, dendritic cells, and tumor-infiltrating lymphocytes. Instead of eliciting tumor immunity, these immune cells with secreting cytokines are capable of facilitating prostate cancer development. For example, a study has demonstrated that fibroblast growth factor 11 (FGF11) released by the recruited $CD4^+$ T cells can induce cell invasion by increasing matrix metalloproteinase 9 (MMP9) in prostate cancer cells (22). In addition, IL4 produced from $CD4^+$ T cells has shown to increase prostate cancer cell survival and proliferation by activating the JNK signaling pathway in cancer cells (23). Moreover, IL17 secreted from T helper cells is capable of facilitating prostate cancer invasiveness by increasing several EMT transcription factors and MMP7 (24).

However, IFNγ, a type II IFN derived predominantly from $CD4^+$/$CD8^+$ lymphocytes and NK cell, is shown to have antitumor activities during innate immune response. Also, IFNγ has been used as a therapeutic agent exhibiting antiproliferative (25), antimetastatic (26), pro-apoptotic (27–30), and anti-angiogenesis (31–34) effects in various cancer types. However, several reports indicate that IFNγ could also facilitate tumor progression. For example, IFNγ can elicit $CD4^+$ T-cell loss and impair secondary antitumor immune responses after initial immunotherapy using tumor-bearing mouse model (35). In colorectal carcinoma, IFNγ has been shown to facilitate the induction of indoleamine 2,3-dioxygenase (IDO) that induces the production of kynurenines metabolites and impairs the function of surrounding T cells (36). In addition to its role in immune modulation, blockade of IFNγ receptor (IFNGR) can inhibit peritoneal disseminated tumor growth of ovarian cancer (37). Noticeably, serum IFNγ levels become elevated after radiotherapy in patients with prostate cancer (38). Nevertheless the effect of IFNγ on the overall survival of patients with prostrate cancer remains controversial (39).

In our study, we provide additional evidence that IFNγ is capable of inducing EMT, leading to cancer invasiveness via IFIT5-mediated turnover of tumor suppressor miRNAs (Fig. 6). We also noticed that low concentration of IFNγ without cytotoxicity is capable of inducing EMT of prostate cancer (Fig. 7). To strengthen the clinical evidence of IFN-induced EMT, we treated *ex vivo* prostate cancer explants with IFNγ and demonstrated that IFNγ could induce similar elevations of IFIT5 and EMT transcriptional factors and suppression of miR-101, miR-128, and miR-363 (Fig. 7G; Supplementary Fig. S7E). Taken together, these data show that IFNγ has a biphasic effect on cancer development. Nevertheless, the protumorigenic effect of IFNγ at low concentration is expected to raise a concern for its application as an antitumor or immunotherapeutic agent.

Unlike other IFIT family proteins, IFIT5 is characterized as a monomeric protein that is capable of binding to viral RNA with 5′-triphosphate group (4) and a broad spectrum of cellular RNA with either 5′-monophosphate or 5′-triphosphate group, including tRNA and other RNA polymerase III transcripts (6). However, the interaction of IFIT5 with miRNA is largely unknown. Knowing that precursor miRNA shares a similar stem loop structure with tRNA and a precursor miRNA still retains 5′-monophosphate group after processing from its primary transcript, we are able to show that IFIT5 is capable of interacting with 5′-end of pre-miRNA molecules. After binding to pre-miRNA, IFIT5 recruits XRN1 to form unique miRNA turnover complex (Fig. 5). For the first time, we demonstrated that the specificity of miRNA recognition by IFIT5 is mainly determined by the 5′-end overhang structure of pre-miRNAs (Figs. 4 and 6). Interestingly, these three tumor suppressor miRNAs (i.e., miR-101, miR-128, and miR-363) share similar 5′-end structure in their pre-miRNA and function in suppressing EMT despite of targeting different EMT transcriptional factors such as ZEB1 and Slug.

To conclude, our study provides a new functional role of IFIT5 in miRNA biogenesis (Fig. 7K), particularly, a new understanding of differential regulation of cluster miRNAs.

Until now, the clinical correlation of IFIT5 in prostate cancer is largely undetermined. In this study, we were able to demonstrate that the expression of IFIT5 is elevated in high-grade prostatic tumor and inverse correlation between IFIT5 and miR-101, -128, and -363 in prostate cancer tumor specimens as well as from prostate cancer TCGA database; this correlative relationship was not observed in other members of the miR-106a-363 cluster. In addition, a significant clinical correlation between IFIT5 and EMT transcription factors (ZEB1 or Slug) was observed from prostate cancer TCGA dataset, which supports the regulatory network of IFIT5-miRNAs-EMT in prostate cancer. Also, data from explants provide additional evidence for the promoting effect of IFNγ on prostate cancer progression, Taking together, we have unveiled new function of IFNγ related with prostate cancer progression and potential therapeutic target(s) from its underlying mechanism.

Disclosure of Potential Conflicts of Interest

G.V. Raj reports receiving other commercial research support from Bayer, has received speakers bureau honoraria from Astellas and Pfizer, and has ownership interest (including stock, patents, etc.) in EtiraRx, GaudiumRx, and C-diagnostics. No potential conflicts of interest were disclosed by the other authors.

Authors' Contributions

Conception and design: U-G. Lo, G.V. Raj

Development of methodology: U-G. Lo, D. Yang, C.-J. Lin, R. Sonavane, P. Kapur, G.V. Raj

Acquisition of data (provided animals, acquired and managed patients, provided facilities, etc.): L. Gandee, E. Hernandez, J. Santoyo, S. Ma, R. Sonavane, J. Huang, P. Kapur, G.V. Raj, C.-H. Lai

Analysis and interpretation of data (e.g., statistical analysis, biostatistics, computational analysis): U-G. Lo, J. Santoyo, L. Moro, A.A. Arbini, P. Kapur, G.V. Raj

Writing, review, and/or revision of the manuscript: U-G. Lo, A.A. Arbini, G.V. Raj, D. He, J.-T. Hsieh

Administrative, technical, or material support (i.e., reporting or organizing data, constructing databases): R.-C. Pong, L. Gandee, A. Dang, J. Santoyo, S.-F. Tseng, H. Lin

Study supervision: J.-T. Hsieh

Acknowledgments

We thank Dr. Collins (University of California, Berkeley, CA) for providing IFIT5 cDNA constructs, Dr. Dong (Emory University, Atlanta, GA) for providing the psiCHECK2-Slug3′UTR plasmid. Drs. Kou-Juey Wu (China Medical University, Taichung, Taiwan) and Dr. Vimal Selvaraj (Cornell University, Ithaca, NY) for the helpful discussion. We also acknowledge the assistance of the Southwestern Small Animal Imaging Resource, which is supported in part by the Harold C. Simmons Cancer Center through an NCI Cancer Center Support Grant (1P30 CA142543), and the Department of Radiology (NIH 1S10RR024757). This work was supported by grants from the United States Army (W81XWH-11-1-0491 and W81XWH-16-1-0474 to J.-T. Hsieh) and (W81XWH-14-1-0249 to U.-G. Lo), and the Ministry of Science and Technology in Taiwan (MOST103-2911-I-005-507 to H. Lin).

The costs of publication of this article were defrayed in part by the payment of page charges. This article must therefore be hereby marked *advertisement* in accordance with 18 U.S.C. Section 1734 solely to indicate this fact.

Received July 18, 2018; revised October 23, 2018; accepted November 27, 2018; published first November 30, 2018.

References

1. Hildenbrand B, Sauer B, Kalis O, Stoll C, Freudenberg MA, Niedermann G, et al. Immunotherapy of patients with hormone-refractory prostate carcinoma pre-treated with interferon-gamma and vaccinated with autologous PSA-peptide loaded dendritic cells—a pilot study. Prostate 2007;67:500–8.
2. Street SE, Cretney E, Smyth MJ. Perforin and interferon-gamma activities independently control tumor initiation, growth, and metastasis. Blood 2001;97:192–7.
3. de Veer MJ, Holko M, Frevel M, Walker E, Der S, Paranjape JM, et al. Functional classification of interferon-stimulated genes identified using microarrays. J Leukoc Biol 2001;69:912–20.
4. Abbas YM, Pichlmair A, Gorna MW, Superti-Furga G, Nagar B. Structural basis for viral 5′-PPP-RNA recognition by human IFIT proteins. Nature 2013;494:60–4.
5. Katibah GE, Lee HJ, Huizar JP, Vogan JM, Alber T, Collins K. tRNA binding, structure, and localization of the human interferon-induced protein IFIT5. Mol Cell 2013;49:743–50.
6. Katibah GE, Qin Y, Sidote DJ, Yao J, Lambowitz AM, Collins K. Broad and adaptable RNA structure recognition by the human interferon-induced tetratricopeptide repeat protein IFIT5. Proc Natl Acad Sci U S A 2014;111:12025–30.
7. Aalto AP, Pasquinelli AE. Small non-coding RNAs mount a silent revolution in gene expression. Curr Opin Cell Biol 2012;24:333–40.
8. Schickel R, Boyerinas B, Park SM, Peter ME. MicroRNAs: key players in the immune system, differentiation, tumorigenesis and cell death. Oncogene 2008;27:5959–74.
9. Obernosterer G, Leuschner PJ, Alenius M, Martinez J. Post-transcriptional regulation of microRNA expression. RNA 2006;12:1161–7.
10. Dylla L, Jedlicka P. Growth-promoting role of the miR-106a∼363 cluster in Ewing sarcoma. PLoS One 2013;8:e63032.
11. Chow TF, Mankaruos M, Scorilas A, Youssef Y, Girgis A, Mossad S, et al. The miR-17-92 cluster is over expressed in and has an oncogenic effect on renal cell carcinoma. J Urol 2010;183:743–51.
12. Diosdado B, van de Wiel MA, Terhaar Sive Droste JS, Mongera S, Postma C, Meijerink WJ, et al. MiR-17-92 cluster is associated with 13q gain and c-myc expression during colorectal adenoma to adenocarcinoma progression. Br J Cancer 2009;101:707–14.
13. Wong P, Iwasaki M, Somervaille TC, Ficara F, Carico C, Arnold C, et al. The miR-17-92 microRNA polycistron regulates MLL leukemia stem cell potential by modulating p21 expression. Cancer Res 2010;70:3833–42.
14. Landais S, Landry S, Legault P, Rassart E. Oncogenic potential of the miR-106–363 cluster and its implication in human T-cell leukemia. Cancer Res 2007;67:5699–707.
15. Xie D, Gore C, Liu J, Pong RC, Mason R, Hao G, et al. Role of DAB2IP in modulating epithelial-to-mesenchymal transition and prostate cancer metastasis. Proc Natl Acad Sci U S A 2010;107:2485–90.
16. Ravindranathan P, Lee TK, Yang L, Centenera MM, Butler L, Tilley WD, et al. Peptidomimetic targeting of critical androgen receptor-coregulator interactions in prostate cancer. Nat Commun 2013;4:1923.
17. Min J, Zaslavsky A, Fedele G, McLaughlin SK, Reczek EE, De Raedt T, et al. An oncogene-tumor suppressor cascade drives metastatic prostate cancer by coordinately activating Ras and nuclear factor-kappaB. Nat Med 2010;16:286–94.
18. Jones CI, Zabolotskaya MV, Newbury SF. The 5′ → 3′ exoribonuclease XRN1/Pacman and its functions in cellular processes and development. Wiley Interdiscip Rev RNA 2012;3:455–68.
19. Nagarajan VK, Jones CI, Newbury SF, Green PJ. XRN 5′→3′ exoribonucleases: structure, mechanisms and functions. Biochim Biophys Acta 2013;1829:590–603.
20. Jones CI, Grima DP, Waldron JA, Jones S, Parker HN, Newbury SF. The 5′-3′ exoribonuclease Pacman (Xrn1) regulates expression of the heat shock protein Hsp67Bc and the microRNA miR-277-3p in Drosophila wing imaginal discs. RNA Biol 2013;10:1345–55.
21. Wall L, Burke F, Barton C, Smyth J, Balkwill F. IFN-gamma induces apoptosis in ovarian cancer cells in vivo and in vitro. Clin Cancer Res 2003;9:2487–96.
22. Hu S, Li L, Yeh S, Cui Y, Li X, Chang HC, et al. Infiltrating T cells promote prostate cancer metastasis via modulation of FGF11→miRNA-541→androgen receptor (AR)→MMP9 signaling. Mol Oncol 2015;9:44–57.
23. Roca H, Craig MJ, Ying C, Varsos ZS, Czarnieski P, Alva AS, et al. IL-4 induces proliferation in prostate cancer PC3 cells under nutrient-depletion stress through the activation of the JNK-pathway and survivin up-regulation. J Cell Biochem 2012;113:1569–80.
24. Zhang Q, Liu S, Parajuli KR, Zhang W, Zhang K, Mo Z, et al. Interleukin-17 promotes prostate cancer via MMP7-induced epithelial-to-mesenchymal transition. Oncogene 2017;36:687–99.
25. Aune TM, Pogue SL. Inhibition of tumor cell growth by interferon-gamma is mediated by two distinct mechanisms dependent upon oxygen tension: induction of tryptophan degradation and depletion of intracellular nicotinamide adenine dinucleotide. J Clin Invest 1989;84:863–75.
26. Addison CL, Arenberg DA, Morris SB, Xue YY, Burdick MD, Mulligan MS, et al. The CXC chemokine, monokine induced by interferon-gamma, inhibits non-small cell lung carcinoma tumor growth and metastasis. Hum Gene Ther 2000;11:247–61.
27. Fukui T, Matsui K, Kato H, Takao H, Sugiyama Y, Kunieda K, et al. Significance of apoptosis induced by tumor necrosis factor-alpha and/or interferon-gamma against human gastric cancer cell lines and the role of the p53 gene. Surg Today 2003;33:847–53.
28. Burke F, East N, Upton C, Patel K, Balkwill FR. Interferon gamma induces cell cycle arrest and apoptosis in a model of ovarian cancer: enhancement of effect by batimastat. Eur J Cancer 1997;33:1114–21.
29. Suk K, Chang I, Kim YH, Kim S, Kim JY, Kim H, et al. Interferon gamma (IFNgamma) and tumor necrosis factor alpha synergism in ME-180 cervical cancer cell apoptosis and necrosis. IFNgamma inhibits cytoprotective NF-kappa B through STAT1/IRF-1 pathways. J Biol Chem 2001;276:13153–9.
30. Chung TW, Tan K-T, Chan H-L, Lai M-D, Yen M-C, Li Y-R, et al. Induction of indoleamine 2,3-dioxygenase (IDO) enzymatic activity contributes to interferon-gamma induced apoptosis and death receptor 5 expression in human non-small cell lung cancer cells. Asian Pac J Cancer Prev 2014;15:7995–8001.
31. Ribatti D, Nico B, Pezzolo A, Vacca A, Meazza R, Cinti R, et al. Angiogenesis in a human neuroblastoma xenograft model: mechanisms and inhibition by tumour-derived interferon-gamma. Br J Cancer 2006;94:1845–52.
32. Saiki I, Sato K, Yoo YC, Murata J, Yoneda J, Kiso M, et al. Inhibition of tumor-induced angiogenesis by the administration of recombinant interferon-gamma followed by a synthetic lipid-A subunit analogue (GLA-60). Int J Cancer 1992;51:641–5.
33. Strieter RM, Kunkel SL, Arenberg DA, Burdick MD, Polverini PJ. Interferon gamma-inducible protein 10 (IP-10), a member of the C-X-C chemokine

Published OnlineFirst November 30, 2018; DOI: 10.1158/0008-5472.CAN-18-2207

family, is an inhibitor of angiogenesis. Biochem Biophys Res Commun 1995;210:51–7.
34. Sun T, Yang Y, Luo X, Cheng Y, Zhang M, Wang K, et al. Inhibition of tumor angiogenesis by interferon-gamma by suppression of tumor-associated macrophage differentiation. Oncol Res 2014;21:227–35.
35. Berner V, Liu H, Zhou Q, Alderson KL, Sun K, Weiss JM, et al. IFN-gamma mediates CD4+ T-cell loss and impairs secondary antitumor responses after successful initial immunotherapy. Nat Med 2007;13:354–60.
36. Mellor AL, Munn DH. Tryptophan catabolism prevents maternal T cells from activating lethal anti-fetal immune responses. J Reprod Immunol 2001;52:5–13.
37. Abiko K, Matsumura N, Hamanishi J, Horikawa N, Murakami R, Yamaguchi K, et al. IFN-gamma from lymphocytes induces PD-L1 expression and promotes progression of ovarian cancer. Br J Cancer 2015;112:1501–9.
38. Tanji N, Kikugawa T, Ochi T, Taguchi S, Sato H, Sato T, et al. Circulating cytokine levels in patients with prostate cancer: effects of neoadjuvant hormonal therapy and external-beam radiotherapy. Anticancer Res 2015;35:3379–83.
39. Hastie C, Masters JR, Moss SE, Naaby-Hansen S. Interferon-gamma reduces cell surface expression of annexin 2 and suppresses the invasive capacity of prostate cancer cells. J Biol Chem 2008;283:12595–603.

Published OnlineFirst November 30, 2018; DOI: 10.1158/0008-5472.CAN-18-2207

Cancer Research
The Journal of Cancer Research (1916–1930) | The American Journal of Cancer (1931–1940)

AACR American Association for Cancer Research

IFNγ-Induced IFIT5 Promotes Epithelial-to-Mesenchymal Transition in Prostate Cancer via miRNA Processing

U-Ging Lo, Rey-Chen Pong, Diane Yang, et al.

Cancer Res 2019;79:1098-1112. Published OnlineFirst November 30, 2018.

Cancer Research

IFNγ, a Double-Edged Sword in Cancer Immunity and Metastasis

Chengfei Liu and Allen C. Gao

IFNγ has antitumorigenic effects; however, the findings of IFNγ in promoting the tumor cell survival and inducing adaptive immune resistance via $CD4^+$ T-cell loss and programmed death ligand 1 (PD-L1) upregulation challenge this concept. Lo and colleagues determined that IFNγ induces epithelial–mesenchymal transition (EMT) by regulating the turnover of miRNA in prostate cancer, emphasizing the duplicitous effects of IFNγ. IFIT5, an IFN-induced tetratricopeptide repeat (IFIT) family member, was found to form a complex with the exoribonuclease-XRN1 to process miRNA maturation. These findings unveil a new IFNγ–STAT1–IFIT5–miRNA–EMT pathway in prostate cancer progression. The biphasic effects of IFNγ in prostate cancer raise concerns about its therapeutic application, which need to be evaluated in future studies.

See related article by Lo et al., p. 1098

In this issue of *Cancer Research*, Lo and colleagues (1) describe an interesting observation wherein IFNγ induces epithelial–mesenchymal transition (EMT) in prostate cancer cells by regulating the degradation of precursor miRNAs through a complex between the known IFNγ-stimulated RNA-binding protein, interferon-induced tetratricopeptide 5 (IFIT5), and the exoribonuclease candidate XRN1 (IFIT5-XRN1). Their study emerged from research on the GTPase-activating protein, DAB2IP, which has long been a focus for this group. They found that IFNγ promotes EMT in prostate cancer cells through DAB2IP, which has been previously identified as an upstream regulator of EMT, and went on to profile the miRNAs and show that miR-363 expression and maturation are specifically regulated by DAB2IP and that IFIT5 is a key factor regulating miR-363 turnover. The authors next sought to further characterize the network among IFIT5, miRNA, and EMT in prostate cancer. They first discovered that miR-363 suppresses EMT by targeting Slug in prostate cancer cells and that IFIT5 recognizes the unique 5′-end overhanging structure of pre-miR-363 to target it for degradation. Because IFIT5 does not possess ribonuclease activity, the authors then demonstrated that IFIT5 alone is not sufficient in regulating miRNA maturation and degradation but needs to form a complex with exoribonuclease-XRN1 to promote miR-363 turnover. To expand the overall effects of the network they established, the authors further examined other miRNAs that could be regulated by IFNγ. Two additional miRNAs, miR-101 and miR-128, were also identified to be involved in the IFIT5-EMT process. Finally, they found that IFIT5 is inversely correlated with miR-363, miR-101, and miR-128 and positively correlated with EMT markers ZEB1, Slug, and vimentin in prostate cancer specimens. From benchwork to clinical validation, Lo and colleagues identified a network of immune factors, transcriptional factors, and miRNAs involved in prostate cancer progression and metastasis.

Although we now recognize that miRNA plays crucial roles in prostate cancer progression, regulation of miRNA expression remains largely unknown. After transcription, pre-miRNA undergoes nuclear and cytoplasmic processing to become mature miRNA. Alteration of mature miRNA expression occurs in many different ways, such as SNP, miRNA tailing, editing, methylation, and regulation of stability (2). XRN1 is a 5′-3′ exoribonuclease that predominantly degrades miRNAs after they have been decapped in cells. Lo and colleagues discovered for the first time that IFIT5 recruits XRN1 to form a unique miRNA complex with the 5′-end of pre-miRNA molecules. The reciprocal correlation of IFIT5 and miR-363 and miR-101 expression in prostate cancer specimens further supports the role of IFNγ signaling in miRNA regulation. Human IFNγ is predominantly from infiltrating immune cells and whether this correlation also exists in these cells in prostate tumors needs to be investigated in future studies. Nevertheless, this function of IFIT5 in miRNA processing provides a new piece of evidence that IFNγ signaling regulates miRNA maturation and turnover in prostate cancer.

Over the last few decades, our understanding of the role of IFNγ in cancer immunity has been evolving. Numerous studies have reported that IFNγ is an important cytokine that facilitates both the innate and adaptive immune systems. Initial induction of IFNγ significantly suppresses tumor growth via immune activation; however, it can also induce $CD4^+$ T-cell apoptosis, alter the CD4:CD8 ratio, and subsequently impair secondary antitumor immune responses (3). As a type II IFN, IFNγ plays both pro- and antitumorigenic roles in immunoediting, a process that consists of immunosurveillance and tumor progression (4). IFNγ plays a role in all three phases of the immunoediting process: elimination, equilibrium, and escape. During the elimination phase, natural killer (NK) cells, NK T cells, $CD8^+$, and $CD4^+$ T cells secrete IFNγ, which then activates macrophages, dendritic cells, Th1 $CD4^+$ helper T cells, and B cells that lead to complete tumor elimination, suggesting that IFNγ is predominantly antitumorigenic in the tumor environment during this phase. During the equilibrium phase, the immune system is able to maintain

Department of Urology, Comprehensive Cancer Center, University of California Davis, Sacramento, California.

Corresponding Author: Allen C. Gao, Department of Urology, School of Medicine, University of California, Davis, Research III Bldg, Suite 1300, 4645 2nd Ave, Sacramento, CA 95817. Phone: 916-734-8718; Fax: 916-734-8714; E-mail: acgao@ucdavis.edu

doi: 10.1158/0008-5472.CAN-19-0083

immune-mediated tumor dormancy. This phase is poorly understood, in part, because of technical challenges in establishing mouse models, but it is known that IFNγ is required for maintaining tumor dormancy by inducing cancer senescence. Finally, during the escape phase, tumor cells grow and expand through mechanisms including adaptive and acquired immune resistance (5). Recent studies suggest that IFNγ can upregulate the expression of programmed-death ligand 1 (PD-L1), a membrane-bound immune inhibitory molecule on the surface of tumor cells. Because PD-L1 binds to programmed cell death protein 1 (PD1) expressed on the activated $CD8^+$ T cells and leads to apoptotic T-cell death, IFNγ signaling activation facilities tumor cells escaping from the antitumor $CD8^+$ T-cell cytotoxicity through formation of the immunosuppressive tumor microenvironment, promotes tumor cell survival, and induces adaptive resistance (6). Therefore, IFNγ possibly plays a protumorigenic role during the tumor immunity escape stage. Although application of immunotherapy in prostate cancer lags behind that in other cancer types, several clinical trials testing immune checkpoint inhibitors in patients with prostate cancer have begun (7). The exact role of IFNγ in prostate cancer immunity remains to be determined and the study by Lo and colleagues brings up more concern into the prostate cancer immunotherapy arena by reinforcing the dual nature of IFNγ in prostate cancer progression.

Metastasis is the primary underlying cause of fatality in patients with prostate cancer. Bone metastases occur in more than 90% of patients with advanced prostate cancer and are associated with poor survival. For men with metastatic prostate cancer, only one-third survive for 5 years after diagnosis (8). There is an urgent need to unravel potential resistant mechanisms that perpetuate disease progression during effective androgen receptor blockade and to devise ways of targeting resistant pathways. EMT is believed to be a crucial step in the conversion of early-stage disease to invasive and metastatic cancer (9). Immortalized human mammary epithelial cells acquire the mesenchymal phenotype and express stem cell markers after induction of EMT (10). The aberrant expression and localization of E-cadherin, N-cadherin, vimentin, Wnt5A, and ZEB1 appears to be important in prostate cancer invasion and bone metastasis. Although strong evidence supports EMT as the essential step in the progression and metastasis of prostate cancer, difficulties in identifying migratory cancer cells have precluded confirmation of the occurrence of EMT *in vivo* for many years. Thus, better understanding of upstream EMT regulators is urgent and important in the clinical arena. EMT can be triggered by tumor-associated fibroblasts, immune cells, and secreted soluble factors, such as Wnt ligands, TGFβ, EGF, and hepatocyte growth factor. These factors and inflammatory cytokines can exert their effects through autocrine or paracrine systems. Slug, Snail, ZEB1, ZEB2, and Twist have been previously identified as classical EMT regulators. In their study, Lo and colleagues report that IFNγ induces EMT in prostate cancer cells by regulating expression of EMT regulators and markers such as ZEB1, Slug, and vimentin as well as miR-363, miR-101, and miR-128. The take-home message from this comprehensive study is that the administration of IFNγ might not benefit patients with prostate cancer and possibly cause some harmful side effects. Nevertheless, clinical evidence and clinical trials would be required before this could be considered as a conclusion.

Together, IFNγ signaling is still largely unfathomable in prostate cancer. Considering the classical role of IFNγ in cancer immunoediting, the possibility of its utility in prostate cancer immunetherapy arena should not be disregarded. Prostate cancer immunotherapy awaits rigorous investigation to define the real targets and pathways involved in the therapy. A better grasp of the detailed mechanisms that underlie the effects of IFNγ in prostate cancer immunoediting appears to be necessary. Lo and colleagues have identified a novel tumor-promoting IFNγ–STAT1–IFIT5–miRNA–EMT pathway in prostate cancer cells, suggesting that IFNγ might serve as a master regulator in controlling several downstream signaling pathways, such as JAK-STAT1, IFIT5, DAB2IP, and miRNA signaling leading to prostate cancer progression and metastasis through EMT, raising concerns about its clinical application.

Disclosure of Potential Conflicts of Interest

No potential conflicts of interest were disclosed.

Acknowledgments

This commentary did not receive any specific grant from any funding agency in the public, commercial, or not-for-profit sector.

Received January 18, 2019; accepted January 18, 2019; published first March 15, 2019.

References

1. Lo UG, Pong RC, Yang D, Gandee L, Hernandez E, Dang A, et al. IFN-γ-induced IFIT5 promotes epithelial-to-mesenchymal transition in prostate cancer via miRNA processing. Cancer Res 2019;79:1098–112.
2. Ha M, Kim VN. Regulation of microRNA biogenesis. Nat Rev Mol Cell Biol 2014;15:509–24.
3. Berner V, Liu H, Zhou Q, Alderson KL, Sun K, Weiss JM, et al. IFN-gamma mediates CD4+ T-cell loss and impairs secondary antitumor responses after successful initial immunotherapy. Nat Med 2007;13:354–60.
4. Kaplan DH, Shankaran V, Dighe AS, Stockert E, Aguet M, Old LJ, et al. Demonstration of an interferon gamma-dependent tumor surveillance system in immunocompetent mice. Proc Natl Acad Sci U S A 1998;95:7556–61.
5. Alspach E, Lussier DM, Schreiber RD. Interferon gamma and its important roles in promoting and inhibiting spontaneous and therapeutic cancer immunity. Cold Spring Harb Perspect Biol 2018 April 16 [Epub ahead of print].
6. Mandai M, Hamanishi J, Abiko K, Matsumura N, Baba T, Konishi I. Dual faces of IFNgamma in cancer progression: a role of PD-L1 induction in the determination of pro- and antitumor immunity. Clin Cancer Res 2016;22:2329–34.
7. Rescigno P, de Bono JS. Immunotherapy for lethal prostate cancer. Nat Rev Urol 2019;16:69–70.
8. Gundem G, Van Loo P, Kremeyer B, Alexandrov LB, Tubio JMC, Papaemmanuil E, et al. The evolutionary history of lethal metastatic prostate cancer. Nature 2015;520:353–7.
9. Thiery JP. Epithelial-mesenchymal transitions in tumour progression. Nat Rev Cancer 2002;2:442–54.
10. Mani SA, Guo W, Liao MJ, Eaton EN, Ayyanan A, Zhou AY, et al. The epithelial-mesenchymal transition generates cells with properties of stem cells. Cell 2008;133:704–15.

IFNγ, a Double-Edged Sword in Cancer Immunity and Metastasis

Chengfei Liu and Allen C. Gao

Cancer Res 2019;79:1032-1033.

亚洲男性学杂志
ISSN 1008-682X (Print)
CN 31-1795/R
ISSN 1745-7262 (Online)

Asian Journal of Andrology

Volume 21, Issue 3, May–June 2019

SPECIAL ISSUE

Guest Editor:
Prof. Jiaoti Huang

Prostate Cancer: Molecular and Cellular Mechanisms

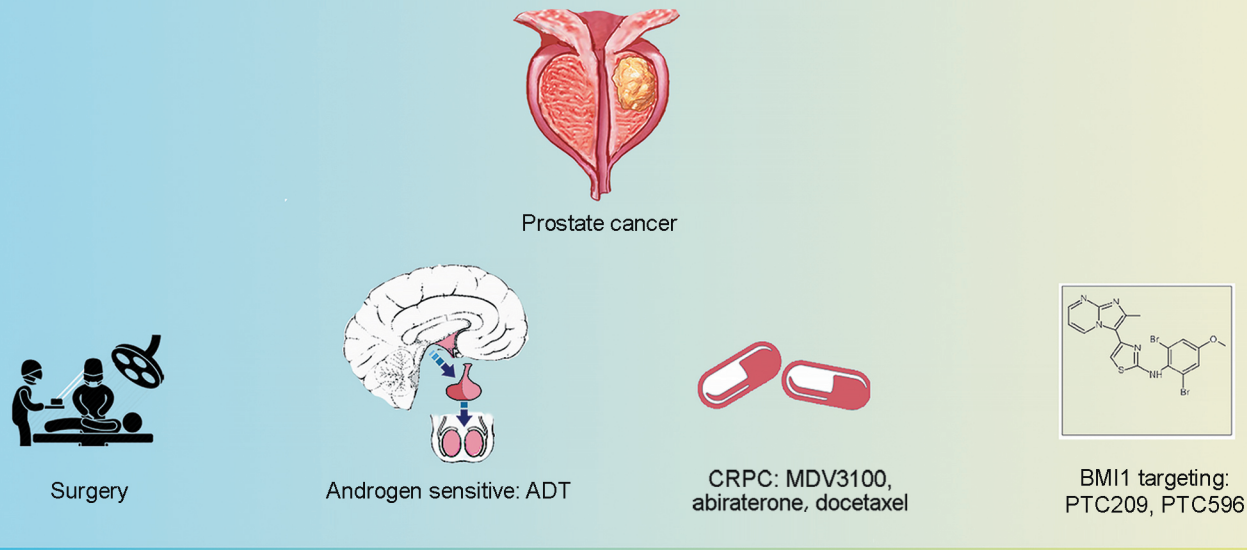

www.asiaandro.com
www.ajandrology.com

Shanghai Institute of Materia Medica (SIMM)
Chinese Academy of Sciences

Shanghai Jiao Tong University (SJTU)

Wolters Kluwer
Medknow

Asian Journal of Andrology (2019) 21, 233–240
www.asiaandro.com; www.ajandrology.com

Open Access

INVITED REVIEW

Prostate Cancer

The regulatory pathways leading to stem-like cells underlie prostate cancer progression

Chun-Jung Lin, U-Ging Lo, Jer-Tsong Hsieh

Prostate cancer (PCa) is the most common cause of malignancy in males and the third leading cause of cancer mortality in the United States. The standard care for primary PCa with local invasive disease mainly is surgery and radiation. For patients with distant metastases, androgen deprivation therapy (ADT) is a gold standard. Regardless of a favorable outcome of ADT, patients inevitably relapse to an end-stage castration-resistant prostate cancer (CRPC) leading to mortality. Therefore, revealing the mechanism and identifying cellular components driving aggressive PCa is critical for prognosis and therapeutic intervention. Cancer stem cell (CSC) phenotypes characterized as poor differentiation, cancer initiation with self-renewal capabilities, and therapeutic resistance are proposed to contribute to the onset of CRPC. In this review, we discuss the role of CSC in CRPC with the evidence of CSC phenotypes and the possible underlying mechanisms.

Asian Journal of Andrology (2019) **21**, 233–240; doi: 10.4103/aja.aja_72_18; published online: 4 September 2018

Keywords: cancer stem cell; castration-resistant prostate cancer; neuroendocrine differentiation; transdifferentiation

INTRODUCTION

Prostate cancer (PCa) remains the most commonly diagnosed cancer, from the 2017 cancer statistic report, there were 180 890 estimated new cases in 2017, and PCa is also the third leading cause of death, with 26 120 estimated deaths in the United States.

Clinical treatment for primary PCa includes radical prostatectomy and radiotherapy. Androgen deprivation therapy (ADT) is commonly used to decrease the androgen-dependent tumor burden of metastatic PCa (mPCa). Castration-resistant PCa (CRPC) is defined as the reappearance of cancer lesion from metastatic site(s) often with rising prostate-specific antigen (PSA) in patient's serum. CRPC is recognized as the end-stage disease since patients do not respond to chemotherapeutics very well with average 6-month to 1-year survival. Although recent introduction of second-line anti-androgen agents has prolonged patients' survival, PCa eventually develops therapy-resistant phenotypes. Clinically, therapy-resistant tumors can be divided into several different phenotypes such as neuroendocrine, androgen receptor (AR) variants, and AR hyperactivation due to gene amplification and/or mutation, which raise a critical question for the cell origin of these subtypes. Many studies have demonstrated the presence of stem-like population in normal prostate and abnormal prostate,[1–3] which raises the potential role of cancer stem cell (CSC) in cancer progression. In this article, we have summarized the potential pathways associated with CSC leading to CRPC and the possible therapeutic strategies to improve the clinical outcomes of PCa patients.

CANCER STEM CELL IN CRPC

Cell markers for CSC

The CSC theory, as a potential mechanism for CRPC, has raised significant attention in recent years. In general, embryonic stem cell is pluripotent with the ability of developing into different tissue types. Somatic stem cell in each organ is considered to be quiescent most of time with limited number and capable of self-renewing and differentiation maintained in a homeostatic balance. Isaacs and Coffey[4] first proposed that prostate stem cell resides in basal cell population; its expansion underlies the development of benign prostatic hyperplasia (BPH). Further study suggested that enrich stem cell is in the proximal duct of prostate.[5] During normal prostate development, androgen binding to the AR in surrounding stromal cells plays a key role of basal stem cell different into luminal cell population.[6] Recent study using gene-tracing technology indicated that luminal cell population has stem cells as well with less potency than basal stem cell.[7] For CSC, its self-renewal ability allows a single cell remained after therapies to repopulate entire tumor population as therapeutic resistance. Further, the pluripotency of CSC is capable of differentiating into different cell types such as neuroendocrine. It has been reported that prostate CSC is likely derived from basal cell population.[8] Normal prostate gland can be divided into epithelial, stromal, and neuroendocrine cells; the epithelial cells include luminal and basal cells. Among all these heterogeneous cell types in the normal prostate, the gene expression profile of basal cell is highly correlated with that of stem cell. Noticeably, the basal cell gene profiles are enriched in advanced, anaplastic, castration-resistant, and metastatic PCa in the human PCa sample set.[9] However, it is still unclear whether clonal expansion and/or adaptation through epithelial-to-mesenchymal transition (EMT)[10–12] or transdifferentiation[13] during therapies results in the expansion of CSC.

Several markers have been commonly used to identify CSC population including CD44, stem cell antigen (Sca-1 or Ly6A), prominin-1 (CD133), and ATP-binding cassette subfamily G member 2 (Junior blood group) (ABCG2). CD44 is often associated

Department of Urology, UT Southwestern Medical Center, Dallas, TX 75390, USA.
Correspondence: Dr. JT Hsieh (jt.hsieh@utsouthwestern.edu)
Received: 21 December 2017; Accepted: 29 June 2018

with CSC, which is a cell membrane receptor that is involved in cell–cell interactions, adhesion, and migration. Especially, cells expressing CD44, but lacking CD24 ($CD44^+CD24^-$) PCa cells, were identified as the CSC population with *in vivo* and *in vitro* models.[14] These $CD44^+CD24^-$ PCa cells have the ability of forming spheres and producing tumor from a single cell, which is known as stem cell self-renewal ability. Sca-1 is a mouse glycosyl phostidylinositol-anchored surface protein that expressed by stem cells or progenitor cells. However, the human homolog of Sca-1 has not been identified yet. Studies in mouse model demonstrated that cells with Sca-1 expression have tumor-initiating ability, and tumor cells expressing higher Sca-1 were correlated with their aggressive phenotype.[15,16] CD133 is a transmembrane glycoprotein, and is known as a marker for basal stem cell as well as PCa-initiating cell. Richardson *et al*.[17] reported that a subset of $CD133^+$ population exhibited higher clonogenic potential than $CD133^-$ population. Furthermore, these $CD133^+$ populating can fully differentiate to prostatic acini from *in vivo* animal model. In addition, studies demonstrated that CD133 involved in cell growth, cell development, and tumor progression, in which the expression of CD133 was significantly increased in cancer-initiating cells using patient-derived primary cell model.[18] ABCG2 is the ATP-binding cassette membrane transporter. Patient-derived cells with high ABCG2 expression correlated with cell that expresses stem cell markers, and these subsets of cells have shown to gain multidrug resistance and be responsible for the recurrence of PCa.[19] Although these CSC markers[20] listed in this review are indeed correlated with CSC population associated with cancer progression, recurrence, and therapy resistance, there is still lacking a specific PCa CSC marker.

Molecular signaling pathways lead to CSC in CPRC

Three signaling pathways have been suggested to be critical for CSC development including Wnt, Sonic Hedgehog, and Notch signaling pathways. Several reports have demonstrated that targeting these signaling pathways along with conventional treatment can prevent the emergence of CRPC.[21,22]

Wnt

In the canonical of Wnt pathway, Wnt ligands bind to Frizzled and low-density lipoprotein receptor–related protein (LRP) 5/6, which activate downstream molecular targets, leading to the accumulation and nuclear translocation of β-catenin, subsequently affecting cell survival; while, in the noncanonical pathways, Wnt activates downstream effectors and activates targeted gene expression and cytoskeleton rearrangement, resulting in altered cell survival. Abnormal Wnt signaling has been found in several cancer types, including brain, breast, and colorectal cancer.[23] In PCa, elevated β-catenin expression was often found in the nucleus of cancer cells.[24] Importantly, Wnt signal regulates self-renewal ability of several cell models including LNCaP, C42B, and PC3 cell in an AR-independent manner,[25,26] while downregulated Wnt/β-catenin pathway significantly suppresses stem cell-like properties.[27] Furthermore, Wnt3 has been shown to increase the expression of its downstream effectors, as well as CSC markers including CD133 and CD44, which subsequently lead to sphere formation.[25] In addition, Zhang *et al*.[23] demonstrated that human telomerase reverse transcriptase (hTERT)-expressing PCa cells have higher Wnt/β-catenin activity and can thereby regulate the self-renewal and differentiation activity of PCa cells. Collectively, Wnt plays a key role in CSC development in CRPC (**Figure 1a**).

Sonic Hedgehog

Sonic Hedgehog signaling pathway is a conserved process that controls cell renewal and cell survival. Hedgehog signaling is initiated by hedgehog family ligands (Sonic, Desert, and Indian). These ligands bind to membrane receptors Patched (Ptch1 and 2) and Smoothened on the primary cilium, leading to the activation and nuclear translocation of glioma-associated oncogene homolog (Gli) (Gli 1, 2, and 3), which trigger the expression of targeted genes that regulate cell survival. Abnormal Hedgehog signaling pathway has been found in several cancer types, including brain, gastrointestinal, lung, breast, and prostate cancers.[28,29] Some studies also demonstrated that Hedgehog involved in tumor progression and CSC proliferation.[30–32] Importantly, using several PCa cell line models,[29] *i.e*., LNCaP, Du145, PC3, 22Rv1, and

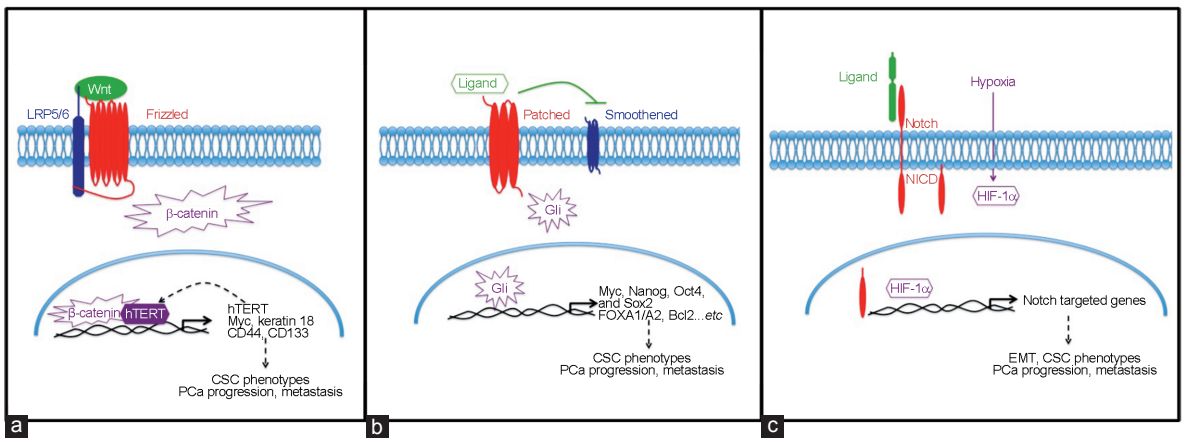

Figure 1: Schematic representation of signal contributes to CSC phenotype. (**a**) Wnt proteins bind to both frizzled receptor proteins and the co-receptor LRP5/6. This binding further facilitates the activation of β-catenin. Activated β-catenin translocates into nucleus and promotes Wnt downstream gene transcription. Furthermore, Wnt/β-catenin induced hTERT also acts as a transcriptional factor, resulting a positive feedback in the enhanced expression of Wnt target genes that leads to cancer-promoting functions and CSC phenotypes. (**b**) Sonic Hedgehog pathway is initiated by binding one of the three secreted Hedgehog ligands to its receptor. This binding releases Smoothened that modulates the expression of three Gli zinc-finger transcription factors. (**c**) The Notch receptor is activated by ligand binding, which is presented by a neighboring cell. Notch activation releases an active fragment, NICD. NICD then translocates into the nucleus and promotes the expression of targeted genes. Notch-dependent signaling induces several genes associated with differentiation, survival, stemness, and EMT, which all relate to PCa progression and metastasis. Further, Notch signaling is often activated by hypoxia through HIF-1α. CSC: cancer stem cell; PCa: prostate cancer; hTERT: human telomerase reverse transcriptase; LRP: low-density lipoprotein receptor-related protein; Gli: glioma-associated oncogene homolog; Sox 2: sex determining region Y-box 2; FOXA1/A2: forkhead box A1/A2; NICD: notch intracellular domain; HIF-1α: hypoxia-inducible factor 1 subunit alpha; EMT: epithelial-to-mesenchymal transition; Bcl2: B-cell lymphoma 2; Oct4: octamer-binding transcription factor 4.

LAPC4, as well as xenograft model (CWR22),[30] several Gli-related genes have been shown to correlate with the progression of CPRC. These Gli-related genes, including *CDKN2A/p16/INK4A*, *Myc*, and *CDK2*, promote AR-independent tumor cell growth[33,34] and lead to tumor recurrence.[35] Data from PCa patients-derived tissue microarray and PCa cell line models (PC3, LNCaP, and Du145) indicated that forkhead box A1 (FOXA1) was found to promote the progression of CRPC.[36,37] Cell model (LNCaP, PC3, Du145, and LAPC4) also showed that the expression of B-cell lymphoma 2 (Bcl2) correlates with therapy resistance ability in CRPC.[38] Importantly, increased Hedgehog signaling was found in PCa CSC population ($CD44^+CD24^-$) *in vivo* and *in vitro*.[14] Taken together, Hedgehog downstream signaling pathway contributes to CRPC progression and therapy-resistant phenotypes of CSC (**Figure 1b**).

Notch

Notch signaling pathway has been extensively studied and has been correlated to promote CSC phenotype in several cancers. Notch signaling is mediated by four Notch receptors, including Notch1–4, and five ligands including delta-like (DLL) 1, DLL 3, DLL4, Jagged 1, and Jagged 2, were involved. Various types of cancers exhibit dysfunction of the Notch pathway in their cells.[39] Importantly, Notch interacts with AR pathway and the phosphoinositide 3-kinase (PI3k)/Akt pathway, which are the two main signaling pathways in controlling prostate development and carcinogenesis.[40–42] Studies from cell culture models and human PCa specimens have demonstrated that higher Notch ligand, Jagged 1-Notch1 signaling contributes to PCa progression and metastasis, and promotes EMT and CSC phenotype.[43–46] Higher Notch3 expression was found in CRPC, which was induced by hypoxia condition.[47] Recently, Notch4-targeted silencing, leading to the inhibition of nuclear factor kappa B (NF-κB) activity, also showed a promising anti-PCa growth and anti-EMT effect.[44,48,49] These reports all point out the importance of Notch signal in PCa progression and the initiation of CSC phenotype (**Figure 1c**).

Caveolin-1 (Cav-1)

The Caveolin protein family including caveolin-1, -2, and -3 is the major component of caveolae; Cav-1 is the first member identified and has been extensively characterized. It is known to regulate multiple cellular functions, including cell cycle, signal transduction, endocytosis, and cholesterol trafficking and efflux. Cav-1 levels are correlated with PCa progression and metastasis.[50–52] Extensive studies using PCa cell line (Du145, LNCaP, and 22Rv1), and human BPH sample model, also indicated that Cav-1 signaling contributes to therapy resistance and the reoccurrence of PCa.[52–54] Using xenograft model, Cav-1 can be secreted into circulation to enhance tumor growth in a paracrine manner, implying that Cav-1 can be a secretory protein.[55,56] Interestingly, other study has demonstrated that Cav-1 can elevate the Notch-1-Akt-NF-kappaB pathway, leading to chemoresistance in ovarian cancer.[57] Studies from PCa cell models (LNCaP, PC3, and Du145) and immunostaining of PCa specimens have indicated that Cav-1 can interact with LRP6 to regulate Wnt-β−catenin signaling.[58,59] Moreover, Cav-1 contributes to the expression of CSC-related genes including *Oct4*, *Nanog*, *CD44*, *CD133*, and *ABCG2* in lung cancer cell and breast cancer models,[59,60] which all strongly suggest that Cav-1 signaling involved in the induction of CSC phenotypes. However, additional data are required to link Cav-1 directly to CSC generation in CRPC.

MicroRNAs contribute to CSC properties of PCa cell

Emerging evidence has implied that microRNA (miRNA) regulation is crucial in promoting or repressing cancer metastasis via regulating the characteristics of CSCs. In particular, dysregulation of miRNAs is associated with tumor initiation and progression of PCa. A coordinated downregulation of miR-34a, let-7b, miR-106a, and miR-200 family has been observed in the progenitor stem cell population of PCa (**Table 1**).[61]

miR-34, a p53 downstream target gene, is known as a tumor-suppressor miRNA. Frequent hypermethylation of miR-34 has been observed in many malignancies with p53 mutation. Cheng *et al.*[62] using conditional knockout/transgenic mouse model demonstrated that inactivation of both p53 and miR-34a in mouse prostate epithelium leads to the expansion of the prostate stem cell compartment, as well as development of early invasive adenocarcinoma and high-grade prostatic intraepithelial neoplasia. Consistent with their *in vivo* observations, combined deficiency of both miR-34 and p53 leads to accelerated EMT-dependent growth, enhanced self-renewal capacity, and increased cell motility in prostate stem/progenitor cells derived from the proximal region of prostatic ducts.[62] In addition, miR-34a is known to be a key negative regulator of CD44, an adhesion molecule that is a key player in metastasis. CSCs derived from multiple malignant tumors have shown high expression of CD44. These CD44-positive CSC populations have colonogenic, tumor-initiating, and metastatic capacities. Liu *et al.*[63] demonstrated that systemic delivery of miR-34a can inhibit PCa metastasis and regeneration by targeting CD44. A recent study done by Bucay *et al.*[64] also revealed that another CD44-targeting miRNA, miR-383, is frequently downregulated due to loss of the chromosome 8p22 locus in the progression of PCa. Functionally, miR-383 is shown to inhibit tumor-initiating potential and metastasis of CD44-positive PCa cells by direct targeting of CD44.[64]

miR-320 is found significantly downregulated in the progression of PCa; reduction of miR-320 associated with increased β-catenin expression has been observed in a CD44-high subpopulation of PCa cells and clinical prostatic tumor specimens. By global gene expression profiling, we reported that ectopic expression of miR-320 in PCa cells leads to suppression of CSC markers such as CD133, CD117, CXCXR4, and ABCG2, as well as downstream target genes of Wnt/β-catenin pathway.[27] Functionally, miR-320 deficiency facilitates the CSC properties including tumor-sphere formation, chemo-resistance, and tumorigenic abilities. Overall, this study strongly suggested that miR-320 is a potent regulator of tumor-initiating cells in prostate.

Similar to miR-320, expression level of miR-7 is also significantly reduced in a subpopulation of CD133-positive/CD44-positive PCa cells, which possess CSC-like features and are sufficient for tumorigenesis based on a limited dilution analysis. On the other hand, restoration of miR-7 in PCa cell lines results in sustained inhibition of CSC characteristics and impaired tumorigenesis via targeting Kruppel-like factor 4 (*Klf4*). Overall, this study implies the critical role of miR-7 in regulating the properties of PCa stem cell.[65]

Meanwhile, loss of the let-7 family has been observed in PCa tissue specimens, particularly in high-grade tumor. Kong *et al.*[66] demonstrated an inverse correlation between let-7 and enhancer of Zeste homolog 2 (EZH2), a putative let-7 family target that is highly expressed in CSCs of many malignancies and is known to regulate expansion and maintenance of CSC.[67] Functionally, let-7 is shown to diminish both colonogenic ability and sphere-forming capacity via targeting *EZH2* in PCa cells.[66]

Similar to let-7, expression level of miR-100 is also significantly decreased particularly in bone metastatic PCa specimens. Wang *et al.*[68] suggested that miR-100 regulates spheroid and colony formation of PCa cells by targeting argonaute 2, RISC catalytic component (Ago2), leading to suppression of stemness markers such as c-Myc, CD44, Klf4, and Oct4. This indicates that loss of miR-100 may promote the stemness

Table 1: MicroRNAs involved in prostate cancer progression to castration-resistant prostate cancer

MicroRNAs	*Target gene*	*Impacts on PCa progression*	*Reference*
miR-34	*CD44*	Inhibits PCa metastasis, regeneration, and carcinogenesis	62,63
miR-383	*CD44*	Inhibits tumor-initiating potential and metastasis of CD44-positive PCa cells	64
miR-320	*CD133, CD117, CXCXR4, ABCG2*	Suppress tumor-sphere formation, chemoresistance, and tumorigenic abilities of prostatic CSCs	27
miR-7	*Klf4*	Inhibits stemness properties and impaires tumorigenesis of PCa stem-like cells	65
let-7	*EZH2*	Diminishes colonogenic ability and sphere-forming capacity of PCa cells	61,66
miR-100	*AGO2*	Regulates spheroid and colony formation of PCa cells	68,69
miR-200b	*Bmi-1*	Suppresses proliferation and migration, as well as enhances chemosensitivity of PCa cells to docetaxel	70
miR-141	*Klf9*	Facilitates spheroid formation and proliferation of PCa cell	73
miR-143 miR-145	*Oct4, Sox2, Klf4, FNDC3B*	Inhibits cell viability and colony formation of bone metastatic PC3 cells. Suppresses tumor sphere formation and CSC marker expression in PC-3 cells	74,76-78
miR-128	*BMI-1, NANOG, TGFBR1*	Reduces sphere formation and colonogenic potential of PCa cells	79
miR-663		Enhances cell proliferation, invasion and neuroendocrine differentiation characteristics in PCa cells	108

PCa: prostate cancer; CRPC: castration-resistant PCa; CSC: cancer stem cell; Sox2: sex determining region Y-box 2; Bmi-1: B-cell-specific Moloney murine leukemia virus insertion site 1; TGFBR1: transforming growth factor beta receptor 1; Klf4: Kruppel-like factor 4; FNDC3B: fibronectin type III domain containing 3B; EZH2: enhancer of Zeste homolog 2; Klf9: Kruppel like factor 9; CXCXR4: C-X-C chemokine receptor type 4; ABCG2: ATP-binding cassette subfamily G member 2 (Junior blood group); AGO2: argonaute 2, RISC catalytic component

properties of PCa. On the contrary, by screening miRNA expression in PCa patient-derived xenograft tumor lineages, a recent study done by Nabavi *et al.*[69] demonstrated that several miRNAs (miR-100-5p, miR-411-5p, and miR-185-5p) are associated with the regression to dormancy status after ADT. Particularly, miR-100 has been recognized as a key component contributing to initiation and evolution of CRPC; it is believed that miR-100 is critical for the cell survival upon AR deprivation in AR-positive PCa cell lines.[69]

The miR-200 family (miR-200a/b/c and miR-141) is known for targeting mesenchymal transcription factors leading to inhibition of EMT. In particular, Yu *et al.*[70] reported that miR-200b is significantly downregulated in PCa *in vivo* and in advanced PCa cell lines (LNCaP, PC3, and DU145), as well as patient samples (BPH) *in vitro*. Ectopic expression of miR-200b sensitizes PCa cells to chemotherapeutic reagent, docetaxel, by targeting the gene, B-cell-specific Moloney murine leukemia virus insertion site 1 (*Bmi-1*),[70] which is a critical regulator of CSC properties in several malignancies such as breast and gastric cancers.[71,72] In contrast, miR-141-3p has an opposite regulatory role. Li *et al.*[73] utilized miR-141-3p mimics to demonstrate its effect on facilitating spheroid formation and proliferation of PCa cell line (PC3). The impact of miR-141 on promoting PC3 stemness is associated with the upregulation of Oct4, Bmi-1, sex-determining region Y-box 9 (Sox9), and CD44, suggesting that miR-141 can target a common repressor of these genes.[73] Certainly, more detailed studies are needed to unveil the mechanism of action of miR-141.

Both miR-143 and miR-145 are known to regulate bone metastasis of PCa. Huang *et al.*[74] reported that both miR-143 and miR-145 can inhibit colony formation, suppress sphere-forming capacity, and reduce expression of CSC markers (CD133, CD44, Oct4, c-Myc, and Klf4) in bone-metastasis-derived PCa cell line. The finding of this study strongly suggested that miR-143 and miR-145 may play a crucial role in regulating CSCs in bone metastatic PCa. Accumulating studies have indicated that miR-145 negatively regulates pluripotency of embryonic stem cells via targeting several stemness markers such as Oct4, Sox2, and Klf4.[75,76] Ozen *et al.*[77] demonstrated that ectopic expression of miR-145 leads to reduced cell renewal of PCa cell lines by targeting *Sox2* gene expression. By screening the miRNA expression between 3D-sphere and 2D-adherent PCa cells, Fan *et al.*[78] unveiled that progressively elevated miR-143 is found in the sphere-re-adherent culture of PCa cells, suggesting that miR-143 is involved in stem cell formation.

In contrast to those miRNAs with CSC-promoting activities, it is significantly reduced miR-128 in PCa compared to benign prostate tissue that may have an opposite function. Indeed, Jin *et al.*[79] demonstrated that overexpression of miR-128 leads to diminished CSC properties by reducing sphere formation and clonogenic potential in PCa cells. Mechanistically, miR-128 is shown to target on several self-renewal genes such as *BMI-1*, *NANOG*, and transforming growth factor beta receptor 1 (*TGFBR1*).[79] Overall, this study highly suggested that miR-128 regulates tumor initiation in PCa by limiting the CSC properties mediated by BMI-1 and NANOG.

NEUROENDOCRINE DIFFERENTIATION (NED) IN CRPC AND CSC

Prostate NED carcinoma is considered as a type of prostatic epithelial neoplasms that have NED feature,[80] which usually identified by histopathological examination with NED markers. Therefore, NED can be found in small cell carcinoma, carcinoid, and carcinoid-like tumors, as well as prostatic adenocarcinoma (**Figure 2**). Importantly, NED has been found in recurrent CPRC after second line of ADT.[81,82] Although small cell carcinoma in prostate only counts for less than 2% of total PCa population,[80] neuroendocrine prostate cancer (NEPC) is detected in 10%–20% of CRPC population.[83] Interestingly, a study with PCa cells (Du145 and PC3) and xenograft models demonstrates that $CD44^+$ is selectively expressed in neuroendocrine cells and these cells are responsible for PCa recurrence.[84] NEPC is an end stage of CRPC and most patients survive less than a year after recurrence.[85] Clinically, NEPC is identified based on histology features. In general, the tumor cell morphology was similar to high-grade neuroendocrine cancers, which have high numbers of mitotic cells with nuclear molding and chromatin-like "salt and pepper" similar to small cell.[81,86] In addition, there are neuroendocrine markers that can be used for validation.

Cell markers for NED in CRPC

There are several general NED markers that are currently used to diagnose NEPC, and the presence of at least one of these is diagnostic of the condition. These markers include (1) neuron-specific enolase (NSE), a cell-specific isoenzyme of the glycolytic enzyme enolase, and it is one of the most reliable markers for the diagnosis of small cell in lung cancer;[87] (2) synaptophysin (SYP), a major synaptic vesicle protein, is usually combined with the neuroendocrine secretory protein, chormogranin A (ChgA), for diagnosis;[88] (3) ChgA, a secretory

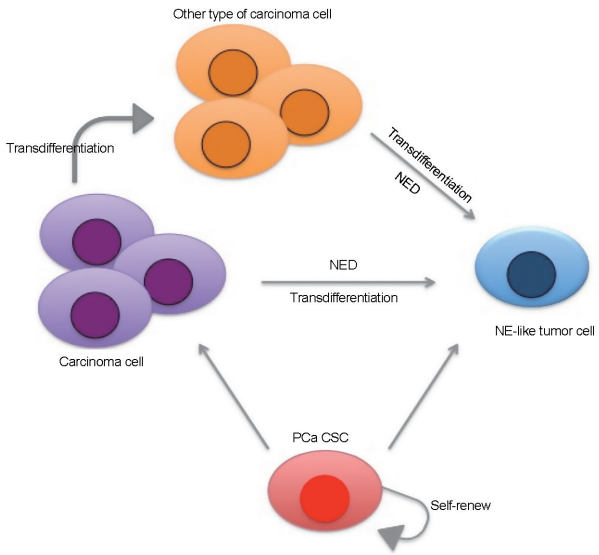

Figure 2: Schematic representation of the relationship of CSC, PCa cells, and NE-like cell. CSC maintains its multipotency to form different types of tumor cell and is capable of self-renewing to expand its progeny. NE-like tumor cell can originate from the same type of tumor cells that undergo NED or transdifferentiation from other type of tumor cell (*i.e.*, adenocarcinoma to small cell adenocarcinoma with NE phenotype). CSC: cancer stem cell; PCa: prostate cancer; NE: neuroendocrine; NED: neuroendocrine differentiation.

protein found in the neuroendocrine cells, has commonly used in detecting neuroendocrine tumors;[89] (4) CD56, also known as neural cell adhesive molecule (NCAM), which belongs to a group of cell surface glycoproteins involved in cell-cell adhesion.[90] On the other hand, NEPC cells often lack the expression of luminal markers such as PSA and prostatic acid phosphatase.[91] Recently, FOXA2 has also been suggested to be a reliable marker in diagnosis of NEPC.[92]

Molecular mechanisms leading to NED in CRPC

Several studies have indicated that Myc (N-Myc or c-Myc) plays a key role in NEPC and also *Myc* gene amplification or protein overexpression is often detected in clinical specimens.[93] Recently, Lee *et al.*[94] have indicated that ectopic expression of N-Myc in basal cell population of prostate potentiates NEPC through the activation of Akt signaling pathway with human patient sample model *in vivo* and *in vitro*. Other embryonic transcription factors such as FOXA1 and FOXA2 are associated with NEPC. FOXA1 is known as a pioneering factor in modulating AR activity, and is also involved in prostate epithelial differentiation by altering chromatin tertiary structure. However, the loss of FOXA1 is found to facilitate NEPC through the mitogen-activated protein kinase/extracellular signal-regulated kinase (MAPK/ERK) signaling pathways in both cell line model (TRAMP-C and 22Rv1) and human patient sample.[95] In contrast, FOXA2 expression was detected in NEPC, but not in primary and metastatic PCa samples (NCI-H660, PC3),[92] and it cooperates with hypoxia-inducible factor 1 subunit alpha (HIF-1α) activity to facilitate NED in PCa cell model (PC3, NCIH660, LAPC4, and LNCaP).[96] In addition, other key regulators in neuronal differentiation such as BRN2, POU-domain transcription factor, have recently shown to regulate Sox2, which contributes to NED in PCa cell model (PC3, NCI-H660, LNCaP, and LAPC4).[97]

Under the influence of tumor microenvironment, studies with mouse PCa *in vitro* and *in vivo* model, as well as LNCaP cell model, have found that interleukin 6/signal transducer and activator of transcription 3 (IL-6/STAT3) pathway associated with aurora kinase A (AURKA), N-Myc, and EZH2 have been shown to induce NEPC.[98,99] Mechanistically, in LNCaP cell model, autophagy process is involved in IL-6-induced NED and therapy-resistant phenotype in PCa model;[100] thus, targeting autophagy synthesis or related signaling pathways can block neuroendocrine cell differentiation.[101,102] In addition, secretory protein secretogranin II (SgII), a neuroendocrine secretory protein-like ChgA that is widely distributed throughout the neuroendocrine system, has been shown to induce NEPC phenotype.[103] G-protein coupled receptor kinase 3 (GRK3) expression correlated with PCa progression has been shown to increase neuroendocrine phenotypes associated with ADT resistance in PCa cells (NCI-H660, PC3, LNCaP, and VCaP).[104] In contrast to oncogenic factors, loss of retinoblastoma 1 (RB1) and tumor protein p53 (TP53) further facilitates ADT resistance of PCa cells that exhibit several NED markers in both clinical patient sample and mouse model.[105,106]

MicroRNAs correlated with NED in PCa

Dang *et al.*[107] demonstrated that the treatment of enzalutamide or casodex increases the infiltration of mast cells secreting C-C motif chemokine ligand 8 (CCL8) and IL-8 that can promote NED phenotypes by upregulating miR-32 in PCa cells. Indeed, overexpression of miR-32 leads to enhanced NED characteristics in PCa cells associated with elevated NSE. Overall, this study demonstrates that the potential impact of immune cells on the emergence of NED in PCa is mediated by microRNA.[107]

Meanwhile, by examining PCa tissue specimens, Jiao *et al.*[108] revealed a significant upregulation of miR-663 in CRPC. Functionally, overexpression of miR-663 in LNCaP cell results in enhanced cell proliferation, invasion, and NED. Clinically, expression level of miR-663 is correlated with PCa grade, node, and metastasis (TNM) staging of PCa,[108] suggesting miR-663 as a potent regulator in NEPC.

In addition, Liang *et al.*[109] reported that hypoxia can promote NED in PCa cell lines such as LNCaP and PC3 by inducing the expression of a polycistronic miRNA cluster containing miR-106b, miR-93, and miR-25, which can suppress the expression of neuron-restrictive silencer factor, also known as RE1-Silencing Transcription factor (*REST*) gene, but increase of pro-neuronal genes such as paired mesoderm homeobox protein 2A (*PHOX2A*), absent small and homeotic disks protein 1 (*ASH-1*), and *ChgA*. Clinically, an inverse correlation between miR-106b-25 and REST is observed in PCa with high Gleason grade.[109] Altogether, this study suggested that loss of REST due to elevation of miR-106b-25 under hypoxia condition might promote NED in PCa.

TRANSDIFFERENTIATION IN CPRC

Transdifferentiation is the process of cell conversion from one type to another type (**Figure 2**). For example, pancreatic progenitor cells transdifferentiate into hepatocyte-like cells.[110] Recent data clearly show that somatic cells can undergo reprograming process by exogenously introducing key transcription factors such as Sox2, Klf4, c-Myc, Oct4, Nanog, and lin-28 homolog A (LIN28).[111,112] For cancer cells, particularly, high-grade poorly differentiated cancer cells exhibiting CSC phenotypes can transdifferentiate into different cell types by turning on similar genes endogenously.[113] For example, loss of Rb1 and TP53 underlying cancer lineage plasticity[106] is mediated by increased Sox2 expression in these cells.[114] Similarly, loss of PTEN and TP53 facilitates ADT resistance and initiates transdifferentation event in adenocarcinoma, which is evidenced by elevated NED markers.[115] All these data conclude that CSC is the result of cancer cell de-differentiation through genetic alteration and/or epigenetic

alteration from tumor microenvironment. In CRPC, accumulating evidence supports that CSC plays a central role of therapeutic resistance, NED. Thus, developing anti-CSC strategy is expected to improve the survival of CRPC patients.

CONCLUSION

The presence of CSC has been identified in hematopoietic and testicular cancers but less known in solid tumors, particularly PCa. Accumulating data support the critical role of prostate CSC in disease progression. Despite these progresses, there is still lacking human PCa-specific CSC marker(s). Further, the underlying mechanisms of transdifferentiation as well as NED in CSC are not fully understood, which will be critical for further developing better therapeutic strategies.

AUTHOR CONTRIBUTIONS

CJL and UGL prepared manuscript. JTH outlined framework and finalized manuscript. All authors read and approved the final manuscript.

COMPETING INTERESTS

All authors declare no competing interests.

ACKNOWLEDGMENTS

We thank Dr. Samarpita Sengupta for editorial assistance. This work was supported in part by grants from the United States Army (W81XWH-16-1-0474 to Jer-Tsong Hsieh).

REFERENCES

1 Patrawala L, Calhoun T, Schneider-Broussard R, Zhou J, Claypool K, *et al*. Side population is enriched in tumorigenic, stem-like cancer cells, whereas ABCG2^{+} and ABCG2^{-} cancer cells are similarly tumorigenic. *Cancer Res* 2005; 65: 6207–19.
2 Maitland NJ, Collins A. A tumour stem cell hypothesis for the origins of prostate cancer. *BJU Int* 2005; 96: 1219–23.
3 Schalken JA, van Leenders G. Cellular and molecular biology of the prostate: stem cell biology. *Urology* 2003; 62: 11–20.
4 Isaacs JT, Coffey DS. Etiology and disease process of benign prostatic hyperplasia. *Prostate Suppl* 1989; 2: 33–50.
5 Goto K, Salm SN, Coetzee S, Xiong X, Burger PE, *et al*. Proximal prostatic stem cells are programmed to regenerate a proximal-distal ductal axis. *Stem Cells* 2006; 24: 1859–68.
6 Cunha GR, Lung B. The possible influence of temporal factors in androgenic responsiveness of urogenital tissue recombinants from wild-type and androgen-insensitive (Tfm) mice. *J Exp Zool* 1978; 205: 181–93.
7 Moad M, Hannezo E, Buczacki SJ, Wilson L, El-Sherif A, *et al*. Multipotent basal stem cells, maintained in localized proximal niches, support directed long-ranging epithelial flows in human prostates. *Cell Rep* 2017; 20: 1609–22.
8 Schalken JA. Molecular and cellular prostate biology: origin of prostate-specific antigen expression and implications for benign prostatic hyperplasia. *BJU Int* 2004; 93 Suppl 1: 5–9.
9 Zhang D, Park D, Zhong Y, Lu Y, Rycaj K, *et al*. Stem cell and neurogenic gene-expression profiles link prostate basal cells to aggressive prostate cancer. *Nat Commun* 2016; 7: 10798.
10 Harner-Foreman N, Vadakekolathu J, Laversin SA, Mathieu MG, Reeder S, *et al*. A novel spontaneous model of epithelial-mesenchymal transition (EMT) using a primary prostate cancer derived cell line demonstrating distinct stem-like characteristics. *Sci Rep* 2017; 7: 40633.
11 Kong D, Sethi S, Li Y, Chen W, Sakr WA, *et al*. Androgen receptor splice variants contribute to prostate cancer aggressiveness through induction of EMT and expression of stem cell marker genes. *Prostate* 2015; 75: 161–74.
12 Abell AN, Johnson GL. Implications of mesenchymal cells in cancer stem cell populations: relevance to EMT. *Curr Pathobiol Rep* 2014; 2: 21–6.
13 Chiou SH, Wang ML, Chou YT, Chen CJ, Hong CF, *et al*. Coexpression of Oct4 and Nanog enhances malignancy in lung adenocarcinoma by inducing cancer stem cell-like properties and epithelial-mesenchymal transdifferentiation. *Cancer Res* 2010; 70: 10433–44.
14 Klarmann GJ, Hurt EM, Mathews LA, Zhang X, Duhagon MA, *et al*. Invasive prostate cancer cells are tumor initiating cells that have a stem cell-like genomic signature. *Clin Exp Metastasis* 2009; 26: 433–46.
15 Xin L, Lawson DA, Witte ON. The Sca-1 cell surface marker enriches for a prostate-regenerating cell subpopulation that can initiate prostate tumorigenesis. *Proc Natl Acad Sci U S A* 2005; 102: 6942–7.
16 Burger PE, Xiong X, Coetzee S, Salm SN, Moscatelli D, *et al*. Sca-1 expression identifies stem cells in the proximal region of prostatic ducts with high capacity to reconstitute prostatic tissue. *Proc Natl Acad Sci U S A* 2005; 102: 7180–5.
17 Richardson GD, Robson CN, Lang SH, Neal DE, Maitland NJ, *et al*. CD133, a novel marker for human prostatic epithelial stem cells. *J Cell Sci* 2004; 117: 3539–45.
18 Vander Griend DJ, Karthaus WL, Dalrymple S, Meeker A, DeMarzo AM, *et al*. The role of CD133 in normal human prostate stem cells and malignant cancer-initiating cells. *Cancer Res* 2008; 68: 9703–11.
19 Guzel E, Karatas OF, Duz MB, Solak M, Ittmann M, *et al*. Differential expression of stem cell markers and ABCG2 in recurrent prostate cancer. *Prostate* 2014; 74: 1498–505.
20 Harris KS, Kerr BA. Prostate cancer stem cell markers drive progression, therapeutic resistance, and bone metastasis. *Stem Cells Int* 2017; 2017: 8629234.
21 Takebe N, Miele L, Harris PJ, Jeong W, Bando H, *et al*. Targeting Notch, Hedgehog, and Wnt pathways in cancer stem cells: clinical update. *Nat Rev Clin Oncol* 2015; 12: 445–64.
22 Gu JW, Rizzo P, Pannuti A, Golde T, Osborne B, *et al*. Notch signals in the endothelium and cancer "stem-like" cells: opportunities for cancer therapy. *Vasc Cell* 2012; 4: 7.
23 Zhang K, Guo Y, Wang X, Zhao H, Ji Z, *et al*. WNT/β-catenin directs self-renewal symmetric cell division of hTERT^{high} prostate cancer stem cells. *Cancer Res* 2017; 77: 2534–47.
24 Chesire DR, Ewing CM, Sauvageot J, Bova GS, Isaacs WB. Detection and analysis of beta-catenin mutations in prostate cancer. *Prostate* 2000; 45: 323–34.
25 Bisson I, Prowse DM. WNT signaling regulates self-renewal and differentiation of prostate cancer cells with stem cell characteristics. *Cell Res* 2009; 19: 683–97.
26 Wan X, Liu J, Lu JF, Tzelepi V, Yang J, *et al*. Activation of β-catenin signaling in androgen receptor-negative prostate cancer cells. *Clin Cancer Res* 2012; 18: 726–36.
27 Hsieh IS, Chang KC, Tsai YT, Ke JY, Lu PJ, *et al*. MicroRNA-320 suppresses the stem cell-like characteristics of prostate cancer cells by downregulating the Wnt/beta-catenin signaling pathway. *Carcinogenesis* 2013; 34: 530–8.
28 Tostar U, Malm CJ, Meis-Kindblom JM, Kindblom LG, Toftgard R, *et al*. Deregulation of the hedgehog signalling pathway: a possible role for the *PTCH* and *SUFU* genes in human rhabdomyoma and rhabdomyosarcoma development. *J Pathol* 2006; 208: 17–25.
29 Giakoustidis A, Giakoustidis D, Mudan S, Sklavos A, Williams R. Molecular signalling in hepatocellular carcinoma: role of and crosstalk among WNT/β-catenin, Sonic Hedgehog, Notch and Dickkopf-1. *Can J Gastroenterol Hepatol* 2015; 29: 209–17.
30 Zunich SM, Valdovinos M, Douglas T, Walterhouse D, Iannaccone P, *et al*. Osteoblast-secreted collagen upregulates paracrine Sonic hedgehog signaling by prostate cancer cells and enhances osteoblast differentiation. *Mol Cancer* 2012; 11: 30.
31 Clement V, Sanchez P, de Tribolet N, Radovanovic I, Ruiz I Altaba A. HEDGEHOG-GLI1 signaling regulates human glioma growth, cancer stem cell self-renewal, and tumorigenicity. *Curr Biol* 2007; 17: 165–72.
32 Chang HH, Chen BY, Wu CY, Tsao ZJ, Chen YY, *et al*. Hedgehog overexpression leads to the formation of prostate cancer stem cells with metastatic property irrespective of androgen receptor expression in the mouse model. *J Biomed Sci* 2011; 18: 6.
33 Bernard D, Pourtier-Manzanedo A, Gil J, Beach DH. Myc confers androgen-independent prostate cancer cell growth. *J Clin Invest* 2003; 112: 1724–31.
34 Gregory CW, Hamil KG, Kim D, Hall SH, Pretlow TG, *et al*. Androgen receptor expression in androgen-independent prostate cancer is associated with increased expression of androgen-regulated genes. *Cancer Res* 1998; 58: 5718–24.
35 Lee CT, Capodieci P, Osman I, Fazzari M, Ferrara J, *et al*. Overexpression of the cyclin-dependent kinase inhibitor p16 is associated with tumor recurrence in human prostate cancer. *Clin Cancer Res* 1999; 5: 977–83.
36 Gerhardt J, Montani M, Wild P, Beer M, Huber F, *et al*. FOXA1 promotes tumor progression in prostate cancer and represents a novel hallmark of castration-resistant prostate cancer. *Am J Pathol* 2012; 180: 848–61.
37 Sahu B, Laakso M, Ovaska K, Mirtti T, Lundin J, *et al*. Dual role of FoxA1 in androgen receptor binding to chromatin, androgen signalling and prostate cancer. *EMBO J* 2011; 30: 3962-76.
38 McCourt C, Maxwell P, Mazzucchelli R, Montironi R, Scarpelli M, *et al*. Elevation of c-FLIP in castrate-resistant prostate cancer antagonizes therapeutic response to androgen receptor-targeted therapy. *Clin Cancer Res* 2012; 18: 3822–33.
39 Espinoza I, Pochampally R, Xing F, Watabe K, Miele L. Notch signaling: targeting cancer stem cells and epithelial-to-mesenchymal transition. *Onco Targets Ther* 2013; 6: 1249–59.
40 Shen MM, Abate-Shen C. Molecular genetics of prostate cancer: new prospects for old challenges. *Genes Dev* 2010; 24: 1967–2000.
41 Chang L, Graham PH, Ni J, Hao J, Bucci J, *et al*. Targeting PI3K/Akt/mTOR signaling pathway in the treatment of prostate cancer radioresistance. *Crit Rev Oncol Hematol* 2015; 96: 507–17.
42 Sarker D, Reid AH, Yap TA, de Bono JS. Targeting the PI3K/AKT pathway for the treatment of prostate cancer. *Clin Cancer Res* 2009; 15: 4799–805.

43 Domingo-Domenech J, Vidal SJ, Rodriguez-Bravo V, Castillo-Martin M, Quinn SA, *et al.* Suppression of acquired docetaxel resistance in prostate cancer through depletion of notch- and hedgehog-dependent tumor-initiating cells. *Cancer Cell* 2012; 22: 373–88.
44 Zhang L, Sha J, Yang G, Huang X, Bo J, *et al.* Activation of Notch pathway is linked with epithelial-mesenchymal transition in prostate cancer cells. *Cell Cycle* 2017; 16: 999–1007.
45 Su Q, Zhang B, Zhang L, Dang T, Rowley D, *et al.* Jagged1 upregulation in prostate epithelial cells promotes formation of reactive stroma in the Pten null mouse model for prostate cancer. *Oncogene* 2017; 36: 618–27.
46 Terada N, Shiraishi T, Zeng Y, Aw-Yong KM, Mooney SM, *et al.* Correlation of Sprouty1 and Jagged1 with aggressive prostate cancer cells with different sensitivities to androgen deprivation. *J Cell Biochem* 2014; 115: 1505–15.
47 Meunier A, Flores AN, McDermott N, Rivera-Figueroa K, Perry A, *et al.* Hypoxia regulates Notch-3 mRNA and receptor activation in prostate cancer cells. *Heliyon* 2016; 2: e00104.
48 Zhang J, Kuang Y, Wang Y, Xu Q, Ren Q. Notch-4 silencing inhibits prostate cancer growth and EMT via the NF-kappaB pathway. *Apoptosis* 2017; 22: 877–84.
49 Wang W, Wang L, Mizokami A, Shi J, Zou C, *et al.* Down-regulation of E-cadherin enhances prostate cancer chemoresistance via Notch signaling. *Chin J Cancer* 2017; 36: 35.
50 Karam JA, Lotan Y, Roehrborn CG, Ashfaq R, Karakiewicz PI, *et al.* Caveolin-1 overexpression is associated with aggressive prostate cancer recurrence. *Prostate* 2007; 67: 614–22.
51 Mouraviev V, Li L, Tahir SA, Yang G, Timme TM, *et al.* The role of caveolin-1 in androgen insensitive prostate cancer. *J Urol* 2002; 168: 1589–96.
52 Thompson TC, Tahir SA, Li L, Watanabe M, Naruishi K, *et al.* The role of caveolin-1 in prostate cancer: clinical implications. *Prostate Cancer Prostatic Dis* 2010; 13: 6–11.
53 Katsogiannou M, El Boustany C, Gackiere F, Delcourt P, Athias A, *et al.* Caveolae contribute to the apoptosis resistance induced by the alpha (1A)-adrenoceptor in androgen-independent prostate cancer cells. *PLoS One* 2009; 4: e7068.
54 Zhang X, Ling MT, Wang Q, Lau CK, Leung SC, *et al.* Identification of a novel inhibitor of differentiation-1 (ID-1) binding partner, caveolin-1, and its role in epithelial-mesenchymal transition and resistance to apoptosis in prostate cancer cells. *J Biol Chem* 2007; 282: 33284–94.
55 Bartz R, Zhou J, Hsieh JT, Ying Y, Li W, *et al.* Caveolin-1 secreting LNCaP cells induce tumor growth of caveolin-1 negative LNCaP cells *in vivo*. *Int J Cancer* 2008; 122: 520–5.
56 Tahir SA, Kurosaka S, Tanimoto R, Goltsov AA, Park S, *et al.* Serum caveolin-1, a biomarker of drug response and therapeutic target in prostate cancer models. *Cancer Biol Ther* 2013; 14: 117–26.
57 Zou W, Ma X, Hua W, Chen B, Cai G. Caveolin-1 mediates chemoresistance in cisplatin-resistant ovarian cancer cells by targeting apoptosis through the Notch-1/Akt/NF-kappaB pathway. *Oncol Rep* 2015; 34: 3256–63.
58 Tahir SA, Yang G, Goltsov A, Song KD, Ren C, *et al.* Caveolin-1-LRP6 signaling module stimulates aerobic glycolysis in prostate cancer. *Cancer Res* 2013; 73: 1900–11.
59 Wang Z, Wang N, Li W, Liu P, Chen Q, *et al.* Caveolin-1 mediates chemoresistance in breast cancer stem cells via β-catenin/ABCG2 signaling pathway. *Carcinogenesis* 2014; 35: 2346–56.
60 Phiboonchaiyanan PP, Kiratipaiboon C, Chanvorachote P. Ciprofloxacin mediates cancer stem cell phenotypes in lung cancer cells through caveolin-1-dependent mechanism. *Chem Biol Interact* 2016; 250: 1–11.
61 Liu C, Kelnar K, Vlassov AV, Brown D, Wang J, *et al.* Distinct microRNA expression profiles in prostate cancer stem/progenitor cells and tumor-suppressive functions of let-7. *Cancer Res* 2012; 72: 3393–404.
62 Cheng CY, Hwang CI, Corney DC, Flesken-Nikitin A, Jiang L, *et al.* miR-34 cooperates with p53 in suppression of prostate cancer by joint regulation of stem cell compartment. *Cell Rep* 2014; 6: 1000–7.
63 Liu C, Kelnar K, Liu B, Chen X, Calhoun-Davis T, *et al.* The microRNA miR-34a inhibits prostate cancer stem cells and metastasis by directly repressing CD44. *Nat Med* 2011; 17: 211–5.
64 Bucay N, Sekhon K, Yang T, Majid S, Shahryari V, *et al.* MicroRNA-383 located in frequently deleted chromosomal locus 8p22 regulates CD44 in prostate cancer. *Oncogene* 2017; 36: 2667–79.
65 Chang YL, Zhou PJ, Wei L, Li W, Ji Z, *et al.* MicroRNA-7 inhibits the stemness of prostate cancer stem-like cells and tumorigenesis by repressing KLF4/PI3K/Akt/p21 pathway. *Oncotarget* 2015; 6: 24017–31.
66 Kong D, Heath E, Chen W, Cher ML, Powell I, *et al.* Loss of let-7 up-regulates EZH2 in prostate cancer consistent with the acquisition of cancer stem cell signatures that are attenuated by BR-DIM. *PLoS One* 2012; 7: e33729.
67 Wen Y, Cai J, Hou Y, Huang Z, Wang Z. Role of EZH2 in cancer stem cells: from biological insight to a therapeutic target. *Oncotarget* 2017; 8: 37974–90.
68 Wang M, Ren D, Guo W, Wang Z, Huang S, *et al.* Loss of miR-100 enhances migration, invasion, epithelial-mesenchymal transition and stemness properties in prostate cancer cells through targeting Argonaute 2. *Int J Oncol* 2014; 45: 362–72.
69 Nabavi N, Saidy NR, Venalainen E, Haegert A, Parolia A, *et al.* miR-100-5p inhibition induces apoptosis in dormant prostate cancer cells and prevents the emergence of castration-resistant prostate cancer. *Sci Rep* 2017; 7: 4079.
70 Yu J, Lu Y, Cui D, Li E, Zhu Y, *et al.* miR-200b suppresses cell proliferation, migration and enhances chemosensitivity in prostate cancer by regulating Bmi-1. *Oncol Rep* 2014; 31: 910–8.
71 Wang X, Wang C, Zhang X, Hua R, Gan L, *et al.* Bmi-1 regulates stem cell-like properties of gastric cancer cells via modulating miRNAs. *J Hematol Oncol* 2016; 9: 90.
72 Kim SH, Singh SV. The role of polycomb group protein Bmi-1 and Notch4 in breast cancer stem cell inhibition by benzyl isothiocyanate. *Breast Cancer Res Treat* 2015; 149: 681–92.
73 Li JZ, Li J, Wang HQ, Li X, Wen B, *et al.* MiR-141-3p promotes prostate cancer cell proliferation through inhibiting kruppel-like factor-9 expression. *Biochem Biophys Res Commun* 2017; 482: 1381–6.
74 Huang S, Guo W, Tang Y, Ren D, Zou X, *et al.* miR-143 and miR-145 inhibit stem cell characteristics of PC-3 prostate cancer cells. *Oncol Rep* 2012; 28: 1831–7.
75 Liu T, Cheng W, Huang Y, Huang Q, Jiang L, *et al.* Human amniotic epithelial cell feeder layers maintain human iPS cell pluripotency via inhibited endogenous microRNA-145 and increased Sox2 expression. *Exp Cell Res* 2012; 318: 424–34.
76 Xu N, Papagiannakopoulos T, Pan G, Thomson JA, Kosik KS. MicroRNA-145 regulates OCT4, SOX2, and KLF4 and represses pluripotency in human embryonic stem cells. *Cell* 2009; 137: 647–58.
77 Ozen M, Karatas OF, Gulluoglu S, Bayrak OF, Sevli S, *et al.* Overexpression of miR-145-5p inhibits proliferation of prostate cancer cells and reduces SOX2 expression. *Cancer Invest* 2015; 33: 251–8.
78 Fan X, Chen X, Deng W, Zhong G, Cai Q, *et al.* Up-regulated microRNA-143 in cancer stem cells differentiation promotes prostate cancer cells metastasis by modulating FNDC3B expression. *BMC Cancer* 2013; 13: 61.
79 Jin M, Zhang T, Liu C, Badeaux MA, Liu B, *et al.* miRNA-128 suppresses prostate cancer by inhibiting BMI-1 to inhibit tumor-initiating cells. *Cancer Res* 2014; 74: 4183–95.
80 Parimi V, Goyal R, Poropatich K, Yang XJ. Neuroendocrine differentiation of prostate cancer: a review. *Am J Clin Exp Urol* 2014; 2: 273–85.
81 Yashi M, Terauchi F, Nukui A, Ochi M, Yuzawa M, *et al.* Small-cell neuroendocrine carcinoma as a variant form of prostate cancer recurrence: a case report and short literature review. *Urol Oncol* 2006; 24: 313–7.
82 Hu CD, Choo R, Huang J. Neuroendocrine differentiation in prostate cancer: a mechanism of radioresistance and treatment failure. *Front Oncol* 2015; 5: 90.
83 Cohen A, Richards KA, Patel S, Weiner A, Eggener SE, *et al.* Metastatic small cell carcinoma of the prostate: population-based analysis of patient characteristics and treatment paradigms. *Urol Oncol* 2015; 33: 70.e1–7.
84 Palapattu GS, Wu C, Silvers CR, Martin HB, Williams K, *et al.* Selective expression of CD44, a putative prostate cancer stem cell marker, in neuroendocrine tumor cells of human prostate cancer. *Prostate* 2009; 69: 787–98.
85 Deorah S, Rao MB, Raman R, Gaitonde K, Donovan JF. Survival of patients with small cell carcinoma of the prostate during 1973-2003: a population-based study. *BJU Int* 2012; 109: 824–30.
86 Stein ME, Bernstein Z, Abacioglu U, Sengoz M, Miller RC, *et al.* Small cell (neuroendocrine) carcinoma of the prostate: etiology, diagnosis, prognosis, and therapeutic implications – a retrospective study of 30 patients from the rare cancer network. *Am J Med Sci* 2008; 336: 478–88.
87 Isgro MA, Bottoni P, Scatena R. Neuron-specific enolase as a biomarker: biochemical and clinical aspects. *Adv Exp Med Biol* 2015; 867: 125–43.
88 Wiedenmann B, Franke WW, Kuhn C, Moll R, Gould VE. Synaptophysin: a marker protein for neuroendocrine cells and neoplasms. *Proc Natl Acad Sci U S A* 1986; 83: 3500-4.
89 Gut P, Czarnywojtek A, Fischbach J, Baczyk M, Ziemnicka K, *et al.* Chromogranin A -unspecific neuroendocrine marker. Clinical utility and potential diagnostic pitfalls. *Arch Med Sci* 2016; 12: 1–9.
90 Farinola MA, Weir EG, Ali SZ. CD56 expression of neuroendocrine neoplasms on immunophenotyping by flow cytometry: a novel diagnostic approach to fine-needle aspiration biopsy. *Cancer* 2003; 99: 240–6.
91 Vlachostergios PJ, Puca L, Beltran H. Emerging variants of castration-resistant prostate cancer. *Curr Oncol Rep* 2017; 19: 32.
92 Park JW, Lee JK, Witte ON, Huang J. FOXA2 is a sensitive and specific marker for small cell neuroendocrine carcinoma of the prostate. *Mod Pathol* 2017; 30: 1262–72.
93 Maina PK, Shao P, Liu Q, Fazli L, Tyler S, *et al.* c-MYC drives histone demethylase PHF8 during neuroendocrine differentiation and in castration-resistant prostate cancer. *Oncotarget* 2016; 7: 75585–602.
94 Lee JK, Phillips JW, Smith BA, Park JW, Stoyanova T, *et al.* N-Myc drives neuroendocrine prostate cancer initiated from human prostate epithelial cells. *Cancer Cell* 2016; 29: 536–47.
95 Kim J, Jin H, Zhao JC, Yang YA, Li Y, *et al.* FOXA1 inhibits prostate cancer neuroendocrine differentiation. *Oncogene* 2017; 36: 4072–80.
96 Qi J, Nakayama K, Cardiff RD, Borowsky AD, Kaul K, *et al.* Siah2-dependent

concerted activity of HIF and FoxA2 regulates formation of neuroendocrine phenotype and neuroendocrine prostate tumors. *Cancer Cell* 2010; 18: 23–38.
97 Bishop JL, Thaper D, Vahid S, Davies A, Ketola K, *et al.* The master neural transcription factor BRN2 is an androgen receptor-suppressed driver of neuroendocrine differentiation in prostate cancer. *Cancer Discov* 2017; 7: 54–71.
98 Dardenne E, Beltran H, Benelli M, Gayvert K, Berger A, *et al.* N-Myc induces an EZH2-mediated transcriptional program driving neuroendocrine prostate cancer. *Cancer Cell* 2016; 30: 563–77.
99 Sun F, Zhang ZW, Tan EM, Lim ZL, Li Y, *et al.* Icaritin suppresses development of neuroendocrine differentiation of prostate cancer through inhibition of IL-6/STAT3 and Aurora kinase A pathways in TRAMP mice. *Carcinogenesis* 2016; 37: 701–11.
100 Chang PC, Wang TY, Chang YT, Chu CY, Lee CL, *et al.* Autophagy pathway is required for IL-6 induced neuroendocrine differentiation and chemoresistance of prostate cancer LNCaP cells. *PLoS One* 2014; 9: e88556.
101 Morell C, Bort A, Vara-Ciruelos D, Ramos-Torres A, Altamirano-Dimas M, *et al.* Up-regulated expression of LAMP2 and autophagy activity during neuroendocrine differentiation of prostate cancer LNCaP cells. *PLoS One* 2016; 11: e0162977.
102 Kanayama M, Hayano T, Koebis M, Maeda T, Tabe Y, *et al.* Hyperactive mTOR induces neuroendocrine differentiation in prostate cancer cell with concurrent up-regulation of IRF1. *Prostate* 2017; 77: 1489–98.
103 Courel M, El Yamani FZ, Alexandre D, El Fatemi H, Delestre C, *et al.* Secretogranin II is overexpressed in advanced prostate cancer and promotes the neuroendocrine differentiation of prostate cancer cells. *Eur J Cancer* 2014; 50: 3039–49.
104 Sang M, Hulsurkar M, Zhang X, Song H, Zheng D, *et al.* GRK3 is a direct target of CREB activation and regulates neuroendocrine differentiation of prostate cancer cells. *Oncotarget* 2016; 7: 45171–85.
105 Tan HL, Sood A, Rahimi HA, Wang W, Gupta N, *et al.* Rb loss is characteristic of prostatic small cell neuroendocrine carcinoma. *Clin Cancer Res* 2014; 20: 890–903.
106 Ku SY, Rosario S, Wang Y, Mu P, Seshadri M, *et al.* Rb1 and Trp53 cooperate to suppress prostate cancer lineage plasticity, metastasis, and antiandrogen resistance. *Science* 2017; 355: 78–83.
107 Dang Q, Li L, Xie H, He D, Chen J, *et al.* Anti-androgen enzalutamide enhances prostate cancer neuroendocrine (NE) differentiation via altering the infiltrated mast cells → androgen receptor (AR) → miRNA32 signals. *Mol Oncol* 2015; 9: 1241–51.
108 Jiao L, Deng Z, Xu C, Yu Y, Li Y, *et al.* miR-663 induces castration-resistant prostate cancer transformation and predicts clinical recurrence. *J Cell Physiol* 2014; 229: 834–44.
109 Liang H, Studach L, Hullinger RL, Xie J, Andrisani OM. Down-regulation of RE-1 silencing transcription factor (REST) in advanced prostate cancer by hypoxia-induced miR-106b ~ 25. *Exp Cell Res* 2014; 320: 188–99.
110 Gratte FD, Pasic S, Olynyk JK, Yeoh GC, Tosh D, *et al.* Transdifferentiation of pancreatic progenitor cells to hepatocyte-like cells is not serum-dependent when facilitated by extracellular matrix proteins. *Sci Rep* 2018; 8: 4385.
111 Takahashi K, Yamanaka S. Induction of pluripotent stem cells from mouse embryonic and adult fibroblast cultures by defined factors. *Cell* 2006; 126: 663–76.
112 Ambasudhan R, Talantova M, Coleman R, Yuan X, Zhu S, *et al.* Direct reprogramming of adult human fibroblasts to functional neurons under defined conditions. *Cell Stem Cell* 2011; 9: 113–8.
113 Prasad A, Manivannan J, Loong DT, Chua SM, Gharibani PM, *et al.* A review of induced pluripotent stem cell, direct conversion by trans-differentiation, direct reprogramming and oligodendrocyte differentiation. *Regen Med* 2016; 11: 181–91.
114 Mu P, Zhang Z, Benelli M, Karthaus WR, Hoover E, *et al.* SOX2 promotes lineage plasticity and antiandrogen resistance in TP53- and RB1-deficient prostate cancer. *Science* 2017; 355: 84–8.
115 Zou M, Toivanen R, Mitrofanova A, Floch N, Hayati S, *et al.* Transdifferentiation as a mechanism of treatment resistance in a mouse model of castration-resistant prostate cancer. *Cancer Discov* 2017; 7: 736–49.

Am J Clin Exp Urol 2019;7(1):31-45
www.ajceu.us /ISSN:2330-1910/AJCEU0092338

Original Article

Interferon-induced IFIT5 promotes epithelial-to-mesenchymal transition leading to renal cancer invasion

U-Ging Lo[1], Jiming Bao[2], Junjie Cen[3], Hsin-Chih Yeh[1,4], Junhang Luo[3], Wanlong Tan[2], Jer-Tsong Hsieh[1,5]

[1]Department of Urology, University of Texas Southwestern Medical Center, Dallas, TX 75390, USA; [2]Department of Urology, Nanfang Hospital, Southern Medical University, Guangzhou 510515, Republic of China; [3]Department of Urology, The First Affiliated Hospital, Sun Yat-sen University, Guangzhou 510080, Republic of China; [4]Department of Urology, Kaohsiung Municipal Ta-Tung Hospital, Kaohsiung Medical University Hospital, Taiwan, Republic of China; [5]Department of Biotechnology, Kaohsiung Medical University, Kaohsiung, Taiwan, Republic of China

Received February 8, 2019; Accepted February 13, 2019; Epub February 18, 2019; Published February 28, 2019

Abstract: Interferon is known as a pleiotropic factor in innate immunity, cancer immunity and therapy. Despite an objective short-term response of interferon (IFN) therapy in renal cell carcinoma (RCC) patients, the potential adverse effect of IFN on RCC cells is not fully understood. In this study, we demonstrate that IFNs can enhance RCC invasion via a new mechanism of IFIT5-mediated tumor suppressor microRNA (miRNA) degradation resulted in the elevation of Slug and ZEB1 and epithelial-to-mesenchymal transition (EMT). Clinically, a significant upregulation of IFNγ signaling pathway (such as IFNGR1, IFNGR2, STAT1 and STAT2) is observed in RCC patients with metastatic disease. Overall, this study provides a new mechanism of action of IFN-elicited canonical pathway in regulating suppressor miRNAs. Most importantly, it highlights the potential pro-metastatic effect of IFNs, which could undermine the clinical applicability of IFNs for treating RCC patients.

Keywords: Interferon (IFN), interferon-induced tetratricopeptide repeat 5 (IFIT5), epithelial-to-mesenchymal transition (EMT)

Introduction

Renal cell carcinoma (RCC) is by far the most lethal urologic malignancy of cancer-specific mortality of 40% compared with 25% of overall mortality of prostate and bladder cancers because it is resistant to chemotherapeutics and radiotherapy [1]. Pathologically, RCC is a heterogenous disease consisting three major types: clear cell RCC (ccRCC) [2], papillary RCC [3] and chromophobe RCC [4]. As for the therapeutic strategy for RCC patients, usually localized primary tumor can be managed successfully with radical nephrectomy. On the contrary, despite the prognosis of metastatic RCC (mRCC) patients has improved with targeted therapies, 20-25% of the patients are refractory to chemotherapy at the first response assessment and acquire drug resistance during the treatment [5].

Accumulating studies have demonstrated that tumor-associated immune cells play a critical role in cancer development. The presence of tumor-associated macrophage (TAM) is able to increase tumor cell proliferation and dissemination in different cancer types [6-12]. Action of these tumor-infiltrating lymphocytes (TILs) is mainly mediated through secretion of cytokines such as interleukins (IL-1, IL-6, IL-8 and IL-10), tumor necrosis factors (TNF), and interferons (IFNs). Many studies have shown that these cytokines could stimulate tumor cell proliferation, protect tumor cells from apoptosis, or promote angiogenesis and metastasis. Interleukin-6 (IL-6) is known to act as pro-tumorigenic cytokine by facilitating cell growth and anti-apoptosis in multiple myeloma [13, 14]. High concentration of interleukin-1 (IL-1) is associated with more malignant tumor phenotype [15-18]. Both IL-1α and IL-β are implied to aggra-

vate tumor angiogenesis and invasiveness via induction of vascular endothelial cell growth factor (VEGF) and tumor necrosis factor (TNF) [18]. On the other hand, the role of IFNs in cancer development remains controversial. For example, both IFN and IFNγ can exhibit antitumor activities [19-25]. IFNγ is also responsible for antigen-specific tumor immunity [26-29]. In contrast, IFNγ was reported to facilitate lung metastasis in melanoma 30 and peritoneal dissemination of ovarian cancer [31]. In prostate cancer, our recent study also indicates that IFNγ can promote epithelial-to-mesenchymal transition (EMT) via a new mechanism of IFIT5 in specific microRNA (miRNA) turnover [32].

Clinically, a significant elevation of several key effectors (such as IFNγ receptor 1 and 2 [IFNGR1, IFNGR2], STAT1, STAT2) in IFNγ signaling pathway is associated with metastatic RCC tumor [33]. Nevertheless, the role of IFNs in RCC development is not fully characterized. In this study, we demonstrate that IFN-elicited RCC invasion is mediated by IFIT5-XRN1 complex responsible for specific microRNA (such as miR-363) turnover; loss of miR-363 expression has been detected in RCC specimens [34]. Taken together, IFN is a potent tumor promoter that is mediated by a new mechanism of action of IFIT5 in degrading tumor suppressor miRNA.

Materials and methods

Cell lines

ACHN, 7680 and 769P cell lines were maintained in RPMI-1640 medium supplemented with 10% fetal bovine serum (FBS). 293 cells were maintained in Dulbecco's Modified Eagle's Medium (DMEM) containing 10% FBS. Stable IFIT5-shRNA knockdown (shIFIT5) and control (shCon) RCC cell lines were established from ACHN, 7860 and 769P cell lines using pLK0.1-shCon or pLK0.1-shIFIT5 plasmids provided from Academia Sinica, Taiwan. All RCC cell lines were authenticated using the short tandem repeat (STR) profiling by Genomic Core in UT Southwestern Medical Center (UTSW). Mycoplasma testing was performed using MycoAlert® kit (Lonza Walkersville, Inc. Walkersville, MD) every quarterly to ensure Mycoplasma-free condition.

Invasion assay

RCC cells cultured in the serum-free RPMI-1640 medium for 18 hrs were plated onto the upper chamber of Transwell (8-um (i.e., 8-micrometer) pore size, Corning) pre-coated with 2.5% Matrigel, and bottom chamber contained RPMI-1640 medium with 10% FBS. After 24 hrs, cells from the bottom side of chamber were fixed by 4% paraformaldehyde, stained with 0.4% Crystal Violet and observed under microscope (Keyance). The crystal-violet-stained cells from each field were quantified using BZ-X Analyzer software. Relative invaded cells were normalized to control group of each experiment. Each experiment was performed in triplicates.

Construction of SSMut and DSMut pre-miRNA-expression plasmid

miR-363 and miR-128 expression plasmid was initially purchased from Origene and Genecopoeia, respectively. Native miR-363 or miR-128 expression plasmid was engineered to generate mutant pre-miR-363 or mutant miR-128 with 5'-end six nucleotides single stranded overhang (pre-SS^{6}Mut-miR-363 or pre-SS^{6}Mut-miR-128) or double-stranded blunt end (pre-DSMut-miR-363 or pre-DSMut-miR-128) constructs using QuickChange II site-directed mutagenesis kit (Agilent Technologies) and the mutated sequence was confirmed by DNA sequencing from Genomic Core in UTSW.

RNA purification

RCC cells were pelleted by centrifuge at 5000 rpm for 2 mins then snap-frozen in liquid nitrogen before RNA extraction. Chilled 1-Thioglycerol/Homogenization Solution (200 µl) was added to re-suspend the pellet, followed by additional of 200 µl Lysis Buffer with 15 µl Proteinase K solution. Samples were vortexed and incubated at room temperature for 10 mins before loading into Maxwell® cartridge. RNA sample was purified in the Maxwell® RSC Instrument using the microRNA Tissue Kit and eluted in 40-60 µl Nuclease-Free Water.

Quantitative real-time RT-PCR (qRT-PCR)

For the quantification of miRNA expression level, total RNA 2.5 ug (i.e., 2.5 microgram) was subjected to miScript II RT kit (QIAGEN) then 2.0 µl cDNA was applied to a 25-µL reaction volume using miScript SYBR® Green PCR kit (QIAGEN) in CFX96 Touch Real-Time PCR detection system (BioRad). Primer assays for each miRNA species were purchased from QIAGEN.

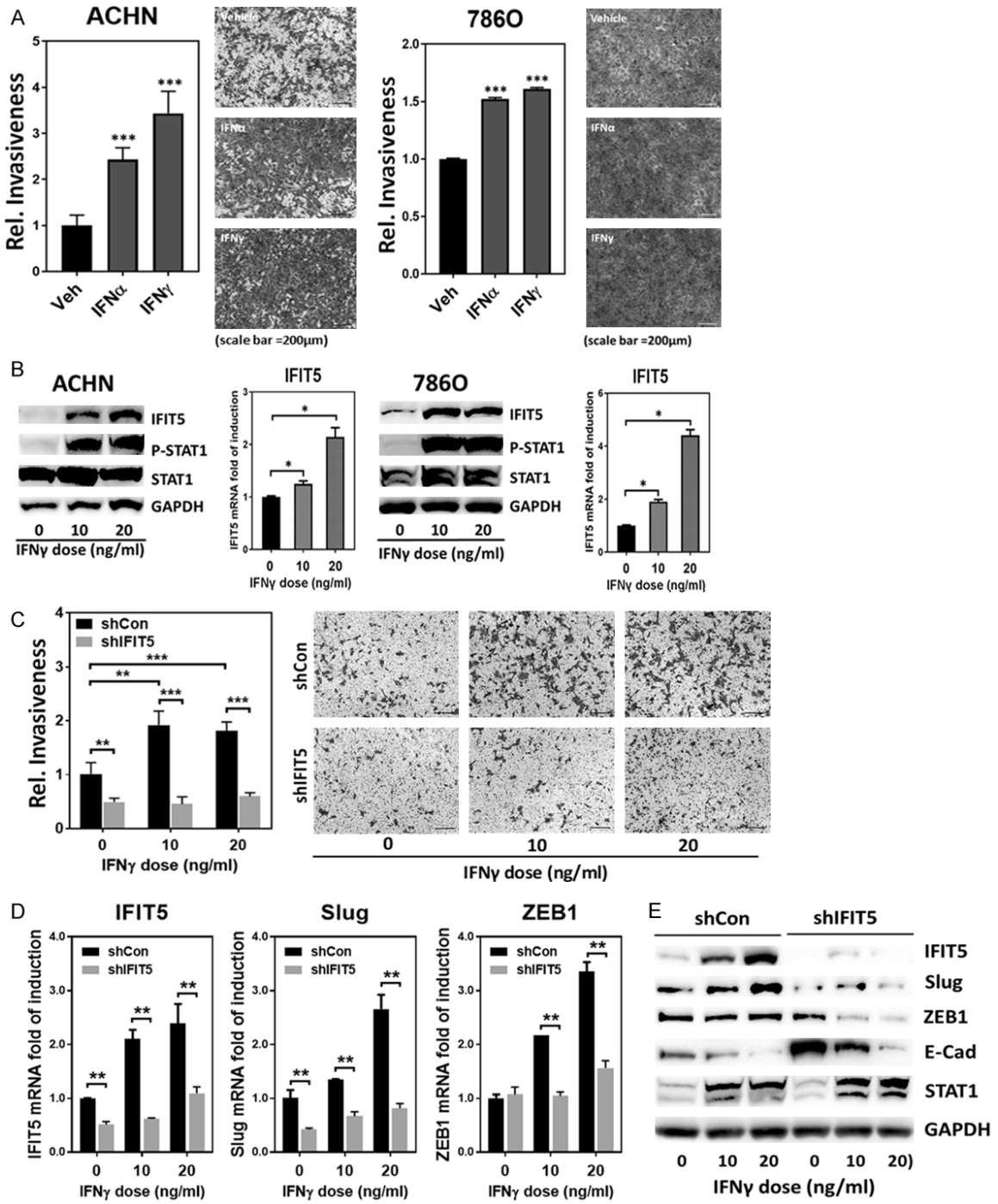

Figure 1. IFNγ promotes renal cancer invasion via induction of IFIT5. A. Increased invasiveness of ACHN or 786O cells after IFNα or IFNγ treatment (20 ng/ml) for 48 hrs, compared to vehicle control. (***P<0.00001). B. Dose-dependent elevation of IFIT5 protein and mRNA level in renal cancer cell lines (ACHN and 786O) treated with IFNγ for 48 hrs, compared to vehicle control. (*P<0.05). C. The impact of IFIT5 loss (shIFIT5) on the IFNγ-enhanced aggravation of invasiveness in ACHN cells, compared to shCon. (**P<0.001, ***P<0.00001). D. The impact of IFIT5 loss (shIFIT5) on the IFNγ-induced elevation of Slug and ZEB1 mRNA level in ACHN cells, compared to shCon (**P<0.001). E. The impact of IFIT5 loss (shIFIT5) on the IFNγ-induced alteration of Slug, ZEB1 and E-Cadherin (E-Cad) protein level in ACHN cells, compared to shCon.

The relative expression levels of matured miRNAs from each sample were determined by normalizing to SNORD95 small RNA. For the quantification of mRNA expression level, total RNA

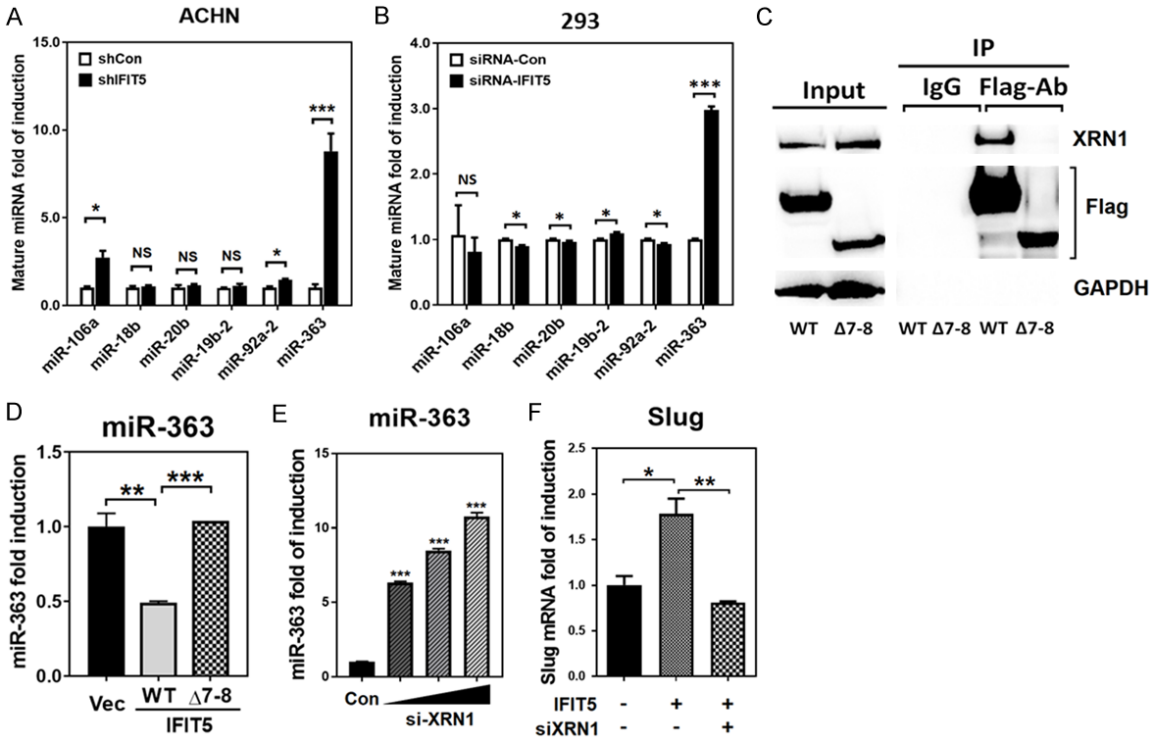

Figure 2. Recruitment of XRN1 is required for the machinery of IFIT5-mediated miR-363 degradation. A, B. The impact of IFIT5 shRNA knockdown (shIFIT5) on the expression level of miRNAs derived from the miR-106a-363 cluster (miR-106a, miR-18b, miR-20b, miR-19b-2, miR-92a-2 and miR-363) in ACHN and 293T cells, compared to control shRNA (shCon). (*P<0.05, ***P<0.00001). C. Co-Immunoprecipitation using flag antibody to pulled down flag-tagged WT or mutant (Δ7-8 TPR deletion) IFIT5 protein overexpressed in 293 cells, and immunoblotted with or and flag antibody. D. Expression level of miR-363 in cells overexpressed with WT or mutant (Δ7-8 TPR deletion) IFIT5, compared to vector control (**P<0.001, ***P<0.0001). E. Dose-dependent expression level of miR-363 in IFIT5-positive 293 cells transfected with siRNA-knockdown of XRN1 (***P<0.0001). F. Expression level of Slug in IFIT5-overexpressed 7860 cells transfected with siRNA-XRN1, compared to vector control (*P<0.05, **P<0.001).

(2 g) was subjected to iScript advanced cDNA synthesis kit (BioRad) then 2.0 μl cDNA was applied to 25-μl qRT-PCR reaction volume using iTaq Universal SYBR® Green supermix (BioRad) in CFX384 Touch Real-Time PCR detection system (BioRad). The relative expression levels of IFIT5, Slug, ZEB1, E-cadherin, and Vimentin mRNA from each sample were determined by normalizing to 18S mRNA. All quantitative data were analyzed using ΔCt (Ct value normalized to internal SNORD95 miRNA or 18S RNA) and the fold change (ΔΔCt) was obtained after normalizing with the control group.

Western blot analysis

RCC Cells were lysed in lysis buffer [50 mM Tris-HCl (pH 7.5), 150 mM NaCl, 0.1% Triton X-100, 1 mM sodium orthovanadate, 1 mM sodium fluoride, 1 mM sodium pyrophosphate, 10 mg/mL, aprotinin, 10 mg/mL leupeptin, 2 mM phenylmethylsulfonyl fluoride, and 1 mM EDTA] for 30 mins on ice. Cell lysates were spin down at 20,000×g for 20 mins at 4°C. Protein extracts were subjected to SDS-PAGE using Bolt 4-12% Bis-Tris Plus gel (Invitrogen), and transferred to nitrocellulose membrane using Trans-Blot Turbo Transfer system (BIORAD). Membranes were incubated with primary antibodies against IFIT5 (ProteinTech), Slug (Cell Signaling Technology), ZEB1 (Cell Signaling Technology), E-Cadherin (BD Transduction Laboratory), Vimentin (Sigma-Aldrich), STAT1 (Santa Cruz Biotechnology), GAPDH (Santa Cruz Biotechnology) or HRP-conjugated Flag (Sigma-Aldrich) antibodies at 4°C for 16-18 hrs, followed by incubation with horseradish peroxidase-conjugated secondary antibodies at room temperature for 1.5 hrs. Results were visualized with ECL chemiluminescent detection system (Thermo Scientific Pierce) using Alphaimager instrument. The relative protein ex-

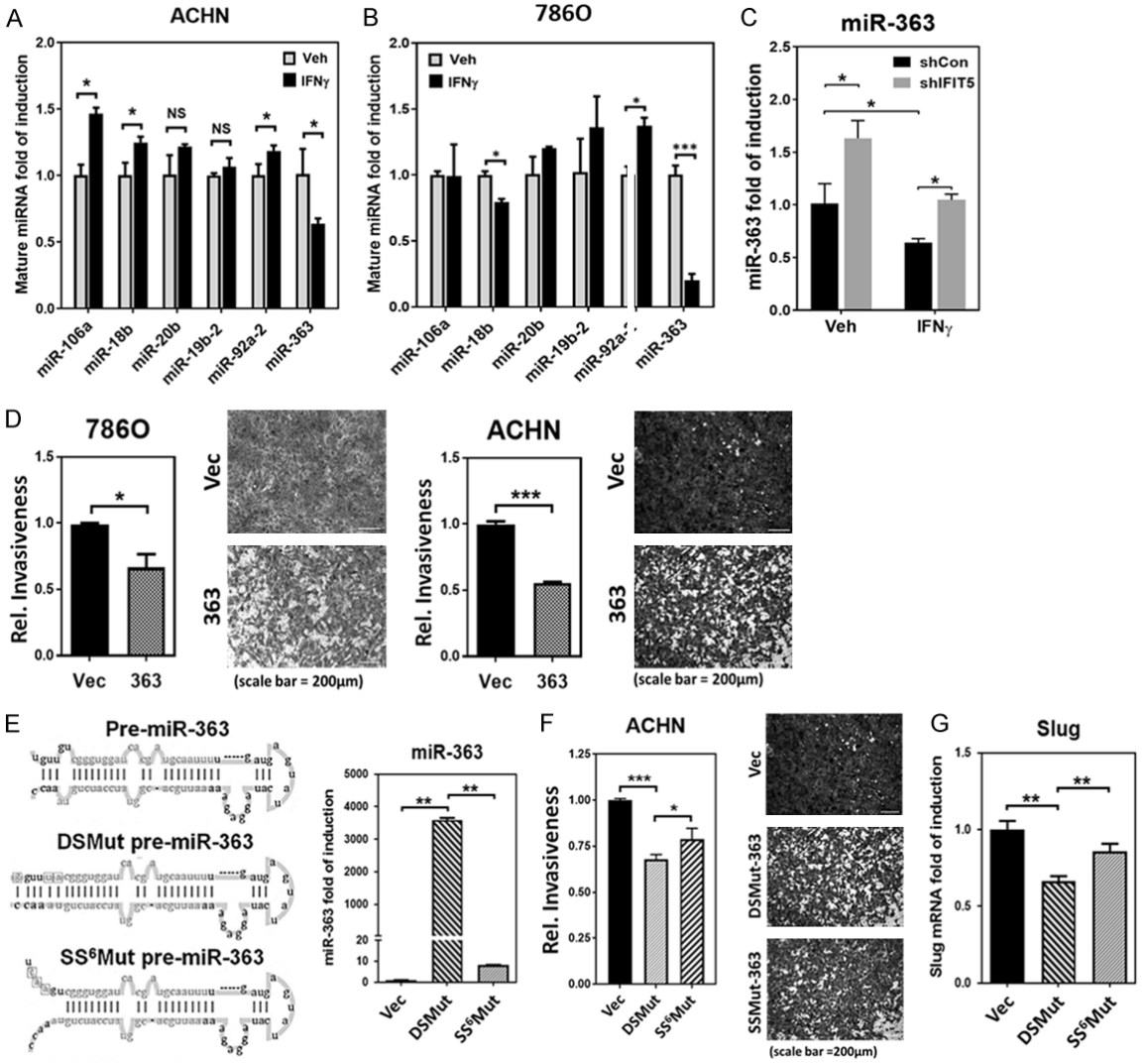

Figure 3. IFIT5 regulates miR-363 turnover via recognition of precursor miRNA 5'end. A, B. The impact of IFNγ on the expression level of miRNAs derived from the miR-106a-363 cluster (miR-106a, miR-18b, miR-20b, miR-19b-2, miR-92a-2 and miR-363) in ACHN and 786O cells, compared to vehicle control (*P<0.05, ***P<0.0001). C. The impact of IFIT5 loss (shIFIT5) on the IFNγ-induced downregulation of miR-363 level in ACHN cells. (*P<0.05). D. Attenuated cancer invasiveness by miR-363 overexpression in 786O or ACHN cells, compared to vector control (*P<0.05, ***P<0.00001). E. Left: Mutation of nucleotides (box) for generating 5'-end 6 nucleotides single stranded pre-miR-363 (SS^6Mut pre-miR-363) and blunt 5'-end double stranded pre-miR-363 (DSMut pre-miR-363). Both mature miR-363 and miR-363* sequence are shown in lighter gray. Right: Expression level of mature miR-363 in 293 cells transfected with plasmids carrying mutant SS^6Mut or DSMut pre-miR-363 sequence. (**P<0.001). F. The impact of mutant SS^6Mut or DSMut pre-miR-363 on suppression of cell invasion in ACHN cells (*P<0.05, ***P<0.00001). G. Expression level of Slug mRNA in 293 cells transfected with plasmids carrying mutant SS^6Mut or DSMut pre-miR-363 sequence. (**P<0.001).

pression level in each sample was normalized by GAPDH levels.

Luciferase reporter assay

Established stable clones of control (shCon) or STAT1-knockdown (shSTAT1) 786O cells (8×10^4) were seeded onto 12-well plates at 75% confluence before transfection with IFIT5 promoter-luciferase reporter plasmid. Cells were harvested and lysed with Passive Lysis buffer (Promega) at 48 hrs after transfection. Luciferase activity was measured using the Firefly luciferase reporter assay (Promega) on the Veritas Microplate Luminometer (Turner Biosystems).

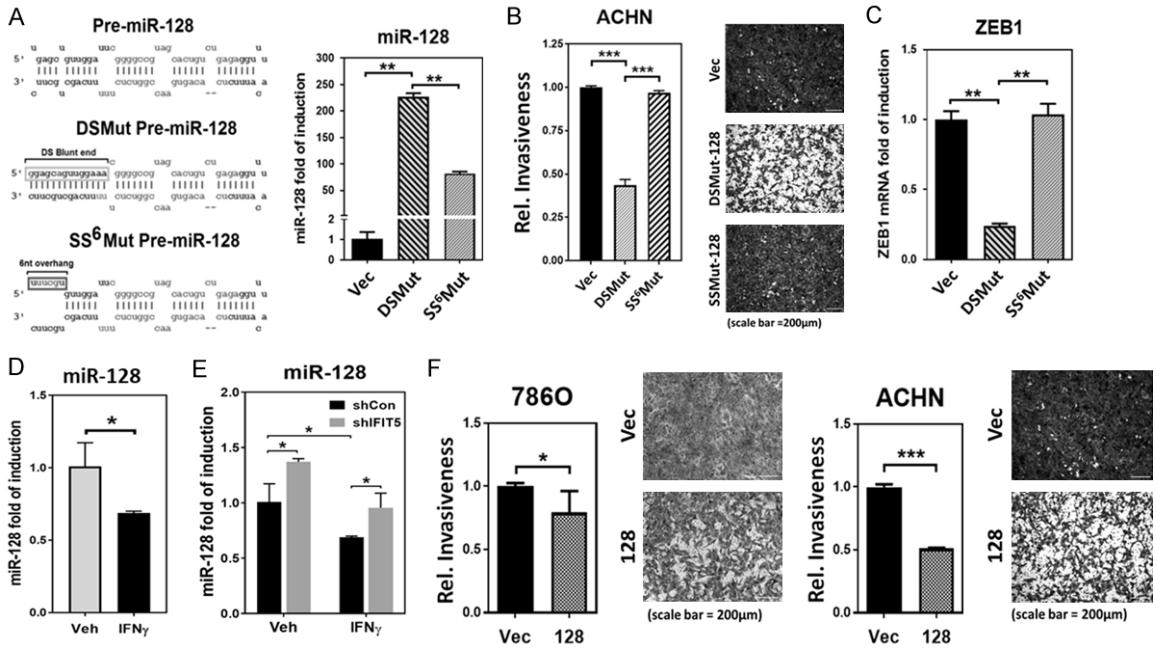

Figure 4. IFIT5 regulates miR-128 turnover via recognition of 5'-end of precursor miRNA. A. Left: Mutation of nucleotides (box) for generating 5'-end 6 nucleotides single stranded pre-miR-128 (SS^{6}Mut pre-miR-128) and blunt 5'-end double stranded pre-miR-128 (DSMut pre-miR-128). Both mature miR-128 and miR-128* sequence are shown in lighter gray. Right: Expression level of mature in 293 cells transfected with plasmids carrying mutant SS^{6}Mut or DSMut pre-miR-128 sequence. (**P<0.001). B. The impact of mutant DSMut or SS^{6}Mut pre-miR-128 on suppression of cell invasion in ACHN cells (***P<0.00001). C. Expression level of ZEB1 mRNA in 293 cells transfected with plasmids carrying mutant SS^{6}Mut or DSMut pre-miR-128 sequence. (**P<0.001). D. The impact of IFNγ and IFIT5 knockdown on the expression level of miR-128, compared to vehicle and control shRNA, respectively. (*P<0.05). E. The impact of IFIT5 loss (shIFIT5) on the IFNγ-induced downregulation of miR-128 level in ACHN cells. (*P<0.05). F. Attenuated cancer invasiveness by miR-128 overexpression in 786O or ACHN cells, compared to vector control (*P<0.05, ***P<0.00001).

Relative luciferase activity was determined by normalizing with control. Each experiment was performed in triplicates.

Statistics analysis

Statistics analyses were performed using GraphPad Prism software. Statistical significance was evaluated using Student t-test. *P* values of P<0.05, P<0.001 and P<0.00001 were considered significant difference between compared groups and marked with asterisks.

Results

IFN promotes RCC invasion via induction of IFIT5

Prior to targeted therapy for RCC patients, IFNα has demonstrated a short-term efficacy as a single agent [35-39] and improved the overall survival by combining with other agents such as cyclooxygenase-2 inhibitor (celecoxib) [40], interleukin-2 [41], capecitabine [42] or sorafenib [43, 39, 44]. On the other hand, IFNγ therapy resulted in minimal anti-tumor activity among mRCC patients [45, 46]. Thus, we decided to study potential adverse effect of IFNγ and observed that either IFNα or IFNγ was able to facilitate cell invasion of ACHN and 786O cell lines using Transwell invasion assay (**Figure 1A**). Since IFNγ appeared more potent than IFNα, we decided to focus IFNγ to unveil its mechanism of action. Indeed, IFNγ treatment is able to activate the canonical pathway of STAT1 phosphorylation to increase IFIT5 expression (**Figures 1B**, S1A and S1B), a bona fide IFN-induced gene [47, 48] that is capable of promoting EMT in prostate cancer [32]. To elucidate the role of IFIT5 in IFNγ-induced RCC cell invasion, we knocked down IFIT5 in ACHN, 786O and 769P cell lines and demonstrated that IFNγ-induced cell invasion is diminished in IFIT5-knockdown (KD) cells (**Figures 1C**, S1C and S1D). Indeed, IFNγ is able to increase both

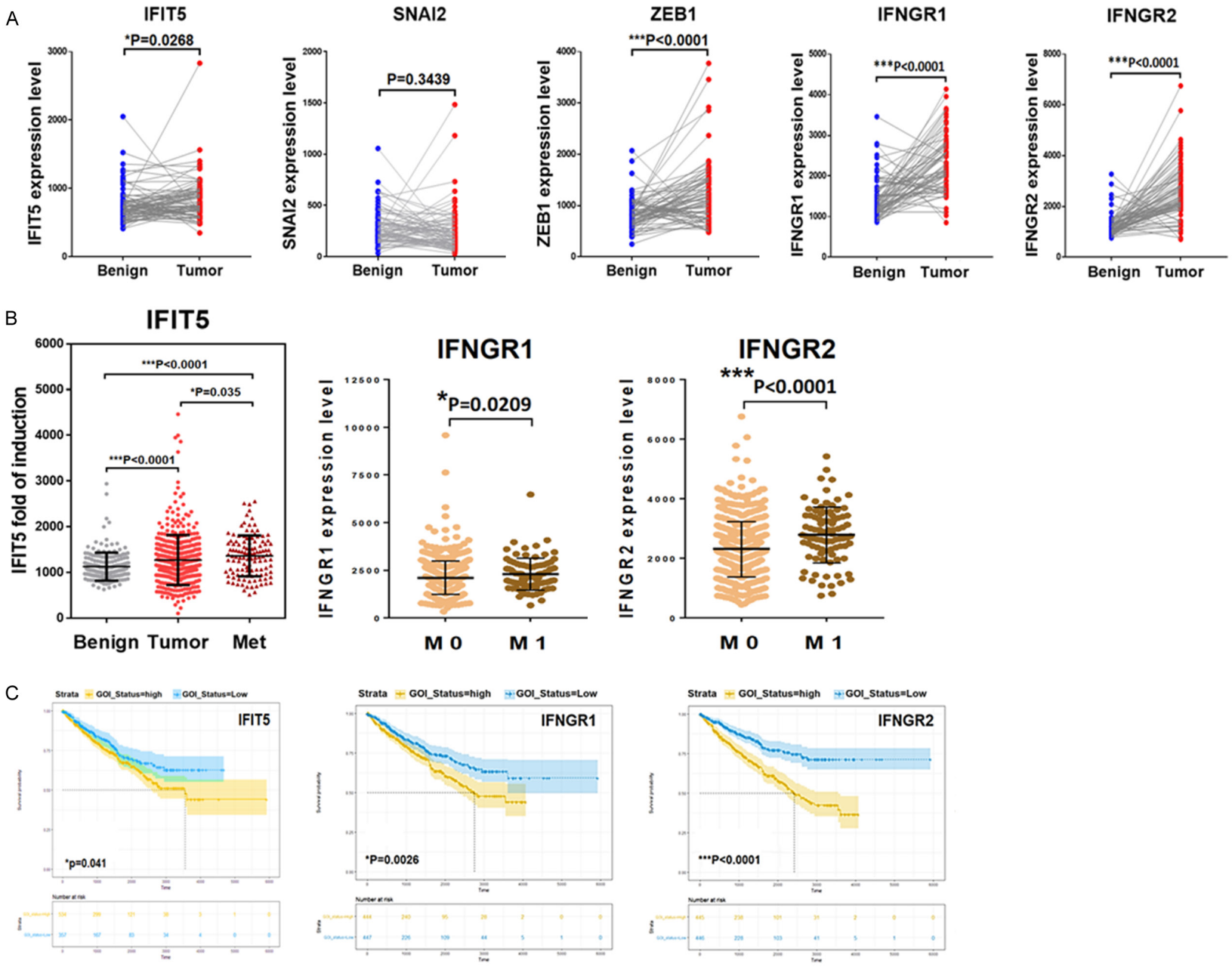
A
IFIT5
*P=0.0268
IFIT5 expression level
Benign
Tumor
SNAI2
P=0.3439
SNAI2 expression level
ZEB1
***P<0.0001
ZEB1 expression level
IFNGR1
***P<0.0001
IFNGR1 expression level
IFNGR2
***P<0.0001
IFNGR2 expression level
B
IFIT5
***P<0.0001
*P=0.035
***P<0.0001
IFIT5 fold of induction
Benign
Tumor
Met
IFNGR1
*P=0.0209
IFNGR1 expression level
M 0
M 1
IFNGR2
***P<0.0001
IFNGR2 expression level
C
Strata
GOI_Status=high
GOI_Status=Low
IFIT5
*p=0.041
IFNGR1
*P=0.0026
IFNGR2
***P<0.0001

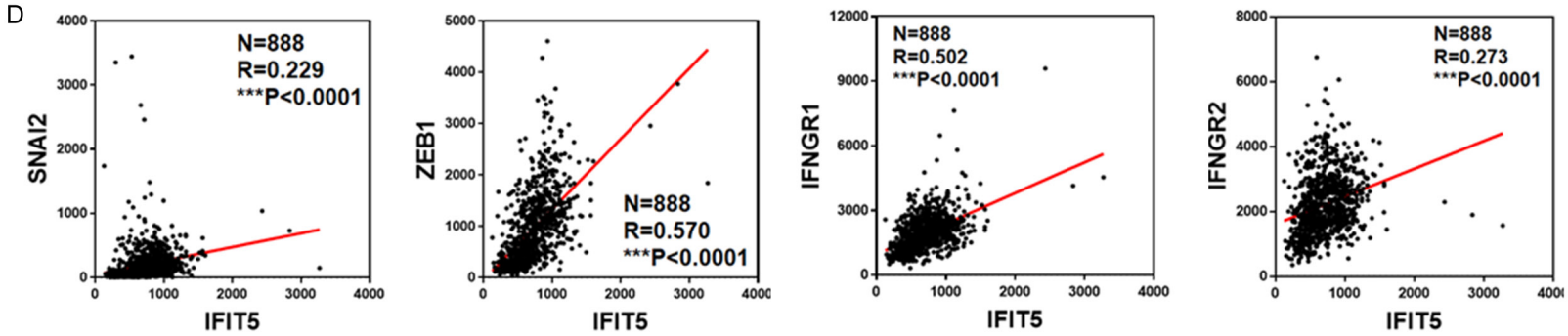

Figure 5. Machinery of IFIT5-mediated miRNA degradation is enhanced in the metastatic progression of RCC. A. Expression level of IFIT5, SNAI2/Slug, ZEB1, IFNGR1 and IFNGR2 in paired adjacent benign and tumor specimens derived from 75 RCC patients. B. Expression of IFIT5 in the patient-derived xenografts from normal benign (N=191), primary (N=294) and metastatic tumors (N=86) of RCC patients. Expression level of IFNGR1 and IFNGR2 genes in tumor specimens derived from RCC patients with non-metastasis (M0, N=550) and metastasis (M1, N=90) status. C. Kaplan-Meier overall survival curves estimate patients with RCC including types of clear cell RCC, papillary RCC and Chromophobe RCC, stratified in low and high expression of IFIT5, IFNGR1 or IFNGR2 genes. D. Clinical correlation between IFIT5 and SNAI2(Slug), ZEB1, IFNGR1 or IFNGR2 in TCGA dataset derived from 888 RCC patient tumor specimens.

Slug and ZEB1 gene expression leading to EMT in ACHN cells (**Figure 1D** and **1E**). However, in IFIT5-knockdown (KD) cells, IFNγ failed to induce Slug and ZEB1 gene expression as well as EMT change based on E-Cadherin and Vimentin expression (**Figures 1D**, **1E** and S1E). Taken together, these data support the notion that IFIT5 is the key mediator in IFNγ-induced RCC invasion.

IFIT5 complex regulates miR-363 turnover

IFIT5 has been characterized to function as a binding protein for various RNA species (such as viral RNA, tRNA) [47, 49, 50]. Our recent data [32] demonstrate that a new function of IFIT5 is to recruit XRN1 exoribonuclease to degrade miRNA by recognizing the unique 5'-structure of precursor miRNA. In addition, loss of miR-363 is detected in RCC specimens [34]. Thus, we further validated whether IFIT5 with a similar functional role could contribute the loss of miR-363 in RCC cells. Noticeably, miR-363 belongs to the miR-106a-363 cluster containing miR-106a, miR-18b, miR-20b, miR-19b, miR-92a-2 and miR-363 [51-54]. As shown in **Figure 2A** and **2B**, only mature miR-363 but no other miRNA species from this cluster was elevated in IFIT5-KD cells.

Since XRN1 is required for the activity of IFIT5 complex, we further determine the binding domain in IFIT5 for XRN1 and found 7-8 TPR domain (Δ7-8) as a key binding domain (**Figure 2C**). This truncated IFIT5 was incapable of degradation of miR-363 (**Figure 2D**). Furthermore, our data demonstrate that XRN1 is required for IFIT5-mediated miRNA degradation (**Figure 2E**). Consistently, the restoration of miR-363 level by siRNA-knockdown of XRN1 resulted in the suppression of Slug mRNA expression in 7860 cells (**Figure 2F**). Taken together, we believe that the presence of IFIT5-XRN1 contributes to the loss of miR-363 in RCC cells.

miR-363 functions as a potent suppressor in IFNγ-induced cell invasion

Knowing IFIT5 as a potent regulator for miR-363 turnover (**Figure 2A** and **2B**), we further demonstrated that IFNγ exhibited the same specific degradation of miR-363 from miR-106a-363 cluster in both ACHN and 7860 cells (**Figure 3A** and **3B**). Also, IFNγ-induced down-regulation of miR-363 can be reversed in IFIT5 KD cells (**Figure 3C**), supporting the mechanism of IFNγ on miRNA turnover is mediated by IFIT5 complex.

By increasing miR-363 expression in either ACHN and 7860 cells, a significant reduction of IFNγ-elicited cell invasion was observed (**Figure 3D**). Recently, we have demonstrated that IFIT5 preferentially bind to 5'-end single-stranded overhang sequence of precursor miRNAs [32]. Thus, the blunt-end (i.e., DSMut) of pre-miR-363 appears more resistant to IFIT5-mediated degradation than open-end (i.e., SS^6Mut) of pre-miR-363 (**Figure 3E**). Functionally, the DSMut of pre-miR-363 is more potent in suppressing cell invasion of several RCC cells (**Figures 3F** and S2A) as well as Slug gene expression (**Figure 3G**). Overall, these data provide some understanding of induction of Slug by IFNγ in RCC cells.

IFIT5 regulates the turnover of miR-128 that can target ZEB1

In addition, ZEB1 induction was detected in IFNγ-treated RCC cells (**Figure 1E**). We hypothesized that this regulation could be mediated by the same mechanism. Thus, by searching IFIT5-binding miRNA candidates, we identified pre-miR-128 with as similar single-stranded overhang structure at its 5'-end (**Figure 4A** left panel) and targeting ZEB1. By modify its native structure, the DSMut of pre-miR-128 became more resistant than the SS^6Mut of pre-miR-128 (**Figure 4A** right panel). Similar to miR-363, the DSMut of pre-miR-128 is more potent in suppressing cell invasion of several RCC cells (**Figures 4B** and S2B) as well as ZEB1 gene expression (**Figure 4C**).

Consistent with the down-regulation of miR-363 by IFNγ (**Figure 3A**), we also observed the reduction of miR-128 level in IFNγ-treated ACHN cells (**Figure 4D**). Moreover, IFNγ-induced down-regulation of miR-128 can be rescued in the IFIT5 KD cells (**Figure 4E**). On the other hand, by increasing miR-128 expression in either ACHN and 7860 cells, a significant reduction of IFNγ-elicited cell invasion was observed (**Figure 4F**). Taken together, we believe that decreased miR-128 regulated by IFIT5 complex underlies IFNγ-induced ZEB1 contributing to RCC cell invasion.

IFNγ-signaling pathway is correlated with RCC progression

To strengthen our observation from in vitro model, we further analyzed the IFNγ-signaling pathway from 75 paired adjacent benign and tumor tissues of ccRCC patients and the results (**Figure 5A**) indicated a significant elevation of IFNγ receptor 1 or 2 (IFNGR1, IFNGR2) and IFIT5 in tumor specimens. In addition, the expression levels of IFNGR1, IFNGR2, and IFIT5 in mRCC patients are significantly higher than primary tumor or benign tissue (**Figure 5B**). Moreover, patients with higher level of elevated IFNGR1, IFNGR2, and IFIT5 predicts poor overall survival of RCC patients based on the Kaplan-Meier curves analyses (**Figure 5C**). As expected, a positive correlation between IFIT5 and Slug, ZEB1, IFNGR1 or IFNGR2 expression level is also observed after analyzing TCGA RCC dataset (**Figure 5D**). Overall, these clinical data support the pro-tumorigenic role of IFNγ-signaling axis in RCC progression.

Discussion

The incidence of RCC has been steadily rising by 2-4% each year; a 5-fold increase in the incidence and a two-fold increase in mortality compared to 1971 [55]. RCC is by far the most lethal urologic malignancy of cancer-specific mortality of 40% compared with 25% of overall mortality of prostate and bladder cancers once it becomes metastatic. The median OS of untreated metastatic disease is 5 months with 1-year survival of only 29%. Although, a recent study elegantly demonstrated the predisposition of different genetic mutation in RCC patients to various organ metastases [56, 57], the influence of tumor microenvironment and its regulatory network are not fully characterized.

At the initial stage of cancer metastasis, tumor cells could undergo a phenotypic change from epithelial type to mesenchymal type (i.e., EMT), leading to loss of cell-cell adhesion, increased cell motility and invasion into vascular circulation [58]. Loss of E-Cadherin (epithelial marker) and gain of Vimentin (mesenchymal marker) is associated with RCC metastasis [59] and the presence of a sarcomatoid component is often found in metastatic lesion of RCC and associated with high mortality. Slug (Snail2), an EMT transcription repressor of E-Cadherin, has been demonstrated to induce EMT in RCC cell lines [60-62]. Slug expression is substantially increased in high-grade ccRCC tissues and sarcomatoid carcinoma, which predicts the worse prognosis for patients with RCC [63]. Tumor surrounding microenvironment is known to play an important role in EMT [64-67] induction by producing several cytokines such as TNF-α [68], TGF-β [69] and IL-10 [67].

In RCC, a number of cytokines have shown anti-tumor activity, the most consistent results have been reported with IFNα [70]. IL-2 and IFNγ have also been given to patients with metastatic RCC with limited success [70]. Although the mechanism of action of these cytokines is poorly understood, anti-tumor effects in murine models have been linked to the direct killing of tumor cells by activated T cells and natural killer cells, as well as to anti-angiogenic effects [71-73]. However, in this study, we demonstrated the pro-tumorigenic role of IFNγ in promoting RCC cancer invasion. IFNγ signaling pathway is highly elevated in primary as well metastatic RCC and significantly correlated with OS RCC patients, suggesting the oncogenic role of IFNγ-IFNGR1/IFNGR2-IFIT5 signal axis in the progression of RCC. Noticeably, this study unveils a new mechanism of action of IFIT5 in regulating turnover of tumor suppressor miRNAs (miR-363 and miR-128), leading to the upregulation of EMT drivers (Slug and ZEB1). Moreover, IFNγ promoting cancer metastasis is not only limited to RCC; it has been recently reported in other malignancies such as prostate [32] and gastric cancer [74]. In summary, we demonstrate an adverse effect of IFNγ on RCC progression via a unique regulation of miRNA turnover. Therefore, targeting IFNγ signaling pathway using inhibitory RNA strategy may provide a new avenue for the clinical management of RCC progression.

Acknowledgements

We thank Dr. Samarpita Sengupta for editorial assistance. This work was in part supported by grants from the United States Army (W81XWH-11-1-0491 and W81XWH-16-1-0474 to JTH) and (W81XWH-14-1-0249 to UGL), and China Scholarship Council (201508440279 to JB).

Disclosure of conflict of interest

None.

Address correspondence to: Dr. Jer-Tsong Hsieh, Department of Urology, University of Texas Southwestern Medical Center, Dallas, 5323 Harry Hines Blvd, J8-134 Dallas, TX 75390, USA. Tel: 214-648-3988; Fax: 214-648-8786; E-mail: jt.hsieh@utsouthwestern.edu

References

[1] Hsieh JJ, Purdue MP, Signoretti S, Swanton C, Albiges L, Schmidinger M, Heng DY, Larkin J, Ficarra V. Renal cell carcinoma. Nat Rev Dis Primers 2017; 3: 17009.

[2] Cancer Genome Atlas Research Network. Comprehensive molecular characterization of clear cell renal cell carcinoma. Nature 2013; 499: 43-9.

[3] Cancer Genome Atlas Research Network, Linehan WM, Spellman PT, Ricketts CJ, Creighton CJ, Fei SS, Davis C, Wheeler DA, Murray BA, Schmidt L, Vocke CD, Peto M, Al Mamun AA, Shinbrot E, Sethi A, Brooks S, Rathmell WK, Brooks AN, Hoadley KA, Robertson AG, Brooks D, Bowlby R, Sadeghi S, Shen H, Weisenberger DJ, Bootwalla M, Baylin SB, Laird PW, Cherniack AD, Saksena G, Haake S, Li J, Liang H, Lu Y, Mills GB, Akbani R, Leiserson MD, Raphael BJ, Anur P, Bottaro D, Albiges L, Barnabas N, Choueiri TK, Czerniak B, Godwin AK, Hakimi AA, Ho TH, Hsieh J, Ittmann M, Kim WY, Krishnan B, Merino MJ, Mills Shaw KR, Reuter VE, Reznik E, Shelley CS, Shuch B, Signoretti S, Srinivasan R, Tamboli P, Thomas G, Tickoo S, Burnett K, Crain D, Gardner J, Lau K, Mallery D, Morris S, Paulauskis JD, Penny RJ, Shelton C, Shelton WT, Sherman M, Thompson E, Yena P, Avedon MT, Bowen J, Gastier-Foster JM, Gerken M, Leraas KM, Lichtenberg TM, Ramirez NC, Santos T, Wise L, Zmuda E, Demchok JA, Felau I, Hutter CM, Sheth M, Sofia HJ, Tarnuzzer R, Wang Z, Yang L, Zenklusen JC, Zhang J, Ayala B, Baboud J, Chudamani S, Liu J, Lolla L, Naresh R, Pihl T, Sun Q, Wan Y, Wu Y, Ally A, Balasundaram M, Balu S, Beroukhim R, Bodenheimer T, Buhay C, Butterfield YS, Carlsen R, Carter SL, Chao H, Chuah E, Clarke A, Covington KR, Dahdouli M, Dewal N, Dhalla N, Doddapaneni HV, Drummond JA, Gabriel SB, Gibbs RA, Guin R, Hale W, Hawes A, Hayes DN, Holt RA, Hoyle AP, Jefferys SR, Jones SJ, Jones CD, Kalra D, Kovar C, Lewis L, Li J, Ma Y, Marra MA, Mayo M, Meng S, Meyerson M, Mieczkowski PA, Moore RA, Morton D, Mose LE, Mungall AJ, Muzny D, Parker JS, Perou CM, Roach J, Schein JE, Schumacher SE, Shi Y, Simons JV, Sipahimalani P, Skelly T, Soloway MG, Sougnez C, Tam A, Tan D, Thiessen N, Veluvolu U, Wang M, Wilkerson MD, Wong T, Wu J, Xi L, Zhou J, Bedford J, Chen F, Fu Y, Gerstein M, Haussler D, Kasaian K, Lai P, Ling S, Radenbaugh A, Van Den Berg D, Weinstein JN, Zhu J, Albert M, Alexopoulou I, Andersen JJ, Auman JT, Bartlett J, Bastacky S, Bergsten J, Blute ML, Boice L, Bollag RJ, Boyd J, Castle E, Chen YB, Cheville JC, Curley E, Davies B, DeVolk A, Dhir R, Dike L, Eckman J, Engel J, Harr J, Hrebinko R, Huang M, Huelsenbeck-Dill L, Iacocca M, Jacobs B, Lobis M, Maranchie JK, McMeekin S, Myers J, Nelson J, Parfitt J, Parwani A, Petrelli N, Rabeno B, Roy S, Salner AL, Slaton J, Stanton M, Thompson RH, Thorne L, Tucker K, Weinberger PM, Winemiller C, Zach LA, Zuna R. Comprehensive molecular characterization of papillary renal-cell carcinoma. N Engl J Med 2016; 374: 135-45.

[4] Davis CF, Ricketts CJ, Wang M, Yang L, Cherniack AD, Shen H, Buhay C, Kang H, Kim SC, Fahey CC, Hacker KE, Bhanot G, Gordenin DA, Chu A, Gunaratne PH, Biehl M, Seth S, Kaipparettu BA, Bristow CA, Donehower LA, Wallen EM, Smith AB, Tickoo SK, Tamboli P, Reuter V, Schmidt LS, Hsieh JJ, Choueiri TK, Hakimi AA; The Cancer Genome Atlas Research Network, Chin L, Meyerson M, Kucherlapati R, Park WY, Robertson AG, Laird PW, Henske EP, Kwiatkowski DJ, Park PJ, Morgan M, Shuch B, Muzny D, Wheeler DA, Linehan WM, Gibbs RA, Rathmell WK, Creighton CJ. The somatic genomic landscape of chromophobe renal cell carcinoma. Cancer Cell 2014; 26: 319-330.

[5] Buti S, Bersanelli M, Sikokis A, Maines F, Facchinetti F, Bria E, Ardizzoni A, Tortora G, Massari F. Chemotherapy in metastatic renal cell carcinoma today? A systematic review. Anticancer Drugs 2013; 24: 535-54.

[6] Zhang C, Gao L, Cai Y, Liu H, Gao D, Lai J, Jia B, Wang F, Liu Z. Inhibition of tumor growth and metastasis by photoimmunotherapy targeting tumor-associated macrophage in a sorafenib-resistant tumor model. Biomaterials 2016; 84: 1-12.

[7] Grossman JG, Nywening TM, Belt BA, Panni RZ, Krasnick BA, DeNardo DG, Hawkins WG, Goedegebuure SP, Linehan DC, Fields RC. Recruitment of CCR2(+) tumor associated macrophage to sites of liver metastasis confers a poor prognosis in human colorectal cancer. Oncoimmunology 2018; 7: e1470729.

[8] Kimura Y, Sumiyoshi M. Resveratrol prevents tumor growth and metastasis by inhibiting lymphangiogenesis and M2 macrophage activation and differentiation in tumor-associated macrophages. Nutr Cancer 2016; 68: 667-78.

[9] Liu B, Jia Y, Ma J, Wu S, Jiang H, Cao Y, Sun X, Yin X, Yan S, Shang M, Mao A. Tumor-associated macrophage-derived CCL20 enhances the growth and metastasis of pancreatic cancer.

Acta Biochim Biophys Sin (Shanghai) 2016; 48: 1067-1074.
[10] Behnes CL, Bremmer F, Hemmerlein B, Strauss A, Ströbel P, Radzun HJ. Tumor-associated macrophages are involved in tumor progression in papillary renal cell carcinoma. Virchows Arch 2014; 464: 191-6.
[11] Buddingh EP, Kuijjer ML, Duim RA, Bürger H, Agelopoulos K, Myklebost O, Serra M, Mertens F, Hogendoorn PC, Lankester AC, Cleton-Jansen AM. Tumor-infiltrating macrophages are associated with metastasis suppression in high-grade osteosarcoma: a rationale for treatment with macrophage activating agents. Clin Cancer Res 2011; 17: 2110-9.
[12] Pollard JW. Tumour-educated macrophages promote tumour progression and metastasis. Nat Rev Cancer 2004; 4: 71-8.
[13] Shen JK, Dong LH, Qi H, Zhang GS. Clinical significance of serum vascular endothelial growth factor and interleukin-6 in multiple myeloma. Zhong Nan Da Xue Xue Bao Yi Xue Ban 2005; 30: 68-71.
[14] Harmer D, Falank C, Reagan MR. Interleukin-6 interweaves the bone marrow microenvironment, bone loss, and multiple myeloma. Front Endocrinol (Lausanne) 2019; 9: 788.
[15] Bani MR, Garofalo A, Scanziani E, Giavazzi R. Effect of interleukin-1-beta on metastasis formation in different tumor systems. J Natl Cancer Inst 1991; 83: 119-23.
[16] Jagielska J, Kapopara PR, Salguero G, Scherr M, Schütt H, Grote K, Schieffer B, Bavendiek U. Interleukin-1 assembles a proangiogenic signaling module consisting of caveolin-1, tumor necrosis factor receptor-associated factor 6, p38-mitogen-activated protein kinase (MAPK), and MAPK-activated protein kinase 2 in endothelial cells. Arterioscler Thromb Vasc Biol 2012; 32: 1280-8.
[17] Watari K, Shibata T, Kawahara A, Sata K, Nabeshima H, Shinoda A, Abe H, Azuma K, Murakami Y, Izumi H, Takahashi T, Kage M, Kuwano M, Ono M. Tumor-derived interleukin-1 promotes lymphangiogenesis and lymph node metastasis through M2-type macrophages. PLoS One 2014; 9: e99568.
[18] Voronov E, Shouval DS, Krelin Y, Cagnano E, Benharroch D, Iwakura Y, Dinarello CA, Apte RN. IL-1 is required for tumor invasiveness and angiogenesis. Proc Natl Acad Sci U S A 2003; 100: 2645-50.
[19] Gresser I. The antitumor effects of interferon: a personal history. Biochimie 2007; 89: 723-8.
[20] Ferrantini M, Proietti E, Santodonato L, Gabriele L, Peretti M, Plavec I, Meyer F, Kaido T, Gresser I, Belardelli F. Alpha 1-interferon gene transfer into metastatic friend leukemia cells abrogated tumorigenicity in immunocompetent mice: antitumor therapy by means of interferon-producing cells. Cancer Res 1993; 53: 1107-12.
[21] Gabriele L, Kaido T, Woodrow D, Moss J, Ferrantini M, Proletti E, Santodonato L, Rozera C, Maury C, Belardelli F, et al. Local and systemic response of mice to interferon-alpha 1-transfected Friend leukemia cells. Am J Pathol 1995; 147: 445-460.
[22] Shin EC, Shin WC, Choi Y, Kim H, Park JH, Kim SJ. Effect of interferon-gamma on the susceptibility to Fas (CD95/APO-1)-mediated cell death in human hepatoma cells. Cancer Immunol Immunother 2001; 50: 23-30.
[23] Egwuagu CE, Li W, Yu CR, Che Mei Lin M, Chan CC, Nakamura T, Chepelinsky AB. Interferon-gamma induces regression of epithelial cell carcinoma: critical roles of IRF-1 and ICSBP transcription factors. Oncogene 2006; 25: 3670-9.
[24] Xu Z, Hurchla MA, Deng H, Uluçkan O, Bu F, Berdy A, Eagleton MC, Heller EA, Floyd DH, Dirksen WP, Shu S, Tanaka Y, Fernandez SA, Rosol TJ, Weilbaecher KN. Interferon-gamma targets cancer cells and osteoclasts to prevent tumor-associated bone loss and bone metastases. J Biol Chem 2009; 284: 4658-66.
[25] Aulitzky W, Gastl G, Aulitzky WE, Herold M, Kemmler J, Mull B, Frick J, Huber C. Successful treatment of metastatic renal cell carcinoma with a biologically active dose of recombinant interferon-gamma. J Clin Oncol 1989; 7: 1875-84.
[26] Shankaran V, Ikeda H, Bruce AT, White JM, Swanson PE, Old LJ, Schreiber RD. IFNgamma and lymphocytes prevent primary tumour development and shape tumour immunogenicity. Nature 2001; 410: 1107-11.
[27] Panelli MC, Wang E, Shen S, Schluter SF, Bernstein RM, Hersh EM, Stopeck A, Gangavalli R, Barber J, Jolly D, Akporiaye ET. Interferon gamma (IFNgamma) gene transfer of an EMT6 tumor that is poorly responsive to IFNgamma stimulation: increase in tumor immunogenicity is accompanied by induction of a mouse class II transactivator and class II MHC. Cancer Immunol Immunother 1996; 42: 99-107.
[28] Phan-Lai V, Kievit FM, Florczyk SJ, Wang K, Disis ML, Zhang M. CCL21 and IFNgamma recruit and activate tumor specific T cells in 3D scaffold model of breast cancer. Anticancer Agents Med Chem 2014; 14: 204-10.
[29] Zhou F. Molecular mechanisms of IFN-gamma to up-regulate MHC class I antigen processing and presentation. Int Rev Immunol 2009; 28: 239-260.
[30] Taniguchi K, Petersson M, Höglund P, Kiessling R, Klein G, Kärre K. Interferon gamma induces lung colonization by intravenously inoculated

B16 melanoma cells in parallel with enhanced expression of class I major histocompatibility complex antigens. Proc Natl Acad Sci U S A 1987; 84: 3405-9.

[31] Abiko K, Matsumura N, Hamanishi J, Horikawa N, Murakami R, Yamaguchi K, Yoshioka Y, Baba T, Konishi I, Mandai M. IFN-gamma from lymphocytes induces PD-L1 expression and promotes progression of ovarian cancer. Br J Cancer 2015; 112: 1501-9.

[32] Lo UG, Pong RC, Yang D, Gandee L, Hernandez E, Dang A, Lin CJ, Santoyo J, Ma S, Sonavane R, Huang J, Tseng SF, Moro L, Arbini AA, Kapur P, Raj GV, He D, Lai CH, Lin H, Hsieh JT. IFN-r-induced IFIT5 promotes epithelial-to-mesenchymal transition in prostate cancer via microRNA processing. Cancer Res 2018; [Epub ahead of print].

[33] Au-Yeung N, Mandhana R, Horvath CM. Transcriptional regulation by STAT1 and STAT2 in the interferon JAK-STAT pathway. JAKSTAT 2013; 2: e23931.

[34] Jung M, Mollenkopf HJ, Grimm C, Wagner I, Albrecht M, Waller T, Pilarsky C, Johannsen M, Stephan C, Lehrach H, Nietfeld W, Rudel T, Jung K, Kristiansen G. MicroRNA profiling of clear cell renal cell cancer identifies a robust signature to define renal malignancy. J Cell Mol Med 2009; 13: 3918-28.

[35] Hofmockel G, Wirth MP, Heimbach D, Frohmüller HG. Results of low dosage cyclic interferon-gamma therapy of metastatic renal cell carcinoma. Urologe A 1993; 32: 290-4.

[36] Nishisaka N, Yoshihara H, Nakatani T, Sugimura K, Maekawa T, Asakawa M, Yasumoto R, Umeda M, Sakamoto W, Kawakita J, et al. Clinical study of immunotherapy with interferon alpha and gamma in metastatic renal cell carcinoma. Nihon Hinyokika Gakkai Zasshi 1993; 84: 1987-93.

[37] Ellerhorst JA, Kilbourn RG, Amato RJ, Zukiwski AA, Jones E, Logothetis CJ. Phase II trial of low dose gamma-interferon in metastatic renal cell carcinoma. J Urol 1994; 152: 841-5.

[38] Farace F, Pallardy M, Angevin E, Hercend T, Escudier B, Triebel F. Metastatic renal-cell carcinoma patients treated with interleukin 2 or interleukin 2 plus interferon gamma: immunological monitoring. Int J Cancer 1994; 57: 814-21.

[39] Fosså SD. Interferon in metastatic renal cell carcinoma. Semin Oncol 2000; 27: 187-93.

[40] Onishi T, Suzuki H, Igarashi T. A case of favorable response after combination treatment with interferon-alpha and cyclooxygenase-2 inhibitor against metastatic renal cell carcinoma. Hinyokika Kiyo 2012; 58: 25-9.

[41] Donskov F, Jensen NV, Smidt-Hansen T, Brøndum L, Geertsen P. A randomized phase II trial of interleukin-2 and interferon-alpha plus bevacizumab versus interleukin-2 and interferon-alpha in metastatic renal-cell carcinoma (mRCC): results from the Danish renal cancer group (DaRenCa) study-1. Acta Oncol 2018; 57: 589-594.

[42] Amato RJ, Mohammad T. Interferon-alpha plus capecitabine and thalidomide in patients with metastatic renal cell cancer. J Exp Ther Oncol 2008; 7: 41-7.

[43] Eto M, Kawano Y, Hirao Y, Mita K, Arai Y, Tsukamoto T, Hashine K, Matsubara A, Fujioka T, Kimura G, Shinohara N, Tatsugami K, Hinotsu S, Naito S; Japan RCC Trialist Collaborative Group (JRTCG) investigators. Phase II clinical trial of sorafenib plus interferon-alpha treatment for patients with metastatic renal cell carcinoma in Japan. BMC Cancer 2015; 15: 667.

[44] Kawano Y, Takahashi W, Eto M, Kamba T, Miyake H, Fujisawa M, Kamai T, Uemura H, Tsukamoto T, Azuma H, Matsubara A, Nishimura K, Nakamura T, Ogawa O, Naito S. Prognosis of metastatic renal cell carcinoma with first-line interferon-alpha therapy in the era of molecular-targeted therapy. Cancer Sci 2016; 107: 1013-7.

[45] Aulitzky WE, Lerche J, Thews A, Lüttichau I, Jacobi N, Herold M, Aulitzky W, Peschel C, Stöckle M, Steinbach F, et al. Low-dose gamma-interferon therapy is ineffective in renal cell carcinoma patients with large tumour burden. Eur J Cancer 1994; 30A: 940-5.

[46] Otto F, Mackensen A, Mertelsmann R, Engelhardt R. Complete response of metastatic renal cell carcinoma to low-dose interferon-gamma treatment. Cancer Immunol Immunother 1995; 40: 115-8.

[47] Katibah GE, Qin Y, Sidote DJ, Yao J, Lambowitz AM, Collins K. Broad and adaptable RNA structure recognition by the human interferon-induced tetratricopeptide repeat protein IFIT5. Proc Natl Acad Sci U S A 2014; 111: 12025-30.

[48] Santhakumar D, Rohaim MAMS, Hussein HA, Hawes P, Ferreira HL, Behboudi S, Iqbal M, Nair V, Arns CW, Munir M. Chicken interferon-induced protein with tetratricopeptide repeats 5 antagonizes replication of RNA viruses. Sci Rep 2018; 8: 6794.

[49] Katibah GE, Lee HJ, Huizar JP, Vogan JM, Alber T, Collins K. tRNA binding, structure, and localization of the human interferon-induced protein IFIT5. Mol Cell 2013; 49: 743-50.

[50] Zhang B, Liu X, Chen W, Chen L. IFIT5 potentiates anti-viral response through enhancing innate immune signaling pathways. Acta Biochim Biophys Sin (Shanghai) 2013; 45: 867-74.

[51] Dylla L, Jedlicka P. Growth-promoting role of the miR-106a~363 cluster in Ewing sarcoma. PLoS One 2013; 8: e63032.
[52] Khuu C, Sehic A, Eide L, Osmundsen H. Antiproliferative properties of miR-20b and miR-363 from the miR-106a-363 cluster on human carcinoma cells. Microrna 2016; 5: 19-35.
[53] Khuu C, Utheim TP, Sehic A. The three paralogous microRNA clusters in development and disease, miR-17-92, miR-106a-363, and miR-106b-25. Scientifica (Cairo) 2016; 2016: 1379643.
[54] Gruszka R, Zakrzewska M. The oncogenic relevance of miR-17-92 cluster and its paralogous miR-106b-25 and miR-106a-363 clusters in brain tumors. Int J Mol Sci 2018; 19.
[55] Siegel RL, Miller KD, Jemal A. Cancer statistics, 2018. CA Cancer J Clin 2018; 68: 7-30.
[56] Turajlic S, Xu H, Litchfield K, Rowan A, Horswell S, Chambers T, O'Brien T, Lopez JI, Watkins TBK, Nicol D, Stares M, Challacombe B, Hazell S, Chandra A, Mitchell TJ, Au L, Eichler-Jonsson C, Jabbar F, Soultati A, Chowdhury S, Rudman S, Lynch J, Fernando A, Stamp G, Nye E, Stewart A, Xing W, Smith JC, Escudero M, Huffman A, Matthews N, Elgar G, Phillimore B, Costa M, Begum S, Ward S, Salm M, Boeing S, Fisher R, Spain L, Navas C, Grönroos E, Hobor S, Sharma S, Aurangzeb I, Lall S, Polson A, Varia M, Horsfield C, Fotiadis N, Pickering L, Schwarz RF, Silva B, Herrero J, Luscombe NM, Jamal-Hanjani M, Rosenthal R, Birkbak NJ, Wilson GA, Pipek O, Ribli D, Krzystanek M, Csabai I, Szallasi Z, Gore M, McGranahan N, Van Loo P, Campbell P, Larkin J, Swanton C; TRACERx Renal Consortium. Deterministic evolutionary trajectories influence primary tumor growth: TRACERx renal. Cell 2018; 173: 595-610, e11.
[57] Mitchell TJ, Turajlic S, Rowan A, Nicol D, Farmery JHR, O'Brien T, Martincorena I, Tarpey P, Angelopoulos N, Yates LR, Butler AP, Raine K, Stewart GD, Challacombe B, Fernando A, Lopez JI, Hazell S, Chandra A, Chowdhury S, Rudman S, Soultati A, Stamp G, Fotiadis N, Pickering L, Au L, Spain L, Lynch J, Stares M, Teague J, Maura F, Wedge DC, Horswell S, Chambers T, Litchfield K, Xu H, Stewart A, Elaidi R, Oudard S, McGranahan N, Csabai I, Gore M, Futreal PA, Larkin J, Lynch AG, Szallasi Z, Swanton C, Campbell PJ; TRACERx Renal Consortium. Timing the landmark events in the evolution of clear cell renal cell cancer: TRACERx renal. Cell 2018; 173: 611-623, e17.
[58] Piva F, Giulietti M, Santoni M, Occhipinti G, Scarpelli M, Lopez-Beltran A, Cheng L, Principato G, Montironi R. Epithelial to mesenchymal transition in renal cell carcinoma: implications for cancer therapy. Mol Diagn Ther 2016; 20: 111-7.
[59] Katagiri A, Watanabe R, Tomita Y. E-cadherin expression in renal cell cancer and its significance in metastasis and survival. Br J Cancer 1995; 71: 376-9.
[60] Harten SK, Shukla D, Barod R, Hergovich A, Balda MS, Matter K, Esteban MA, Maxwell PH. Regulation of renal epithelial tight junctions by the von Hippel-Lindau tumor suppressor gene involves occludin and claudin 1 and is independent of E-cadherin. Mol Biol Cell 2009; 20: 1089-101.
[61] Evans AJ, Russell RC, Roche O, Burry TN, Fish JE, Chow VW, Kim WY, Saravanan A, Maynard MA, Gervais ML, Sufan RI, Roberts AM, Wilson LA, Betten M, Vandewalle C, Berx G, Marsden PA, Irwin MS, Teh BT, Jewett MA, Ohh M. VHL promotes E2 box-dependent E-cadherin transcription by HIF-mediated regulation of SIP1 and snail. Mol Cell Biol 2007; 27: 157-69.
[62] Esteban MA, Tran MG, Harten SK, Hill P, Castellanos MC, Chandra A, Raval R, O'brien TS, Maxwell PH. Regulation of E-cadherin expression by VHL and hypoxia-inducible factor. Cancer Res 2006; 66: 3567-75.
[63] Mikami S, Katsube K, Oya M, Ishida M, Kosaka T, Mizuno R, Mukai M, Okada Y. Expression of Snail and Slug in renal cell carcinoma: E-cadherin repressor Snail is associated with cancer invasion and prognosis. Lab Invest 2011; 91: 1443-58.
[64] Li S, Xu F, Zhang J, Wang L, Zheng Y, Wu X, Wang J, Huang Q, Lai M. Tumor-associated macrophages remodeling EMT and predicting survival in colorectal carcinoma. Oncoimmunology 2017; 7: e1380765.
[65] Su S, Liu Q, Chen J, Chen J, Chen F, He C, Huang D, Wu W, Lin L, Huang W, Zhang J, Cui X, Zheng F, Li H, Yao H, Su F, Song E. A positive feedback loop between mesenchymal-like cancer cells and macrophages is essential to breast cancer metastasis. Cancer Cell 2014; 25: 605-20.
[66] Yuan ZY, Luo RZ, Peng RJ, Wang SS, Xue C. High infiltration of tumor-associated macrophages in triple-negative breast cancer is associated with a higher risk of distant metastasis. Onco Targets Ther 2014; 7: 1475-80.
[67] Liu CY, Xu JY, Shi XY, Huang W, Ruan TY, Xie P, Ding JL. M2-polarized tumor-associated macrophages promoted epithelial-mesenchymal transition in pancreatic cancer cells, partially through TLR4/IL-10 signaling pathway. Lab Invest 2013; 93: 844-54.
[68] Hagemann T, Robinson SC, Schulz M, Trümper L, Balkwill FR, Binder C. Enhanced invasiveness of breast cancer cell lines upon co-cultivation with macrophages is due to TNF-alpha dependent up-regulation of matrix metalloproteases. Carcinogenesis 2004; 25: 1543-9.

[69] Zhang S, Che D, Yang F, Chi C, Meng H, Shen J, Qi L, Liu F, Lv L, Li Y, Meng Q, Liu J, Shang L, Yu Y. Tumor-associated macrophages promote tumor metastasis via the TGF-beta/SOX9 axis in non-small cell lung cancer. Oncotarget 2017; 8: 99801-99815.

[70] McDermott DF, Atkins MB. Application of IL-2 and other cytokines in renal cancer. Expert Opin Biol Ther 2004; 4: 455-68.

[71] Rosenberg SA, Mulé JJ, Spiess PJ, Reichert CM, Schwarz SL. Regression of established pulmonary metastases and subcutaneous tumor mediated by the systemic administration of high-dose recombinant interleukin 2. J Exp Med 1985; 161: 1169-88.

[72] Mulé JJ, Yang JC, Afreniere RL, Shu SY, Rosenberg SA. Identification of cellular mechanisms operational in vivo during the regression of established pulmonary metastases by the systemic administration of high-dose recombinant interleukin 2. J Immunol 1987; 139: 285-94.

[73] Neidhart JA. Interferon therapy for the treatment of renal cancer. Cancer 1986; 57: 1696-1699.

[74] Xu YH, Li ZL, Qiu SF. IFN-gamma induces gastric cancer cell proliferation and metastasis through upregulation of integrin beta3-mediated NF-kappaB signaling. Transl Oncol 2018; 11: 182-192.

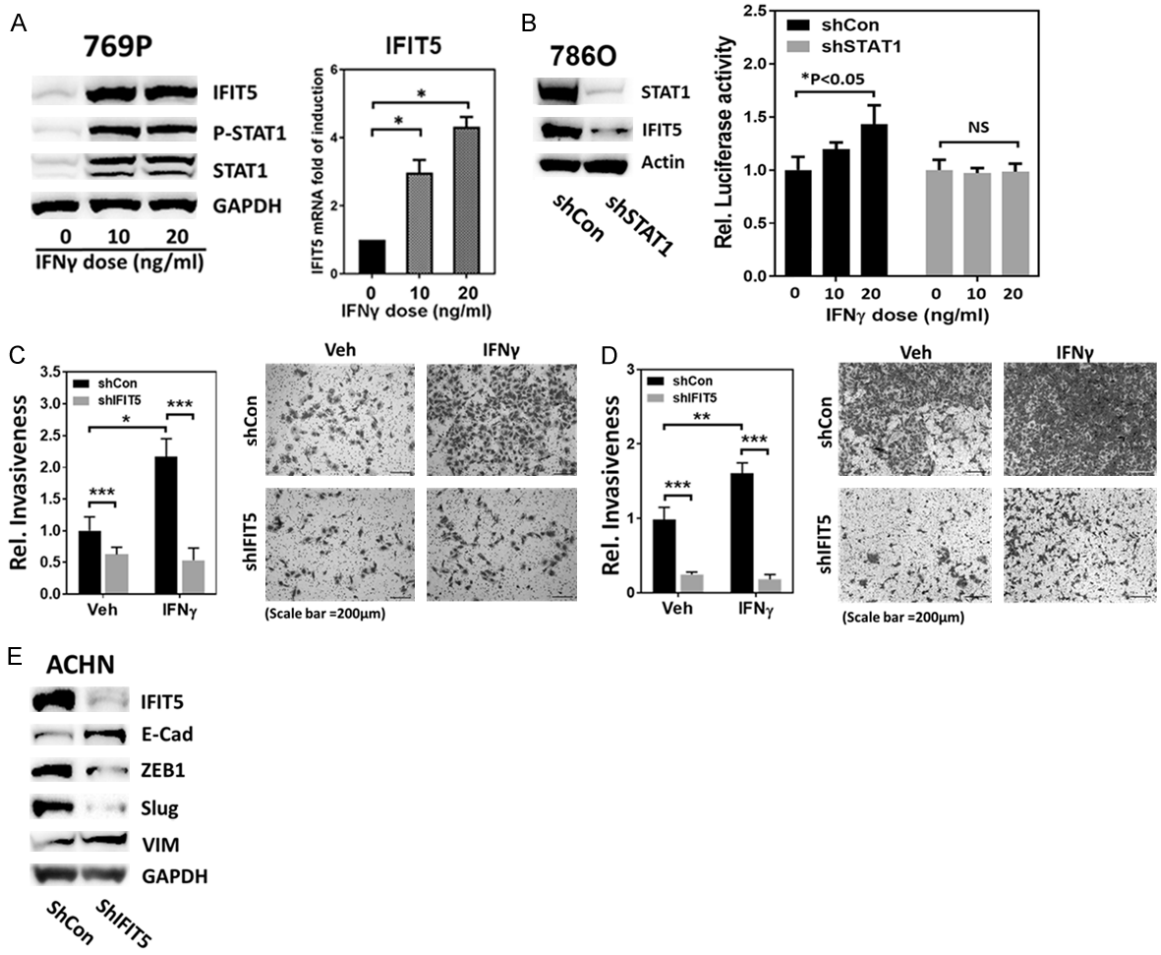

Figure S1. A. Dose-dependent elevation of IFIT5 protein and mRNA level in 769P cells treated with IFNγ for 48 hrs, compared to vehicle control. (*P<0.05). B. The impact of STAT1 shRNA knockdown (shSTAT1) on IFIT5 promoter activity using luciferase reporter assay. C. The impact of IFIT5 loss (shIFIT5) on the IFNγ-enhanced aggravation of invasiveness in 786O cells, compared to shCon. (*P<0.05, ***P<0.00001). D. The impact of IFIT5 loss (shIFIT5) on the IFNγ-enhanced aggravation of invasiveness in 769P cells, compared to shCon. (**P<0.001, ***P<0.00001). E. The impact of IFIT5 shRNA knockdown (shIFIT5) on the protein expression level of E-Cad, ZEB1, Slug and Vimentin (VIM) in ACHN cells, compared to control shRNA (shCon).

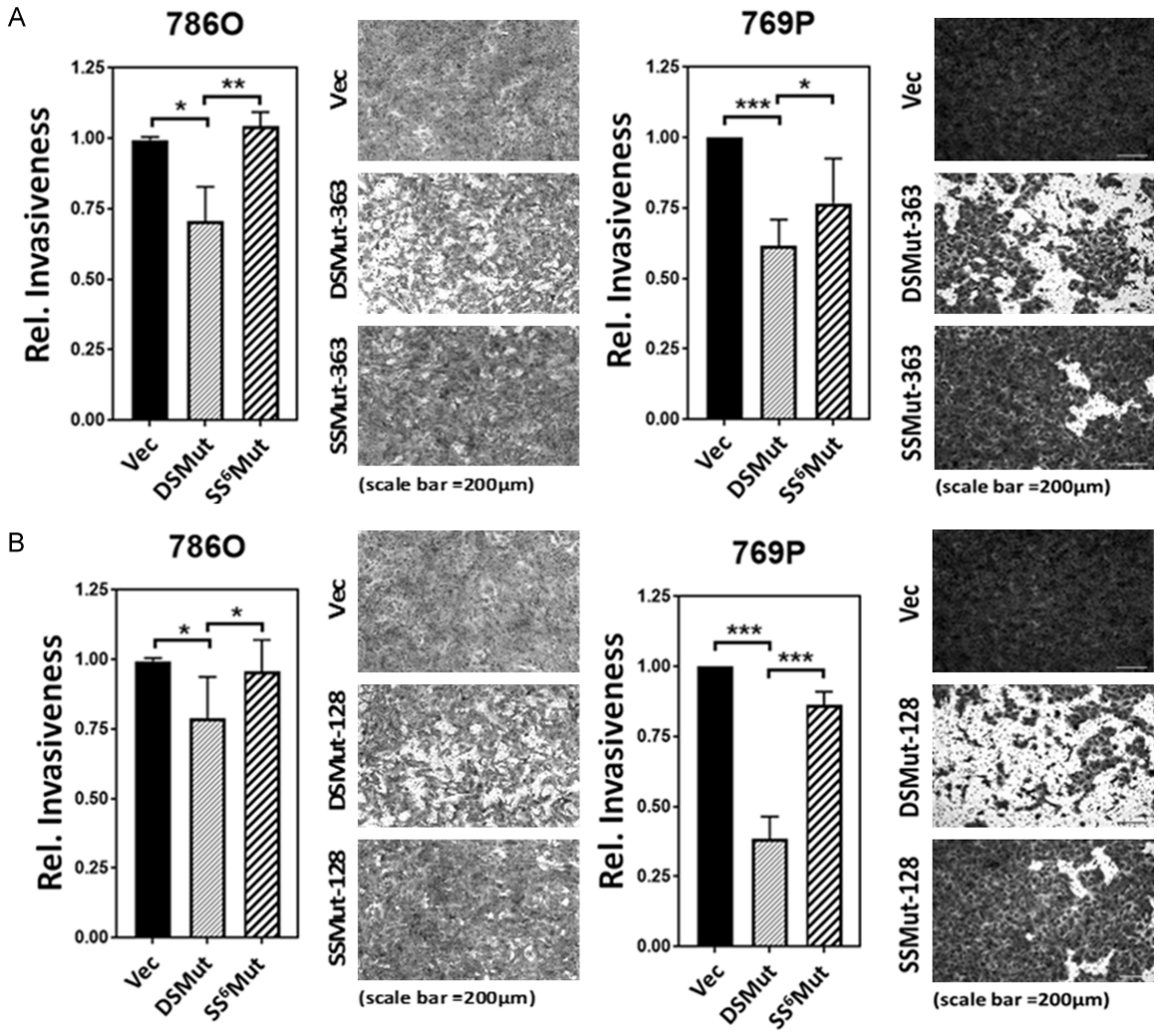

Figure S2. A. The impact of mutant DSMut or SS^{6}Mut pre-miR-363 on suppression of cell invasion in 786O and 769P cells (*P<0.05, **P<0.001, ***P<0.00001). B. The impact of mutant DSMut or SS^{6}Mut pre-miR-128 on suppression of cell invasion in 786O and 769P cells (*P<0.05, ***P<0.00001).

International Journal of
Molecular Sciences

MDPI

Review

The Role and Mechanism of Epithelial-to-Mesenchymal Transition in Prostate Cancer Progression

U-Ging Lo [1], Cheng-Fan Lee [1,2], Ming-Shyue Lee [2] and Jer-Tsong Hsieh [1,*]

[1] Department of Urology, University of Texas Southwestern Medical Center, Dallas, TX 75390, USA; U-Ging.Lo@utsouthwestern.edu (U.-G.L.); Cheng-Fan.Lee@utsouthwestern.edu (C.-F.L.)
[2] Department of Biochemistry and Molecular Biology, College of Medicine, National Taiwan University, Taipei 10617, Taiwan; mslee2006@ntu.edu.tw
* Correspondence: jt.hsieh@utsouthwestern.edu; Tel.: +1-214-648-3988

Received: 23 August 2017; Accepted: 27 September 2017; Published: 30 September 2017

Abstract: In prostate cancer (PCa), similar to many other cancers, distant organ metastasis symbolizes the beginning of the end disease, which eventually leads to cancer death. Many mechanisms have been identified in this process that can be rationalized into targeted therapy. Among them, epithelial-to-mesenchymal transition (EMT) is originally characterized as a critical step for cell trans-differentiation during embryo development and now recognized in promoting cancer cells invasiveness because of high mobility and migratory abilities of mesenchymal cells once converted from carcinoma cells. Nevertheless, the underlying pathways leading to EMT appear to be very diverse in different cancer types, which certainly represent a challenge for developing effective intervention. In this article, we have carefully reviewed the key factors involved in EMT of PCa with clinical correlation in hope to facilitate the development of new therapeutic strategy that is expected to reduce the disease mortality.

Keywords: epithelial-to-mesenchymal transition; metastasis; prostate cancer progression

1. Introduction

The plasticity of cellular phenotypic transformation is fundamental to embryonic development. During gastrulation stage, the reprogramming process of epithelial-to-mesenchymal transition (EMT) mainly governs the phenotypic change of polarized ectodermal epithelial cells into migratory mesenchymal cells that ultimately constitute the mesodermal layer of the embryo [1]. EMT occurs by breakdown of cell-to-cell or cell-to-extracellular matrix (ECM) adherence at the polarized epithelium lining. E-cadherin is a major component of epithelial adherence junction and acts as the master gatekeeper of EMT. Loss of E-cadherin, considered to be the key step to initiate EMT, leads to collapse of intercellular mechanical communication. In contrast, critical mesenchymal markers such as vimentin and *N*-cadherin, as well as several E-cadherin transcriptional repressors including zinc finger proteins Snail/SNAI1 and Slug/SNAI2, twist-related protein 1 (Twist 1) and zinc finger E-box-binding homeobox 1 and 2 (ZEB1 and ZEB2) are highly elevated during EMT (Figure 1), leading to acquisition of mesenchymal phenotype of enhanced cell mobility [2]. EMT is critical for tissue remodeling during embryonic morphogenesis [3–6]; however, this reprogramming process is also observed in different pathological process such as organ fibrosis, wound healing and carcinoma progression. In particular, primary carcinoma cells switch from epithelial characteristics to mesenchymal-like phenotype while responding to either intrinsic genetic and molecular alteration or extrinsic microenvironmental stimuli, which leads to the invasion into surrounding stroma and subsequent vasculature, ultimately colonization at a distant pre-metastatic niche [6,7]. Particularly, the role of EMT in metastasis has

been demonstrated in many cancer types including prostate cancer (PCa) to elicit their metastatic potentials [2,8,9], which is supported by significant correlation between TGF-β and EMT-related genes detected from circulating prostate cancer cells of PCa patients [10]. PCa is the most common male malignancy and the second leading cause of cancer mortality in the men of US. Current treatments for primary prostatic tumor involve radical prostatectomy, external radiotherapy, brachytherapy, and androgen deprivation therapy (ADT). The major cause of PCa mortality is the onset of metastatic castration-resistant PCa (mCRPC). Although none of these therapeutic strategies are curative for PCa, surgery and radiation remain the most effective regimen for patients with organ-confined disease. It is known that PCa is a multifocal disease with heterogeneous cell population. Thus, understanding cellular and molecular mechanisms underlying metastatic dissemination of PCa, such as EMT could generate potential therapeutic strategies to prevent PCa related mortality. In this review, we will discuss several key players in driving EMT in PCa and the different mechanisms that produce distinct signaling cascades to modulate gene transcription or epigenetic regulation, and post-transcriptional regulation by microRNA (miRNA) or long non-coding RNAs (lncRNAs).

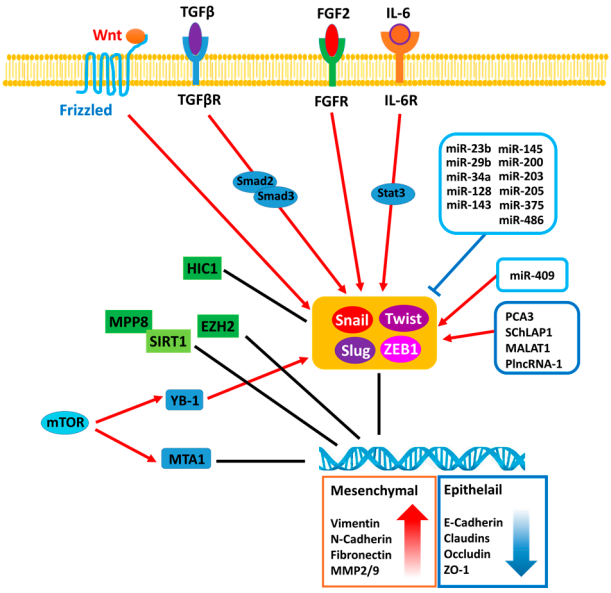

Figure 1. The regulatory mechanisms associated with epithelial-to-mesenchymal transition (EMT) in prostate cancer (PCa). MPP8: M-phase phosphoprotein 8; SIRT1: NAD-dependent deacetylase sirtuin-1; HIC1: Hypermethylated in cancer 1; EZH2: Enhancer of zeste homolog 2; YB-1: Y-box binding protein 1; MTA1: Metastasis Associated 1 protein; mTOR: Mammalian target of rapamycin; TGFβR: Transforming growth factor beta receptor; FGFR: Fibroblast growth factor receptor; IL-6R: Interleukin 6 receptor; Snail: Zinc finger protein SNAI1; Slug: Zinc finger protein SNAI2; ZEB1: Zinc finger E-box-binding homeobox 1; Twist: Twist-related protein 1.

Accumulating studies have demonstrated that activation of EMT transcription factors induces acquisition of stem cell properties in epithelial cells and contributes to the emergence of tumor-initiating cell population in several cancer types such as breast and pancreatic cancer [11–13]. In PCa, one study also indicates that *N*-cadherin can increase prostate tumor spheroid formation by elevating expression of stemness markers such as c-Myc, Klf4, Sox2 and Oct4 via ErbB signaling pathway [14]. In addition, the ectopic expression of Semaphorin 3 C can concurrently enhance the invasiveness and stemness in normal prostate epithelial cells, and that mesenchymal markers such as *N*-cadherin and Vimentin are highly upregulated in CD44-positive populations, compared to CD44-negative ones [15]. Using transgenic mouse model, prostate tumor cells with mesenchymal characteristics displayed enhanced invasiveness and stemness [16]. However, using primary prostate cancer-derived cells, there is no significant correlation between stemness and the expression level of EMT markers such as

vimentin and *N*-cadherin [17], suggesting that more studies are needed to delineate the regulation of EMT leading to PCa stemness.

EMT-related transcription factors such as Snail, Slug and Twist are shown to confer chemo-resistance in ovarian, breast and nasopharyngeal carcinoma [18–20]. In PCa, a study demonstrated that reintroduction of E-cadherin significantly sensitizes chemo-resistant PCa cell lines to paclitaxel [21]. A recent study showed that Skp2-mediated Twist stabilization can facilitate the acquisition of chemo-resistant to paclitaxel or doxorubicin during PCa progression toward CRPC [22]. In addition, ZEB1 has been shown to promote the chemo-resistance in Paclitaxel-resistant PCa [23]. Taken together, the onset of EMT can lead to PCa cells acquiring drug resistance during progression.

2. The Signal Pathways Leading to Epithelial-To-Mesenchymal Transition (EMT) in Prostate Cancer (PCa)

The tumor surrounding microenvironment has been shown to play an important role in eliciting EMT of carcinoma cell through paracrine/endocrine fashion. Many extracellular signals are responsible for cell–cell communication that alter PCa cell behavior through a receptor-dependent manner. Several peptide hormones such as TGF-β, IL-6, FGF and Wnt are detected in prostatic stromal cells, which are associated with cancer progression [24–27] (Table 1). Among these factors existing in the tumor microenvironment, TGF-β is one of the most well characterized EMT inducer in PCa. It is known that TGF-β can promote EMT via induction of vimentin, fibronectin and suppression of E-cadherin level in vitro [28,29]. It appears that the canonical pathway of TGF-β plays a key role in increasing the expression of EMT transcriptional factor such as (Snail1/2 or ZEB1), which is supported by the evidence that E74-like factor (Elf5), a member of the large E-twenty-six (ETS) transcription factor family, can directly bind to Smad3 and block EMT [30]. Noticeably, the expression of this protein is associated with and E-cadherin expression in PCa specimens [30]. In addition to the canonical pathway, TGF-β-induced Twist expression appears to be mediated by non-canonical pathway of Stat3 in PCa cell lines such as PC3 and DU145 [31,32].

IL-6 is also demonstrated to be an EMT inducer leading to PCa invasiveness [33] and its elevated level is found in metastatic specimens of PCa patients [34]. A study investigating TRAMP (transgenic adenocarcinoma of the mouse prostate) mouse-derived PCa cell lines demonstrated elevated IL-6 levels in hormone resistant cells. Knocking down IL-6 can increase E-cadherin expression and decrease vimentin expression via Stat3 pathway, which also reduces tumor invasion in vivo [35]. Consistently, in LNCaP cells, IL-6 can induce cell migration as well as altered mesenchymal morphology. Mechanistically, IL-6 can induce Twist expression via State3 pathway and lead to the increased fibronectin expression and the inhibited E-cadherin expression [36]. In addition, a similar effect of IL-6 on EMT has been reported using BPH cells [37].

Accumulating evidence has demonstrated that fibroblast growth factor (FGF) family is associated with EMT in PCa. An in vitro study using PCa cell lines demonstrated that FGF2 increases mesenchymal markers, *N*-cadherin, vimentin and decreases epithelial marker, E-cadherin, leading to cell invasion [38]. Moreover, by using a transgenic mouse-expressing FGF9 in PrECs crossed with the TRAMP mouse model, the authors found that forced expression of FGF9 can accelerate the PCa progression in TRAMP mice. Mechanistically, FGF9 derived from LNCaP cells is shown to activate c-Jun dependent TGF-β secretion from prostatic stromal cells, which in turns triggers EMT of LNCaP cells in a paracrine manner [39].

PCa is a typical androgen-dependent disease and ADT is a standard treatment for patients with metastatic disease. It is known that androgen receptor (AR) can induce the expression of several proteases such as MMP2/9 and TMPRSS2 underlying cell invasion [40–42]. In contrast, AR ablation has been shown to induce EMT genes [43]. Mechanistically, AR directly represses Snail gene expression by directly binding to its responsive elements of the promoter. Thus, enzalutamide can promote PCa EMT by de-repressing Snail [44]. Similarly, AR-negative PCa cell lines, PC3 and DU145, show higher mesenchymal gene expression and lower epithelial characteristics than androgen-dependent PCa

cell lines, LNCaP [45]. By using patient-derived xenograft model, a study demonstrated that both *N*-cadherin and vimentin become elevated after ADT [46]. Furthermore, ADT can affect EMT gene expression partly due to the emergence of AR variants [47,48]. For example, one of AR variant such as AR-V7 has been shown to induce mesenchymal genes such as ZEB1 and vimentin, and stem cell marker, Nanog, leading to metastasis [49–51].

Clinically, there is a positive correlation between AR and β-catenin in high-grade PCa [52]. It certainly implies Wnt/β-catenin signaling is associated to PCa [53]. Indeed, DAB2IP, a potent tumor suppressor, is able to block Wnt-induced EMT by facilitating β-catenin degradation resulted in increasing E-cadherin expression through the canonical pathway [54]. It has been reported that up-regulation of Frizzled 8 (FZD8), which is a subtype of Wnt family receptor, induces PCa to metastasize to bone [55]. Moreover, osteoblast derived Wnt-induced secreted protein-1 (WISP1) facilitated PC3 and DU145 invasion through up-regulation of VCAM-1 [56]. In addition, non-canonical Wnt signaling could also contribute EMT, for example, in high-grade PCa specimens exhibiting elevated Wnt5A, *N*-cadherin and vimentin expression but no change in E-cadherin expression [57].

Table 1. Microenvironment soluble factors involved in EMT progression of PCa.

Soluble Factors	Role in EMT	Impacts on PCa Progression	Reference
TGF-β1	Inducer	Invasion, Migration, Metastasis, Sphere formation	[28–32]
BMP	Inducer	Sphere formation	[58]
IL-6	Inducer	Invasion, Metastasis, Sphere formation, Tumor incidence	[33–35,37]
FGF	Inducer	Invasion, Metastasis	[38,39]
AR	Suppressor	EMT Suppression	[24,43,44,52]
AR variants	Inducer	Metastasis	[47–50]
Wnt/β-catenin	Inducer	Invasion, Metastasis, Stemness	[42,52,53,55–57]

EMT: epithelial-to-mesenchymal transition; PCa: prostate cancer.

Accumulating evidence has demonstrated that interplay between signal transduction pathways in response to external stimuli is a critical mechanism to drive the development of metastatic CRPC. In particular, signaling pathways involved in the initiation of EMT often lead to suppression of E-cadherin, resulting in enhanced cell proliferation and metastasis. Particularly, the phosphoinositide 3-kinase (PI3K)-Akt signaling pathway integrates external growth factor stimulations with internal cellular processes. TGF-β can initiate EMT by dissociation of E-cadherin/catenin complexes from the actin cytoskeleton via PI3K/Akt signaling [58]. In this study, the authors demonstrated that TGF-β treatment induces PI3K activation, phosphorylation on either α- or β-catenin associated with E-cadherin localized at the actin cytoskeleton. Dissociation of phosphorylated α- or β-catenin molecules from the E-cadherin results in diminished cell–cell adhesion, as well as enhanced cell migration and invasion. Moreover, TGF-β treatment also leads to significant down-regulation of E-cadherin protein level, accompanied by dramatic change of cancer cell shape from epithelial-like to spindle-like morphology. In contrast, PTEN is a PI3K-Akt signaling regulator involved in stabilization of adherent junctions via de-phosphorylation of β-catenin. TGF-β treatment causes PTEN dissociation from β-catenin, and thus reduced β-catenin dephosphorylation further facilitates PI3K-induced β- and α-catenin phosphorylation, leading to reduction of E-cadherin/catenin complex at the adherent junction and transformation into a more mesenchymal-like phenotype. Meanwhile, bone morphogenetic protein-7 (BMP-7) is shown to induce activation of PI3K and ERK signaling and contributes to the morphological conversion of bone metastatic PCa cell line in both 2D monolayer and 3D spheroid culture system [59]. In particular, the authors observed a significant down-regulation of E-cadherin, accompanied by up-regulation of both Twist and Slug in 3D-cultured PC3 spheroids after exposure to BMP7 treatment. In contrast, inhibition of both Akt and ERK signaling cascades abolishes BMP7-mediated EMT in PC3 cells by diminishing cell migration motility. Overall, this study suggests that initiation of EMT by BMP7 can be regulated through PI3K and ERK signaling in PCa.

Moreover, another critical downstream effector of Akt during prostate tumorigenesis is the mammalian target of rapamycin (mTOR) kinase. Hyper-activation of mTOR is observed in nearly 100%

of advanced PCa [60,61]. In a study using ribosomal profiling approach, mTOR signaling mediates the translation of a specific repertoire of PCa genes involved in cell proliferation, metabolism and invasion. Based on the profiling outcome, mTOR translationally regulates genes including YB-1 (Y-box binding protein 1), vimentin, and MTA1 (metastasis associated 1) that are mainly involved in PCa invasion and metastasis [62]. Notably, ectopic expression of YB-1 can enhance translational activation of Snail and Twist, leading to down-regulation of E-cadherin and enhanced cell migration motility. In contrast, loss of YB-1 results in significant reduction of several mesenchymal factors such as Twist, *N*-cadherin and Snail [63]. Overall, this study demonstrated a critical impact of YB-1 on EMT, MTA1 is a chromatin remodeler playing an important role in PCa invasiveness. A study using MTA1 transgenic knock-in mouse model displayed an inverse correlation between MTA1 and E-cadherin level in the murine prostate tissue, and that MTA1 is shown to suppress E-cadherin expression at post-transcriptional level [64]. Meanwhile, another study also showed that MTA1 impacts on the invasiveness of PCa cells through regulating E-cadherin expression [65]. Functionally, ectopic expression of MTA1 leads to increased invasive capacity of untransformed prostate epithelial cell line [64,66,67]. In addition, studies using clinical specimen and tumor model also demonstrated a significant elevation of MTA1 in highly aggressive PCa, and that loss of MTA1 diminishes PCa invasion, bone metastasis and angiogenesis [68–70]. Overall, these studies demonstrated a significant role of MTA1 and YB-1 in the EMT of PCa leading to metastatic progression of the disease. In addition, different protein components of the mTOR complex such as mTORC1 and mTORC2 exhibit its significant impact on PCa metastasis. Loss of the mTORC1 or mTORC2 complex components, Raptor or Rictor, leads to attenuation of PCa migration and invasion due to elevated E-cadherin and β-catenin expression and reduced mesenchymal markers such as *N*-cadherin and vimentin [71]. Moreover, it appears that paclitaxel-resistant PCa cells are invasive [21]; this is initiated by EMT via Notch-1 signaling and suppression of E-cadherin expression. Overall, this study implies that Notch-1 signaling facilitates the mesenchymal phenotype associated with the acquisition of chemo-resistance in PCa cells.

3. Transcription Factors Associated with EMT

E-cadherin is an essential cell–cell adhesion molecule involved in maintaining the epithelial integrity of the carcinoma cell. Hence, loss of E-cadherin becomes a critical step for EMT initiation and is mainly regulated by several transcriptional repressors such as Snail [72], Slug [73], Twist [74,75] and ZEB1 [76].

Snail is a zinc-finger protein binding to E-box sequences of the E-cadherin promoter [72]. Aberrant up-regulation of Snail has been observed in many malignancies such as breast cancer, ovarian cancer [77,78], colorectal cancer [79,80] and PCa [44,81]. In particular, elevation of Snail protein expression has been seen in both enzalutamide-resistant PCa cell line as well as highly metastatic PCa patient specimens [81]. Particularly, ectopic expression of Snail results in enhanced elevation of both AR and AR variants, which might be an initial cause of enzalutamide resistance in PCa lines, suggesting the impact of Snail on the recurrence of metastatic CRPC. In addition to its suppressor function, Snail may facilitate cancer metastasis via enhancing the protein expression and enzymatic activity of urokinase-type plasminogen activator (uPA) leading to enhanced motility in PCa cell lines [82]. In addition, Snail impacts on the expression level of several tight junction protein components by repressing the promoter activity of claudins and occludin genes, and inhibiting Zona occludin 1 (ZO-1) expression at post-transcriptional level [83,84]. Overall, the impact of Snail on EMT process and cell adhesion molecules demonstrates its crucial regulatory role in the disease progression of PCa.

Slug is a dominant regulator of EMT in many cancers including PCa. In addition to acting as an E-cadherin transcriptional repressor, Slug also regulates other factors leading to EMT in PCa. An in vitro study showed that Slug up-regulates both CXCL12 and CXCR4 and impacts on CXCL12/CXCR4 signaling downstream target gene, MMP9, leading to highly invasiveness of PCa [85], implying that up-regulation of autocrine CXCL12 is a critical mechanism underlying Slug-mediated migration and invasion of PCa. In primary PCa, Slug/SNAI2 gene expression are often down

regulated due to the promoter methylation; the expression of Slug is restored or elevated in the invasion front of high grade PCa and lymph node metastases [86]. In addition, Slug can suppress several metastasis-suppressor genes such as KISS1. Particularly, KISS1 is able to inhibit EMT by via suppressing *N*-cadherin and vimentin, and increasing E-cadherin expression then diminish tumor cell migration and invasion motility [87]. Clinically, loss of KISS1 is widely observed in primary and metastatic PCa compared with benign tissue. Restoring KISS1 expression in highly metastatic PCa cell lines results in diminishing cell invasion motility [88]. Taken together, Slug is a highly potent promoter for PCa metastasis via EMT induction, cytokine production and metalloprotease secretion.

Twist is a basic helix-loop-helix protein that plays critical roles during development and tumorigenesis. Many studies have demonstrated that Twist can activate EMT, and that it enhances cell migration via binding to the promoter of the E-cadherin gene. In the past, the mechanistic association between Twist and transcriptional repression of E-cadherin has been shown in many malignancies including esophageal squamous cell carcinoma [89], bladder cancer [90], breast cancer [91] and PCa [92]. Clinically, Twist is found highly expressed in malignant prostatic tissue when compared to BPH tissue, and its protein level is significantly correlated with Gleason grades and metastasis [75]. Meanwhile, overexpression of Twist at the marginal area of prostatic tumor has been correlated with capsule invasion and biochemical recurrence (BCR) in PCa patients receiving radical prostatectomy [93]. In addition to acting as E-cadherin repressor, Twist also facilitates EMT by regulating *N*-cadherin expression [94]. This study demonstrated that β1 integrin-mediated nuclear translocation of Twist is capable of inducing *N*-cadherin transcriptional activation via binding of Twist to the E-box regulatory element within the *N*-cadherin gene, suggesting that Twist acts as pivotal transcription factor in the metastatic progression of PCa.

ZEB1 is a zinc finger homeodomain transcriptional repressor that regulates skeletal patterning during development and suppresses E-cadherin transcriptional activity in multiple malignancies.

Clinically, ZEB1 is elevated in high-grade prostatic tumors, compared to benign or lower grade PCa specimens [95]. A recent study demonstrated that ZEB1 is physically associated with the histone H4K20-specific methyltransferase, SET8. Mechanistically, SET8-induced H4K20 methylation is implied to exert a dual function in ZEB1-regulated gene expression. Functionally, ZEB1 and SET8 cooperatively trigger EMT by suppression of E-cadherin and induction of vimentin in PCa cells, leading to the invasive potential of PCa [96]. Moreover, an in vitro study has demonstrated that elevation of ZEB1 and loss of E-cadherin is concurrently observed in a subpopulation of PC3 cells that acquired trans-endothelial migration characteristics in vitro, compared to the parental cell line. In contrast, loss of ZEB1 partially restores the epithelial phenotype and reduces trans-endothelial extravasation of PC3 cells [76]. Overall, this study suggests that ZEB1 is a critical regulator of EMT and mediates vascular extravasation of PCa cells during the disease progression.

Forkhead box (FOX) proteins constitute a large family of 19 subgroups of transcriptional regulators that contain an evolutionary conserved DNA binding domain (Forkhead or winged-helix). Among them, FOXA1 is known as a pioneering transcription factor for AR [97–99]. However, FOXA1 loss is often detected in metastatic PCa specimen [100] because FOXA1 has an AR-independent function on suppressing EMT via regulating Slug in PCa cells. In contrast, FoxO family is able to block EMT in malignant cells of multiple cancers [101,102]. Clinically, emerging evidence has demonstrated an inverse correlation between FoxOs level and PCa grade as well as tumor dissemination, indicating its suppressor role in PCa metastasis [103]. Mechanistically, the transcriptional activity of FoxO3a is negatively regulated by PI3K/Akt signaling through post-translational phosphorylate modification. During PCa progression, progressive activation of Akt leads to increased phosphorylation of FoxO3a, which impacts on its nuclear localization and hence FoxO3a-dependent transcriptional activity is further inhibited [104]. Functionally, FoxO3a can directly compete with T-cell factor (TCF) for the interaction with β-catenin, leading to inhibition of β-catenin/TCF transcriptional activity and thus reduction in expression of β-catenin-target genes, such as ZEB1 and Snail. Moreover, knockdown of FoxO3a leads to elevation of *N*-cadherin, fibronectin, ZEB1 and vimentin in highly metastatic

PC3 cells [105]. Overall, these data demonstrated a crucial role of FoxO family in PCa metastasis via targeting EMT factors.

4. Epigenetic Regulation of EMT

Epigenetic regulation is considered as a key initial step in mammalian development. Since EMT occurs during embryogenesis, it is conceivable that epigenetics also plays a critical role in pathologic EMT. Accumulating evidence has demonstrated that both hyper- and hypomethylation of DNA are involved in the deregulation of several genes contributing to PCa progression [106–108]. In particular, aberrant DNA hypermethylation in cancer may lead to inactivation of tumor suppressor genes, leading to increased invasiveness of PCa. HIC1 is a tumor suppressor gene located at 17p13.3, a chromosomal region that is frequently hyper-methylated or deleted in human tumors. HIC1 acts as a transcriptional repressor involved in the suppression of SIRT1 and the regulation of TP53-dependent apoptotic DNA-damage responses [109]. A study using PCa specimens showed that high frequency of HIC1 gene hypermethylation is observed in metastatic PCa, compared to primary and benign tissue. Moreover, hypermethylation of HIC1 gene in PCa cells leads to induction of cell migration and metastasis by promoting EMT via enhancing both Slug and CXCR4 expression that are crucial to PCa metastasis [110]. Meanwhile, restoring HIC1 expression in several PCa cell lines markedly inhibits cell proliferation, migration and invasion in vitro, as well as reduces tumor growth, tissue metastasis and bone destruction in vivo [111,112]. Clearly, epigenetic modification of HIC1 promoter can impact EMT induction in PCa.

Moreover, histone modification of critical genes has similar effect on EMT induction during PCa metastasis. The histone methyltransferase, MMSET/WHSC1 (Multiple Myeloma SET domain), is capable of facilitating EMT in PCa cells via induction of Twist1, which in turns suppresses E-cadherin expression [113]. In addition, Zeste homolog 2 (EZH2) is a critical component of Polycomb repressive complex 2 (PRC2) and causes gene silencing by increasing histone methylation. Increased level of EZH2 has been observed in PCa and many other cancer types. Particularly, transcriptional repression of E-cadherin by EZH2 is often observed in highly aggressive PCa [114–116]. In addition, EMT-related transcription factor can be an epigenetic regulator to orchestrate EMT process. SIRT1 is, known as class III Histone deacetylase, also characterized as an EMT-related transcription factor. By silencing of SIRT1 can cause down-regulation of ZEB1. In addition, recruitment of SIRT1 at the promoter region of E-cadherin can be facilitated by the presence of ZEB1 in PCa cells, leading to transcriptional suppression of E-cadherin [117]. A recent study demonstrated that silencing of SIRT1 can suppress PCa cell migration and invasion via down-regulation of Vimentin and *N*-cadherin, leading to subsequent up-regulation of E-cadherin [118]. Overall, SIRT1 is a unique epigenetic regulator as well as EMT-related transcription factor in PCa.

5. MicroRNA Associated with EMT during PCa Progression

MicroRNAs (miRNAs) are small non-coding RNA molecules regulating gene expression via post-transcriptional silencing of target genes. miRNA regulation is highly associated with multiple biological processes such as differentiation, proliferation, migration, survival and invasion. Several miRNAs are known to target transcription factors contributing to the mesenchymal phenotype in PCa (Table 2). For incidence, members of the miR-200 family (miR-200a, miR-200b, miR-200c, miR-141 and miR-449) are markedly down-regulated during PCa progression and are shown to suppress EMT mainly by inhibiting E-cadherin repressors such as ZEB1 and ZEB2 at the post-transcriptional level [119–121]. Both miR-203 and miR-205 are known to restore epithelial phenotype in PCa cells by targeting Slug/SNAI2 and ZEB2. Clinically, expression level of miR-203 is significantly attenuated in bone metastatic PCa specimens compared with benign tissue, while miR-205 is found to be decreased dramatically in lymph node metastasis when compared to primary prostatic tumor [122,123]. Meanwhile, by miRNA microarray analysis, miR-508-5p, miR-145, miR-143, miR-33a and miR-100 were found to be significantly down-regulated in metastatic PCa compared to

the primary tumor. In particular, miR-143 and miR-145 derived from the same cluster are shown to reverse EMT and reduce PCa cell migration and invasion by targeting fibronectin and ZEB2 [124,125]. Moreover, several mesenchymal factors such as *N*-cadherin, Twist and Snail are regulated by miR-29b, which is also down-regulated significantly in PCa cell lines and PCa patient specimens when compared to normal prostate epithelial cells and adjacent benign tissue, respectively. Ectopic expression of miR-29b in PCa cells is capable of suppressing PCa invasiveness in vitro, and diminishing secondary colonization at the lungs and liver following intravenous injection in vivo, suggesting miR-29b acts as an anti-metastatic miRNA that is down-regulated during PCa progression [126]. Meanwhile, miR-23b is found to be a methylation-silenced tumor suppressor that inhibits EMT via directly targeting Src kinase and Akt. Moreover, this study also demonstrated that ectopic expression of miR-23b in PC3 cells causes decline in mesenchymal markers vimentin and Snail, and increase of epithelial marker, E-cadherin [127]. Similarly, miR-34a is a tumor suppressive miRNA implicated in EMT and cancer stemness in multiple tumors. A study showed that miR-34a is negatively correlated with PCa migration and invasion by targeting lymphoid enhancer-binding factor-1 (LEF1), a key transcription factor involved in regulation of cell proliferation and invasion. This study also demonstrated that ectopic expression of miR-34a causes the down regulation of *N*-cadherin and Snail, and induction of E-cadherin in LNCaP and C4-2B cell lines, overall suggesting that miR-34a-LEF1 regulation plays an important role in the metastatic progression of PCa [128]. In addition, miR-486 is significantly down-regulated in metastatic C4-2 cells as well as disseminated tumors in PCa patients, compared to parental LNCaP cell and localized PCa tissues, respectively. Functionally, miR-486 is demonstrated to target Snail by post-transcriptional suppression and functionally inhibit PCa cell migration and invasion [129]. Findings from this study suggest that miR-486 negatively mediates the migration and invasion potential of PCa via targeting Snail.

In contrast to tumor suppressor miRNAs, aberrant expression of oncogenic miRNAs is observed in highly aggressive PCa associated with EMT. A study using intra-cardiac inoculation of PCa cells in mice demonstrated the oncogenic role of miR-409 in PCa bone metastasis [130]. Inhibition of miR-409 in highly metastatic PCa cells reverses EMT process by increasing E-Cadherin expression, reducing *N*-cadherin level, and causing morphological change to the epithelial phenotype.

In addition, several studies demonstrated a negative feedback loop between miRNA and EMT transcription factors. For example, ZEB2 known as a direct target of miR-145 can also suppress miR-145 at transcription level. This double negative feedback loop between ZEB2 and miR-145 determines the invasiveness and stemness properties of PCa and contributes to the bone metastasis [131]. Moreover, ZEB1 can suppress the transcription of miR-375 that can inhibit EMT-elicited cell migration and invasion via targeting YAP1 [132].

Table 2. MicroRNAs involved in the EMT and metastatic progression of PCa.

MicroRNAs	Role in EMT	Target	Impacts on PCa Progression	Reference
miR-200b	Suppressor	ZEB1, ZEB2	Suppress cell proliferation, EMT, invasion, and inhibit prostate tumor growth and metastasis.	[120,133,134]
miR-141	Suppressor	ZEB1, CD44, EZH2, Rac1	Inhibits cell sphere formation, invasion, and suppresses tumor regeneration and metastasis.	[119]
miR-203	Suppressor	ZEB2, Bmi, Survivin, RunX2	Suppress prostate tumor metastasis, inhibit cell proliferation, EMT, and invasion motility	[122]
miR-205	Suppressor	c-SRC, ZEB1, ZEB2	Attenuate cell proliferation, invasion and tumor growth	[123,135,136]
miR-143	Suppressor	Fibronectin, ZEB2, MMP13	Suppress cell invasion and migration	[125,137]
miR-145	Suppressor	Fibronectin, ZEB2	Repress cell bone metastasis, invasion and migration	[125]
miR-29b	Suppressor	*N*-cadherin, Twist1, Snail	Suppress cell invasion, migration and attenuate prostate tumor lung metastasis	[126]
miR-23b	Suppressor	Slug, Vimentin, Src	Suppress cell migration, invasion and attenuate prostate tumorigenecity	[127]
miR-34a	Suppressor	LEF1, *N*-cadherin, Snail	Attenuate cell invasion and migration	[128,138]
miR-486	Suppressor	Snail	Suppresses migration and invasion of cells.	[129]
miR-409	Inducer	STAG2, RBL2, RSU1, NPRL2	Increase invasiveness and aggressiveness, and promotes tumorigenecity, EMT and stemness of prostate tumor	[130]

6. Long Non-Coding RNA Regulation of EMT in PCa

Long non-coding RNAs (lncRNAs), such as the prostate specific prostate cancer antigen 3 (PCA3/DD3), also plays a critical role in PCa EMT. Silencing of PCA3 in LNCaP cells modulates the expression pattern of several cancer-related genes coding EMT markers such as MTA2 and PLAUR. Meanwhile, PCA3 is shown to facilitate PRKD3-mediated invasion and migration via competitive sponging of miR-1261 [139]. In addition, SChLAP1 (Second Chromosome Locus Associated with Prostate-1) is prevalently expressed in a subset of metastatic PCa, compared to localized primary PCa. Mechanistically, SChLAP1 is able to enhance PCa metastasis by altering the cellular localization and gene regulation of tumor-suppressive SWI/SNF (Switch/Sucrose Nonfermenting) chromatin-modifying complex through interaction with SNF5 [140]. In addition, a recent study also demonstrates that SChLAP1 can modulate the MAPK1 signaling pathway, leading to accelerating cell proliferation and enhancing metastatic potential of PCa in vitro and in vivo [141]. Another highly up-regulated lncRNA in PCa is Metastasis-associated Lung Adenocarcinoma Transcript 1 (MALAT1) that is shown to enhance EZH2-mediated repression of Polycomb-dependent target gene, E-Cadherin. Mechanistically, by interacting with the Polycomb protein enhancer of EZH2, MALAT1 is capable of facilitating EZH2 recruitment to target genes, such as E-cadherin and DAB2IP, resulting in enhanced EZH2-mediated migration and invasion in aggressive CRPC cell lines [142–144]. PlncRNA-1 has been shown to induce *N*-cadherin expression through modulating TGF-β1 signaling, and hence increase PCa cell migration and invasion motility [145].

7. Conclusions

The initiation of EMT is considered the initial step leading to cancer metastasis that is expected to contribute to the poor prognosis of cancer patient. Thus, targeting EMT is likely to improve the overall survival of a patient. EMT is a highly regulated process that can be engaged by the reciprocal interaction between tumor surrounding microenvironment and cancer cells. Through extensive survey in PCa, several key inducers associated with the specific signaling pathways and their regulations have been reported. With respect to the role of EMT in cancer metastasis, stemness, and chemo-resistance, apparently, these key regulators can be druggable targets to be a new generation of cancer medicine as

a targeted therapeutic strategy. In this case, small molecule inhibitor such as EZH2 inhibitor or certain unique miRNA such as miR-200 [146] and miR-145 [147] can be further tested in vivo to evaluate their efficacy and validate their mechanism of action.

Acknowledgments: We thank Samarpita Sengupta for editorial assistance. This work was supported in part by grants from the United States Army (W81XWH-11-1-0491 and W81XWH-16-1-0474 to Jer-Tsong Hsieh) and (W81XWH-14-1-0249 to U-Ging Lo), and the Ministry of Science and Technology, Taiwan (MOST 104-2911-I-002-578 and MOST 105-2911-I-002-521 to Ming-Shyue Lee and Cheng-Fan Lee).

Author Contributions: U-Ging Lo and Cheng-Fan Lee collected reference and wrote manuscript. Ming-Shyue and Jer-Tsong Hsieh determined framework and finalized manuscript.

Conflicts of Interest: The authors declare no conflicts of interest.

References

1. Nakaya, Y.; Sheng, G. Epithelial to mesenchymal transition during gastrulation: An embryological view. *Dev. Growth Differ.* **2008**, *50*, 755–766. [CrossRef] [PubMed]
2. Grant, C.M.; Kyprianou, N. Epithelial mesenchymal transition (EMT) in prostate growth and tumor progression. *Transl. Androl. Urol.* **2013**, *2*, 202–211. [PubMed]
3. Krainock, M.; Toubat, O.; Danopoulos, S.; Beckham, A.; Warburton, D.; Kim, R. Epicardial epithelial-to-mesenchymal transition in heart development and disease. *J. Clin. Med.* **2016**, *5*, 27. [CrossRef] [PubMed]
4. Bartis, D.; Mise, N.; Mahida, R.Y.; Eickelberg, O.; Thickett, D.R. Epithelial-mesenchymal transition in lung development and disease: Does it exist and is it important? *Thorax* **2014**, *69*, 760–765. [CrossRef] [PubMed]
5. Chaffer, C.L.; Thompson, E.W.; Williams, E.D. Mesenchymal to epithelial transition in development and disease. *Cells Tissues Organs* **2007**, *185*, 7–19. [CrossRef] [PubMed]
6. Lee, J.M.; Dedhar, S.; Kalluri, R.; Thompson, E.W. The epithelial-mesenchymal transition: New insights in signaling, development, and disease. *J. Cell Biol.* **2006**, *172*, 973–981. [CrossRef] [PubMed]
7. Perl, A.K.; Wilgenbus, P.; Dahl, U.; Semb, H.; Christofori, G. A causal role for e-cadherin in the transition from adenoma to carcinoma. *Nature* **1998**, *392*, 190–193. [CrossRef] [PubMed]
8. Nakaya, Y.; Sheng, G. Emt in developmental morphogenesis. *Cancer Lett.* **2013**, *341*, 9–15. [CrossRef] [PubMed]
9. Fan, L.; Wang, H.; Xia, X.; Rao, Y.; Ma, X.; Ma, D.; Wu, P.; Chen, G. Loss of e-cadherin promotes prostate cancer metastasis via upregulation of metastasis-associated gene 1 expression. *Oncol. Lett.* **2012**, *4*, 1225–1233. [PubMed]
10. Chen, C.L.; Mahalingam, D.; Osmulski, P.; Jadhav, R.R.; Wang, C.M.; Leach, R.J.; Chang, T.C.; Weitman, S.D.; Kumar, A.P.; Sun, L.; et al. Single-cell analysis of circulating tumor cells identifies cumulative expression patterns of emt-related genes in metastatic prostate cancer. *Prostate* **2013**, *73*, 813–826. [CrossRef] [PubMed]
11. Mani, S.A.; Guo, W.; Liao, M.J.; Eaton, E.N.; Ayyanan, A.; Zhou, A.Y.; Brooks, M.; Reinhard, F.; Zhang, C.C.; Shipitsin, M.; et al. The epithelial-mesenchymal transition generates cells with properties of stem cells. *Cell* **2008**, *133*, 704–715. [CrossRef] [PubMed]
12. Morel, A.P.; Lievre, M.; Thomas, C.; Hinkal, G.; Ansieau, S.; Puisieux, A. Generation of breast cancer stem cells through epithelial-mesenchymal transition. *PLoS ONE* **2008**, *3*, e2888. [CrossRef] [PubMed]
13. Wellner, U.; Schubert, J.; Burk, U.C.; Schmalhofer, O.; Zhu, F.; Sonntag, A.; Waldvogel, B.; Vannier, C.; Darling, D.; zur Hausen, A.; et al. The emt-activator ZEB1 promotes tumorigenicity by repressing stemness-inhibiting microRNAs. *Nat. Cell Biol.* **2009**, *11*, 1487–1495. [CrossRef] [PubMed]
14. Wang, M.; Ren, D.; Guo, W.; Huang, S.; Wang, Z.; Li, Q.; Du, H.; Song, L.; Peng, X. *N*-cadherin promotes epithelial-mesenchymal transition and cancer stem cell-like traits via erbb signaling in prostate cancer cells. *Int. J. Oncol.* **2016**, *48*, 595–606. [CrossRef] [PubMed]
15. Tam, K.J.; Hui, D.H.F.; Lee, W.W.; Dong, M.; Tombe, T.; Jiao, I.Z.F.; Khosravi, S.; Takeuchi, A.; Peacock, J.W.; Ivanova, L.; et al. Semaphorin 3 c drives epithelial-to-mesenchymal transition, invasiveness, and stem-like characteristics in prostate cells. *Sci. Rep.* **2017**, *7*, 11501. [CrossRef] [PubMed]
16. Ruscetti, M.; Quach, B.; Dadashian, E.L.; Mulholland, D.J.; Wu, H. Tracking and functional characterization of epithelial-mesenchymal transition and mesenchymal tumor cells during prostate cancer metastasis. *Cancer Res.* **2015**, *75*, 2749–2759. [CrossRef] [PubMed]

17. Harner-Foreman, N.; Vadakekolathu, J.; Laversin, S.A.; Mathieu, M.G.; Reeder, S.; Pockley, A.G.; Rees, R.C.; Boocock, D.J. A novel spontaneous model of epithelial-mesenchymal transition (EMT) using a primary prostate cancer derived cell line demonstrating distinct stem-like characteristics. *Sci. Rep.* **2017**, *7*, 40633. [CrossRef] [PubMed]
18. Wang, X.; Ling, M.T.; Guan, X.Y.; Tsao, S.W.; Cheung, H.W.; Lee, D.T.; Wong, Y.C. Identification of a novel function of twist, a bhlh protein, in the development of acquired taxol resistance in human cancer cells. *Oncogene* **2004**, *23*, 474–482. [CrossRef] [PubMed]
19. Kurrey, N.K.; Jalgaonkar, S.P.; Joglekar, A.V.; Ghanate, A.D.; Chaskar, P.D.; Doiphode, R.Y.; Bapat, S.A. Snail and slug mediate radioresistance and chemoresistance by antagonizing p53-mediated apoptosis and acquiring a stem-like phenotype in ovarian cancer cells. *Stem Cells* **2009**, *27*, 2059–2068. [CrossRef] [PubMed]
20. Saxena, M.; Stephens, M.A.; Pathak, H.; Rangarajan, A. Transcription factors that mediate epithelial-mesenchymal transition lead to multidrug resistance by upregulating abc transporters. *Cell Death Dis.* **2011**, *2*, e179. [CrossRef] [PubMed]
21. Wang, W.; Wang, L.; Mizokami, A.; Shi, J.; Zou, C.; Dai, J.; Keller, E.T.; Lu, Y.; Zhang, J. Down-regulation of e-cadherin enhances prostate cancer chemoresistance via notch signaling. *Chin. J. Cancer* **2017**, *36*, 35. [CrossRef] [PubMed]
22. Ruan, D.; He, J.; Li, C.F.; Lee, H.J.; Liu, J.; Lin, H.K.; Chan, C.H. SKP2 deficiency restricts the progression and stem cell features of castration-resistant prostate cancer by destabilizing twist. *Oncogene* **2017**, *36*, 4299–4310. [CrossRef] [PubMed]
23. Hanrahan, K.; O'Neill, A.; Prencipe, M.; Bugler, J.; Murphy, L.; Fabre, A.; Puhr, M.; Culig, Z.; Murphy, K.; Watson, R.W. The role of epithelial-mesenchymal transition drivers ZEB1 and ZEB2 in mediating docetaxel-resistant prostate cancer. *Mol. Oncol.* **2017**, *11*, 251–265. [CrossRef] [PubMed]
24. Ricke, E.A.; Williams, K.; Lee, Y.F.; Couto, S.; Wang, Y.; Hayward, S.W.; Cunha, G.R.; Ricke, W.A. Androgen hormone action in prostatic carcinogenesis: Stromal androgen receptors mediate prostate cancer progression, malignant transformation and metastasis. *Carcinogenesis* **2012**, *33*, 1391–1398. [CrossRef] [PubMed]
25. Yu, S.H.; Zheng, Q.; Esopi, D.; Macgregor-Das, A.; Luo, J.; Antonarakis, E.S.; Drake, C.G.; Vessella, R.; Morrissey, C.; De Marzo, A.M.; et al. A paracrine role for il6 in prostate cancer patients: Lack of production by primary or metastatic tumor cells. *Cancer Immunol. Res.* **2015**, *3*, 1175–1184. [CrossRef] [PubMed]
26. Shigemura, K.; Huang, W.C.; Li, X.; Zhau, H.E.; Zhu, G.; Gotoh, A.; Fujisawa, M.; Xie, J.; Marshall, F.F.; Chung, L.W. Active sonic hedgehog signaling between androgen independent human prostate cancer cells and normal/benign but not cancer-associated prostate stromal cells. *Prostate* **2011**, *71*, 1711–1722. [CrossRef] [PubMed]
27. Zong, Y.; Huang, J.; Sankarasharma, D.; Morikawa, T.; Fukayama, M.; Epstein, J.I.; Chada, K.K.; Witte, O.N. Stromal epigenetic dysregulation is sufficient to initiate mouse prostate cancer via paracrine WNT signaling. *Proc. Natl. Acad. Sci. USA* **2012**, *109*, E3395–E3404. [CrossRef] [PubMed]
28. Chen, X.H.; Liu, Z.C.; Zhang, G.; Wei, W.; Wang, X.X.; Wang, H.; Ke, H.P.; Zhang, F.; Wang, H.S.; Cai, S.H.; et al. Tgf-beta and egf induced hla-i downregulation is associated with epithelial-mesenchymal transition (EMT) through upregulation of snail in prostate cancer cells. *Mol. Immunol.* **2015**, *65*, 34–42. [CrossRef] [PubMed]
29. Shiota, M.; Zardan, A.; Takeuchi, A.; Kumano, M.; Beraldi, E.; Naito, S.; Zoubeidi, A.; Gleave, M.E. Clusterin mediates TGF-beta-induced epithelial-mesenchymal transition and metastasis via twist1 in prostate cancer cells. *Cancer Res.* **2012**, *72*, 5261–5272. [CrossRef] [PubMed]
30. Yao, B.; Zhao, J.; Li, Y.; Li, H.; Hu, Z.; Pan, P.; Zhang, Y.; Du, E.; Liu, R.; Xu, Y. ELF5 inhibits TGF-beta-driven epithelial-mesenchymal transition in prostate cancer by repressing SMAD3 activation. *Prostate* **2015**, *75*, 872–882. [CrossRef] [PubMed]
31. Hu, Q.; Tong, S.; Zhao, X.; Ding, W.; Gou, Y.; Xu, K.; Sun, C.; Xia, G. Periostin mediates tgf-beta-induced epithelial mesenchymal transition in prostate cancer cells. *Cell. Physiol. Biochem.* **2015**, *36*, 799–809. [CrossRef] [PubMed]
32. Cho, K.H.; Jeong, K.J.; Shin, S.C.; Kang, J.; Park, C.G.; Lee, H.Y. STAT3 mediates tgf-beta1-induced twist1 expression and prostate cancer invasion. *Cancer Lett.* **2013**, *336*, 167–173. [CrossRef] [PubMed]
33. Nguyen, D.P.; Li, J.; Tewari, A.K. Inflammation and prostate cancer: The role of interleukin 6 (IL-6). *BJU Int.* **2014**, *113*, 986–992. [CrossRef] [PubMed]

34. Gu, L.; Talati, P.; Vogiatzi, P.; Romero-Weaver, A.L.; Abdulghani, J.; Liao, Z.; Leiby, B.; Hoang, D.T.; Mirtti, T.; Alanen, K.; et al. Pharmacologic suppression of JAK1/2 by JAK1/2 inhibitor AZD1480 potently inhibits IL-6-induced experimental prostate cancer metastases formation. *Mol. Cancer Ther.* **2014**, *13*, 1246–1258. [CrossRef] [PubMed]
35. Wu, C.T.; Hsieh, C.C.; Lin, C.C.; Chen, W.C.; Hong, J.H.; Chen, M.F. Significance of IL-6 in the transition of hormone-resistant prostate cancer and the induction of myeloid-derived suppressor cells. *J. Mol. Med.* **2012**, *90*, 1343–1355. [CrossRef] [PubMed]
36. Shiota, M.; Bishop, J.L.; Nip, K.M.; Zardan, A.; Takeuchi, A.; Cordonnier, T.; Beraldi, E.; Bazov, J.; Fazli, L.; Chi, K.; et al. Hsp27 regulates epithelial mesenchymal transition, metastasis, and circulating tumor cells in prostate cancer. *Cancer Res.* **2013**, *73*, 3109–3119. [CrossRef] [PubMed]
37. Rojas, A.; Liu, G.; Coleman, I.; Nelson, P.S.; Zhang, M.; Dash, R.; Fisher, P.B.; Plymate, S.R.; Wu, J.D. IL-6 promotes prostate tumorigenesis and progression through autocrine cross-activation of IGF-IR. *Oncogene* **2011**, *30*, 2345–2355. [CrossRef] [PubMed]
38. Liu, C.; Guan, H.; Wang, Y.; Chen, M.; Xu, B.; Zhang, L.; Lu, K.; Tao, T.; Zhang, X.; Huang, Y. Mir-195 inhibits emt by targeting FGF2 in prostate cancer cells. *PLoS ONE* **2015**, *10*, e0144073. [CrossRef] [PubMed]
39. Huang, Y.; Jin, C.; Hamana, T.; Liu, J.; Wang, C.; An, L.; McKeehan, W.L.; Wang, F. Overexpression of FGF9 in prostate epithelial cells augments reactive stroma formation and promotes prostate cancer progression. *Int. J. Biol. Sci.* **2015**, *11*, 948–960. [CrossRef] [PubMed]
40. Ko, C.J.; Huang, C.C.; Lin, H.Y.; Juan, C.P.; Lan, S.W.; Shyu, H.Y.; Wu, S.R.; Hsiao, P.W.; Huang, H.P.; Shun, C.T.; et al. Androgen-induced TMPRSS2 activates matriptase and promotes extracellular matrix degradation, prostate cancer cell invasion, tumor growth, and metastasis. *Cancer Res.* **2015**, *75*, 2949–2960. [CrossRef] [PubMed]
41. Liao, X.; Thrasher, J.B.; Pelling, J.; Holzbeierlein, J.; Sang, Q.X.; Li, B. Androgen stimulates matrix metalloproteinase-2 expression in human prostate cancer. *Endocrinology* **2003**, *144*, 1656–1663. [CrossRef] [PubMed]
42. Yang, Y.; Jiao, L.; Hou, J.; Xu, C.; Wang, L.; Yu, Y.; Li, Y.; Yang, C.; Wang, X.; Sun, Y. Dishevelled-2 silencing reduces androgen-dependent prostate tumor cell proliferation and migration and expression of WNT-3a and matrix metalloproteinases. *Mol. Biol. Rep.* **2013**, *40*, 4241–4250. [CrossRef] [PubMed]
43. Zhu, M.L.; Kyprianou, N. Role of androgens and the androgen receptor in epithelial-mesenchymal transition and invasion of prostate cancer cells. *FASEB J.* **2010**, *24*, 769–777. [CrossRef] [PubMed]
44. Miao, L.; Yang, L.; Li, R.; Rodrigues, D.N.; Crespo, M.; Hsieh, J.T.; Tilley, W.D.; de Bono, J.; Selth, L.A.; Raj, G.V. Disrupting androgen receptor signaling induces snail-mediated epithelial-mesenchymal plasticity in prostate cancer. *Cancer Res.* **2017**, *77*, 3101–3112. [CrossRef] [PubMed]
45. Tran, N.L.; Nagle, R.B.; Cress, A.E.; Heimark, R.L. *N*-cadherin expression in human prostate carcinoma cell lines. An epithelial-mesenchymal transformation mediating adhesion withstromal cells. *Am. J. Pathol.* **1999**, *155*, 787–798. [CrossRef]
46. Wang, M.; Liu, X.; Guo, J.; Weng, X.; Jiang, G.; Wang, Z.; He, L. Inhibition of lsd1 by pargyline inhibited process of emt and delayed progression of prostate cancer in vivo. *Biochem. Biophys. Res. Commun.* **2015**, *467*, 310–315. [CrossRef] [PubMed]
47. Zhang, X.; Morrissey, C.; Sun, S.; Ketchandji, M.; Nelson, P.S.; True, L.D.; Vakar-Lopez, F.; Vessella, R.L.; Plymate, S.R. Androgen receptor variants occur frequently in castration resistant prostate cancer metastases. *PLoS ONE* **2011**, *6*, e27970. [CrossRef] [PubMed]
48. Ware, K.E.; Garcia-Blanco, M.A.; Armstrong, A.J.; Dehm, S.M. Biologic and clinical significance of androgen receptor variants in castration resistant prostate cancer. *Endocr. Relat. Cancer* **2014**, *21*, T87–T103. [CrossRef] [PubMed]
49. Xu, J.; Qiu, Y. Role of androgen receptor splice variants in prostate cancer metastasis. *Asian J. Urol.* **2016**, *3*, 177–184. [CrossRef] [PubMed]
50. Sun, F.; Chen, H.G.; Li, W.; Yang, X.; Wang, X.; Jiang, R.; Guo, Z.; Chen, H.; Huang, J.; Borowsky, A.D.; et al. Androgen receptor splice variant ar3 promotes prostate cancer via modulating expression of autocrine/paracrine factors. *J. Biol. Chem.* **2014**, *289*, 1529–1539. [CrossRef] [PubMed]
51. Li, Y.; Li, C.X.; Ye, H.; Chen, F.; Melamed, J.; Peng, Y.; Liu, J.; Wang, Z.; Tsou, H.C.; Wei, J.; et al. Decrease in stromal androgen receptor associates with androgen-independent disease and promotes prostate cancer cell proliferation and invasion. *J. Cell. Mol. Med.* **2008**, *12*, 2790–2798. [CrossRef] [PubMed]

52. Jung, S.J.; Oh, S.; Lee, G.T.; Chung, J.; Min, K.; Yoon, J.; Kim, W.; Ryu, D.S.; Kim, I.Y.; Kang, D.I. Clinical significance of WNT/beta-catenin signalling and androgen receptor expression in prostate cancer. *World J. Mens Health* **2013**, *31*, 36–46. [CrossRef] [PubMed]
53. Baruah, M.M.; Khandwekar, A.P.; Sharma, N. Quercetin modulates wnt signaling components in prostate cancer cell line by inhibiting cell viability, migration, and metastases. *Tumour Biol.* **2016**, *37*, 14025–14034. [CrossRef] [PubMed]
54. Yun, E.J.; Zhou, J.; Lin, C.J.; Hernandez, E.; Fazli, L.; Gleave, M.; Hsieh, J.T. Targeting cancer stem cells in castration-resistant prostate cancer. *Clin. Cancer Res.* **2016**, *22*, 670–679. [CrossRef] [PubMed]
55. Li, Q.; Ye, L.; Xin, Z.; Wang, M.; Lin, C.; Huang, S.; Guo, W.; Lai, Y.; Du, H.; Li, J.; et al. Fzd8, a target of p53, promotes bone metastasis in prostate cancer by activating canonical wnt/beta-catenin signaling. *Cancer Lett.* **2017**, *402*, 166–176. [CrossRef] [PubMed]
56. Tai, H.C.; Chang, A.C.; Yu, H.J.; Huang, C.Y.; Tsai, Y.C.; Lai, Y.W.; Sun, H.L.; Tang, C.H.; Wang, S.W. Osteoblast-derived wnt-induced secreted protein 1 increases VCAM-1 expression and enhances prostate cancer metastasis by down-regulating mir-126. *Oncotarget* **2014**, *5*, 7589–7598. [CrossRef] [PubMed]
57. Sandsmark, E.; Hansen, A.F.; Selnaes, K.M.; Bertilsson, H.; Bofin, A.M.; Wright, A.J.; Viset, T.; Richardsen, E.; Drablos, F.; Bathen, T.F.; et al. A novel non-canonical wnt signature for prostate cancer aggressiveness. *Oncotarget* **2017**, *8*, 9572–9586. [CrossRef] [PubMed]
58. Vogelmann, R.; Nguyen-Tat, M.D.; Giehl, K.; Adler, G.; Wedlich, D.; Menke, A. Tgfbeta-induced downregulation of e-cadherin-based cell-cell adhesion depends on pi3-kinase and pten. *J. Cell. Sci.* **2005**, *118*, 4901–4912. [CrossRef] [PubMed]
59. Lim, M.; Chuong, C.M.; Roy-Burman, P. Pi3k, erk signaling in bmp7-induced epithelial-mesenchymal transition (emt) of PC-3 prostate cancer cells in 2- and 3-dimensional cultures. *Horm. Cancer* **2011**, *2*, 298–309. [CrossRef] [PubMed]
60. Kaarbo, M.; Mikkelsen, O.L.; Malerod, L.; Qu, S.; Lobert, V.H.; Akgul, G.; Halvorsen, T.; Maelandsmo, G.M.; Saatcioglu, F. Pi3k-akt-mtor pathway is dominant over androgen receptor signaling in prostate cancer cells. *Cell Oncol.* **2010**, *32*, 11–27. [PubMed]
61. Gao, N.; Zhang, Z.; Jiang, B.H.; Shi, X. Role of pi3k/akt/mtor signaling in the cell cycle progression of human prostate cancer. *Biochem. Biophys. Res. Commun.* **2003**, *310*, 1124–1132. [CrossRef] [PubMed]
62. Hsieh, A.C.; Liu, Y.; Edlind, M.P.; Ingolia, N.T.; Janes, M.R.; Sher, A.; Shi, E.Y.; Stumpf, C.R.; Christensen, C.; Bonham, M.J.; et al. The translational landscape of mtor signalling steers cancer initiation and metastasis. *Nature* **2012**, *485*, 55–61. [CrossRef] [PubMed]
63. Evdokimova, V.; Tognon, C.; Ng, T.; Ruzanov, P.; Melnyk, N.; Fink, D.; Sorokin, A.; Ovchinnikov, L.P.; Davicioni, E.; Triche, T.J.; et al. Translational activation of snail1 and other developmentally regulated transcription factors by yb-1 promotes an epithelial-mesenchymal transition. *Cancer Cell* **2009**, *15*, 402–415. [CrossRef] [PubMed]
64. Dhar, S.; Kumar, A.; Gomez, C.R.; Akhtar, I.; Hancock, J.C.; Lage, J.M.; Pound, C.R.; Levenson, A.S. MTA1-activated Epi-microRNA-22 regulates e-cadherin and prostate cancer invasiveness. *FEBS Lett.* **2017**, *591*, 924–933. [CrossRef] [PubMed]
65. Wang, H.; Fan, L.; Wei, J.; Weng, Y.; Zhou, L.; Shi, Y.; Zhou, W.; Ma, D.; Wang, C. Akt mediates metastasis-associated gene 1 (MTA1) regulating the expression of e-cadherin and promoting the invasiveness of prostate cancer cells. *PLoS ONE* **2012**, *7*, e46888. [CrossRef] [PubMed]
66. Sheridan, C.M.; Grogan, T.R.; Nguyen, H.G.; Galet, C.; Rettig, M.B.; Hsieh, A.C.; Ruggero, D. YB-1 and MTA1 protein levels and not DNA or mRNA alterations predict for prostate cancer recurrence. *Oncotarget* **2015**, *6*, 7470–7480. [CrossRef] [PubMed]
67. Khan, M.I.; Adhami, V.M.; Lall, R.K.; Sechi, M.; Joshi, D.C.; Haidar, O.M.; Syed, D.N.; Siddiqui, I.A.; Chiu, S.Y.; Mukhtar, H. YB-1 expression promotes epithelial-to-mesenchymal transition in prostate cancer that is inhibited by a small molecule fisetin. *Oncotarget* **2014**, *5*, 2462–2474. [CrossRef] [PubMed]
68. Dias, S.J.; Zhou, X.; Ivanovic, M.; Gailey, M.P.; Dhar, S.; Zhang, L.; He, Z.; Penman, A.D.; Vijayakumar, S.; Levenson, A.S. Nuclear MTA1 overexpression is associated with aggressive prostate cancer, recurrence and metastasis in african americans. *Sci. Rep.* **2013**, *3*, 2331. [CrossRef] [PubMed]
69. Kai, L.; Wang, J.; Ivanovic, M.; Chung, Y.T.; Laskin, W.B.; Schulze-Hoepfner, F.; Mirochnik, Y.; Satcher, R.L., Jr.; Levenson, A.S. Targeting prostate cancer angiogenesis through metastasis-associated protein 1 (MTA1). *Prostate* **2011**, *71*, 268–280. [CrossRef] [PubMed]

70. Hofer, M.D.; Kuefer, R.; Varambally, S.; Li, H.; Ma, J.; Shapiro, G.I.; Gschwend, J.E.; Hautmann, R.E.; Sanda, M.G.; Giehl, K.; et al. The role of metastasis-associated protein 1 in prostate cancer progression. *Cancer Res.* **2004**, *64*, 825–829. [CrossRef] [PubMed]
71. Chen, X.; Cheng, H.; Pan, T.; Liu, Y.; Su, Y.; Ren, C.; Huang, D.; Zha, X.; Liang, C. Mtor regulate emt through rhoa and rac1 pathway in prostate cancer. *Mol. Carcinog.* **2015**, *54*, 1086–1095. [CrossRef] [PubMed]
72. Batlle, E.; Sancho, E.; Franci, C.; Dominguez, D.; Monfar, M.; Baulida, J.; Garcia De Herreros, A. The transcription factor snail is a repressor of e-cadherin gene expression in epithelial tumour cells. *Nat. Cell Biol.* **2000**, *2*, 84–89. [CrossRef] [PubMed]
73. Liu, Y.N.; Abou-Kheir, W.; Yin, J.J.; Fang, L.; Hynes, P.; Casey, O.; Hu, D.; Wan, Y.; Seng, V.; Sheppard-Tillman, H.; et al. Critical and reciprocal regulation of KLF4 and SLUG in transforming growth factor beta-initiated prostate cancer epithelial-mesenchymal transition. *Mol. Cell. Biol.* **2012**, *32*, 941–953. [CrossRef] [PubMed]
74. Liu, G.L.; Yang, H.J.; Liu, T.; Lin, Y.Z. Expression and significance of E-cadherin, *N*-cadherin, transforming growth factor-beta1 and twist in prostate cancer. *Asian Pac. J. Trop. Med.* **2014**, *7*, 76–82. [CrossRef]
75. Kwok, W.K.; Ling, M.T.; Lee, T.W.; Lau, T.C.; Zhou, C.; Zhang, X.; Chua, C.W.; Chan, K.W.; Chan, F.L.; Glackin, C.; et al. Up-regulation of twist in prostate cancer and its implication as a therapeutic target. *Cancer Res.* **2005**, *65*, 5153–5162. [CrossRef] [PubMed]
76. Drake, J.M.; Strohbehn, G.; Bair, T.B.; Moreland, J.G.; Henry, M.D. Zeb1 enhances transendothelial migration and represses the epithelial phenotype of prostate cancer cells. *Mol. Biol. Cell* **2009**, *20*, 2207–2217. [CrossRef] [PubMed]
77. Moody, S.E.; Perez, D.; Pan, T.C.; Sarkisian, C.J.; Portocarrero, C.P.; Sterner, C.J.; Notorfrancesco, K.L.; Cardiff, R.D.; Chodosh, L.A. The transcriptional repressor snail promotes mammary tumor recurrence. *Cancer Cell* **2005**, *8*, 197–209. [CrossRef] [PubMed]
78. Elloul, S.; Elstrand, M.B.; Nesland, J.M.; Trope, C.G.; Kvalheim, G.; Goldberg, I.; Reich, R.; Davidson, B. Snail, slug, and smad-interacting protein 1 as novel parameters of disease aggressiveness in metastatic ovarian and breast carcinoma. *Cancer* **2005**, *103*, 1631–1643. [CrossRef] [PubMed]
79. Kwon, C.H.; Park, H.J.; Choi, J.H.; Lee, J.R.; Kim, H.K.; Jo, H.J.; Kim, H.S.; Oh, N.; Song, G.A.; Park, D.Y. Snail and serpina1 promote tumor progression and predict prognosis in colorectal cancer. *Oncotarget* **2015**, *6*, 20312–20326. [CrossRef] [PubMed]
80. Fan, X.J.; Wan, X.B.; Yang, Z.L.; Fu, X.H.; Huang, Y.; Chen, D.K.; Song, S.X.; Liu, Q.; Xiao, H.Y.; Wang, L.; et al. Snail promotes lymph node metastasis and twist enhances tumor deposit formation through epithelial-mesenchymal transition in colorectal cancer. *Hum. Pathol.* **2013**, *44*, 173–180. [CrossRef] [PubMed]
81. Ware, K.E.; Somarelli, J.A.; Schaeffer, D.; Li, J.; Zhang, T.; Park, S.; Patierno, S.R.; Freedman, J.; Foo, W.C.; Garcia-Blanco, M.A.; et al. Snail promotes resistance to enzalutamide through regulation of androgen receptor activity in prostate cancer. *Oncotarget* **2016**, *7*, 50507–50521. [CrossRef] [PubMed]
82. Randle, D.D.; Clarke, S.; Henderson, V.; Odero-Marah, V.A. Snail mediates invasion through upa/upar and the mapk signaling pathway in prostate cancer cells. *Oncol. Lett.* **2013**, *6*, 1767–1773. [PubMed]
83. Ikenouchi, J.; Matsuda, M.; Furuse, M.; Tsukita, S. Regulation of tight junctions during the epithelium-mesenchyme transition: Direct repression of the gene expression of claudins/occludin by snail. *J. Cell. Sci.* **2003**, *116*, 1959–1967. [CrossRef] [PubMed]
84. Ohkubo, T.; Ozawa, M. The transcription factor snail downregulates the tight junction components independently of e-cadherin downregulation. *J. Cell. Sci.* **2004**, *117*, 1675–1685. [CrossRef] [PubMed]
85. Uygur, B.; Wu, W.S. Slug promotes prostate cancer cell migration and invasion via cxcr4/cxcl12 axis. *Mol. Cancer* **2011**, *10*, 139. [CrossRef] [PubMed]
86. Esposito, S.; Russo, M.V.; Airoldi, I.; Tupone, M.G.; Sorrentino, C.; Barbarito, G.; Di Meo, S.; Di Carlo, E. Snai2/slug gene is silenced in prostate cancer and regulates neuroendocrine differentiation, metastasis-suppressor and pluripotency gene expression. *Oncotarget* **2015**, *6*, 17121–17134. [CrossRef] [PubMed]
87. Song, G.Q.; Zhao, Y. Kisspeptin-10 inhibits the migration of breast cancer cells by regulating epithelial-mesenchymal transition. *Oncol. Rep.* **2015**, *33*, 669–674. [CrossRef] [PubMed]
88. Wang, H.; Jones, J.; Turner, T.; He, Q.P.; Hardy, S.; Grizzle, W.E.; Welch, D.R.; Yates, C. Clinical and biological significance of kiss1 expression in prostate cancer. *Am. J. Pathol.* **2012**, *180*, 1170–1178. [CrossRef] [PubMed]

89. Sasaki, K.; Natsugoe, S.; Ishigami, S.; Matsumoto, M.; Okumura, H.; Setoyama, T.; Uchikado, Y.; Kita, Y.; Tamotsu, K.; Sakamoto, A.; et al. Significance of twist expression and its association with e-cadherin in esophageal squamous cell carcinoma. *J. Exp. Clin. Cancer Res.* **2009**, *28*, 158. [CrossRef] [PubMed]
90. Zhang, Z.; Xie, D.; Li, X.; Wong, Y.C.; Xin, D.; Guan, X.Y.; Chua, C.W.; Leung, S.C.; Na, Y.; Wang, X. Significance of twist expression and its association with e-cadherin in bladder cancer. *Hum. Pathol.* **2007**, *38*, 598–606. [CrossRef] [PubMed]
91. Vesuna, F.; van Diest, P.; Chen, J.H.; Raman, V. Twist is a transcriptional repressor of e-cadherin gene expression in breast cancer. *Biochem. Biophys. Res. Commun.* **2008**, *367*, 235–241. [CrossRef] [PubMed]
92. Yuen, H.F.; Chua, C.W.; Chan, Y.P.; Wong, Y.C.; Wang, X.; Chan, K.W. Significance of twist and e-cadherin expression in the metastatic progression of prostatic cancer. *Histopathology* **2007**, *50*, 648–658. [CrossRef] [PubMed]
93. Raatikainen, S.; Aaltomaa, S.; Palvimo, J.J.; Karja, V.; Soini, Y. Twist overexpression predicts biochemical recurrence-free survival in prostate cancer patients treated with radical prostatectomy. *Scand. J. Urol.* **2015**, *49*, 51–57. [CrossRef] [PubMed]
94. Alexander, N.R.; Tran, N.L.; Rekapally, H.; Summers, C.E.; Glackin, C.; Heimark, R.L. *N*-cadherin gene expression in prostate carcinoma is modulated by integrin-dependent nuclear translocation of twist1. *Cancer Res.* **2006**, *66*, 3365–3369. [CrossRef] [PubMed]
95. Graham, T.R.; Zhau, H.E.; Odero-Marah, V.A.; Osunkoya, A.O.; Kimbro, K.S.; Tighiouart, M.; Liu, T.; Simons, J.W.; O'Regan, R.M. Insulin-like growth factor-i-dependent up-regulation of ZEB1 drives epithelial-to-mesenchymal transition in human prostate cancer cells. *Cancer Res.* **2008**, *68*, 2479–2488. [CrossRef] [PubMed]
96. Hou, L.; Li, Q.; Yu, Y.; Li, M.; Zhang, D. Set8 induces epithelialmesenchymal transition and enhances prostate cancer cell metastasis by cooperating with ZEB1. *Mol. Med. Rep.* **2016**, *13*, 1681–1688. [CrossRef] [PubMed]
97. Sahu, B.; Laakso, M.; Ovaska, K.; Mirtti, T.; Lundin, J.; Rannikko, A.; Sankila, A.; Turunen, J.P.; Lundin, M.; Konsti, J.; et al. Dual role of foxa1 in androgen receptor binding to chromatin, androgen signalling and prostate cancer. *EMBO J.* **2011**, *30*, 3962–3976. [CrossRef] [PubMed]
98. Robinson, J.L.; Hickey, T.E.; Warren, A.Y.; Vowler, S.L.; Carroll, T.; Lamb, A.D.; Papoutsoglou, N.; Neal, D.E.; Tilley, W.D.; Carroll, J.S. Elevated levels of foxa1 facilitate androgen receptor chromatin binding resulting in a crpc-like phenotype. *Oncogene* **2014**, *33*, 5666–5674. [CrossRef] [PubMed]
99. Jones, D.; Wade, M.; Nakjang, S.; Chaytor, L.; Grey, J.; Robson, C.N.; Gaughan, L. Foxa1 regulates androgen receptor variant activity in models of castrate-resistant prostate cancer. *Oncotarget* **2015**, *6*, 29782–29794. [CrossRef] [PubMed]
100. Jin, H.J.; Zhao, J.C.; Ogden, I.; Bergan, R.C.; Yu, J. Androgen receptor-independent function of foxa1 in prostate cancer metastasis. *Cancer Res.* **2013**, *73*, 3725–3736. [CrossRef] [PubMed]
101. Dong, T.; Zhang, Y.; Chen, Y.; Liu, P.; An, T.; Zhang, J.; Yang, H.; Zhu, W.; Yang, X. FOXO1 inhibits the invasion and metastasis of hepatocellular carcinoma by reversing ZEB2-induced epithelial-mesenchymal transition. *Oncotarget* **2017**, *8*, 1703–1713. [CrossRef] [PubMed]
102. Ni, D.; Ma, X.; Li, H.Z.; Gao, Y.; Li, X.T.; Zhang, Y.; Ai, Q.; Zhang, P.; Song, E.L.; Huang, Q.B.; et al. Downregulation of FOXO3a promotes tumor metastasis and is associated with metastasis-free survival of patients with clear cell renal cell carcinoma. *Clin. Cancer Res.* **2014**, *20*, 1779–1790. [CrossRef] [PubMed]
103. Shukla, S.; Shukla, M.; Maclennan, G.T.; Fu, P.; Gupta, S. Deregulation of FOXO3a during prostate cancer progression. *Int. J. Oncol.* **2009**, *34*, 1613–1620. [PubMed]
104. Brunet, A.; Bonni, A.; Zigmond, M.J.; Lin, M.Z.; Juo, P.; Hu, L.S.; Anderson, M.J.; Arden, K.C.; Blenis, J.; Greenberg, M.E. Akt promotes cell survival by phosphorylating and inhibiting a forkhead transcription factor. *Cell* **1999**, *96*, 857–868. [CrossRef]
105. Liu, H.; Yin, J.; Wang, H.; Jiang, G.; Deng, M.; Zhang, G.; Bu, X.; Cai, S.; Du, J.; He, Z. FOXO3a modulates WNT/beta-catenin signaling and suppresses epithelial-to-mesenchymal transition in prostate cancer cells. *Cell Signal.* **2015**, *27*, 510–518. [CrossRef] [PubMed]
106. Angulo, J.C.; Andres, G.; Ashour, N.; Sanchez-Chapado, M.; Lopez, J.I.; Ropero, S. Development of castration resistant prostate cancer can be predicted by a DNA hypermethylation profile. *J. Urol.* **2016**, *195*, 619–626. [CrossRef] [PubMed]

107. Ellinger, J.; Bastian, P.J.; Jurgan, T.; Biermann, K.; Kahl, P.; Heukamp, L.C.; Wernert, N.; Muller, S.C.; von Ruecker, A. Cpg island hypermethylation at multiple gene sites in diagnosis and prognosis of prostate cancer. *Urology* **2008**, *71*, 161–167. [CrossRef] [PubMed]
108. Yegnasubramanian, S.; Kowalski, J.; Gonzalgo, M.L.; Zahurak, M.; Piantadosi, S.; Walsh, P.C.; Bova, G.S.; De Marzo, A.M.; Isaacs, W.B.; Nelson, W.G. Hypermethylation of CpG islands in primary and metastatic human prostate cancer. *Cancer Res.* **2004**, *64*, 1975–1986. [CrossRef] [PubMed]
109. Chen, W.Y.; Wang, D.H.; Yen, R.C.; Luo, J.; Gu, W.; Baylin, S.B. Tumor suppressor hic1 directly regulates SIRT1 to modulate p53-dependent DNA-damage responses. *Cell* **2005**, *123*, 437–448. [CrossRef] [PubMed]
110. Hao, M.; Li, Y.; Wang, J.; Qin, J.; Wang, Y.; Ding, Y.; Jiang, M.; Sun, X.; Zu, L.; Chang, K.; et al. Hic1 loss promotes prostate cancer metastasis by triggering epithelial-mesenchymal transition. *J. Pathol.* **2017**, *242*, 409–420. [CrossRef] [PubMed]
111. Zheng, J.; Wang, J.; Sun, X.; Hao, M.; Ding, T.; Xiong, D.; Wang, X.; Zhu, Y.; Xiao, G.; Cheng, G.; et al. Hic1 modulates prostate cancer progression by epigenetic modification. *Clin. Cancer Res.* **2013**, *19*, 1400–1410. [CrossRef] [PubMed]
112. Van Rechem, C.; Rood, B.R.; Touka, M.; Pinte, S.; Jenal, M.; Guerardel, C.; Ramsey, K.; Monte, D.; Begue, A.; Tschan, M.P.; et al. Scavenger chemokine (CXC motif) receptor 7 (CXCR7) is a direct target gene of *hic1* (hypermethylated in cancer 1). *J. Biol. Chem.* **2009**, *284*, 20927–20935. [CrossRef] [PubMed]
113. Ezponda, T.; Popovic, R.; Shah, M.Y.; Martinez-Garcia, E.; Zheng, Y.; Min, D.J.; Will, C.; Neri, A.; Kelleher, N.L.; Yu, J.; et al. The histone methyltransferase MMSET/WHSC1 activates TWIST1 to promote an epithelial-mesenchymal transition and invasive properties of prostate cancer. *Oncogene* **2013**, *32*, 2882–2890. [CrossRef] [PubMed]
114. Shin, Y.J.; Kim, J.H. The role of EZH2 in the regulation of the activity of matrix metalloproteinases in prostate cancer cells. *PLoS ONE* **2012**, *7*, e30393. [CrossRef] [PubMed]
115. Ren, G.; Baritaki, S.; Marathe, H.; Feng, J.; Park, S.; Beach, S.; Bazeley, P.S.; Beshir, A.B.; Fenteany, G.; Mehra, R.; et al. Polycomb protein EZH2 regulates tumor invasion via the transcriptional repression of the metastasis suppressor rkip in breast and prostate cancer. *Cancer Res.* **2012**, *72*, 3091–3104. [CrossRef] [PubMed]
116. Cho, K.S.; Oh, H.Y.; Lee, E.J.; Hong, S.J. Identification of enhancer of zeste homolog 2 expression in peripheral circulating tumor cells in metastatic prostate cancer patients: A preliminary study. *Yonsei Med. J.* **2007**, *48*, 1009–1014. [CrossRef] [PubMed]
117. Byles, V.; Zhu, L.; Lovaas, J.D.; Chmilewski, L.K.; Wang, J.; Faller, D.V.; Dai, Y. SIRT1 induces emt by cooperating with emt transcription factors and enhances prostate cancer cell migration and metastasis. *Oncogene* **2012**, *31*, 4619–4629. [CrossRef] [PubMed]
118. Cui, Y.; Li, J.; Zheng, F.; Ouyang, Y.; Chen, X.; Zhang, L.; Chen, Y.; Wang, L.; Mu, S.; Zhang, H. Effect of SIRT1 gene on epithelial-mesenchymal transition of human prostate cancer PC-3 cells. *Med. Sci. Monit.* **2016**, *22*, 380–386. [CrossRef] [PubMed]
119. Liu, C.; Liu, R.; Zhang, D.; Deng, Q.; Liu, B.; Chao, H.P.; Rycaj, K.; Takata, Y.; Lin, K.; Lu, Y.; et al. MicroRNA-141 suppresses prostate cancer stem cells and metastasis by targeting a cohort of pro-metastasis genes. *Nat. Commun.* **2017**, *8*, 14270. [CrossRef] [PubMed]
120. Williams, L.V.; Veliceasa, D.; Vinokour, E.; Volpert, O.V. Mir-200b inhibits prostate cancer emt, growth and metastasis. *PLoS ONE* **2013**, *8*, e83991. [CrossRef] [PubMed]
121. Banyard, J.; Chung, I.; Wilson, A.M.; Vetter, G.; Le Bechec, A.; Bielenberg, D.R.; Zetter, B.R. Regulation of epithelial plasticity by mir-424 and mir-200 in a new prostate cancer metastasis model. *Sci. Rep.* **2013**, *3*, 3151. [CrossRef] [PubMed]
122. Saini, S.; Majid, S.; Yamamura, S.; Tabatabai, L.; Suh, S.O.; Shahryari, V.; Chen, Y.; Deng, G.; Tanaka, Y.; Dahiya, R. Regulatory role of mir-203 in prostate cancer progression and metastasis. *Clin. Cancer Res.* **2011**, *17*, 5287–5298. [CrossRef] [PubMed]
123. Kalogirou, C.; Spahn, M.; Krebs, M.; Joniau, S.; Lerut, E.; Burger, M.; Scholz, C.J.; Kneitz, S.; Riedmiller, H.; Kneitz, B. Mir-205 is progressively down-regulated in lymph node metastasis but fails as a prognostic biomarker in high-risk prostate cancer. *Int. J. Mol. Sci.* **2013**, *14*, 21414–21434. [CrossRef] [PubMed]
124. Fan, X.; Chen, X.; Deng, W.; Zhong, G.; Cai, Q.; Lin, T. Up-regulated microRNA-143 in cancer stem cells differentiation promotes prostate cancer cells metastasis by modulating fndc3b expression. *BMC Cancer* **2013**, *13*, 61. [CrossRef] [PubMed]

125. Peng, X.; Guo, W.; Liu, T.; Wang, X.; Tu, X.; Xiong, D.; Chen, S.; Lai, Y.; Du, H.; Chen, G.; et al. Identification of mirs-143 and -145 that is associated with bone metastasis of prostate cancer and involved in the regulation of emt. *PLoS ONE* **2011**, *6*, e20341. [CrossRef] [PubMed]
126. Ru, P.; Steele, R.; Newhall, P.; Phillips, N.J.; Toth, K.; Ray, R.B. MiRNA-29b suppresses prostate cancer metastasis by regulating epithelial-mesenchymal transition signaling. *Mol. Cancer Ther.* **2012**, *11*, 1166–1173. [CrossRef] [PubMed]
127. Majid, S.; Dar, A.A.; Saini, S.; Arora, S.; Shahryari, V.; Zaman, M.S.; Chang, I.; Yamamura, S.; Tanaka, Y.; Deng, G.; et al. Mir-23b represses proto-oncogene src kinase and functions as methylation-silenced tumor suppressor with diagnostic and prognostic significance in prostate cancer. *Cancer Res.* **2012**, *72*, 6435–6446. [CrossRef] [PubMed]
128. Liang, J.; Li, Y.; Daniels, G.; Sfanos, K.; De Marzo, A.; Wei, J.; Li, X.; Chen, W.; Wang, J.; Zhong, X.; et al. Lef1 targeting emt in prostate cancer invasion is regulated by mir-34a. *Mol. Cancer Res.* **2015**, *13*, 681–688. [CrossRef] [PubMed]
129. Zhang, X.; Zhang, T.; Yang, K.; Zhang, M.; Wang, K. Mir-486–5p suppresses prostate cancer metastasis by targeting snail and regulating epithelial-mesenchymal transition. *Onco Targets Ther.* **2016**, *9*, 6909–6914. [CrossRef] [PubMed]
130. Josson, S.; Gururajan, M.; Hu, P.; Shao, C.; Chu, G.Y.; Zhau, H.E.; Liu, C.; Lao, K.; Lu, C.L.; Lu, Y.T.; et al. Mir-409–3p/-5p promotes tumorigenesis, epithelial-to-mesenchymal transition, and bone metastasis of human prostate cancer. *Clin. Cancer Res.* **2014**, *20*, 4636–4646. [CrossRef] [PubMed]
131. Ren, D.; Wang, M.; Guo, W.; Huang, S.; Wang, Z.; Zhao, X.; Du, H.; Song, L.; Peng, X. Double-negative feedback loop between ZEB2 and mir-145 regulates epithelial-mesenchymal transition and stem cell properties in prostate cancer cells. *Cell Tissue Res.* **2014**, *358*, 763–778. [CrossRef] [PubMed]
132. Selth, L.A.; Das, R.; Townley, S.L.; Coutinho, I.; Hanson, A.R.; Centenera, M.M.; Stylianou, N.; Sweeney, K.; Soekmadji, C.; Jovanovic, L.; et al. A ZEB1-mir-375-YAP1 pathway regulates epithelial plasticity in prostate cancer. *Oncogene* **2017**, *36*, 24–34. [CrossRef] [PubMed]
133. Kong, D.; Li, Y.; Wang, Z.; Banerjee, S.; Ahmad, A.; Kim, H.R.; Sarkar, F.H. Mir-200 regulates pdgf-d-mediated epithelial-mesenchymal transition, adhesion, and invasion of prostate cancer cells. *Stem Cells* **2009**, *27*, 1712–1721. [CrossRef] [PubMed]
134. Liu, Y.N.; Yin, J.J.; Abou-Kheir, W.; Hynes, P.G.; Casey, O.M.; Fang, L.; Yi, M.; Stephens, R.M.; Seng, V.; Sheppard-Tillman, H.; et al. Mir-1 and mir-200 inhibit emt via slug-dependent and tumorigenesis via slug-independent mechanisms. *Oncogene* **2013**, *32*, 296–306. [CrossRef] [PubMed]
135. Puhr, M.; Hoefer, J.; Schafer, G.; Erb, H.H.; Oh, S.J.; Klocker, H.; Heidegger, I.; Neuwirt, H.; Culig, Z. Epithelial-to-mesenchymal transition leads to docetaxel resistance in prostate cancer and is mediated by reduced expression of mir-200c and mir-205. *Am. J. Pathol.* **2012**, *181*, 2188–2201. [CrossRef] [PubMed]
136. Wang, N.; Li, Q.; Feng, N.H.; Cheng, G.; Guan, Z.L.; Wang, Y.; Qin, C.; Yin, C.J.; Hua, L.X. Mir-205 is frequently downregulated in prostate cancer and acts as a tumor suppressor by inhibiting tumor growth. *Asian J. Androl.* **2013**, *15*, 735–741. [CrossRef] [PubMed]
137. Wu, D.; Huang, P.; Wang, L.; Zhou, Y.; Pan, H.; Qu, P. MicroRNA-143 inhibits cell migration and invasion by targeting matrix metalloproteinase 13 in prostate cancer. *Mol. Med. Rep.* **2013**, *8*, 626–630. [CrossRef] [PubMed]
138. Liu, C.; Kelnar, K.; Liu, B.; Chen, X.; Calhoun-Davis, T.; Li, H.; Patrawala, L.; Yan, H.; Jeter, C.; Honorio, S.; et al. The microRNA mir-34a inhibits prostate cancer stem cells and metastasis by directly repressing cd44. *Nat. Med.* **2011**, *17*, 211–215. [CrossRef] [PubMed]
139. He, J.H.; Li, B.X.; Han, Z.P.; Zou, M.X.; Wang, L.; Lv, Y.B.; Zhou, J.B.; Cao, M.R.; Li, Y.G.; Zhang, J.Z. Snail-activated long non-coding RNA pca3 up-regulates prkd3 expression by mir-1261 sponging, thereby promotes invasion and migration of prostate cancer cells. *Tumour Biol.* **2016**. [CrossRef] [PubMed]
140. Prensner, J.R.; Iyer, M.K.; Sahu, A.; Asangani, I.A.; Cao, Q.; Patel, L.; Vergara, I.A.; Davicioni, E.; Erho, N.; Ghadessi, M.; et al. The long noncoding RNA schlap1 promotes aggressive prostate cancer and antagonizes the swi/snf complex. *Nat. Genet.* **2013**, *45*, 1392–1398. [CrossRef] [PubMed]
141. Li, Y.; Luo, H.; Xiao, N.; Duan, J.; Wang, Z.; Wang, S. Long noncoding RNA schlap1 accelerates the proliferation and metastasis of prostate cancer via targeting mir-198 and promoting the mapk1 pathway. *Oncol. Res.* **2017**. [CrossRef] [PubMed]

142. Aiello, A.; Bacci, L.; Re, A.; Ripoli, C.; Pierconti, F.; Pinto, F.; Masetti, R.; Grassi, C.; Gaetano, C.; Bassi, P.F.; et al. Malat1 and hotair long non-coding RNAs play opposite role in estrogen-mediated transcriptional regulation in prostate cancer cells. *Sci. Rep.* **2016**, *6*, 38414. [CrossRef] [PubMed]
143. Wang, D.; Ding, L.; Wang, L.; Zhao, Y.; Sun, Z.; Karnes, R.J.; Zhang, J.; Huang, H. LncRNA *MALAT1* enhances oncogenic activities of EZH2 in castration-resistant prostate cancer. *Oncotarget* **2015**, *6*, 41045–41055. [CrossRef] [PubMed]
144. Sebastian, A.; Hum, N.R.; Hudson, B.D.; Loots, G.G. Cancer-osteoblast interaction reduces *Sost* expression in osteoblasts and up-regulates lncRNA *MALAT1* in prostate cancer. *Microarrays* **2015**, *4*, 503–519. [CrossRef] [PubMed]
145. Jin, Y.; Cui, Z.; Li, X.; Jin, X.; Peng, J. Upregulation of long non-coding RNA plncRNA-1 promotes proliferation and induces epithelial-mesenchymal transition in prostate cancer. *Oncotarget* **2017**, *8*, 26090–26099. [CrossRef] [PubMed]
146. Cortez, M.A.; Valdecanas, D.; Zhang, X.; Zhan, Y.; Bhardwaj, V.; Calin, G.A.; Komaki, R.; Giri, D.K.; Quini, C.C.; Wolfe, T.; et al. Therapeutic delivery of mir-200c enhances radiosensitivity in lung cancer. *Mol. Ther.* **2014**, *22*, 1494–1503. [CrossRef] [PubMed]
147. Ibrahim, A.F.; Weirauch, U.; Thomas, M.; Grunweller, A.; Hartmann, R.K.; Aigner, A. MicroRNA replacement therapy for mir-145 and mir-33a is efficacious in a model of colon carcinoma. *Cancer Res.* **2011**, *71*, 5214–5224. [CrossRef] [PubMed]